# Integrating kinematics, mechanics of deformation, thermal modelling and diagenesis in orogenic systems: the Dinarides example

**Geïntegreerde kinematica, mechanismen van deformatie, thermisch modelleren en diagenese in orogene systemen: het Dinarische voorbeeld**
(met een samenvatting in het Nederlands)

**Cinématique intégratrice, mécanique de la déformation, modélisation thermique et diagénèse dans les systèmes orogéniques: l'exemple des Dinarides**
(avec un résumé en français)

## Proefschrift

ter verkrijging van de graad van doctor aan de Universiteit Utrecht
op gezag van de rector magnificus, prof. dr. H.R.B.M. Kummeling,
ingevolge het besluit van het college voor promoties in het openbaar
te verdedigen op woensdag 26 juni 2019 des ochtends te 10.30 uur

door

**Marianne van Unen**

geboren op 20 juli 1992 te ‘s-Gravenhage

| | |
|---|---|
| **Promotor:** | Prof. dr. L.C. Matenco |
| **Copromotoren:** | Dr. F.H. Nader |
| | Dr. J.-L. Rudkiewicz |

This study was financially supported by IFP Energies Nouvelles, Rueil-Malmaison, France

*"Geologists have a saying – rocks remember."*

Neil Armstrong

Members of the reading committee:

| | |
|---|---|
| Prof. dr. Mark Handy | Freie Universität Berlin, Germany |
| Prof. dr. Rudy Swennen | Katholieke Universiteit Leuven, Belgium |
| Prof. dr. Marinko Toljić | University of Belgrade, Serbia |
| Prof. dr. Giovanni Bertotti | Technische Universiteit Delft, The Netherlands |
| Dr. Gabor Tari | Österreichische Mineralölverwaltung, Vienna, Austria |

The research presented in this thesis was carried out at :

Department of Geo-resources, Geosciences Division
IFP Energies Nouvelles
1 - 4 avenue de Bois-Préau
92852 Rueil-Malmaison Cedex
France

and

Tectonics Research Group, Department of Earth Sciences
Faculty of Geosciences, Utrecht University
Princetonlaan 4
3584 CB Utrecht
The Netherlands

This is Utrecht Studies in Earth Sciences volume 191
ISBN 978-90-6266-548-8



Printed in the Netherlands by Drukkerij Haveka te Alblasserdam.

*Cover: Photo taken during my fieldwork, illustrating a large-scale overview of the Kotor Bay in Montenegro, where significant amounts of shortening are being accommodated (further details are described in Chapter 3, see also Figure 3.9e).*

# Contents

# Acknowledgements

This thesis includes three years of intensive research as well as professional and personal development. This project allowed me to work in France and in the Netherlands and involved many travelling including field work, workshops, courses, conferences and meetings. This gave me the chance to meet a lot of new and great people from all over the world with whom I have exchanged great ideas and knowledge.

First, I want to thank my promotor Liviu Matenco for his great scientific and moral support, and constructive criticism. Liviu, your great help started from the first month of my PhD during the first field research. This was an effective way for me to understand the kinematic background of the Dinarides and also the Bosnian culture and history. I want to thank you for transferring your great knowledge and for your contribution in reviewing and writing three scientific papers. Your continuous motivation until the end of my PhD allowed me to significantly progress as a scientist and to defend my thesis in Utrecht.

Second, I would like to thank my co-promotor Fadi Nader for his contribution in reviewing the three scientific papers, for his support during the fieldwork and his help in the lab. During my stay in France you often checked on me if everything was going well both personally and with work. You presented me to a lot of professionals, which allowed me to expand my professional network. I also appreciated your great support, ideas and advice regarding my future career.

Great appreciation also goes to Romain Darnault. I want to thank you for your great support and help, not only when you were my co-promotor during the initial phases of my PhD, but also after. Especially, I enjoyed the fieldwork together with you and also working with you in IFPEN. Also many thanks for your contribution in reviewing the scientific papers.

Jean-Luc, even though you became my co-promotor at the end of the PhD, I want to thank you for your great help with the basin modelling and for the discussions we had on the results. I also want to thank you for your contribution and revision of the third paper and the thesis.

I would like to thank the members of the reading committee: Mark Handy, Rudy Swennen, Marinko Toljić, Giovanni Bertotti and Gabor Tari, for taking the time to review my thesis and providing me with valuable comments and for highlighting the added value of this thesis.

Vedad, Bruno, Matija, Milos and Oleg are greatly acknowledged for their collaboration, great discussions and moments of fun during fieldwork.

Mark Handy, Douwe van Hinsbergen, Stefan Schmid and Kamil Ustaszewski are acknowledged for the great discussions during meetings and conferences, which helped in understanding the large-scale orogenic correlations.

Hazim Hrvatović and Marinko Toljić are acknowledged for their collaboration, discussions and logistic support in the field.

Prof. dr. M. Joachimski is acknowledged for doing the carbon and oxygen isotope analyses on our rock-samples.

Ljiljana Vucic and her colleagues from the Montenegro Seismological Observatory is acknowledged for insight into the seismic data of Montenegro, for providing us with seismic lines, for the great discussions and for being very welcoming during our stay in Montenegro.

Daniel Pillot is acknowledged for teaching me to do the Rock-Eval pyrolysis and for doing Rock-Eval on my first set of samples. Herman Ravelojaona is acknowledged for his help in the lab and during the thin-section preparation.

Francois Roure is acknowledged for the discussions on the geometry of the cross-sections, which helped us to better understand the offshore structural deformation and to improve the cross-sections.

Many thanks to Margot Stoete and Ton Markus from the Geoscience Faculty Office for making the cover and invitations and for providing me with helpful information that aided me in designing my thesis.

During my stay in IFP Energies Nouvelles and Beicip in France I have met a lot of great new friends and colleagues who supported me both personally and professionally. Great thanks go to: Anouk, Pauline, DanDan, Amanda, Adriana, Martina, Damaris, Jean, Cedric, Fadi, Romain, Jean-Luc, Vanessa, Renaud, Sylvie, Remy, Sebastian, Djamila, Jamila, Meriem, Mickaele, Olga, Benoit, Vincent-Richard, Jean-Claude, Marie and many others.

During my stay at Utrecht University in the Netherlands, during meetings and at conferences, friends and colleagues from the Tectonics Group were very welcoming and always invited me for social events. I appreciated this a lot and want to thank all of you: Nevena, Atilla, Eszter, Kristóf, Antoine, Jeroen, Inge, Fred, Ernst, Sierd, Magdala, Liviu and others.

Great thanks go to my mother, father and brother, and other family, and my friends from home, who always gave me great advice and supported me in difficult and successful moments.

# Summary

Continental collision and subduction dynamics are often the main tectonic processes responsible for the formation of mountain belts. Understanding the mechanics of deformation across collisional orogens is of prime importance in order to determine the mountains architecture and the associated deep mantle-scale geodynamic processes.

In this thesis I aim to determine the mechanics of tectonic-driven deformation associated with the migration of subducting slabs, indentation of microplates and lower crustal accretion. Subsequently, the effect of these mechanisms of deformation on the thermal, fluid-flow and maturity of organic matter evolution has been determined.

The Dinarides orogen is a world-class example of a collisional orogen that was affected by a number of critical processes driving mountain building and subsequent collapse during its Jurassic-Eocene evolution associated with the convergence between Europe- and Adriatic-derived units in the Central Mediterranean area. Such processes include linked migration of slab and magmatism during continental collision, indentation of continental micro-plates, changes in polarities in respect to neighboring orogens or transfer of deformation between active areas driving the distribution of present-day seismicity and crustal stresses. All these processes are critical for the evaluation of geo-resources in the upper crustal domain and their quantification is important to be ported to the understanding of other orogens worldwide.

Chapter 2 analyses the large-scale kinematic evolution of the Dinarides by the means of an extensive surface kinematic study performed in the less known area of the external Dinarides. By correlating the kinematics with available geophysical and evolutionary constraints, we constructed two large-scale, kinematically controlled regional transects. The results demonstrate a long-lived evolution of shortening that affected the Dinarides lower orogenic plate. While the Late Jurassic-earliest Cretaceous deformation was associated with an earlier obduction moment, the latest Cretaceous onset of continental collision has gradually focused deformation at inherited rheological weakness zones. We show that shortening was interrupted by a period of Miocene extension that affected all orogenic areas and created the Dinarides Lake System. The extension was followed by renewed shortening, which started during the late Miocene and remains presently active. This renewed shortening was induced by the indentation of the Adriatic microplate. These results indicate a lower plate crustal accretion mechanism that was spatially and temporally connected with gradual slab retreat in the Dinarides.

The structural and kinematic effects of the post- middle Miocene Adriatic indentation in the NW-SE oriented Dinarides structure have been analysed in more details in Chapter 3. The results demonstrate that deformation was characterized by a coherent regional system of large offset dextral strike-slip faults, which transfer gradually their offsets to thrusts and high-angle reverse faults. As the Dinarides is situated at the critical transition between the Alps, Albanides and Hellenides, and across the Adriatic margin of the Apennines, we have discussed the results of the mechanics of deformation associated with the Adriatic indentation in the larger scale geodynamic context. This shows that the post-middle Miocene Dinarides fault system accommodates the differential motion between the N- ward Adriatic indentation in the Alps and the rapid S- to SW- ward movement of a Hellenides area situated SE of the Kefalonia Fault (that was driven by the Aegean slab-roll back).

The effects of the extensively acquired kinematic, structural and regional geodynamic knowledge on the thermal, fluid-flow and organic matter maturity evolutions were further explored by the means of a numerical modelling study presented in Chapter 4. This 2D modelling approach is based on a kinematically controlled cross-section across the Dinarides orogen, which was analysed in previous chapters. First, this cross-section was reconstructed to its pre-orogenic configuration. The modelling results demonstrate that deformation-, burial- and exhumation-, and erosion- and sedimentation- rates significantly contribute to changes in the thermal distribution across the orogen. In addition, petrographic and geochemical (stable oxygen and carbon isotopic) investigations of samples that were taken from major fault contacts, demonstrate the significant impact of the tectonic-induced paleo-fluid flow on the diagenetic evolution of rocks across the external Dinarides.

# Samenvatting

Continentale botsing en subductie-dynamica zijn vaak de belangrijkste tektonische processen die verantwoordelijk zijn voor de vorming van bergketen. Het begrijpen van de deformatie mechanica van botsende orogenen, is van groot belang om de berg-architectuur en de bijbehorende geo-dynamische processen op diepe mantel-schaal te bepalen.

Mijn doel in dit proefschrift is het bepalen van de mechanica van tektonisch aangedreven deformatie geassocieerd met de migratie van subductiezones, botsing van microplaten en het omhoog komen van de lagere aardkorst. Vervolgens, kan het effect van deze deformatie mechanismen op de evolutie van thermische patronen, vloeistof stromingen en maturiteit van organische materie worden bepaald.

Het Dinariden orogeen is een wereldklasse voorbeeld van continentale orogenen die werd getroffen door een aantal kritieke processen die de bergopbouw en daaropvolgende instorting tijdens zijn Jura – Eoceen evolutie geassocieerd met de convergentie tussen de Europese en Adriatische platen in het centrale Middellandse Zee Gebied. Dit soort processen omvatten gekoppelde migratie van subductiezones en magmatisme tijdens continentale botsingen, botsingen van continentale microplaten, veranderingen in polariteiten met betrekking tot naburige orogenen, of overdracht van deformatie tussen actieve gebieden die de distributie van de huidige aardbevingen en aardkorstspanningen sturen. Al deze processen zijn cruciaal voor de evaluatie van aardreserves in de bovenste korst laag en hun kwantificatie is belangrijk om gebruikt te worden voor het begrijpen van andere orogenen wereldwijd.

Hoofdstuk 2 analyseert de grootschalige kinematische evolutie van de Dinariden aan de hand van een uitgebreide kinematische studie op het aardoppervlak van de minder bekende omgeving van de externe Dinariden. Door de kinematica te correleren met beschikbare geofysische en evolutionaire informatie, construeerden we twee grootschalige, kinematisch gecontroleerde regionale dwarsprofielen. De resultaten tonen een langdurige ontwikkeling van de verkorting die de lagere orogene plaat van de Dinariden beïnvloedde. Hoewel de vroege Jura tot vroegste Krijt-deformatie geassocieerd was met een eerder obductiemoment, de opeenvolgende continentale botsing van het jongste Krijt geleidelijk concentreerde de deformatie in reologische zwaktezones. We laten zien dat de periode van verkorting werd onderbroken door een periode van Mioceen-extensie die alle orogene gebieden aantastten en het Dinariden-bekkensysteem creëerde. De extensie werd gevolgd door hernieuwde verkorting, wat begon tijdens het late Mioceen en is momenteel nog steeds actief is. Deze verkorting wordt aangedreven door de botsing van de Adriatische microplaat. Deze resultaten duiden op een mechanisme waarbij materialen van de lagere aardkorst, die ruimtelijk en met tijd verbonden was met het geleidelijk terugtrekken van een subductie zone in de Dinariden.

De structurele en kinematische effecten van de post-midden Mioceen Adriatische botsing in de noordwest - zuidoost georiënteerde Dinariden structuur zijn in meer detail geanalyseerd in Hoofdstuk 3. De resultaten tonen aan dat deformatie werd gekenmerkt door een coherent regionaal systeem van grote afschuivings dextrale zijschuivings-breuken, die geleidelijk hun afschuiving overbrengen naar opschuivings-breuken die een hoge hoek kunnen hebben. Aangezien de Dinariden zich bevinden op de kritieke overgang tussen de Alpen, Albaniden en Helleniden, en aan de overkant van de Adriatische rand van de Apennijnen, hebben we de resultaten besproken van de deformatie mechanismen geassocieerd met de Adriatische botsing

in de geodynamische context op grotere schaal. Dit toont aan dat het Dinariden breuksysteem dat gevormd was na het midden-Mioceen resulteerde in de differentiële beweging tussen de noordwaarts bewegende Adriatische plaat en botsing tegen de Alpen, en de snelle zuid-zuidwest-waartse beweging van een Hellenides-gebied gelegen ten zuidoosten van de Kefalonia-breuk (dat was aangedreven door de terugtrekking van de Egeïsche subductiezone).

Het effect van de uitgebreid verworven kinematische, structurele en regionale geodynamische kennis op de evolutie van de thermische eigenschappen, vloeistofstromingen en maturiteit van organische materie, werden verder onderzocht door middel van een numerieke modeleer studie gepresenteerd in Hoofdstuk 4. Deze 2D modellering is gebaseerd op de analyse van een representatieve kinematisch gecontroleerde dwarsprofiel door het Dinariden orogeen, geanalyseerd in voorgaande hoofdstukken. In de eerste fase werd dit dwarsprofiel gereconstrueerd naar zijn pre-orogene configuratie. De modellerings-resultaten tonen aan dat deformatie-, begraaf- en opheffing-, en erosie- en sedimentatie-snelheden significant bijdragen aan veranderingen in de thermische verdeling door het orogeen. Daarnaast, zijn petrografische en geo-chemische (stabiele zuurstof- en koolstofisotopen) onderzoeken gedaan op monsters genomen van de grootste breukcontacten, wat de significante impact van de tektonisch geïnduceerde paleo-vloeistofstroom op de diagenetische evolutie van gesteenten in de externe Dinariden aantoonde.

# Résumé

La collision continentale associée au mécanisme de subduction sont souvent les principaux processus tectoniques responsables de la formation des chaînes de montagne. Comprendre la mécanique de la déformation au sein de ces orogènes en collision est primordiale pour déterminer l'architecture de ces édifices et les processus géodynamiques associés à l'échelle du manteau profond.

L'objectif de cette thèse est d'étudier les déformations induites par la tectonique associée à la migration du plan de subduction, à l'indentation et l'accrétion de la partie inférieure de la croûte terrestre, et à l'augmentation de l'épaisseur de l'écorce terrestre. Ce travail permettra également de déterminer l'effet de ces mécanismes sur la thermicité, la migration des fluides et l'évolution de maturité de la matière organique dans ces contextes géologiques particuliers.

Les Dinarides, situées en méditerranée centrale et issues de la collision entre la microplaque adriatique et la plaque européenne, sont un exemple de classe mondiale d'un orogène collisionnel marqué, au cours de son évolution jurassique-éocène, par un certain nombre de processus géologiques entrainant la formation de montagnes et l'effondrement qui s'en suit.

Parmi les processus impactant cet orogène, les suivant sont recensés : la migration du plan de subduction et du magmatisme associé, l'indentation des microplaques continentales, les changements de polarités par rapport aux orogènes voisins et, de façon associée, l'évolution au cours du temps de la distribution des contraintes dans le système crustal global. La compréhension et la quantification de chacun de ces processus est clé dans l'évaluation des géo-ressources. De plus, cet exemple constitue un analogue de qualité pour mieux comprendre les processus géologiques similaires à l'échelle mondiale.

Le chapitre 2 de la thèse porte sur l'évolution cinématique des Dinarides à grande échelle. Une étude sur la cinématique de déformation menée dans la partie externe des Dinarides la moins connue y est présentée. La corrélation des données de terrain sur la cinématique de déformations et des données géophysiques ont permis de construire deux coupes géologiques régionales d'échelle crustale. Les résultats montrent une évolution long-terme du raccourcissement qui affecte la partie inférieure des Dinarides. De la fin du Jurassique jusqu'au début du Crétacé, les déformations de la chaîne sont associées à une obduction. La collision continentale tardi-crétacée est quant à elle marquée par des déformations se focalisant dans les zones de faiblesses rhéologiques. Nous démontrons dans ce travail que le raccourcissement a été interrompu par une période d'extension miocène qui affecte toute la chaine et crée le système de lacs présents dans les Dinarides. La fin du Miocène est marquée par le regain du raccourcissement qui perdure aujourd'hui et qui est associé à l'indentation de la microplaque adriatique. Ces résultats indiquent une accrétion de la partie profonde de la croute qui est spatialement et temporellement connectée au retrait graduel du plan de subduction des Dinarides.

L'impact des déformations structurales datées du post Miocène moyen et générées par l'indentation de la microplaque adriatique (structures orientées NW-SE dans les Dinarides) a été analysé en détails et fait l'objet du chapitre 3 de cette thèse. Les résultats démontrent que cette déformation est caractérisée par un système de grandes failles décrochantes dextres qui génèrent des chevauchements et des failles inverses à fort pendage. Etant donné que les Dinarides sont situées au point de transition critique entre les Alpes, les Albanides et les

Hellenides, et à travers la marge des Apennins, nous avons discuté des résultats obtenus en les situant dans ce contexte géodynamique. Cette démarche montre que le système de failles post Miocène moyen structurant les Dinarides accommode les déplacements relatifs des Alpes vers le Nord et le mouvement rapide vers le Sud – Sud-Ouest des Hellenides, au Sud-Est de la faille Kefalonia. Ces déplacements sont contrôlés par les déformations profondes liées au retrait du plan de subduction Egéen.

Les connaissances acquises sur la cinématique, la structure et la géodynamique régionale ont permis de créer des modèles numériques pour étudier les effets de ces paramètres sur les évolutions de température, de flux et de maturité sur les systèmes pétroliers existants. Les résultats sont présentés dans le chapitre 4 de la thèse. Cette 2D modélisation est basée sur les coupes géologiques créées pendant le travail de thèse et sur leur restauration. La modélisation montre à quel point les taux de déformation, d'enfouissement et d'exhumation, et d'érosion et de sédimentation contribuent de manière significative à la distribution de la thermicité et les migrations des fluides à travers la chaîne de montagne. De plus, les investigations petrographiques et géochimiques (isotopes stables du carbone et de l'oxygène) menées sur des échantillons prélevés dans les failles majeures démontrent l'impact significatif des paléo-écoulements des fluides induits par la tectonique dans l'évolution diagénétique des roches au travers des Dinarides externes.

## Chapter 1.

# Introduction

The geometry and evolution of collisional mountain belts are commonly controlled by processes of lower crustal accretion associated with a gradual migration of deformation, exhumation and subduction zones towards the orogenic foreland (Burov & Yamato, 2008; Doglioni et al., 2007; Faccenna et al., 2014; Forte et al., 2014; Gerya & Yuen, 2003; Matenco et al., 2010). Quantifying the kinematics responsible for the formation of such collisional orogens is of prime importance in order to determine and understand the mechanics of deformation responsible for the structuration of convergence zones. The convergent deformation and exhumation across these orogens is mainly rheologically controlled and also depends on the distribution of surface processes in space and with time, such as rates of erosion and sedimentation, and on mantle dynamics (Matenco et al., 2017; Willingshofer et al., 2013). Kinematically controlled restorations across such orogens are an effective way to understand the superposition and localization of deformation. The restoration of cross-sections to a pre-orogenic configuration allows to better estimate the amounts shortening, subsidence and exhumation, erosion and sedimentation, together with the evolution of diagenesis and fluid-rock interactions (Davis et al., 1983; Mitra, 1994; Roure & Sassi, 1995; Vergés et al., 1995). Thermal (basin) modelling on such restored cross-sections take into account realistic mechanisms of deformation and their evolution through time. Therefore, a qualitative simulation of the porous medium deformation, heat transfer, and hydrocarbon generation and accumulation can be made (Schneider, 2003). Subsequently, quantitative predictions on the petroleum system or other geo-resources potential (e.g. reservoir properties, timing of hydrocarbon generation and accumulation) can be achieved together with better constraining the fluid-rock interactions.

## 1.1 Tectonics and sedimentation in the Dinarides collisional orogen

A world-class example of collisional orogens is the Dinarides orogen situated in central-eastern Europe, as part of the Mediterranean system of mountain belts (Figure 1.1). The Dinarides orogen started its evolution with the opening of a northern branch of the Neotethys Ocean (e.g., Stampfli & Borel, 2002; Schmid et al., 2008) during the Middle Triassic, which also triggered the formation of the Budva graben in the external parts of the SE-Dinarides. This graben was gradually filled with deep marine carbonates, whereas in the remainder of the external Dinarides only shallow water carbonate sedimentation took place (Dimitrijević, 1997; Vlahovic et al., 2005). During late Early Jurassic times the shallow water deposition continued in the Adriatic carbonate platform, while being separated by intervening deep marine basins to the north and south (Vlahović et al., 2005). The shallow marine platform carbonates continued to be deposited in the platform areas of the Dinarides until Eocene times (Cosović et al., 1994). These platform carbonates were alternating with intra-platform deep marine troughs, which were filled with deep marine turbidites (e.g. Korbar et al., 2001; Tišljar et al., 1998). Within the internal parts of the Dinarides the carbonate platform deposition was interrupted by the deposition of deep-marine turbidites during the Kimmeridgian (i.e. Vranduk Flysch) that continued with thickest deposition during the uppermost Cretaceous (i.e. the Ugar and Durmitor flysches).

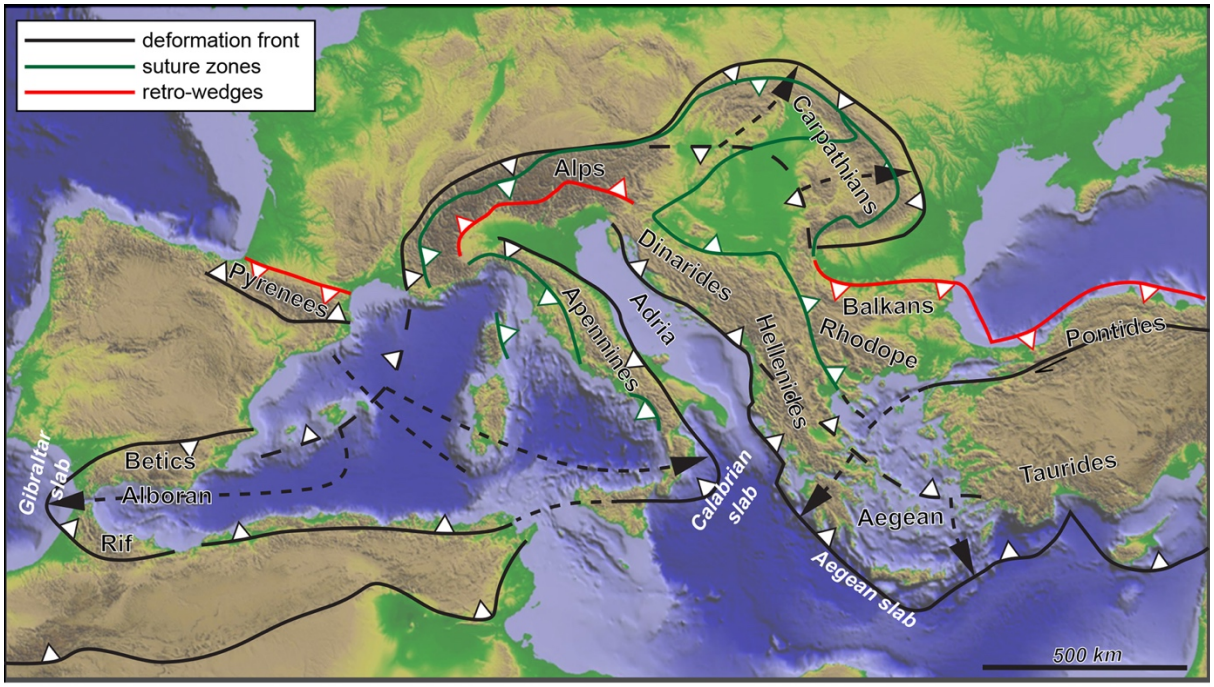


Figure 1.1 Topographic map at the scale of the Central Mediterranean illustrating the main orogenic features (inspired from Wortel & Spakman, 2000).

The main tectonic units in the Dinarides formed in response to a Cretaceous – Oligocene phase of NE-SW oriented contraction created by the convergence between the Europe- and Adriatic-derived units (e.g. Dimitrijević, 1997; Schmid et al., 2008). The SW-vergent thrusting gradually migrated towards the external parts of the Dinarides (Aubouin et al., 1970; Dimitrijević, 2001). The last phase of orogenic deformation was associated with the deposition of late Eocene clastic turbidites and late Eocene - Oligocene coarse conglomeratic molasse deposits (the Promina Beds) near thrust contacts and inside the basins (Mrinjek, 1993; Zupanič & Babić, 2011).

This was followed by a generalized moment of early – middle Miocene extension as a result of orogenic collapse and slab retreat, which created the Miocene Dinarides Lake System (Figure 1.2; Andrić et al., 2017; Harzhauser & Manidc, 2008; Harzhauser et al., 2011; Mandic et al., 2012). The largest such lake basin is the Sarajevo-Zenica, which is situated SW of the Bosnian Flysch in Bosnia and Herzegovina. In this basin, late Oligocene – early Miocene continental to shallow-marine lacustrine contractional flexural deposition was followed by an early - middle Miocene asymmetric extension featuring coarse clastic deposits and by an upper Miocene continental alluvial to deltaic sedimentary deposition that was partly coeval with the late stage inversion of the basin (Andrić et al., 2017; Hrvatović, 2006).

This phase of extension affected the entire Dinarides and provide critical stratigraphic constraints for a post-middle Miocene phase of contraction, driven by the N- to NE-ward indentation of the Adriatic microplate (Figure 1.2; Grenerczy et al., 2005; Pinter et al., 2005; Ustaszewski et al., 2008). This deformation is also associated with a presently observed slab in a far external Dinarides position as indicated from large-scale high-velocity anomalies along the entire external part of the Dinarides (Šumanovac et al., 2017; Šumanovac & Dudjak, 2016; Ustaszewski et al., 2008).

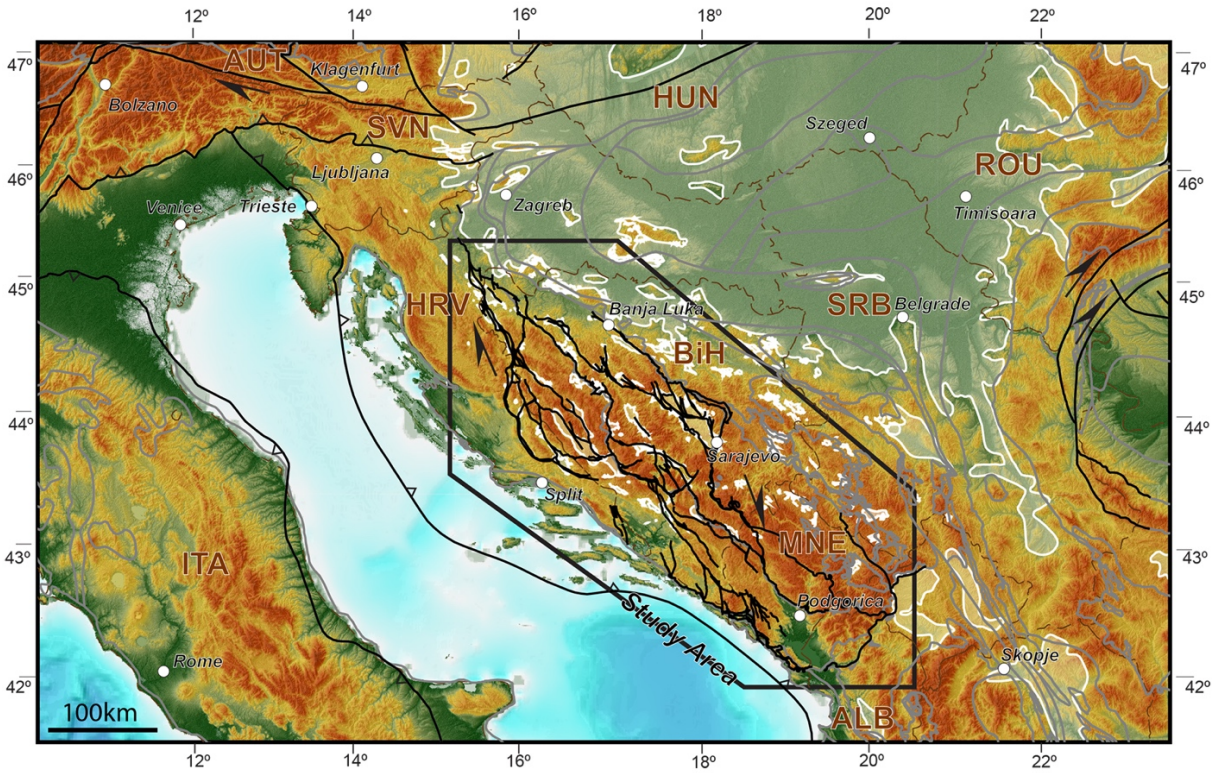


Figure 1.2 Relief map of the Dinarides and their junction with the Alps and the Albanides in SE Europe, showing the post-9Ma fault system described in this thesis. Black outline is the location of the studied area presented in this thesis. White outlines are the Miocene Pannonian Basin and the Miocene Dinarides Lake System (DLS), (after Harzhauser & Mandic, 2008; de Leeuw et al., 2012). AUT= Austria, SVN= Slovenia, HUN= Hungary, ITA= Italy, HRV= Croatia, SRB= Serbia, BiH= Bosnia-and-Herzegovina, MNE= Montenegro, ROU= Romania, ALB= Albania.

## 1.2 Research objectives

Collisional orogens can often be associated with the migration of deformation and associated subduction zones towards the orogenic foreland. The Dinarides orogen is a world-class example of such an orogen, which formed in response to continental collision and a latest phase of indentation, and where the remnant of the subducted slab is presently observed in a far external position. In this orogen, understanding the mechanics of contractional deformation is hampered by the lack of structural and kinematic data in the central and SE-Dinarides, which is a critical area for understanding the evolution of the collisional system and associated subduction. This combination between interesting processes and lack of data provided the motivation to study the mechanics of orogenic building by performing a structural and kinematic study on the complex geometry of the Dinarides orogen, combined with the construction of regional scale kinematically controlled restorations along cross-sections over the central and southeastern Dinarides.

Furthermore, among the many examples worldwide, the evolution of the Adriatic continental microplate in the Mediterranean domain provides one of the best places to study the mechanics of indentation. This is a rare opportunity when compared with many other indentation areas worldwide, where understanding the structural and kinematic effects of indentation is rather

difficult due to the large number of competing mechanisms responsible for the complex orogenic build-up. Therefore, we focused on understanding the structures and kinematics that formed as a result of the Adriatic indentation and their driving mechanisms. This offers also the opportunity to understand the larger geodynamic context connecting the Dinarides with their critical transitions to the Southern Alps and Albanides-Hellenides system and across the Adriatic margin of the Apennines in the overall context of the Adriatic indentation.

In order to estimate the shortening, sedimentation and erosion, and subsidence and exhumation through space and time, a kinematically controlled cross-section across the Dinarides has been restored into its pre-orogenic configuration. Thermal/basin numerical modelling was applied on these restorations in order to derive a novel understanding of the thermal and maturity evolution, in the overall context of tectonic and geodynamic processes driving the temperature, maturity and fluid flow characteristics across the orogen. Additional information concerning the tectonic-related paleo- fluid flow was derived from preliminary petrographic and geochemical investigations of representative fracture-cemented samples.

## 1.3 Outline of the thesis

This thesis consists of five chapters. The introduction of Chapter 1 is followed by Chapter 2, which descibes the overall large-scale kinematic evolution responsible for the formation of the Dinarides orogen. This has been done by the means of a large-scale surface kinematic study, which contributed to a new extensive kinematic dataset focused on the main phases of deformation. By correlating the kinematics with available geophysical and evolutionary constraints we constructed two large-scale kinematically controlled regional transects, of which one extends through the central- and the other one through the SE-Dinarides.

Chapter 3 provides a focused kinematic dataset associated with the structural effects induced during the post- middle Miocene Adriatic indentation onto the Dinarides orogen. The post-9 Ma structures can be characterized by a regional system of large offset dextral strike-slip faults which transfer gradually their offsets to thrusts and high-angle reverse faults. The mechanics of deformation associated with the Adriatic indentation in the Dinarides has been correlated at the larger scale context of the Alps, Albanides and Hellenides, and across the Adriatic margin of the Apennines.

Chapter 4 focusses on the restoration and numerical modelling of one of the constructed cross-sections presented in Chapter 2. From the restoration the minimum amounts of shortening, erosion and sedimentation, and subsidence- and exhumation have been estimated. The basin model results indicate that the tectonic processes significantly contribute to changes in the thermal distribution across the orogen. Petrographic and geochemical (stable oxygen and carbon isotopic) studies of samples from major fault contacts demonstrate the character of the tectonic-induced paleo-fluid flow during the main episodes of thrusting.

The thesis ends with a synthesis of the main results obtained in the present thesis presented in Chapter 5, where the crustal-scale kinematic evolution is connected with the mantle-scale processes and subsequently the effect on the geometry, thermal and maturity evolution across the studied orogen.

## Chapter 2.

# Kinematics of foreland-vergent crustal accretion: inferences from the Dinarides evolution

*This chapter is based on:*
*van Unen, M., Matenco, L., Nader, F. H., Darnault, R., Mandic, O., & Demir, V. (2019). Kinematics of foreland-vergent crustal accretion: Inferences from the Dinarides evolution. Tectonics, 38, 49–76. doi: 10.1029/2018TC005066*

## 2.1 Introduction

The geometry and evolution of mountain chains are primarily controlled by the mechanics of accreting sediments and crustal basement units during subduction and continental collision, coupled with magmatism and larger-scale mantle dynamic processes (Burov & Yamato, 2008; Doglioni et al., 2007; Faccenna et al., 2014; Gerya & Yuen, 2003). This interplay results in a large geometric variability, from double-vergent wedges to highly-curved orogens associated with the formation of large-scale extensional back-arcs or wide orogenic plateaus affected by regional magmatism (Beaumont et al., 2000; Heuret & Lallemand, 2005; Molnar et al., 1993; Sengör et al., 2008; Willett et al., 1993). Among this variety of mountain chains, observation studies have shown that deformation during collision may accrete lower continental plate material by a gradual migration of deformation and associated exhumation towards orogenic forelands (e.g., Forte et al., 2014; Matenco et al., 2010). Modelling studies have inferred that this sequence of deformation and exhumation is rheologically controlled. For instance, a rheological weak lower plate decouples from the upper crust, creating prolonged periods of continental subduction and orogens that display one dominant structural vergence (Vogt et al., 2017a, 2017b; Willingshofer et al., 2013). Many such single-sided orogens are associated with periods of rapid slab retreat, where back-arc extension often overprints the pre-dating nappe stacking during their gradual migration of deformation towards the foreland, as observed in many Mediterranean orogens or SE-Asia convergence zones (Brun & Faccenna, 2008; Faccenna et al., 2013; Jolivet & Brun, 2010; Pubellier & Morley, 2014). This extensional overprint makes it difficult to understand the mechanics of continental collision in these foreland accretion orogens, as well as its relationships with back-arc extension, slab retreat and exhumation.

One interesting exception of such single-sided orogens are the Dinarides system of Central Europe (Figure 2.1a), which are less affected by the frequent large-scale extensional overprint observed in orogenic areas such as the Aegean or the Apennines system (Jolivet & Faccenna, 2000; Jolivet et al., 2013). The Dinarides orogen mainly formed during the Jurassic-Eocene convergence between Europe- and Adriatic- derived units, associated with gradual subduction and continental collision (e.g., Schmid et al., 2008). The NE-vergent nappe system observed in European-derived units (Figure 2.1b) formed due to the Cretaceous closure of one other ocean, Ceahlau-Severin, which was located more to the north and formed the orogenic structure of the Carpathians and Balkan Mountains (e.g., Iancu et al., 2005; Schmid et al., 2008). A number of recent studies have demonstrated an interplay between contraction and a period of Late Oligocene - Miocene extension that affected the internal part of the Dinarides and their contact with the Carpathian units (Andrić et al., 2017; Erak et al., 2017; Matenco & Radivojević, 2012; Stojadinović et al., 2017; Ustaszewski et al., 2010). Shortening resumed during the late Miocene and is still active at present in the external part of the Dinarides. This is interpreted to be an effect of the Adriatic plate indentation, associated with the subduction of a slab remnant observed in the external-most part of the orogen (e.g., Bennett et al., 2008 and references therein). The internal part of the Dinarides and their contact with the European-derived upper plate along the Sava Zone have recently benefitted from a number of detailed kinematic analyses (Erak et al., 2017; Ilić & Neubauer, 2005; Ilić et al., 2005; Mladenović et al., 2015;

Schefer, 2010; Schefer et al., 2011; Stojadinović et al., 2013; Stojadinović et al., 2017; Toljić et al., 2013; Ustaszewski et al., 2010; van Gelder et al., 2015).

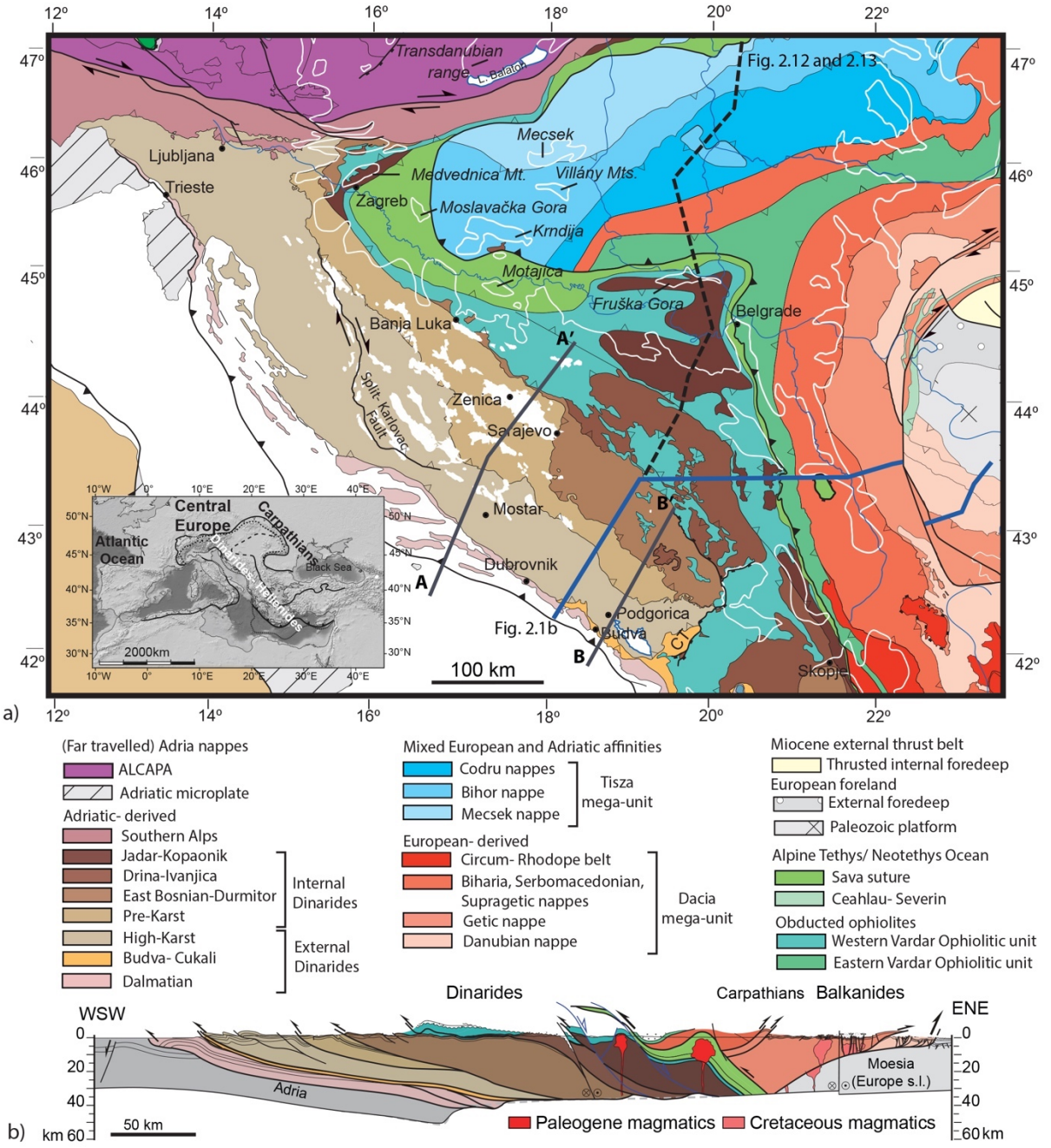


Figure 2.1 a) Tectonic map of the Dinarides and their junction with the Alps and the Albanides in the SE Europe (location in the lower left inset, modified from Schmid et al., 2008). White line is the outline of the Miocene Pannonian Basin and the white zones are the location of the Miocene Dinarides Lake System (DLS), (after Harzhauser & Mandic, 2008; de Leeuw et al., 2012). Thick blue line is the location of the cross-section in Figure 2.1b. Grey lines are the locations of the crustal-scale cross-sections of Figure 2.11. The black dashed line is the location of the reconstruction displayed in Figures 2.12 and 2.13. CT= Cukali tectonic half-window; b) Regional crustal cross-section illustrating the main tectonic units and deformation along a Dinarides–Carpathians transect (modified from Matenco & Radivojević, 2012). The location of the cross-section is displayed by the thick blue line in Figure 2.1a.

In contrast, there are no regional kinematic studies available in the central and south-eastern part of the Dinarides, a critical area for understanding the evolution of the collision system and the associated subducted slab (e.g., Bennett et al., 2008; Šumanovac et al., 2017). Therefore, in order to understand the regional Dinarides deformation and evolution, we have performed a kinematic study that was focused in this critical area (Figures 2.1 and 2.2, Dalmatian, Budva, High–Karst, Pre–Karst units and their contact with the overlying East Bosnian–Durmitor unit along the Bosnian Flysch zone).

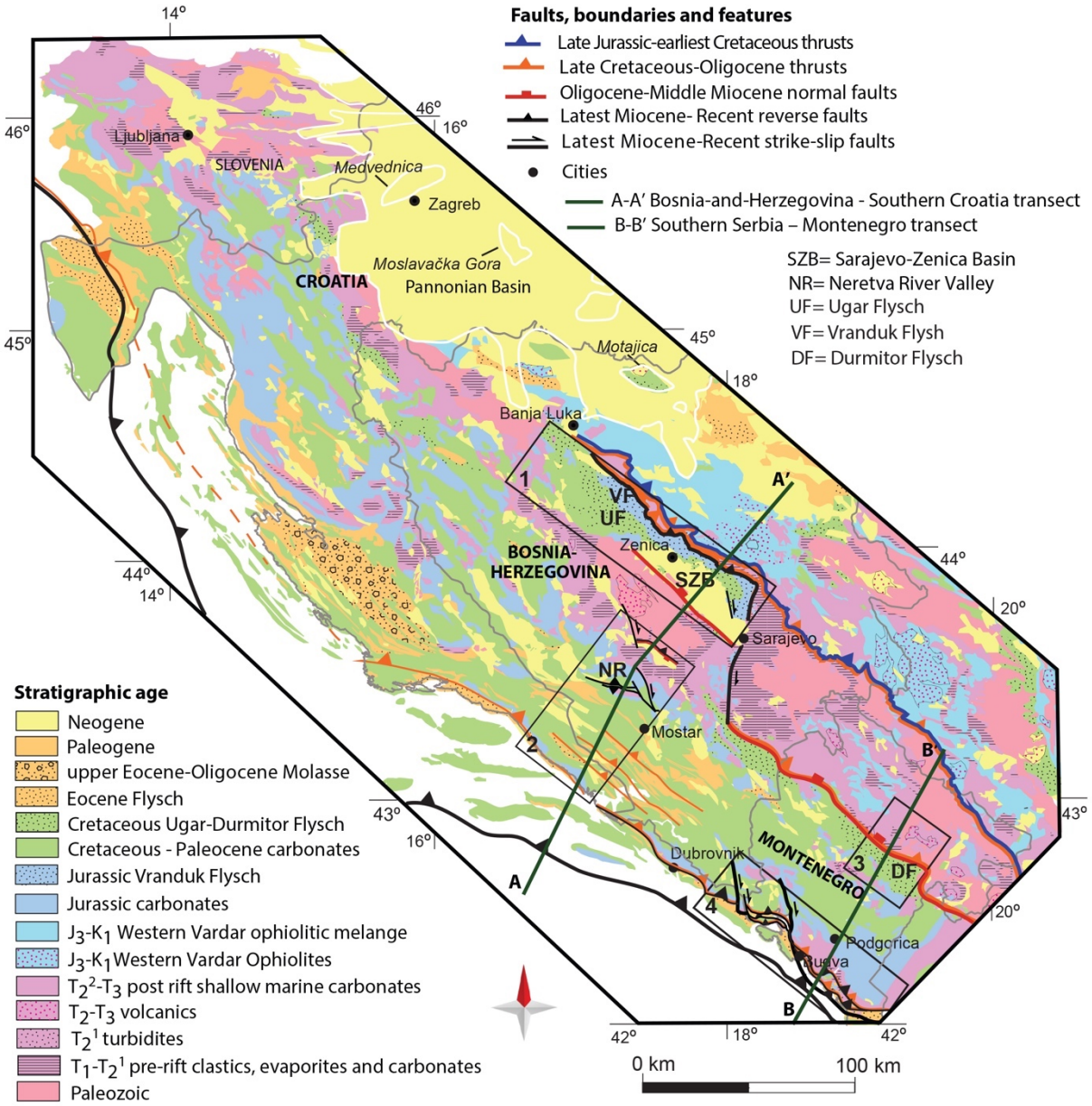


Figure 2.2 Geological map of the Dinarides compiled and simplified from the sheets of the 1:100.000 geological map of former Yugoslavia (Osnovna Geološka Karta SFRJ), with the locations of the four focus areas (black rectangles) and the two main crustal-scale transects investigated in this study. Note that outside the main tectonic contacts (slightly modified when compared with Figure 2.1a) and focus areas, lower amounts of deformation are observed elsewhere. $K_1$= Early Cretaceous, $J_3$= Late Jurassic, $T_3$= Late Triassic, $T_2^2$= late Middle Triassic, $T_2^1$= early Middle Triassic, $T_2$= Middle Triassic, $T_1$= Early Triassic.

Given the known shortening variability along the strike of the orogen, we have constructed two regional orogenic cross-sections in Bosnia and Herzegovina – Croatia and Serbia – Montenegro, respectively (Figure 2.2). In order to understand the superposition and localization of deformation, these cross-sections are constrained by higher resolution field kinematic studies in areas that retained larger amounts of shortening or extensional deformation (Figure 2.2). The overall kinematic data is combined with previous studies (e.g. Balazs et al., 2017; Šumanovac et al., 2017) to create larger orogenic transects, which were interpreted in the overall crustal and lithospheric context of the Dinarides. We specifically note that our kinematic observations were not aimed at characterizing the entire deformation of the studied Dinarides, which is otherwise not possible in one study for such a large area. Outside the Miocene basins, which provided critical timing constraints for our kinematic data, we focused our observations in understanding the kinematics of highly deformed areas. These areas are known to have localized deformation and created large-offset structures, which are important to derive the succession of orogenic deformation. Following the regional characterization of deformation, we focused our study in understanding the relationship between orogenic build-up and the evolution of the retreating slab in the Dinarides.

## 2.2 Regional Dinarides background

The Dinarides are part of the Mediterranean orogenic system that formed during Mesozoic–Cenozoic times in response to the closure of a northern branch of the Neotethys Ocean located between Europe- and Adria- derived continental units (Kreemer et al., 2003; Stampfli & Borel, 2002). The Middle Triassic opening of this ocean was associated with rift-related intermediate and basic magmatism and was followed by the formation of a wide Adriatic passive continental margin (Figure 2.3, Dimitrijević, 1997; Pamić, 1984). The distal part of this margin has recorded a gradual Middle Triassic–Late Jurassic deepening in depositional environment, changing from shallow water carbonates to deep water radiolarites and pelagic sediments (Djerić et al., 2007; Djerić & Gerzina, 2008; Goričan et al., 1999; Schefer et al., 2010; Toljić et al., 2013; van Gelder et al., 2015). In contrast, the proximal part of this passive continental margin (i.e. the external part of the Dinarides) recorded a ~2.2 km thick, shallow water carbonate sedimentation during Middle Triassic-Eocene, part of the larger Adriatic carbonate platform system (Figure 2.3, Dimitrijević, 1997; Vlahovic et al., 2005). The exception is the formation of a Middle Triassic extensional (graben) structure in the external part of the Dinarides. This graben was gradually filled with Mesozoic deep-water carbonate and more pelagic sediments and was subsequently inverted, being presently exposed in the Budva thrusted unit of Southern Montenegro (Figures 2.2 and 2.3, Cadjenović et al., 2008; Crne et al., 2011; Goričan, 1994).

Starting with Middle Jurassic times, oceanic subduction took place in the Dinarides, which was followed by the obduction over the Dinarides passive continental margin of an up to ~180 km wide sheet of ophiolites and the formation of a genetically related ophiolitic mélange during Late Jurassic-earliest Cretaceous times (the Western Vardar Ophiolitic unit, Figures 2.1, 2.2 and 2.3, Chiari et al., 2011; Robertson et al., 2009; Schmid et al., 2008; Ustaszewski et al., 2009).

Figure 2.3 Correlation of lithostratigraphic columns across various tectonic units along the two studied transects: a) Bosnia and Herzegovina – Southern Croatia transect, b) Serbia – Montenegro transect. Abbreviations (from Pz to Plio) are standard stratigraphic periods of the Paleozoic, Mesozoic and Cenozoic eras. Subscript numbers are stratigraphic epoch during

*Figure 2.3 (continued)* periods. Superscript numbers are chronostratigraphic stages during epochs. The Variscan basement is generally overlain by Permian–Lower Triassic continental deposits with thin evaporitic intercalations. The evaporites have higher thicknesses only in the external parts of the High-Karst and more external areas in the Bosnian - Croatian profile. 2-3 km thick, generally shallow water upper Lower Triassic–Paleocene carbonates, were deposited in the external parts of the Dinarides nappes. Note the gradual deepening of depositional environment towards more internal units, where deep water carbonates, clastics and pelagic sediments were deposited along the former passive continental margin. Ages: Plio= Pliocene–Pleistocene, M= Miocene, Ec= Eocene, Ol= Oligocene, K-Pg= Cretaceous–Paleocene, $K_2$= Upper Cretaceous, K= Cretaceous, J= Jurassic, $J_3$= Upper Jurassic, $J_2$= Middle Jurassic, $J_1$= Lower Jurassic, $T_3$= Upper Triassic, $T_2^2$= upper Middle Triassic, $T_2^1$= lower Middle Triassic, $T_1^2$= upper Lower Triassic, $T_1^1$= lower Lower Triassic, $T_1$= Lower Triassic, P-$T_1$= Permo–Triassic, P= Permian and Pz= metamorphosed Paleozoic.

This was followed by the late Early Cretaceous formation of an unconformity well observed in the internal parts of the Dinarides (Figure 2.3b), which is likely associated with localized thrusting and metamorphism, possibly as an effect of a continuation of the obduction-related shortening (Dimitrijević, 1997; Ilić & Neubauer, 2005; Ilić et al., 2005; Schmid et al., 2008). Oceanic subduction subsequently continued, while the onset of continental collision between the Adria- and European- derived continental units took place during the latest Cretaceous, which resulted in the formation of the Sava zone as the suture of the Neotethys Ocean (Schmid et al., 2008). This suture separates the Adriatic-derived Dinarides from the European-derived Serbomacedonian and Tisza units in the orogenic upper plate (Pamić, 2002; Ustaszewski et al., 2009; Ustaszewski et al., 2010). The onset of collision was associated with the thick deposition of syn-contractional Campanian–Maastrichtian turbidites in a deep-water environment, which localized deformation during nappe stacking (Figure 2.3, Dimitrijević & Dimitrijević, 1987; Toljić et al., 2018). The collision continued during Paleogene times and was associated with an overall migration of the NE-SW oriented shortening towards more external areas of the Dinarides (Figures 2.1, 2.2 and 2.3, Aubouin et al., 1970; Dimitrijević, 2001; Ustaszewski et al., 2010). The peak Eocene-Oligocene shortening in the External Dinarides created SW–ward thrusting and was associated with the deposition of Eocene turbidites and a late Eocene–Oligocene coarse conglomeratic regressive molasse sequence (the Promina Beds) deposited near thrust contacts (Figure 2.3, Mrinjek, 1993; Zupanič & Babić, 2011). Shortening during this period was also recorded in more internal units and near the Sava zone (Stojadinović et al., 2017; Ustaszewski et al., 2010). Among all syn-contractional turbidites observed in the Dinarides, the thickest deposition is observed in the Bosnian Flysch zone (Figure 2.2). This zone is located in the footwall of more internal units carrying obducted ophiolites in an upper structural position in the Dinarides or in the footwall of the Southern Alps thrusting (Figure 2.1, Dimitrijević, 1997; Goričan et al., 2012; Hrvatović & Pamić, 2005; Tari, 2002). The deposition of these turbidites started during the Kimmeridgian (the Vranduk Flysch, Figure 2.3), and continued during Cretaceous times, with thickest deposition being recorded during the latest Cretaceous (Maastrichtian, the Ugar–Durmitor Flysch, Figure 2.3). The Bosnian Flysch deposition was interrupted by local unconformities (Dimitrijević, 1997; Hrvatović & Pamić, 2005; Hrvatović, 2006; Mikes et al., 2008; Schmid et al., 2008), which may suggest several pulses of thrusting of the overlying East Bosnian – Durmitor unit.

The Late Oligocene - Miocene extension has affected the internal part of the Dinarides and their contact with the Carpathians. Generally, this extension was thought to be at least partly related to the formation of the Pannonian Basin back-arc that started at ~20 Ma during the roll-back of the Carpathian and Dinarides slabs (Figure 2.2, Horváth et al., 2015; Matenco & Radivojević, 2012). This extension has created large-scale detachments and other listric normal faults along the entire length of the Sava zone and other Dinarides nappe contacts, previously documented to have reached as far to the foreland as the Sarajevo–Zenica Basin (Figure 2.2, Andrić et al., 2017; Erak et al., 2017; Stojadinovic et al., 2013; Toljić et al., 2013; Ustaszewski et al., 2010; van Gelder et al., 2015). Outside the Pannonian Basin, the extension was partly coeval with the creation of the Dinarides Lake System, a group of Miocene intra-montane basins that recorded lacustrine endemic fauna and endorheic sedimentation (Figures 2.2 and 2.3, Harzhauser & Mandic, 2008; Mandic et al., 2012). Among all basins, the largest observed is the Oligocene–Miocene Sarajevo–Zenica Basin (Figure 2.2). This basin started its evolution with Oligocene–Early Miocene continental to shallow-water lacustrine foreland flexural deposition over the Bosnian Flysch in the footwall of the East Bosnian–Durmitor thrusting (Figure 2.3a) and was affected by a large-scale asymmetric extension leading to the deposition of ~ 2 km of middle–upper Miocene continental alluvial to deltaic sediments (Figure 2.3a, Andrić et al., 2017; Hrvatović, 2006).

The extension was followed by an overall inversion that started somewhere in the late Miocene and is presently active. This deformation took place in response to a general indentation and counterclockwise rotation of the Adriatic microplate, which has been documented from present-day crustal stress patterns, GPS velocities and paleomagnetic studies (e.g., D'Agostino et al., 2008; Grenerczy et al., 2005; Handy et al., 2010; Heidbach et al., 2016; Márton et al., 2003; Pinter et al., 2005; Ustaszewski et al., 2014; Weber et al., 2010). These studies indicate that the present Adria kinematics is related to ~N-ward indentation in the NW Dinarides near the contact with the Southern Alps, while this indentation is oriented towards the NE in the central and SE part of this orogen, which agrees with the overall counterclockwise rotation of Adria (see also Vrabec, 2006). However, no significant rotation took place in the thrusted Dinarides units during post- Eocene times (de Leeuw et al., 2012), which would point to a decoupling between the kinematics of Adria and the one of the Dinarides during the presently active continental subduction. The geometry of this subduction is observed by the high-velocity mantle anomaly located beneath the External Dinarides of Montenegro (e.g., Bennett et al., 2008). To the NW, the presence of such a subducted slab is debated, although recent studies have envisaged a large scale high-velocity anomaly along the entire external part of the Dinarides (Šumanovac & Dudjak, 2016; Šumanovac et al., 2017; Ustaszewski et al., 2008) that may continue beneath the Eastern Alps (Lippitsch et al., 2003; Kissling et al., 2006).

## 2.3 Methodology

In order to understand the deformation in the external part of the Dinarides, we have first performed an outcrop kinematic study. Most of the structures measured are brittle, such as faults with kinematic senses of shear, folds, joints or larger cataclastic-shear zones. Shear-sense criteria used are: slickensides, Riedel shears, tension gashes, drag folds and, in rheological weak or poorly consolidated sediments and fault gouges, brittle shear bands. Structures were subsequently plotted on stereograms, with joints, faults and shear zones as planes, and kinematic senses of shear, folds and associated hinges as points. Timing indicators were derived from superposition criteria, such as cross-cutting faults or reactivated fault planes, tilted fault planes, re-folded geometries, and from stratigraphic constraints. Deformation of Miocene sediments have provided critical timing constraints used to derive the relationship between the pre-Miocene shortening from the subsequent Miocene extension and late Miocene–Recent inversion. These constraints have been used to derive a relative chronology of deformation events, which was further interpreted in a regional context.

Since the area is unusually large for one kinematic study, we focussed and restricted our structural analysis only to define the kinematics of the main faults or shear zones observed along two main structural transects, one in central-eastern Bosnia and Herzegovina – Southern Croatia, and one other in Southern Serbia – Montenegro (Figure 2.2). Such faults and shear zones were identified to have significant stratigraphic offset in map view and observed in the field to be associated with shear zones or faults with large (hundreds of metres to kilometres) displacements, aided by the exceptional good quality and full coverage of the 1:100.000 scale geological maps available (OGK Former Yugoslavia). We specifically note that most of our measurements are taken in such major shear zones along the chosen transects, characterized often by the development of wide fault gouge foliations or high density of faults having the same kinematics in a narrow deformation zone.

In a first stage, the measured kinematic structures at outcrop-scale were grouped at local scale by calculating paleostress directions for the same deformation event (Figures 2.4, 2.6, 2.8 and 2.9, see also the supporting information). The measured kinematic structures were plotted in the Win-Tensor software (Delvaux & Sperner, 2003) for each deformation event separately, by using a combination of PBT (Turner, 1953) and direct inversion methods (Angelier, 1984), accounting for confidence criteria (Sperner & Zweigel, 2010). The analysis has demonstrated that only paleostress is not suitable for defining regional tectonic phases. This is due to large amounts of strain partitioning observed near and at large distance from large-offset structures during the same deformation event (e.g., coeval strike-slip faulting and thrusting), or because of large amounts of vertical axis rotation that took place during deformation or subsequent tectonic events. Such limitations of the paleostress methodology are otherwise widely known (see also Lacombe, 2012). Therefore, we have followed one other methodology (e.g., Andrić et al., 2017; van Gelder et al., 2015), where the observed deformation was described by defining directions of regional tectonic transport along main observed structures in map and cross-sections scale (i.e. by performing a strain analysis). The differentiation between stress calculations (compression-tension) and strain observations (contraction-extension) is subsequently used in the description of deformation events.

This approach also means that our study does not utilize the typical paleostress approach where all faults are measured in specific restricted areas where the paleostress field is calculated, but we specifically targeted and measured the kinematics of large offset faults along the chosen transects, while the typical statistical definition of a succession of paleostress fields remains less relevant. This type of kinematic approach is better suited for the large size of our study area, when compared with the typical local stations paleostress approach measuring all faults that create stress patterns often difficult to connect at regional scale. This is also justified by the previous observation that the overall deformation in the Dinarides is generally focused at or near the main tectonic contacts that localized the strain in weakness zones and allowed the formation of large-offset thrusts or normal faults, an observation confirmed by our structural analysis. These larger amounts of deformation are observed in particular in the Bosnian Flysch zone and the Budva unit of Montenegro, which were the main focus areas of our study (areas 1, 3 and 4 in Figure 2.2). Furthermore, the balance between shortening and intervening extension was studied in one other focus area, where the latter displays larger offsets, i.e. the Herzegovina lower Neretva River Valley (area 2 in Figure 2.2). Our results and previous studies were integrated in these two onshore crustal profiles, the Southern Serbia–Montenegro profile being prolonged offshore over the frontal thrusting over the Adriatic unit by using previously published cross-sections and our own reflection seismic interpretations (Bega, 2015; see also Chapter 4). Given the lack of other reflection seismic data, our depth projections were combined with other available information of crustal thickness or potential fields, such as gravity maps (Marović et al., 2002; Šumanovac, 2010). Therefore, the deep part of the crustal profiles is fairly speculative and has to be viewed qualitatively. Kinematic and superposition criteria were used to extrapolate deformation to depth and to define the relative timing of deformation, which has subsequently been used to conceptually restore the crustal profiles. In order to discuss the results in the larger scale context of the subduction zone evolution, the crustal profiles were extrapolated at lithospheric-scale by using available mantle constraints derived from teleseismic tomography (Artemieva et al., 2006; Balazs et al., 2017; Bennett et al., 2008; Piromallo & Morelli, 2003; Šumanovac et al., 2017).

## 2.4 Kinematic analyses in focus areas

### 2.4.1 The Bosnian Flysch zone near the Sarajevo–Zenica Basin

The Bosnian Flysch zone is mostly exposed north of the Sarajevo–Zenica Basin (Figure 2.4a). This zone is characterized by intense deformation as a result of multiple phases of folding, thrusting, strike-slip faulting and normal faulting, associated with strata generally being tilted to steep sub-vertical positions.

The first deformation event observed in this area is characterized by the formation of thrusts, and isoclinal and décollement folds (Figures 2.4b and 2.5a,b). These structures are strongly overprinted by all subsequent deformation events. The few fold hinges and thrusts we were able to document are NE-SW oriented and indicate an overall NW–SE oriented contraction direction (Figure 2.4b). One can derive an associated NW-SE oriented compressional stress field, but the number of measurements is too low to be regionally significant. Décollement and isoclinal drag folding can be associated with layer-parallel shearing and low-angle thrusting (Figure 2.5b).

No large-offset structures that may be significant at regional scale could be associated with this deformation event.

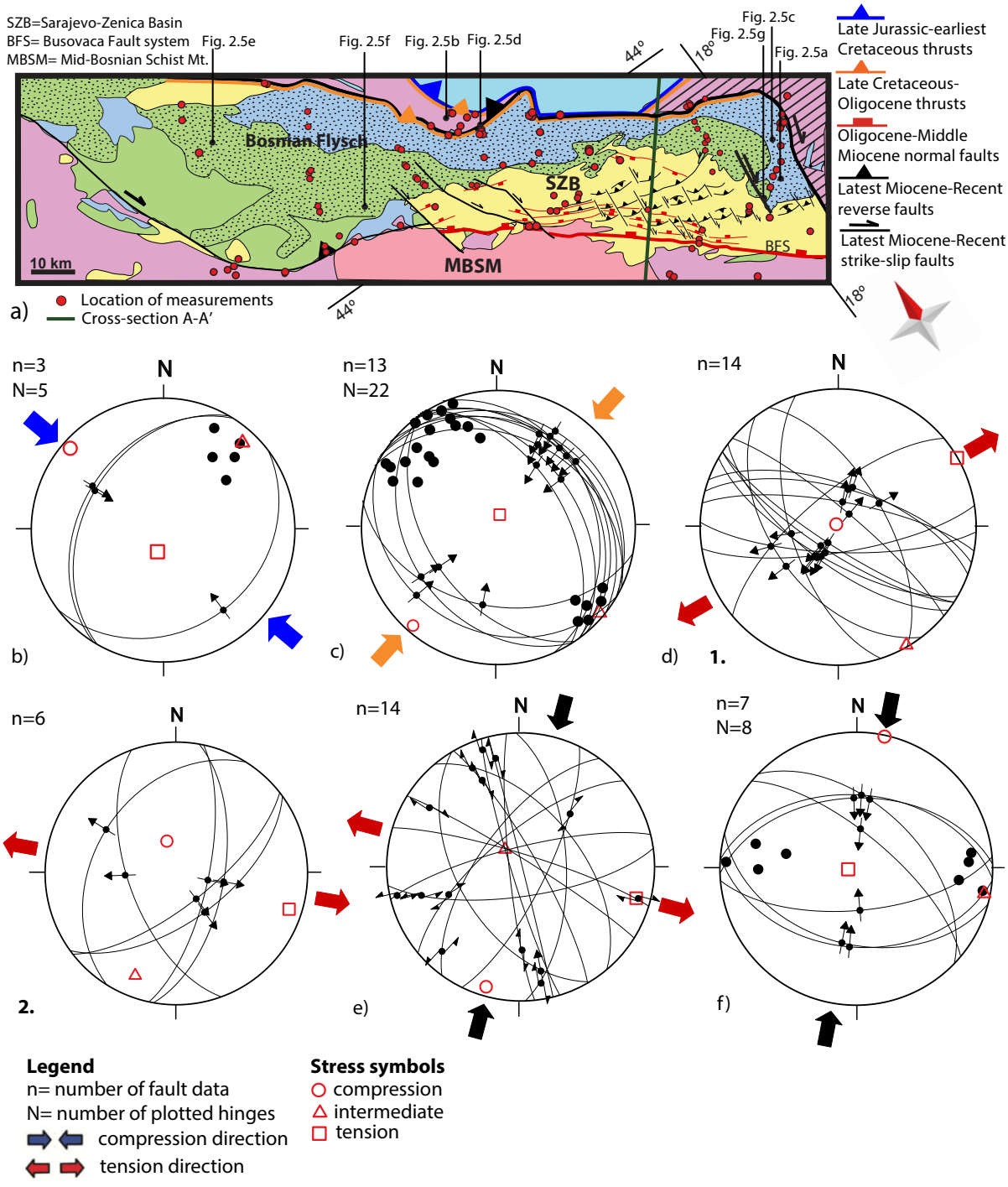


Figure 2.4 Kinematic data grouped per deformational event in the first focus area, the Bosnian Flysch zone and the Sarajevo-Zenica Basin. These data correspond to the NE part of cross-section A-A' (Figure 2.11a). The data is plotted in Schmidt stereoplots, lower hemisphere projection. Lines with arrow symbols are projections of fault planes with kinematic sense of shear. Thick black dots are projections of fold hinges. Colors of the maximum and minimum stress directions, symbolized by arrows next to stereoplots, indicates the deformation event corresponding to the same color of map structures. a) Geological and structural map of the Bosnian Flysch zone and the Sarajevo-Zenica Basin, where faults are color coded according to

*Figure 2.4 (continued)* deformation events (compiled and simplified from sheets of the 1:100.000 geological map of former Yugoslavia, Osnovna Geološka Karta SFRJ). The same legend for the stratigraphic age applies as in Figure 2.2. The location of the map is given in Figure 2.2 (rectangle 1); b) Stereoplot showing the faults and folds associated with the Late Jurassic – earliest Cretaceous contractional event; c) Stereoplot showing the faults and folds associated with the latest Cretaceous-Oligocene contractional event; d) Stereoplots showing faults associated with the Miocene extensional event: 1 – normal faults characterizing a stress field with a NE-SW direction of tension, 2 – normal faults characterizing a stress field with a WNW-ESE direction of tension; e) Stereoplot showing strike-slip faults associated with the inversion starting during late Miocene times; f) Stereoplot showing reverse faults and folds associated with the inversion starting during late Miocene times.

The folds from the first deformation event are re-folded by a second generation of asymmetric folds with NW–SE oriented hinges indicating a NE-SW oriented contraction direction (Figures 2.4c and 2.5c), often associated with hinge collapse structures between more competent layers (Figure 2.5d). These folds are centimetres to tens of metres scale in outcrops and form the main bulk of structures observed in the field. The folds are genetically associated with NW–SE oriented thrusts (Figure 2.4c), with larger offset SW-vergent thrusts and smaller offset NE-vergent thrusts. The overall stress field was characterized by a NE-SW oriented compression direction. The relationship between thrusts and asymmetric folds is visible in footwalls, where folds often form asymmetric drag folds or the overturned flank is truncated by thrust faults in a break-thrust folding mechanism (sensu Fischer et al., 1992). Fault-bend fold structures were observed in more competent strata, locally associated with syn-kinematic deposition in uppermost Cretaceous strata (Figure 2.5e). This is an important timing indicator, which demonstrates a latest Cretaceous age of deformation.

The NW–SE oriented thrusts and asymmetric folds are truncated by younger normal faults (Figure 2.4d). A typical situation is when normal faulting truncates imbricated thrust fans, formed by layer-parallel shear in fine sediments (Figure 2.5f). The normal faults are generally high-angle to listric and show little to no tilting by subsequent deformation. The orientations of these normal faults are quite widespread (Figure 2.4d), but is in general agreement with the identification of two directions of tension in the reconstructed stress fields, NE–SW (Figure 2.4d-1) and WNW-ESE (Figure 2.4d-2). Similar directions of extension were previously documented in the much larger dataset measured in the sediments of the adjacent Sarajevo–Zenica Basin, controlled by the large-scale Busovača fault system associated with syn-kinematic lower-middle Miocene sedimentation (Andrić et al., 2017; Hrvatović, 2006).

The last deformation event observed in the Bosnian Flysch is characterized by frequent large-offset NW–SE to NNW-SSE oriented dextral, and more rare and lower offset NE–SW to ENE-WSW oriented sinistral strike-slip faults (Figure 2.4e). These faults define a stress field with NNE-SSW oriented compression and WNW-ESE oriented tension. In the field, strike-slip faults are associated with E–W to (W)NW-(E)SE oriented high-angle reverse faults combined with drag and upright folds, which define a stress field with a NNE-SSW oriented compression direction (Figure 2.4f).

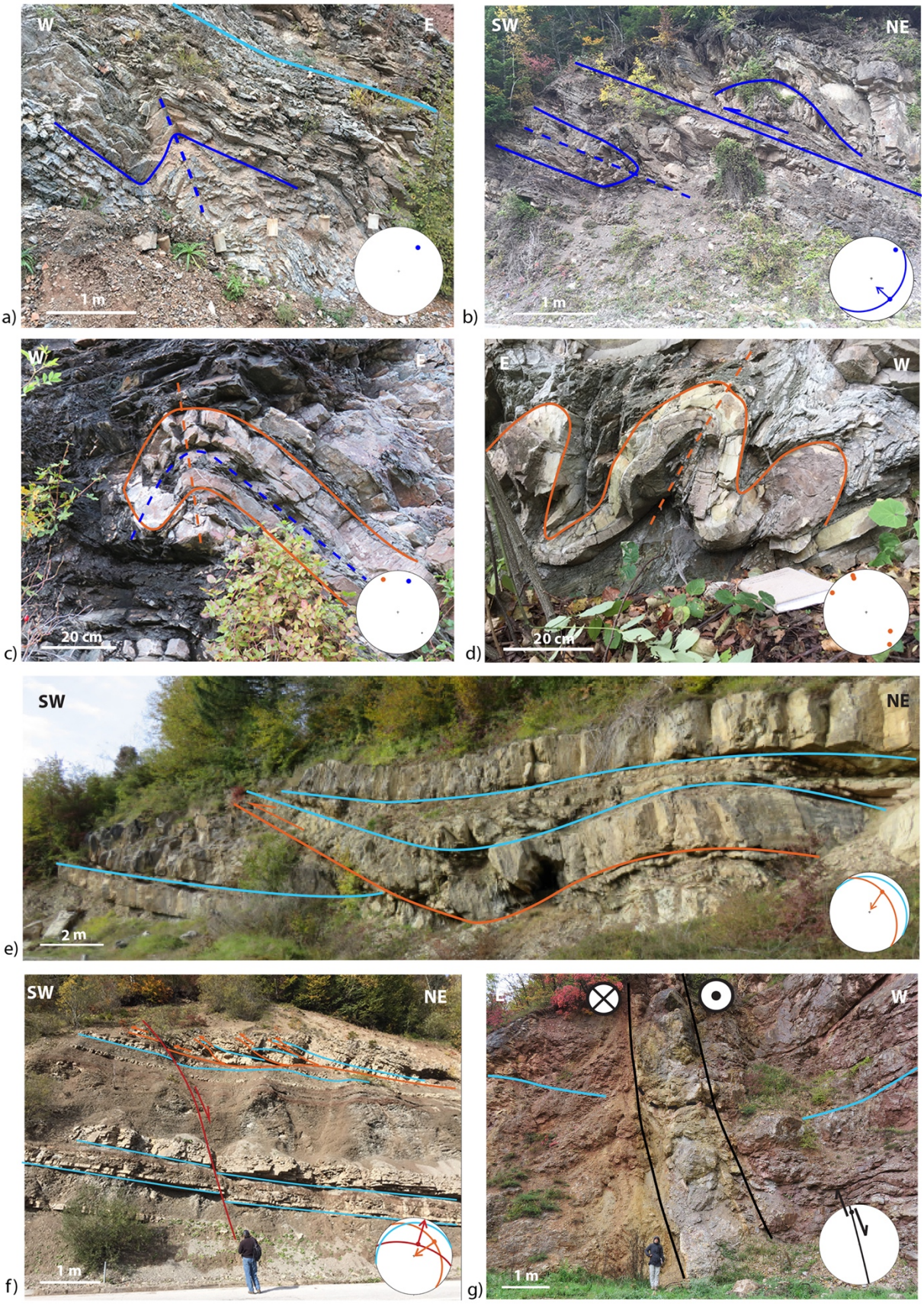


Figure 2.5 Interpreted field photos illustrating structures and their kinematics in the Bosnian Flysch Zone and the Sarajevo–Zenica Basin. Location of the field photos are displayed in Figure 2.4a. Colors of the lines and symbols, indicates the age of the deformation event corresponding to the same color of map structures Dark blue: Late Jurassic–earliest Cretaceous,

*Figure 2.5 (continued)* orange: latest Cretaceous–Oligocene, red: Early–Middle Miocene, black: late Miocene–Recent, light blue: bedding plane. a) An asymmetric fold with a NE-oriented hinge; b) A NW-verging low-angle thrust associated with décollement and isoclinal drag folds with NE-oriented hinges; c) An isoclinal fold with a NE-oriented hinge is refolded by a younger asymmetric fold with a NW-oriented hinge; d) Asymmetric folding associated with NW–SE oriented hinges and hinge collapse structures; e) A fault-bend fold structure with a SW-vergence, associated with syn-kinematic deposition; f) A high-angle NNE-verging normal fault truncates an imbricated SW-vergent thrust fan; g) A large-offset NNW–SSE oriented dextral strike-slip shear zone.

Among all, a spectacular large-offset NNW–SSE oriented strike-slip shear zone is observed at the eastern termination of the Sarajevo–Zenica Basin (Figure 2.5g), which likely accommodated 10-20 km of dextral offset, indicated by the change in strike of the East Bosnian–Durmitor unit and Bosnian Flysch strata (Figures 2.4a). Furthermore, reactivation of the NW-SE oriented East Bosnian–Durmitor thrusting contact resulted in the formation of S-vergent high-angle reverse faults. These faults placed, or locally repeated, the Triassic strata of the East Bosnian – Durmitor units over the Jurassic strata of the Vranduk Bosnian Flysch (Figure 2.4a). Both the strike-slip and reverse faults can be grouped to a deformation event characterized by NNE-SSW oriented contraction (Figures 2.4e,f).

### 2.4.2 The lower Neretva Valley area

The lower Neretva Valley area (Figure 2.6a) shows multiple phases of thrusting, strike-slip and normal faulting. The oldest structures in this area were observed in the SW, where most of the deformation is made up of NW–SE oriented, SW-vergent thrusts and NE-vergent backthrusts (Figure 2.6b). These thrusts are often quite prominent in the topography, where they usually thrust Cretaceous limestones in their hanging-wall over more distal Eocene mudstones to immature carbonate turbidites in their footwall (Figure 2.7a). These thrusts generally have offsets of less than 2 km.

On the flanks of the Konjic Basin, the NW-SE oriented thrusts are cross-cut by normal faults that are associated with syn-kinematic Miocene sedimentation inside the same basin. Similar with the Sarajevo-Zenica Basin and its flanks, the extension has two directions in the Konjic Basin and neighboring area. Larger offset normal faults are NW-SE oriented and define a stress field with a NE-SW oriented tension direction (Figure 2.6c-1), while smaller offset normal faults are NNE-SSW to NE-SW oriented and define a stress field with a (W)NW-(E)SE oriented tension direction (Figure 2.6c-2).

In the Miocene Konjic Basin and elsewhere to the south and southwest, the normal faults and pre-dating NW–SE oriented thrusts are truncated by two types of structures. A large number of strike-slip faults were observed in the field, where larger offset (W)NW–(E)SE to NNW-SSE oriented dextral transpressive faults are associated with smaller offset NNE–SSW to NE-SW oriented sinistral strike-slip faults. These faults define a stress field with a roughly N-S oriented compression and a E-W oriented tension direction (Figure 2.6d). In the Konjic Basin, these dextral faults cross-cut the earlier formed normal faults (Figure 2.7b). These normal faults are also truncated by ~E–W oriented reverse faults and similarly oriented large-offset shear zones with both N- and S-vergence, which define a stress field with a NNE-SSW oriented compression direction (Figure 2.6e).

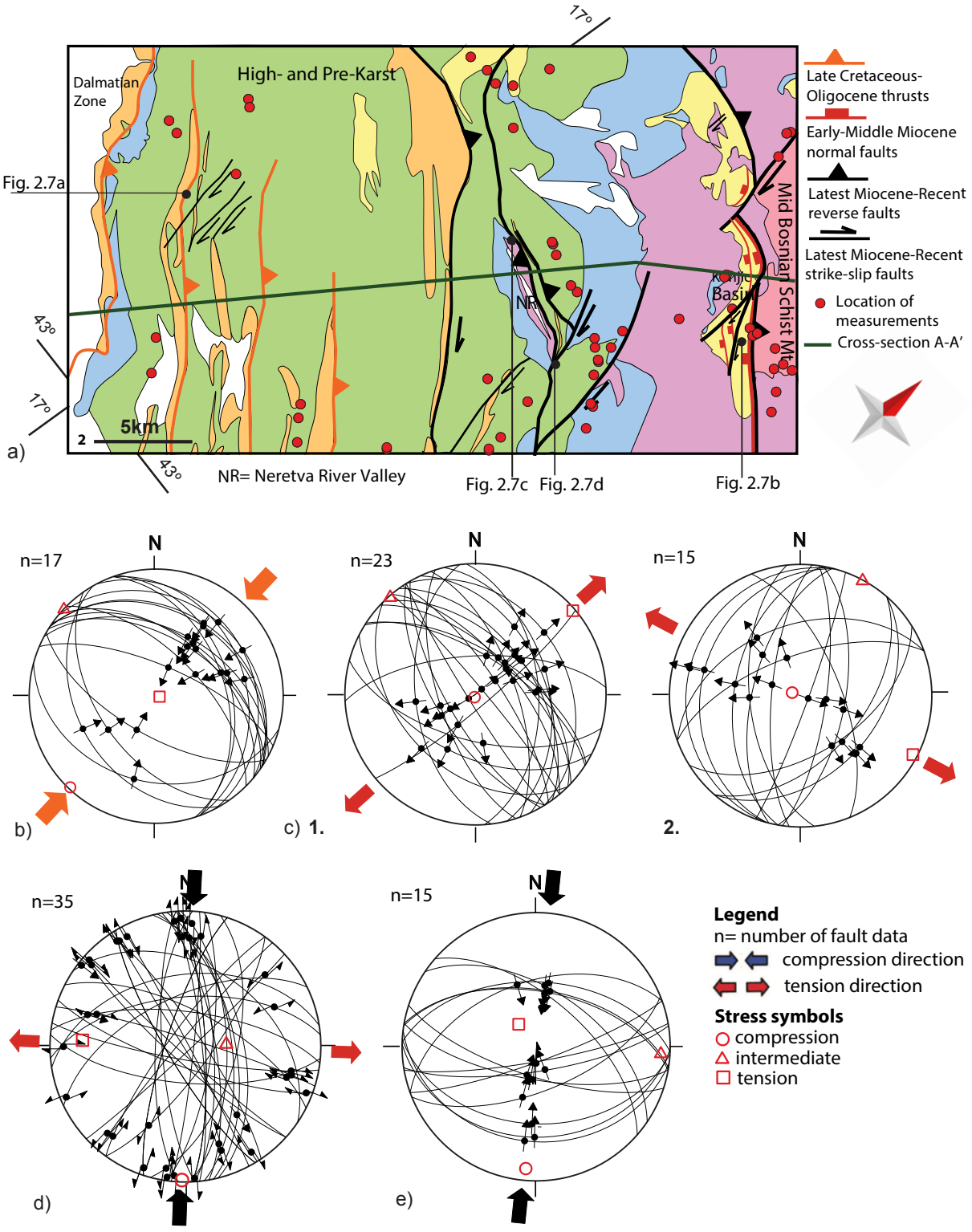


Figure 2.6 Kinematic data grouped per deformational event in the second focus area, central Bosnia and Herzegovina and Southern Croatia. These data correspond to the SW part of cross-section A-A' (Figure 2.11a). Further figure conventions as in Figure 2.4. a) Geological and structural map of central Bosnia and Herzegovina and Southern Croatia (compiled and simplified from sheets of the 1:100.000 geological map of former Yugoslavia, Osnovna Geološka Karta SFRJ). The same legend for the stratigraphic age applies as in Figure 2.2. The location of the map is given in Figure 2.2 (rectangle 2); b) Stereoplot showing the faults associated with the latest Cretaceous-Oligocene contractional event; c) Stereoplots showing

*Figure 2.6 (continued)* faults associated with the Miocene extensional event: 1 – normal faults characterizing a stress field with a NE-SW direction of tension, 2 – normal faults characterizing a stress field with a NW-SE direction of tension; d) Stereoplot showing strike-slip faults, associated with the inversion starting during late Miocene times; e) Stereoplot showing reverse faults, associated with the inversion starting during late Miocene times.

Furthermore, the (N)NW–(S)SE dextral transpressive and ~E–W oriented reverse faults connect with each other along their strike, which is also fairly obvious in map view in the NE (Figure 2.6a). The largest structure can be observed along the Neretva River Valley, where combined strike-slip and reverse faults (larger offset backthrusts and lower offset thrusts) are connected with strike-slip faults (Figures 2.7c,d). One backthrust with offset in the order of 8 km has been observed in the field (fault on the right in Figure 2.7d). Both the strike-slip and reverse faults can be grouped to a deformation event characterized by N-S to NNE-SSW oriented contraction.

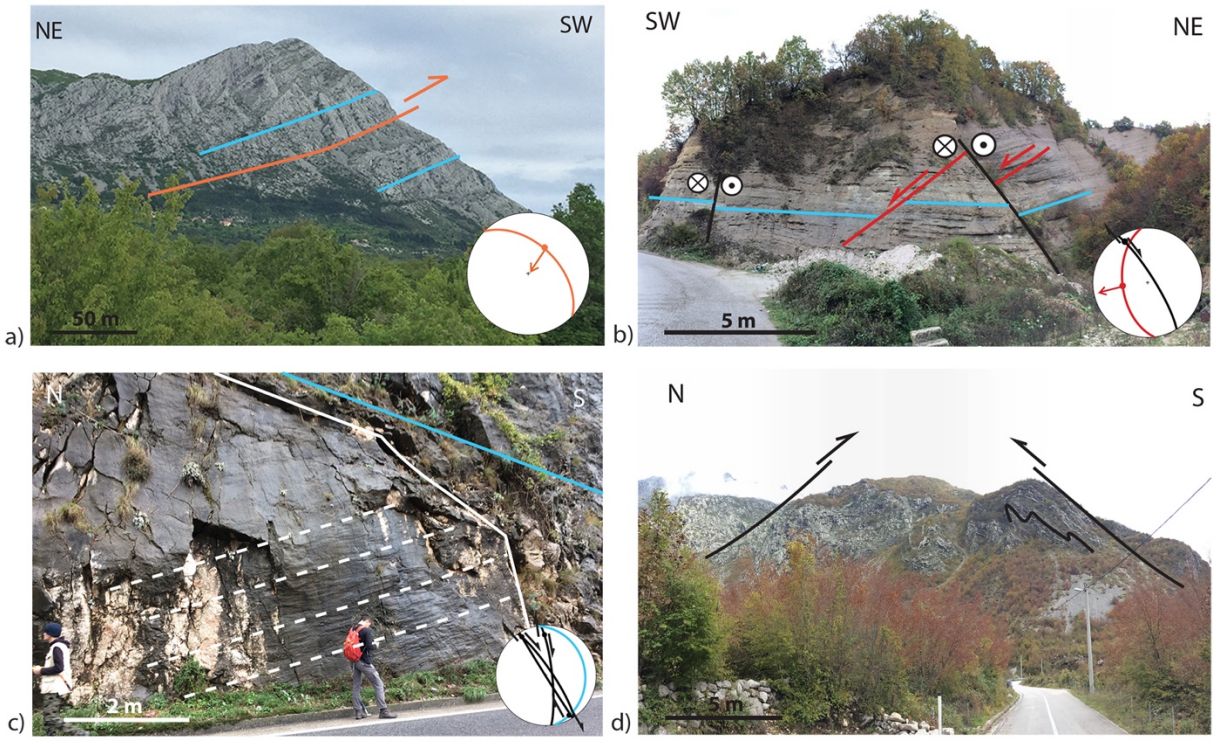


Figure 2.7 Interpreted field photos illustrating structures and their kinematics in the second focus area, central Bosnia and Herzegovina and Southern Croatia. Location of the field photos are displayed in Figure 2.6a. Further figure conventions as in Figure 2.5. a) A low angle NW–SE oriented SW-vergent thrust; b) A NW–SE oriented dextral strike-slip fault cross-cuts a Miocene WSW-verging normal fault; c) Large-offset NW-SE and NNW-SSE oriented dextral strike-slip faults; d) High-angle ~E–W oriented N- and S- verging reverse faults associated with tight asymmetric folding.

### 2.4.3 The Durmitor Flysch of Montenegro

Only few observations have been done in the Bosnian Flysch zone exposed in Montenegro, i.e. the Durmitor Flysch in the footwall of the East Bosnian–Durmitor thrusting (Figure 2.8a).

These observations are in general agreement with the larger data set available in previous studies (Dohmen, 2012), which are plotted for comparison in Figure 2.8c.

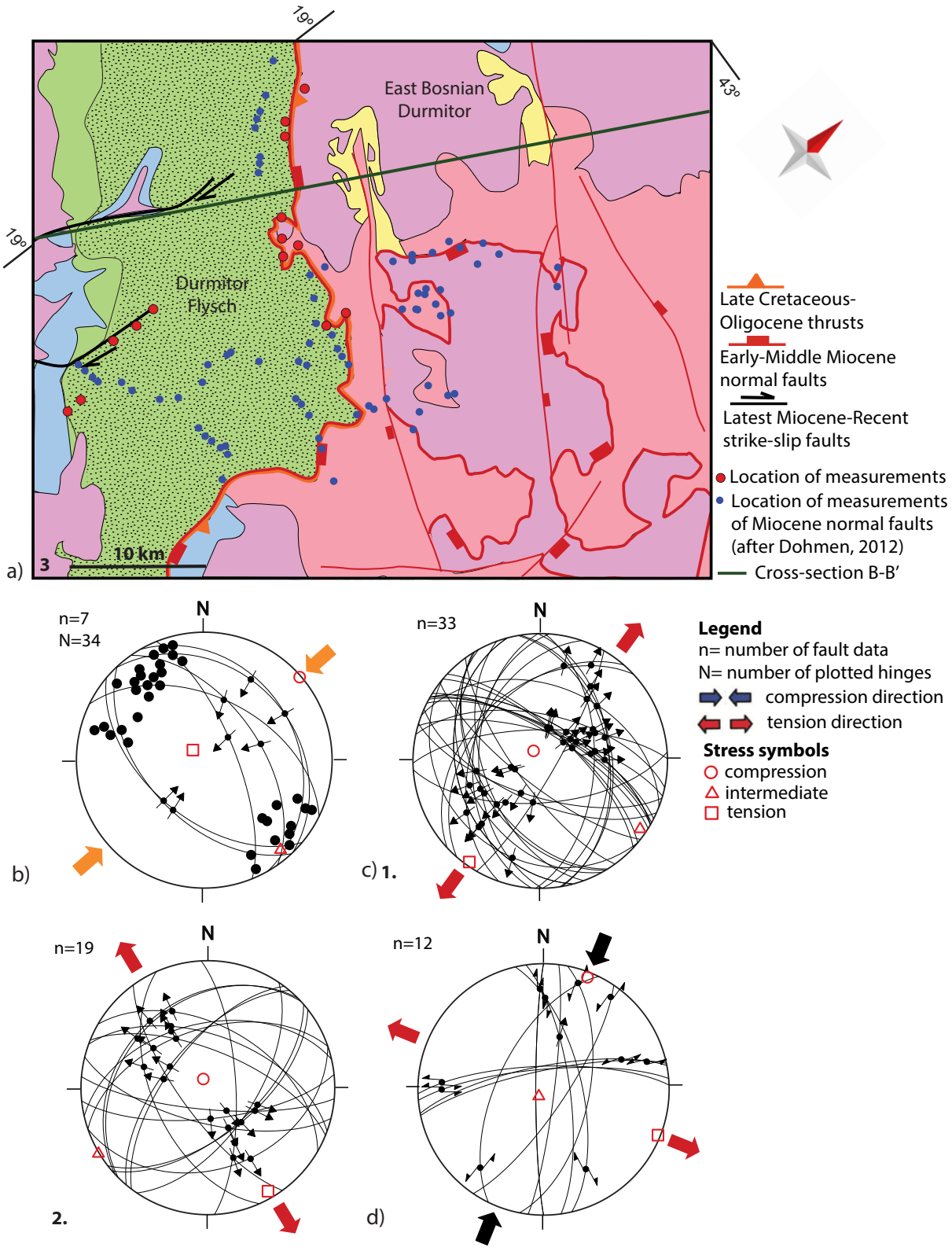


Figure 2.8 Kinematic data grouped per deformational event in the third focus area, the Durmitor Flysch zone of Montenegro. These data correspond to the NE part of cross-section B-B' (Figure 2.11b). Further figure conventions as in Figure 2.4. a) Geological and structural map of the

*Figure 2.8 (continued)* Durmitor Flysch zone of Montenegro (compiled and simplified from sheets of the 1:100.000 geological map of former Yugoslavia, Osnovna Geološka Karta SFRJ). The same legend for the stratigraphic age applies as in Figure 2.2. The location of the map is given in Figure 2.2 (rectangle 3); b) Stereoplot showing the faults and folds associated with the latest Cretaceous-Oligocene contractional event; c) Stereoplots showing faults associated with the Miocene extensional event (part of the fault data is taken from Dohmen, 2012): 1 – normal faults characterizing a stress field with a NE-SW direction of tension, 2 – normal faults characterizing a stress field with a NW-SE direction of tension; d) Stereoplot showing strike-slip faults, associated with the inversion starting during late Miocene times.

Previous studies and our observations document a first deformation event characterized by NW–SE oriented thrusts with both a SW- and NE-vergence, associated with folds with NW-SE oriented hinges (Figure 2.8b). These structures define a stress field with a NE-SW oriented compression direction. Outcrop kinematics and the relationship with major structures show that this deformation event was responsible for the initial thrusting of the East Bosnian–Durmitor unit (Figure 2.8a).

The thrusts formed during the first deformational event (Figure 2.8b), were subsequently truncated by numerous normal faults that show, yet again, two directions of extension. Roughly NW–SE oriented normal faults document a stress field with a NE-SW oriented extension direction (Figure 2.8c-1), while ~NE–SW oriented normal faults document a stress field with a NW-SE oriented extension direction (Figure 2.8c-2). The largest offset is observed along the NW-SE oriented normal faults, that can be kinematically connected with the reactivation of the East Bosnian–Durmitor thrust as a listric normal fault and the formation of extensional klippens of the overlying Drina-Ivanjica unit in its hanging-wall (Figures 2.1a and 2.8a).

A number of strike-slip faults have been observed in the field, dextral strike-slip faults are predominantly NNW-SSE to N-S oriented, associated with NE-SW to ENE-WSW oriented sinistral strike-slip faults (Figure 2.8d). These strike-slip faults formed during a deformation characterized by a stress field with a NNE-SSW to NE-SW oriented compression direction associated with a WNW-ESE to NW-SE oriented tension direction.

### 2.4.4 The southern High–Karst, Budva and northern Dalmatian units of coastal Montenegro

A large amount of kinematic data was obtained in coastal Montenegro, in the highly deformed area of the southern High–Karst, Budva and northern Dalmatian units (Figure 2.9a). This area shows multiple phases of folding, normal faulting, thrusting, strike-slip faulting and high-angle reverse faulting (Figures 2.9b-g).

The first phase of deformation observed in the field is characterized by NW–SE oriented normal faults dipping both to the NE and SW, that define a stress field with a NE–SW oriented tension direction (Figure 2.9b). Most of these faults cross-cut Lower Triassic–Anisian sediments and are syn-kinematic with the onset of Uppermost Anisian–Ladinian deep water carbonatic, calci-turbiditic, radiolaritic and volcanoclastic deposits (Figure 2.10a).

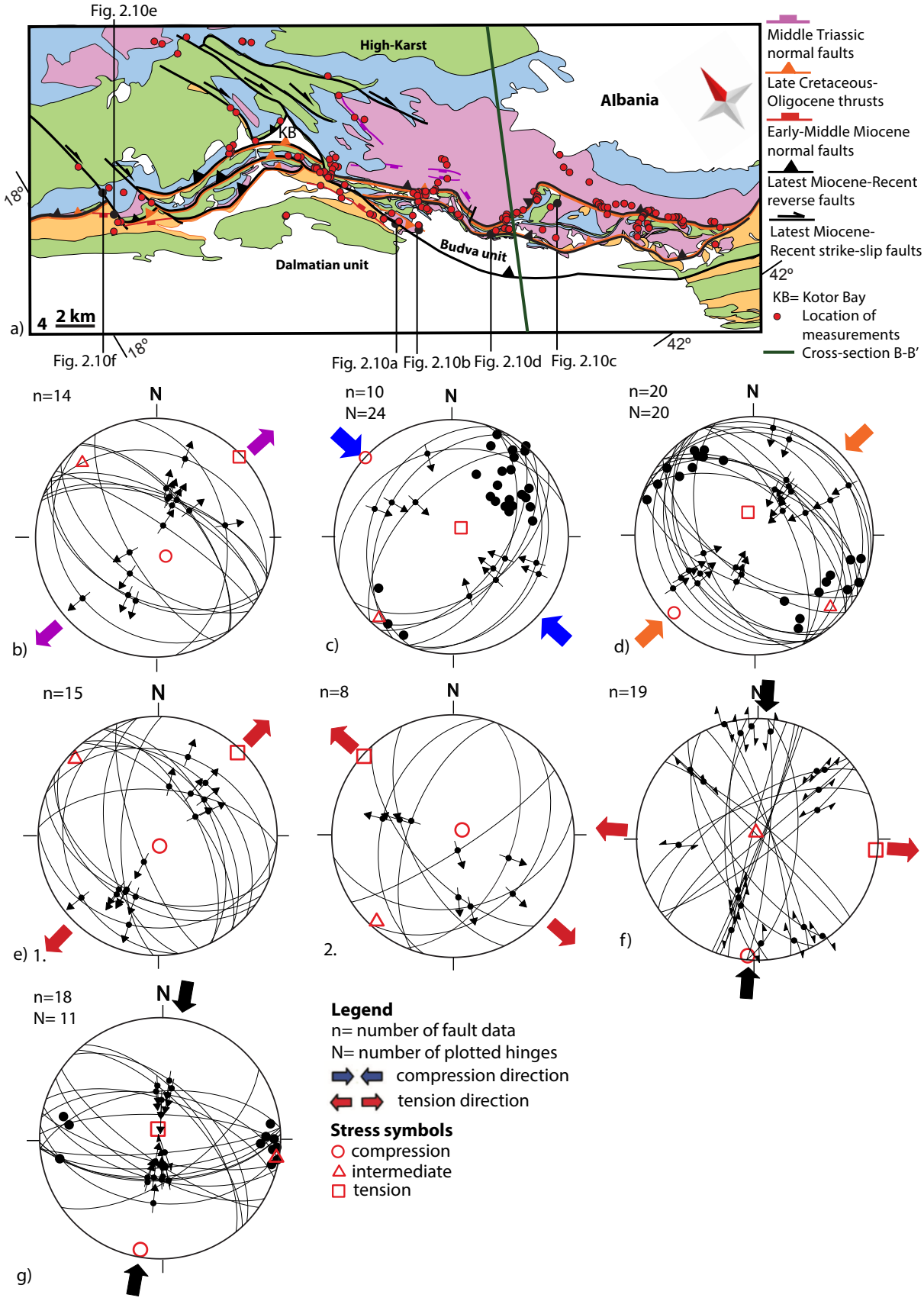


Figure 2.9 Kinematic data grouped per deformational event in the fourth focus area, coastal Montenegro. These data correspond to the SW part of cross-section B-B' (Figure 2.11b).

*Figure 2.9 (continued)* Further figure conventions as in Figure 2.4. a) Geological and structural map of coastal Montenegro (compiled and simplified from sheets of the 1:100.000 geological map of former Yugoslavia, Osnovna Geološka Karta SFRJ). The same legend for the stratigraphic age applies as in Figure 2.2. The location of the map is given in Figure 2.2 (rectangle 4); b) Stereoplot showing the faults associated with the Middle Triassic rifting event; c) Stereoplot showing the faults and folds associated with the Late Jurassic – earliest Cretaceous contractional event; d) Stereoplot showing the faults and folds associated with the latest Cretaceous-Oligocene contractional event; e) Stereoplots showing the faults associated with the Miocene extensional event: 1 – normal faults characterizing a stress field with a NE-SW direction of tension, 2 - normal faults characterizing a stress field with a NW-SE direction of tension; f) Stereoplot showing strike-slip faults, associated with the inversion starting during late Miocene times; g) Stereoplot showing reverse faults, associated with the inversion starting during late Miocene times.

In places, normal faults served as conduits for the emplacement of volcanic and sub-volcanic basaltic to andesitic bodies, which induced local contact metamorphism in neighboring Lower – Middle Triassic sediments, while the overlying Upper Triassic sediment are not metamorphosed. No larger, map-scale structures can be assigned to this deformation event, most likely due to significant overprinting by subsequent deformation events.

A second phase of deformation has been characterized by the formation of isoclinal and tight asymmetric folds with NE-SW oriented hinges commonly associated in outcrops with NE-SW oriented thrusts with both NW- and SE-ward vergences that affect strata as young as the Jurassic (Figures 2.9c and 2.10b). These structures define a stress-field with a NW–SE oriented compression direction (Figure 2.9c). Although such deformation is quite obvious in particular in the deep-water sediments of the Budva unit, no large-scale structures could be associated with this deformation phase.

These structures are being deformed by a second contractional event observed in the field by numerous folds and large-offset thrusts (Figures 2.9a,d). Isoclinal to tight asymmetric folds with NW–SE oriented hinges are often observed at outcrop scale in the deep-water sediments of the Budva unit, and the Eocene turbidites of the Budva and Dalmatian units (Figure 2.10c). These asymmetric folds become more open and larger (hundreds of metres to kilometres) in the massive Mesozoic shallow water limestones of the High–Karst and Dalmatian units. The folds are associated with numerous NW-SE oriented thrusts with both SW- and NE-ward vergences (Figure 2.9d). Compared to the NE-vergent thrusts, the SW-ward vergent thrusts have larger, kilometer-size offsets and created thick fault gouges and brittle shear zones. Such shear zones typically emplace more massive limestone layers over a sheared mudstone-siltstone matrix containing rotated blocks of limestones (Figure 2.10d). The folds and thrusts demonstrate an event characterized by a stress field with a NE–SW oriented compression direction. Lateral changes in thicknesses suggest that the Eocene turbidites of the Budva unit were partly syn-kinematic deposited with this deformation. The deformation is particularly intense in these turbidites, which also have syn-kinematic patterns when they are overlying the upper part of the Dalmatian unit that is situated beneath the Budva thrust (Figure 2.9a). East of the Kotor Bay, thrusting can be correlated inside the Budva unit and along its thrusting plane over the Dalmatian unit (Figure 2.9a). In the area of the Kotor Bay, intense internal folding and thrusting of the Budva unit was affected by a subsequent event characterized by the re-activation of both the Budva and High–Karst thrusts and strike-slip displacements.

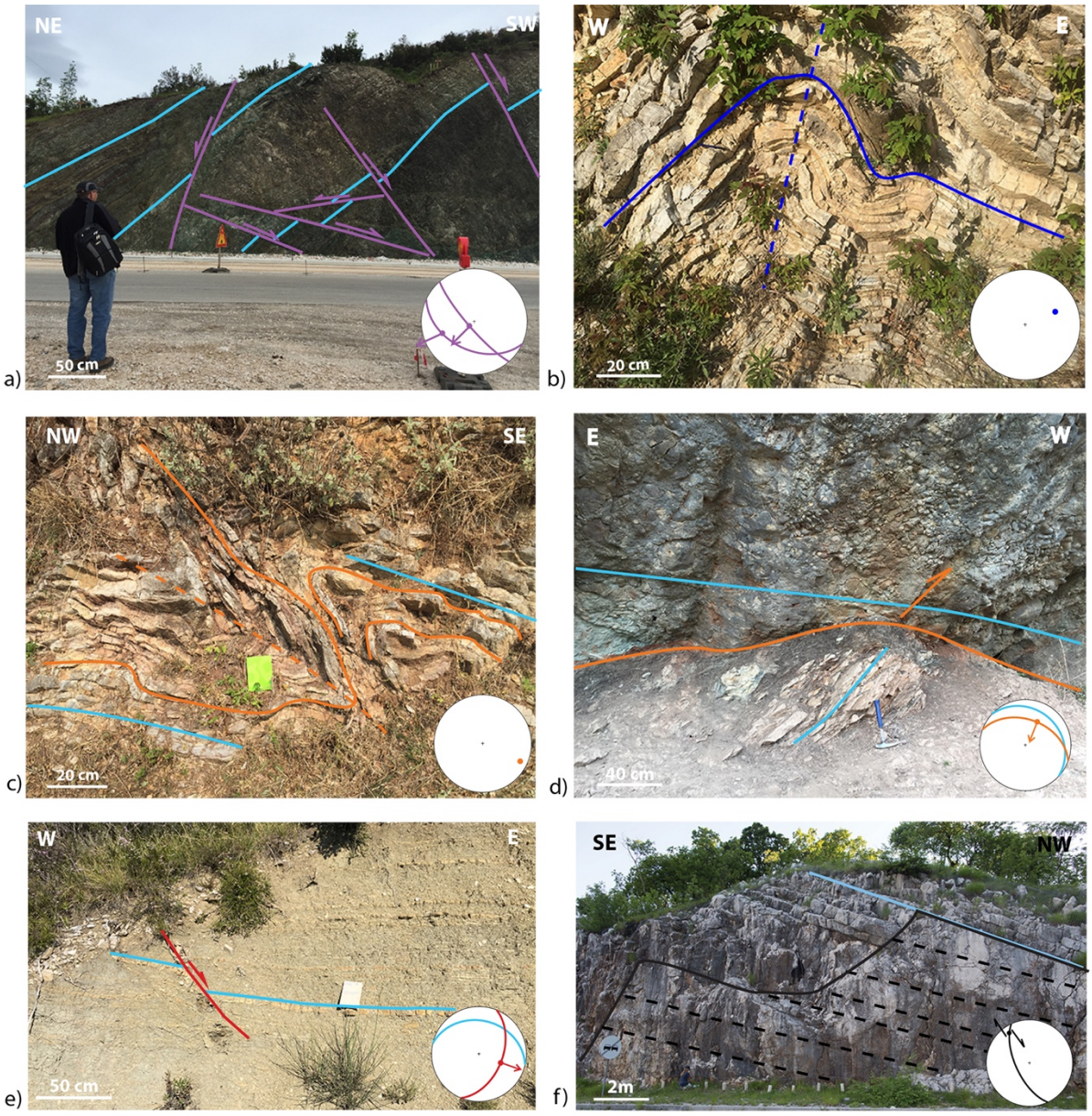


Figure 2.10 Interpreted field photos illustrating structures and their kinematics in the fourth focus area, coastal Montenegro. Location of the field photos are displayed in Figure 2.9a. Further figure conventions as in Figure 2.5. a) NW–SE oriented normal faults with NE– and SW-vergences within Triassic strata; b) A tight asymmetric fold with a NE-oriented hinge; c) Asymmetric folding with a SE oriented hinge; d) A NW–SE oriented SW-vergent thrust; e) A NE–SW oriented normal fault with a SE-vergence; f) A large-offset NW–SE oriented dextral strike-slip fault.

The large-offset thrusts and tight folds are truncated by normal faults, which were observed to cross-cut sediments as young as the Eocene (Figures 2.9a and 2.10e). Similar with elsewhere, normal faults can be subdivided into two extensional events, larger offset normal faults are NW-SE oriented and define a stress field with a NE-SW oriented tension direction (Figure 2.9e-1), while smaller offset mostly NE-SW oriented normal faults define one other stress field with a NW-SE oriented tension direction (Figure 2.9e-2). The offsets of such normal faults are generally centimetres to metres scale (Figure 2.10e). These normal faults do not appear to be associated with larger offset map-scale structures.

All previous structures are truncated or tilted by a last deformation event that is characterized by two different types of structures. In the Kotor Bay area, large-offset NW–SE to NNW–SSE oriented dextral strike-slip faults are associated with lower offset NNE–SSW to NE-SW oriented sinistral strike-slip faults and define a stress field with a NNE-SSW oriented compression and a WNW-ESE oriented tension direction (Figure 2.9f). Large strike-slip faults are commonly truncating entire outcrops (Figure 2.10f) and are distributed throughout the area. The offsets of strike-slip faults decrease significantly at outcrop and map-scale east of the Kotor area (Figure 2.9a), where the second type of deformation is more dominant (Figure 2.9g). This second type is characterized by a large number of ~E–W to (W)NW-(E)SE oriented thrusts or high-angle reverse faults that are both N-and S-vergent. These faults define a stress field with a NNE-SSW oriented compression direction (Figure 2.9g). Outcrop-scale faults observed in all areas can be connected in map view along large-offset dextral strike-slip faults, that often reach up more than 5 km in offset (Figures 2.9a and 2.10f). These faults are associated with significant rotations by forming large drag-folds with E–W oriented hinges, such as in the area of the Kotor Bay (Figure 2.9g).

## 2.5 Interpreting the kinematic data in the focus areas constraining the crustal scale transects

The analysis of kinematic data obtained in the four focus areas, demonstrate that the Dinarides orogen was affected by a long-lasting poly-phase tectonic evolution. This evolution shows that the largest amounts of thrusting have migrated gradually with time towards the foreland and was interrupted by periods of regional extension.

### 2.5.1 From Middle Triassic rifting to Late Jurassic–earliest Cretaceous obduction

The first moment of deformation recorded by our data is the Middle Triassic (latest Anisian–Ladinian) rifting and the formation of the Budva extensional structure, which is presently located in an external position in the Dinarides orogen (Figures 2.1 and 2.2). This interpretation agrees with previous studies that suggested a continental graben geometry, filled gradually by deep water sediments (Gorican, 1994; Schmid et al., 2008). Our observations demonstrate that extension of the Budva graben was NE–SW oriented (Figure 2.9b) and was associated with intermediate and mafic magmatism and a syn-kinematic deposition that shows rapid deepening of the basin, illustrated by the sedimentation of pelagic radiolarites interbedded with calci-turbidites, which are likely transported across the slope formed by normal faults. Deep water deposition continued until Upper Cretaceous times, although a gradual progradation and shallowing of facies is observed at the margins of the presently exposed Budva thrusted unit (Goričan, 1994). This deposition was also affected by regional geochemical changes induced by the onset of magmatism in the larger area of the Tethys, such as those that prevailed near the Triassic-Jurassic boundary (Crne et al., 2011). Our interpretation of a Middle Triassic NE-SW oriented extension in the Budva graben is also compatible with the rifting, drifting and the gradual deepening of the Middle Triassic–Early Jurassic carbonate facies interpreted at farther distances in the internal part of the Dinarides (Figure 2.3, e.g., Dimitrijević, 1997; van Gelder

et al., 2015). No indications of oceanic crust are found in the Budva unit, which has a rather limited extent along the Dinarides strike, being restricted to the SE-Montenegro area (Figure 2.1). Therefore, Budva was likely a symmetric continental graben that terminated to the NW and formed during the same Middle Triassic moment of continental rifting that opened the much larger Neotethys area situated northwards, as previously interpreted (Schmid et al., 2008). Whether or not Budva becomes an ocean in its lateral prolongation in the Cukali-Pindos units of the Albanides and Hellenides is still unclear (e.g., Menant et al., 2016).

The exact onset of Neotethys oceanic subduction is unclear in the study area, but available ages of ophiolites and metamorphic soles at the base of the ophiolitic sequences in the Dinarides and Hellenides indicate that it took place during Middle Jurassic times (e.g., Ustaszewski et al., 2009 and references therein). Our data from the Kimmeridgian–Valanginian Vranduk Flysch (e.g., Djeric et al., 2007), show a contractional event associated with a low number of top-NW thrusts and associated folds (Figures 2.4b and 2.5a,b). Such folds with NE–SW oriented hinges have been mapped also in the Budva graben of Montenegro (Figures 2.9c and 2.10b). The NW–SE orientation of this contraction direction is rather unique in more internal Dinarides units, interpreted to be the result of the Late Jurassic – earliest Cretaceous obduction event. The low number of kinematic data is otherwise similar with the internal part of the Dinarides, where a low number of similarly oriented folds and shears have been observed in the underlying ophiolitic mélange (Chiari et al., 2011; Schmid et al., 2008). We have not observed any syn-kinematic deposition in the Vranduk Flysch and, therefore, the deposition of these sediments may be assigned to any process that creates deep water turbidities, such as along the slope of a continental passive margin. However, the switch from carbonatic to siliciclastic turbidites overlying the Pre–Karst unit is almost coeval with the moment of obduction of the Western Vardar Ophiolites over more internal Adriatic units and the related formation of an active source area for these turbidites (Mikes et al., 2008). Therefore, this first NW-SE oriented contractional event can possibly be correlated with the NW-verging Kimmeridgian–Valanginian obduction of the Western Vardar ophiolites. The influence of this tectonic event on the formation of the NE-SW oriented fold hinges and thrusts observed in the Budva units is rather unclear in our study, most likely due to severe overprint by subsequent deformation events. It is possible that a far-field contractional effect, induced by the obduction of the neighboring Albanian ophiolites (Figure 2.1) (Bortolotti et al., 2012), has affected also the deep-water sedimentation of the Budva graben, but such a correlation is beyond the data available in our study.

### 2.5.2 Top-SW Late Cretaceous – Oligocene thrusting

The Bosnian Flysch zone was affected by large-scale thrusting and folding that started during Late Cretaceous times (Figures 2.4c and 2.8b). This is documented by syn-depositional thrusts and folds observed in the dominantly Campanian–Maastrichtian sediments of the Ugar and Durmitor flysches (e.g., Figures 2.5c-e). However, the depositional onset of these turbidites may have started earlier, during the Upper Cretaceous, owing to differences in biostratigraphic interpretations (Dimitrijević, 1997; Rampnoux, 1970). The termination of thrusting in this area is constrained by observations of syn-kinematic sedimentation along the northern margin of the Sarajevo–Zenica Basin (Figure 2.4a), which demonstrate Eocene thrusting that continued during Oligocene times (Andrić et al., 2017).

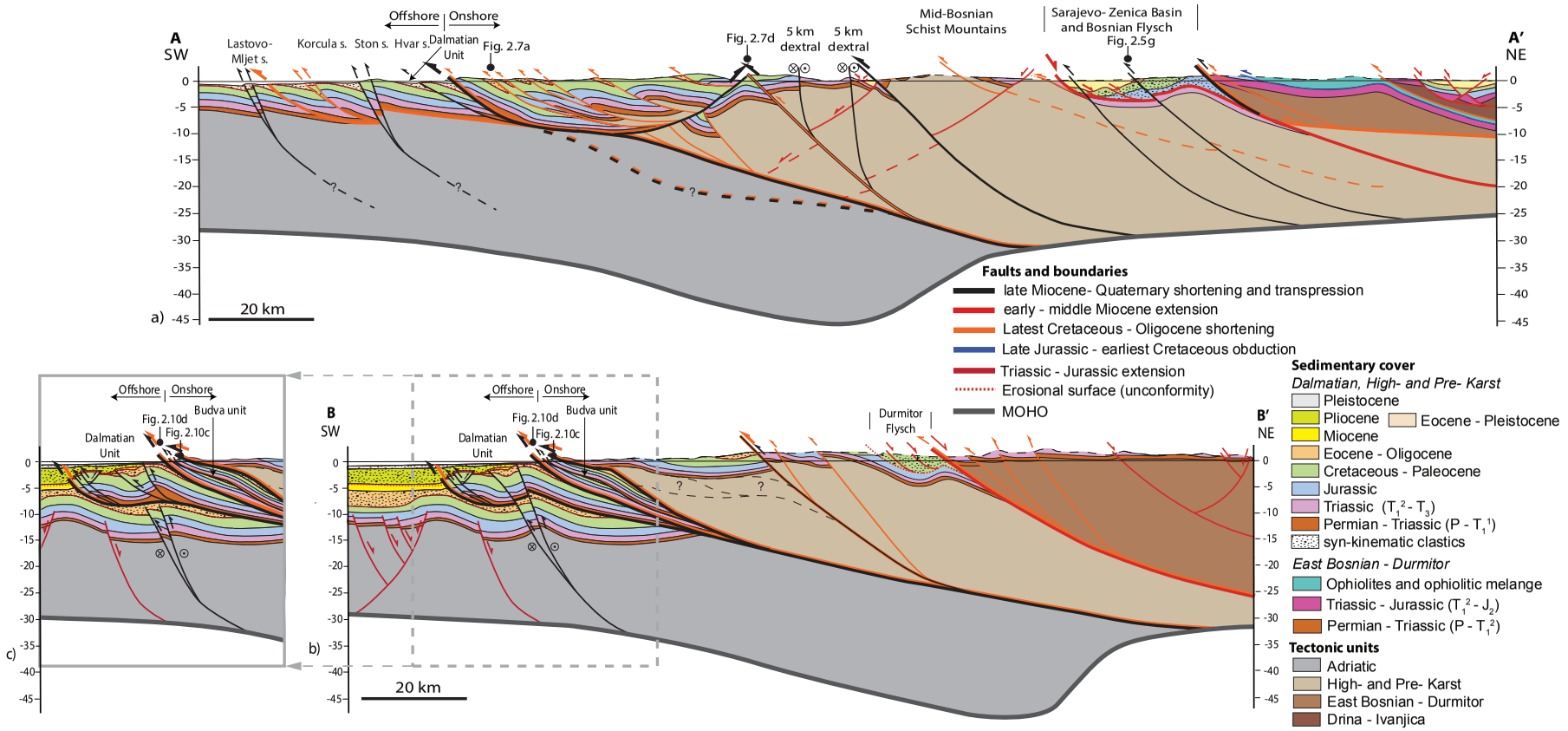


Figure 2.11 Two regional orogenic cross-sections built from depth projections of surface kinematics. The offshore structure of the profiles was studied and is explained with details in Chapter 4. The color of faults represents the timing of the most significant deformation. The Moho depth has been taken from Šumanovac et al. (2010). The location of the cross-sections is displayed in Figures 2.1a and 2.2. a) Cross-section A–A′ extends from the East Bosnian–Durmitor unit in central-eastern Bosnia and Herzegovina towards the Dalmatian zone in Southern Croatia and ends in the Adriatic foreland in the area of the Lastovo and Mljet structural highs. Note that the offshore extension is not based on seismic interpretations and, therefore, is only conceptual (see further details in Chapter 4).

*Figure 2.11 (continued)* Given the limited depth extent of our surface data projection, we do not have information on the presence of thin-skinned lower structural levels (i.e., duplexes) in the external part of the High-Karst unit (marked with thick dashed lines). Such deeper levels would significantly increase the shortening to amounts that are difficult to correlate across the strike of the Dinarides, but cannot be completely excluded. The part of the cross-section NE of the Bosnian Flysch and East Bosnian-Durmitor contact is modified after Ustaszewski et al. (2010); b) Cross-section B–B' extends from the East Bosnian–Durmitor unit in Southern Serbia crossing the Dalmatian zone of Montenegro and ends in the Adriatic foreland. The offshore structure is based on the interpretation of seismic reflection profiles and is explained in Chapter 4. Note that this offshore structure displays one possible interpretation of the cross-cutting and timing relationships between the thin- and thick- skinned deformation in the Dalmatian unit. In this interpretation, the Dalmatian thin-skinned emplacement pre-dates the thick-skinned deformation in the Adriatic foreland, which cross-cuts the Dalmatian unit (See also Chapter 4 for a more detailed description); c) Alternative interpretation of the cross-cutting and timing relationships between the thin- and thick- skinned deformation in the Dalmatian unit. In this interpretation, the Dalmatian thin-skinned emplacement post-dates the thick-skinned deformation in the Adriatic foreland, while the internal deformation inside the Adriatic unit is accommodated by the formation of a Permo-Triassic salt diapir.

Our field observations and the distribution of the syn-kinematic sediments show that the bulk of shortening taken by the Bosnian Flysch zone and its southern margin is Campanian–Maastrichtian in age, while the subsequent Eocene–Oligocene contraction is relatively minor by comparison (Figure 2.11a).

In contrast, the Eocene–Oligocene thrusting has significantly affected the external part of the Dinarides and was localized with larger thrusting and folding effects in the Budva unit of Montenegro (Figures 2.9d and 2.11b). Large-offset thrusts separate this unit in two main thrust sheets affected by intense internal deformation, which were subsequently truncated by the strike-slip faults and thrusting in post- middle Miocene times (Figure 2.9a). Outside the Budva unit, this deformation is observed by lower offset thrusts and widely spaced (hundreds of metres to kilometres) open folds (Figure 2.11). The onset of this deformation is constrained by the syn-kinematic deposition of Eocene turbidites in the footwall of numerous thrusts. Outside the Sarajevo–Zenica Basin, we have not obtained data of prolongation of this tectonic event in the studied area during Oligocene times, but such an age is compatible with the deposition of the late Eocene–Oligocene Promina Beds (Mrinjek, 1993) that are highly eroded in the studied area. However, deformation during the deposition of this orogenic regressive sequence is likely. Outcrop observations at the thrust contact of the East Bosnian–Durmitor unit overthrusting the Bosnian Flysch zone indicate an inclination between 45 and 60° of the thrust fault (Figure 2.11). However, the present geometry of this fault reflects rather its large-scale reactivation during the subsequent Miocene extension, while depth projections suggest an initial Late Cretaceous–Oligocene cumulated offset in the order of 10 km.

### 2.5.3 Bi-directional Miocene extension

Thrusting was followed by a period of Miocene extension. In all studied areas of the Dinarides, large offset normal faults define a NE-SW oriented extension, while smaller offset normal faults define a NW-SE oriented extension (Figures 2.4d, 2.6c, 2.8c and 2.9e). These are likely two successive episodes of Miocene extension, although clear superposition criteria are

missing in our dataset. The largest effects of this deformation are observed by the formation of a low-angle normal fault system that follows the NE direction of burial of the Bosnian Flysch beneath the thrusting of the overlying East Bosnian–Durmitor unit (Figure 2.11a). In other words, the thrusting of the East Bosnian–Durmitor unit was reactivated by large-offset normal faults dipping NE-wards in the Bosnian Flysch. The formation of this asymmetric fault system was likely influenced by the rheological weakness of the NE-dipping Bosnian Flysch turbidites, which are squeezed between the southern Paleozoic basement and overlying carbonate platform of the Pre–Karst unit, and the northern Paleozoic basement, carbonate platform and overlying ophiolites of the East Bosnian–Durmitor unit (Figures 2.4a and 2.11a). In the area of the Sarajevo–Zenica Basin, the main offset of the normal fault system is located at the base of the Bosnian Flysch and created ~ 8 km of Miocene exhumation in the footwall of the Busovača Fault, which is also partially responsible for the exhumation of the Mid-Bosnian Schist Mountains (Figures 2.11a, see also Andrić et al., 2017). The faults geometry suggests an isostatic rebound in the footwall of an extensional detachment. The same geometry is also inferred by observations in Montenegro, with the difference that the main Miocene extensional detachment reactivates the inherited Late Cretaceous East Bosnian–Durmitor thrust, which overlies the Durmitor Flysch (Figure 2.11b).

SW-ward of the Bosnian Flysch, the demonstration of Miocene extensional deformation that affected the external part of the Dinarides is novel and implies that the formation of the entire Dinarides Lake System during the Early Miocene was associated with extension, as observed for instance in the Konjic Basin (Figure 2.6a). The Miocene normal faults in the external parts of the Dinarides cumulate hundreds of metres of offsets and formed similarly thick lacustrine basins (see also de Leeuw et al., 2010, 2011, 2012; Harzhauser & Mandic, 2008; Mandic et al., 2011, 2012). Similar extensional structures have been observed in the NE-Dinarides, interpreted to be active during Neogene times (e.g., Žibret & Vrabec, 2016). These offsets are lower when compared with the kilometres-scale offsets observed in the Bosnian Flysch and numerous other large-offset low-angle normal faults and detachments accompanying the formation of several kilometres thick Miocene basins in more internal parts of the Dinarides. When combined, all these observations demonstrate that the Miocene period of extension affected all areas of the Dinarides until the Sava zone (Figures 2.1 and 2.2).

### 2.5.4 Late Miocene–Recent N-S to NNE-SSW oriented contraction

The Miocene extension was followed by the late Miocene (after 9 Ma) onset of strike-slip faulting (NW–SE to NNW–SSE oriented dextral strike-slip and NE–SW oriented sinistral strike-slip), thrusting (top-S and top-N), high-angle reverse faulting and folding with E-W oriented hinges. Field observations clearly demonstrate that these structures connect each other and the two paleostress fields measured (strike-slip and compression), reflect in fact the same N-S to NNE-SSW contraction event, which partitions deformation to either strike-slip, thrusting, or reverse faulting and folding. This observed deformation is roughly compatible with the mechanism of N- to NE-ward Adriatic indentation in the Dinarides (Handy et al., 2010; Pinter et al., 2005).

In more details, the inherited rheological structure and localization of deformation plays an important role on the type of structures formed. The inherited rheological weakness and the

geometry of the Bosnian Flysch turbidites and deep-water sediments of the Budva unit localizes deformation by the formation of major low-angle thrusts, reactivating such inherited structures or low-angle normal faults (Figure 2.11). This mechanism is in agreement with the Bosnian Flysch localization of southward thrusting that deformed the sediments of the Sarajevo–Zenica Basin starting with late Miocene times (Andrić et al., 2017). We have not found clear field evidence for such a localization in the along-strike prolongation of the Bosnian Flysch in Montenegro. Instead, most of the localization of this deformation in the Serbia – Montenegro profile takes place in the Budva unit, observed by the large thrusting of the High–Karst and Budva units and local truncation of its previous Eocene-Oligocene thrust sheets (Figure 2.11b). This is also compatible with the coeval emplacement of the Dalmatian unit over the Adriatic margin, observed in offshore seismic interpretations (Figure 2.11b, see also Bega, 2015).

The total amounts of thrusting in the External Dinarides units can be estimated based on minimum cumulative offsets. For the Montenegro profile (Figure 2.11b), the geometry of the Cukali tectonic half-window and the one of the Peshkopia window, where the sediments of Budva–Cukali unit are outcropping in neighboring Albania (Figure 2.1), suggest a minimum 50-60 km cumulated Eocene-Oligocene and post- 9 Ma thrusting offset of the High–Karst from the Budva unit. Given the fact that Budva unit pinches out to the north-west until Dubrovnik, a gradual decrease in minimum thrusting offset is likely to around 25-30 km along the trace of our profile (Figure 2.11b). The depth projection shows that a cumulated offset for the same period, is in the order of ~15-25 km for the thrusting of the Budva unit over the Dalmatian unit, while the internal deformation of Budva is in the order of minimum 15-20 km (Figure 2.11b). This means that the total cumulated shortening from the High–Karst thrust to the Budva over Dalmatian thrust in the order of minimum 60-75 km. This estimate, contrasts with the depth projection of the equivalent High–Karst over Dalmatian thrusting in the Bosnia and Herzegovina – Croatia profile, which is in the order of 10 km (Figure 2.11a). All these observations and depth extrapolations show that the bulk of the post – 9 Ma thrusting was transferred along the strike from the Bosnian Flysch in the Bosnia and Herzegovina – Croatia profile to the High–Karst, Budva and Dalmatian units in the Serbia – Montenegro profile (Figures 2.2 and 2.11). Parts of this differential amounts of shortening may have been accommodated by the counterclockwise rotation of the Adriatic lower plate, while most Dinarides thrusted units do not record this rotation (de Leeuw et al., 2012).

The large-scale thrusting in the more internal Bosnian Flysch in the Bosnia and Herzegovina – Croatia profile and the more external Budva unit in the Serbia – Montenegro profile is likely connected along the orogenic strike by the numerous larger offset dextral strike-slip and high-angle reverse faults observed in the field, which may allow an effective deformation transfer between the two areas. The total amount of shortening recorded during this deformation event, which started during the late Miocene and is still presently active, can be evaluated by the differential shortening and strike-slip transfer between the Bosnia and Herzegovina – Croatia and Serbia – Montenegro profiles, which is in the order of minimum 45 km.

## 2.6 Mechanics of orogenic deformation

Given the scarcity of depth information, such as wells or seismic lines, in the onshore external part of the Dinarides, the depth prolongation of major structures in our crustal profiles

(Figure 2.11) is rather estimative and based mostly on surface-to-depth projections. Understanding the balance between thin- versus thick-skinned deformation relies on the availability of décollement horizons located stratigraphically above the Paleozoic. These Paleozoic rocks crop out in all internal parts of the Dinarides units in the hanging-wall of the major thrusts or nappe contacts, which shows that deformation is thick-skinned relative to this basement. Thin-skinned deformation is proved or inferred in the High–Karst unit located in the northeastern and central Dinarides of Croatia, which is facilitated by the presence of thicker Permo–Triassic salt or other evaporite layers that serves as the main décollement level for a number of thrust systems (Korbar, 2009; Kulušić & Borojević Šoštarić, 2014). However, such evaporite layers decrease in thickness and finally disappear along the strike of the onshore Dinarides to the SE, being replaced in Montenegro by dominantly Permo–Triassic continental sediments, rarely intercalated with scarce or thin layers of mostly gypsum deposits (Figure 2.3). A good place to find such potential décollement horizons are the Mid-Bosnian Schist Mountains (Figure 2.2 and 2.11a), where the Paleozoic basement and its overlying Mesozoic sedimentary cover were exhumed during the Paleogene contraction and the Miocene extension in the footwall of the Busovača Fault (Figures 2.11a, Hrvatović, 2006). We note this Paleozoic basement contains late Early Cretaceous metamorphic ages (Pamić et al., 2004) and, therefore, at least the upper part of the ductile lower orogenic crust is exposed in the Bosnian Schist Mountains. Our field observations have failed so far to find a pre-Miocene décollement horizon potentially located at or near the contact between the metamorphosed Paleozoic basement and its Permo–Mesozoic cover or inside this cover (Kulušić & Borojević Šoštarić, 2014), as we have only observed unconformable or continuous sedimentation. These types of contacts show that the orogenic deformation is thick-skinned, rooted below the exposed Paleozoic metamorphosed basement that crops out or was also drilled in our studied area (Pamić et al., 2002; Velić et al., 2015). However, note that that thin-skinned lower structural levels (i.e., duplexes) may be present in limited areas of the High-Karst unit (marked with dashed lines in Figure 2.11).We do not have any information that such levels are present in our study, but at the same time we cannot exclude them given the scarce availability of deep data. The surface to depth projection and the wavelength of deformation in the studied area indicate that almost all thrusts or high-angle reverse faults must be rooted in the lower crust in the internal parts of our profiles (Figure 2.11). Therefore, similar with previous Dinarides interpretations (Figure 2.1b, see also Schmid et al., 2008), we have chosen to root such faults at the base of the crust, which agrees with the mechanics of such orogenic systems accounting for a rheological weakness zone at the crust-mantle transition (Erdös et al., 2015; Jammes & Huismans, 2012; Lacombe & Bellahsen, 2016; Ziegler et al., 1995).

### 2.6.1 Gradual transfer of deformation towards the orogenic foreland

From Late Jurassic times all units in the studied external part of the Dinarides recorded the main orogenic phases of deformation. The top-NW Late Jurassic–earliest Cretaceous obduction (e.g., Dimitrijevic, 1997; Schmid et al., 2008) has resulted in the onset of deposition and deformation of the Bosnian Flysch in the frontal part of the obduction system and similar deformation affected also the Budva deep water deposits, the latter possibly in connection with the emplacement of the Albanian ophiolites. The detailed effects of this deformation are difficult

to be assessed in the studied area, being almost completely overprinted by subsequent deformation events. Subduction continued in Cretaceous time until the latest Cretaceous peak moment of continental collision between the Dinarides and Tisza-Dacia continental units. The accretionary wedge sediments presently observed farther NE-wards in the Sava zone show significant Early Cretaceous–Cenomanian contractional deformation followed by the Turonian–Santonian formation of an extensional fore-arc basin (Figure 2.1, Toljić et al., 2018). The effects of this ongoing Cretaceous subduction at farther distances from the Sava zone in the Dinarides are significantly reduced, mostly observed by a late Early Cretaceous moment of burial and the formation of a regional unconformity recorded in the internal part of the Dinarides (Ilić & Neubauer, 2005; Schefer, 2010). No clear effects of these deformation events can be defined in the studied area, but it cannot be completely excluded also.

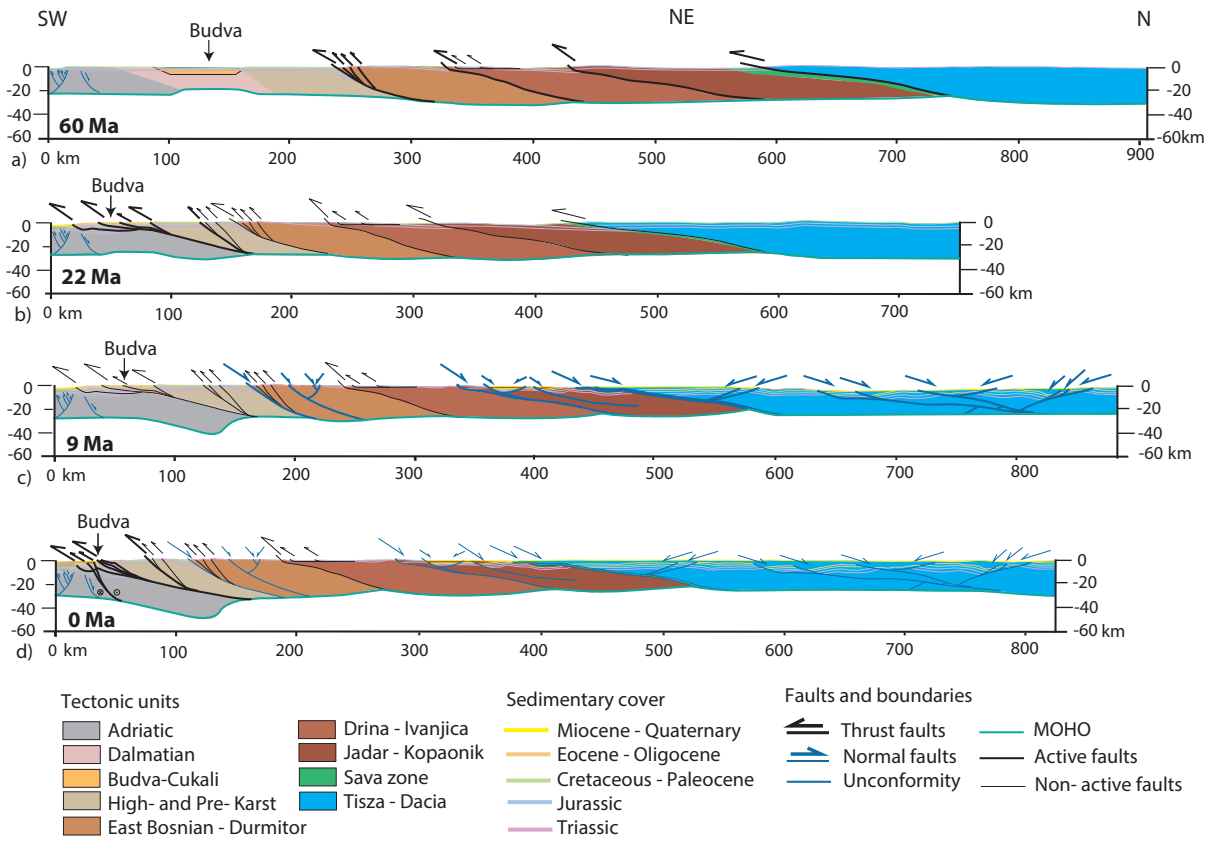


Figure 2.12 Kinematic reconstruction of a cross-section that combines the crustal scale cross-section displayed in Figure 2.11b in the external part of the Dinarides with its prolongation in the internal part of the Dinarides, Sava Zone and Tisza unit (modified after Balazs et al., 2017). The trace of the combined cross-section is displayed in Figure 2.1 (grey line B-B' – black dotted line). a) The latest Cretaceous moment of continental collision resulted in the gradual migration of contractional deformation towards the orogenic foreland, associated with SW-ward nappe stacking in the internal part of the Dinarides; b) Continued contraction until Oligocene times affected mainly the external parts of the Dinarides, characterized by the SW-ward nappe stacking of the High-Karst, Budva and Dalmatian units; c) Miocene extension induced normal faulting and reactivation of former thrusts in the entire Dinarides, Sava zone and Tisza unit; d) The N-S to NNE-SSW oriented contraction that started during late Miocene times induced high-angle reverse faulting and reactivated former structures and nappe contacts in the Dinarides.

The large-scale deformation shows a gradual migration towards the orogenic foreland during the latest Cretaceous onset of continental collision (Figure 2.12a) and its continuation of contractional deformation until Oligocene times (Figure 2.12b). This overall pattern was influenced by the pre-existence of the Bosnian Flysch and the Budva unit, that contained rheological weak sediments and localized larger amounts of contractional deformation, although at different times. The main moment of latest Cretaceous continental collision was recorded especially at the contact between the Dinarides and European-derived units along the Sava zone and at the contact between the Jadar–Kopaonik and Drina–Ivanjica units (e.g., Schmid et al., 2008; Toljić et al., 2018; Ustaszewski et al., 2010). Significant deformation is documented by our study in the Bosnian Flysch zone, most likely an effect of localization along this inherited weakness zone. The continuation of contraction during Eocene–Oligocene, concentrated in a second, more external rheological weak zone, the Budva unit of Montenegro (Figure 2.12b). However, given this unit gradual lateral reduction to disappearance along the strike of the orogen towards the NW, deformation becomes more regionally distributed in this direction along the entire pre–Karst, High-Karst to Dalmatian area, where a large number of thrusts with lower offsets are observed (comparing Figure 2.11a with 2.11b). The total amount of Eocene–Oligocene offset is similar in both areas in the order of 30 km. In other words, the Eocene–Oligocene shortening is similar along the strike of the orogen, but the deformation is largely localized in the Serbia – Montenegro transect due to the presence of the rheologically weaker sediments of the Budva unit. Elsewhere in more internal areas of the Dinarides, coeval deformation has significantly smaller effects in the order of hundreds of metres to possibly few kilometres. The Budva unit cannot reflect an oceanic suture zone connected to the present-day observed slab, because this unit does not retain any oceanic characteristics and pinches out along the orogenic strike towards the NW, in the SE Dinarides (Figure 2.11), while the high-velocity slab anomaly is continuous more to the NW. Therefore, the overall latest Cretaceous–Oligocene migration of peak deformation towards the orogenic foreland (Figure 2.12b) cannot have any other mechanism, but a general migration of the subduction zone during collision (Figures 2.13a,b) on its way to the presently observed location in the frontal part of the orogen (Figure 2.13c). This mechanism is the only one compatible with the observed SW-ward migration towards the orogenic foreland of the Cretaceous – Oligocene subduction-related magmatism that crosses the oceanic suture (Sava) zone (see discussion in Andrić et al., 2018; Cvetković et al., 2013). This mechanism is also compatible with the present thermal, crustal and lithospheric configuration (Figure 2.13c) and with an overall migration of the onset of Dinarides extension, from Oligocene near the Sava zone (e.g., Erak et al., 2017; Stojadinović et al., 2017) to Miocene in more external parts.

The lithospheric configuration and evolution (Figure 2.13) as well as the overall pattern of foreland migration of deformation and slab retreat during continental collision is observed in many other orogens, such as the Carpathians, Betics or the Aegean system (e.g., Faccenna et al., 2014; Jolivet & Brun, 2010; Matenco et al., 2016; Vergés & Fernàndez, 2012). The migration implies a change in location of the subduction zone by accretion of continental material from the lower tectonic plate during collision. Such a gradual accretion of continental material and migration of the subduction zone in single-vergent orogens agrees with the prediction from numerical or analogue modelling studies (Vogt et al., 2017a, 2017b; Willingshofer et al., 2013). These studies have inferred that such orogenic wedges form when

significant rheological decoupling exist between crustal and/or mantle lithospheric layers, or when the upper tectonic plate is rheologically stronger during collision. Such rheological inheritance may result in foreland migration of deformation and of the subduction zone that can be associated with significant amounts of continental subduction (Figure 2.13, Vogt et al., 2017a, 2017b; Willingshofer et al., 2013). The main difference of the Dinarides in our studied sector is that the entire accretion of continental material during collision is inferred to be thick- and thin- skinned, as opposed to for instance the Carpathians or the Apennines (e.g., Matenco et al., 2016; Picotti & Pazzaglia, 2008), where most of the accretion is thin-skinned and only the last phases of deformation are thick-skinned.

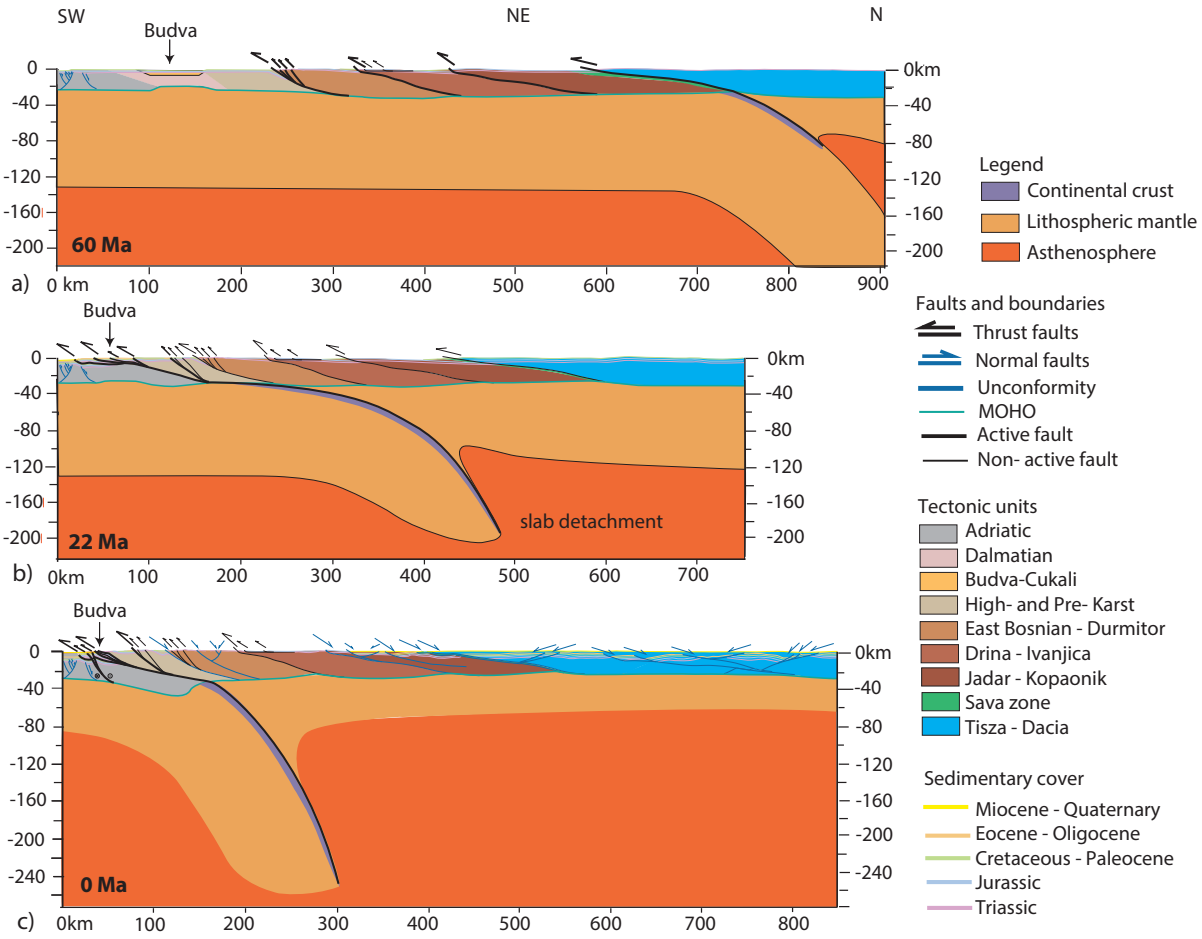


Figure 2.13 Schematic representation of the lithospheric evolution by using the reconstruction of the cross-section displayed in Figure 2.12. a) Immediately after the first stage of the latest Cretaceous collision (~60 Ma) we assumed that the location of the slab is in the prolongation of the Sava suture zone, which is in agreement with the position of the Late Cretaceous back-arc magmatism (see Gallhofer et al., 2015); b) Slab break-off took place during Oligocene times, at a time when the slab was located more to the foreland, which is in agreement with the observed Eocene-Oligocene foreland migration of magmatism (see Andrić et al., 2018); c) The crustal structure derived from the present study combined with the present-day lithospheric configuration, indicates that the position of the detached slab is beneath the frontal part of the Dinarides orogen, which has been derived from teleseismic tomography (modified after Balazs et al., 2017).

Alternatively, one other explanation for the overall foreland migration observed in the Dinarides may be the indentation of the lower crust of the upper plate during collision, when only the overlying upper crust is being shortened (Andrić et al., 2018). In this hypothesis, decoupling between the upper and lower crust will create a mid-crustal décollement level where all Late Cretaceous–Oligocene thrusts are rooted, which is less likely in our depth extrapolations (Figure 2.11).

Structural, kinematic, magmatism and numerical modelling studies have inferred that slab detachment took place in the Dinarides during Oligocene times (Figure 2.13b, e.g., Andrić et al., 2018; Schefer et al., 2011). Our observation that the Miocene extension was observed in all areas of the Dinarides (Figure 2.12c), implies that this extension was related to a post-orogenic process with respect to the Dinarides mechanics, which pre-dated the onset of the Adriatic indentation during the late Miocene (Figure 2.12d). Whether this post-orogenic process is related to eduction (exhumation of the lower plate by reversing the motion of the subduction plane, e.g., Andersen et al., 1991; Andrić et al., 2018) during or after slab-detachment or the typical gravitational collapse of an over-thickened orogen is difficult to be quantified based only on crustal-scale information, as often discussed for instance in other Mediterranean orogens, such as the Betics-Rift system (e.g., Platt et al., 2013; Vergés & Fernàndez, 2012).

## 2.7 Conclusions

The field kinematic study and the construction of regional scale transects in the central and SE part of the External Dinarides, has demonstrated a long and poly-phase tectonic evolution that started with the Middle Triassic rifting and continued with the Late Jurassic onset of orogenic deformations that are still presently active.

The Middle Triassic rifting is observed in the studied area by the formation of the Budva graben and a widespread magmatism that has also created, north of our studied area, the Vardar branch of the Neotethys ocean. The Middle Jurassic onset of oceanic subduction and intra-oceanic obduction was followed by the Late Jurassic–earliest Cretaceous emplacement of ophiolites and mélanges onto the Dinarides northern continental margin. The effects of this tectonic event were largely overprinted by re-activations during subsequent deformations, but few relict structures testifying the typical NW–SE direction of contraction were still observed in the Bosnian Flysch and the Budva unit of Montenegro.

This deformation was followed in the studied area by a long lasting latest Cretaceous–Oligocene continental collision. Although the effects of this tectonic event are observed in the entire studied area, our analysis of its maximum effects shows a gradual migration of the main deformation towards the orogenic foreland, interpreted to result from a migration of the subduction zone by continental accretion during collision.

Following the likely Oligocene moment of slab detachment, our study demonstrates that the Miocene extension previously observed in the internal Dinarides units has affected the entire orogen, including the external part of the Dinarides foreland. This extension may be related to either eduction during and after slab detachment or to the extensional gravitational potential collapse of an over-thickened orogen after slab detachment.

The Miocene extension was followed by the late Miocene onset of Adriatic indentation in the Dinarides, a process that is still active today and is not intrinsically related to the Dinarides orogenic evolution, but likely related to the much larger Africa-Europe convergence.

The localization of latest Cretaceous–Oligocene shortening was significantly influenced by the existence of deep-water sediments, pre-conditioning rheological weakness zones in the Bosnian Flysch and the Budva unit of Montenegro. These units have localized large amount of thrusting during Late Cretaceous and Eocene - Oligocene, respectively. Although the total amount of latest Cretaceous–Oligocene deformation is similar in the two studied profiles, the lateral disappearance of the Budva unit to the NW and its rheological weakness along the strike of the orogen has distributed the localized deformation over a much larger area to the north in the High–Karst and Dalmatian units. The specificity of the Dinarides collision is the thick- and thin- skinned accretion that was active during the entire collisional moment. Interesting is also that the continental subduction has continued after slab-detachment and post-orogenic extension, driven by the subsequent Adriatic indentation. The differential and rotational ~N–S to NE-SW direction of indentation, when compared with the overall NW–SE strike of the inherited orogen, has resulted in localization of oblique thrusting along the inherited rheological weak zones that were connected by a system of strike-slip and high-angle reverse faults elsewhere. This overall evolution shows that the evolution of the Dinarides was driven initially by the evolution of its genetically related slab. Once this slab was detached, the Dinarides evolution was conditioned by the more regional mechanism of Adriatic indentation, which has similar continental subduction effects, but with slightly different kinematics. Such a differentiation between two different geodynamic mechanisms, producing similar effects during mountain building, is very interesting also for other orogens situated elsewhere. Therefore, the Dinarides may represent a prime example of such a geodynamic juxtaposition.

## Chapter 3.

# Transfer of deformation during indentation: inferences from the post-middle Miocene evolution of the Dinarides

*This chapter is based on*
*van Unen, M., Matenco, L., Demir, V., Nader, F. H., Darnault, R., & Mandic, O. (2019). Transfer of deformation during indentation: inferences from the post- middle Miocene evolution of the Dinarides. Submitted to Global and Planetary Change*

## 3.1 Introduction

The architecture of mountain belts is often controlled by the evolution and dynamics of subducted slabs during the final stages of continental collision (e.g., Andrić et al., 2018; Burov et al., 2014; Duretz & Gerya, 2013; Faccenna et al., 2014; Matenco et al., 2010). The term indentation has been used to define the collisional mechanics of a small continental plate flanked by subduction zones, creating significant crustal thickening and/or lateral escape of blocks against strike-slip faults, facilitated by rheological strength contrasts or changes in subduction mechanics, such as lateral slab retreat (e.g., Davy & Cobbold, 1988; Molnar & Tapponnier, 1975; Regard et al., 2005). Understanding the structural and kinematic effects of indentation has been a subject of debate due to the large number of competing mechanism, ranging from crustal and lithospheric thickening and folding, lower crustal flow, lateral extrusion, to oblique oceanic or continental subduction (e.g., Houseman & England, 1993; Meissner & Mooney, 1998; Molnar & Tapponnier, 1975; Rosenberg et al., 2007; Smit et al., 2013; van Gelder et al., 2017). In many situations observed in the India-Asia or Mediterranean collision systems, indentation is associated with the evolution of opposite dipping subduction zones situated at the margins of the continental plate fragment, where a lateral transfer of contractional deformation across multiple orogens is observed (Doglioni et al., 2007; Faccenna et al., 2014; Faccenna et al., 2004; Jolivet et al., 2018). While the significant thickening of the continental fragments is usually described as indentation, the same convergence process is described laterally in the opposite polarity subduction systems as oceanic or continental subduction (Faccenna & Becker, 2010; Jolivet et al., 2018; Munteanu et al., 2014; Peral et al., 2018; Regard et al., 2005). This contrast leads to a situation where a clear process-based discrimination between subduction and indentation, based on observations in transition zones, is too often unclear. In particular, kinematic studies are required in such transitional zones to discriminate processes and understand indentation effects.

One typical example of the interplay between indentation, opposite polarity subduction zones and associated deep mantle processes is the one observed for the post-Paleogene evolution of the Adriatic micro-plate, which is situated between the opposite polarity orogenic systems of the Alps and the ones of the Dinarides and Apennines (Figure 3.1, Handy et al., 2014; Király et al., 2018; Le Breton et al., 2017; Ustaszewski et al., 2008). The kinematics and timing of deformation is relatively well understood in the rapid transition zone between the Alps and Apennines (e.g., Bertotti et al., 2006; Handy et al., 2010; Picotti & Pazzaglia, 2008; Schmid et al., 2017). In contrast, the balance between the Alps-Dinarides subduction polarity change, Adria indentation and subduction of the Adriatic plate in the Dinarides (Figure 3.1) is much less understood (e.g., Bennett et al., 2008; Kissling et al., 2006; Schmid et al., 2008; Šumanovac et al., 2017). This understanding is hampered in particular by the poor knowledge of the post-Paleogene kinematics in the external Dinarides (Figure 3.1). This 700 km long orogen connects the intense post-Paleogene and active deformation presently observed in the Southern Alps, defined as Adriatic indentation, with the active subduction and retreat of the Aegean slab that still drives the evolution of the Albanides – Hellenides orogenic system (e.g., Jolivet & Brun, 2010; Jolivet et al., 2015; Schmid et al., 2008; van Gelder et al., 2017).

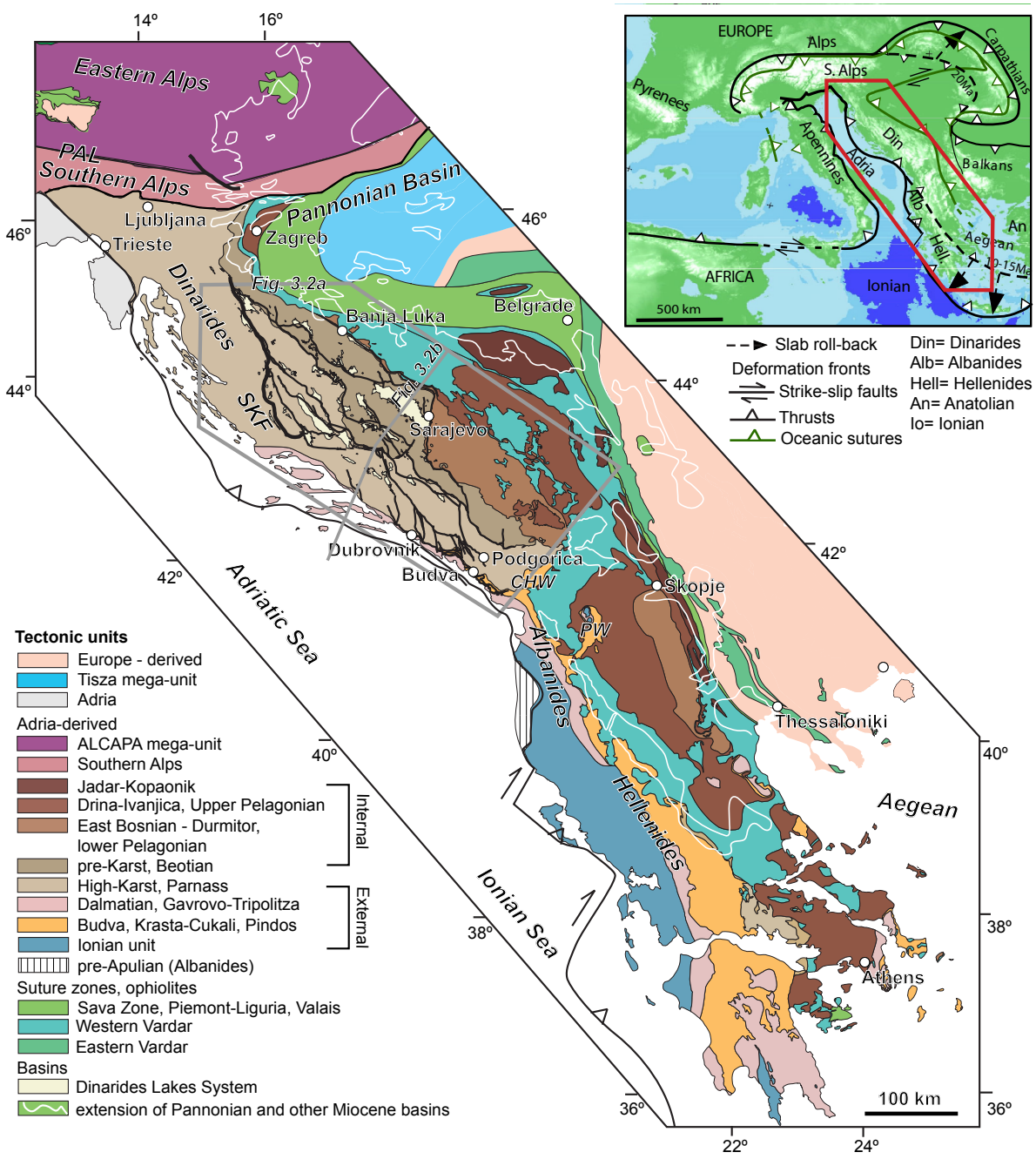


Figure 3.1 Tectonic map of the external parts of the Dinarides, Albanides and Hellenides, as well as the neighbouring parts of Pannonian Basin, Southern and Eastern Alps (after Schmid et al., 2008 ; Schmid et al., 2011). In the Dinarides, the map is overlain by the post- 9 Ma fault system depicted in Mthis study and by Miocene basins belonging to the Dinarides Lake System (Harzhauser & Mandic, 2008; Mandic et al., 2012). The grey polygon is the location of the map in Figure 3.2. The map in the upper right corner is the localisation of the tectonic map in the larger European orogenic context. PAL = Peri – Adriatic Lineament; SKF= Split – Karlovac Fault; CHW - Cukali half-window; PW - Peshkopia Window. Dashed lines are locations of the orogenic front in the Carpathians and Aegean domain at 20 and 15 Ma, respectively (modified after Wortel & Spakman, 2000).

The Adriatic indentation was associated in the Southern Alps and internal part of the Dinarides with thrusting, dextral movements and/or extrusions along the Peri-Adriatic Lineament (e.g., Fodor et al., 1998; Frisch et al., 2000; Tomljenović & Csontos, 2001; Ustaszewski et al., 2014; Vrabec et al., 2006; Wölfler et al., 2011; Žibret & Vrabec, 2016). In contrast, there is almost no kinematic and timing documentation available for structures in the central and south-eastern part of the external Dinarides that would explain the present-day intense seismicity, crustal stress pattern and the up to 5 mm/yr N- to NE-ward movement with respect to stable Europe detected by GPS studies (Bennett et al., 2008; Caporali et al., 2009; Grenerczy et al., 2005; Heidbach et al., 2018; Métois et al., 2015; Pinter et al., 2005). This lack of data renders all previously inferred large-scale (up to 100 km) motions along various structures in the external part of the Dinarides, such as the NNW-SSE oriented dextral strike-slip Split-Karlovac Fault System (Figure 3.1, e.g., Chorowicz, 2016; Ustaszewski et al., 2008) and resulting reconstructions of Adriatic indentation (e.g., Picha, 2002) as highly speculative. Therefore, a quantitative understanding of the effects and mechanics of the N-ward Adriatic indentation and its relationship with the inherited NW-SE oriented Dinarides structure is still not available.

We aim to fill this gap in regional and process-oriented knowledge by quantifying the post-Paleogene kinematics and timing of structures associated with the indentation of the Adriatic continental micro-plate and its continental subduction observed in the external parts of the Dinarides. We have collected a new kinematic dataset for structures that postdate the main Late Jurassic – Paleogene orogenic evolution in the central and south-eastern Dinarides (Figure 3.2). We use one critical timing indicator not previously accounted for, which is the deformation of Miocene sediments deposited during the development of the Dinarides Lake System, an endemic and isolated group of intra-montane lakes that overlies the previous orogenic structure and whose areal extent was enhanced by the Miocene Climatic Optimum (Figures 3.1 and 3.2a, Harzhauser & Mandic, 2008; Harzhauser et al., 2011; Mandic et al., 2012). Given the unusual large extent of our studied area, we have focused our observations to characterize only post-Paleogene large offset faults that affect the Miocene sediments and can be followed regionally outside the Miocene basins. A quantification is achieved by the means of a field kinematic study correlated with available information on timing, orogenic structure and evolution, seismicity, crustal stress pattern and GPS motions. The results are discussed in the context of characterizing deformation mechanics and understanding regional effects associated with the Adriatic indentation in the larger framework of the neighbouring Southern Alps, Albanides, Hellenides and Apennines orogens.

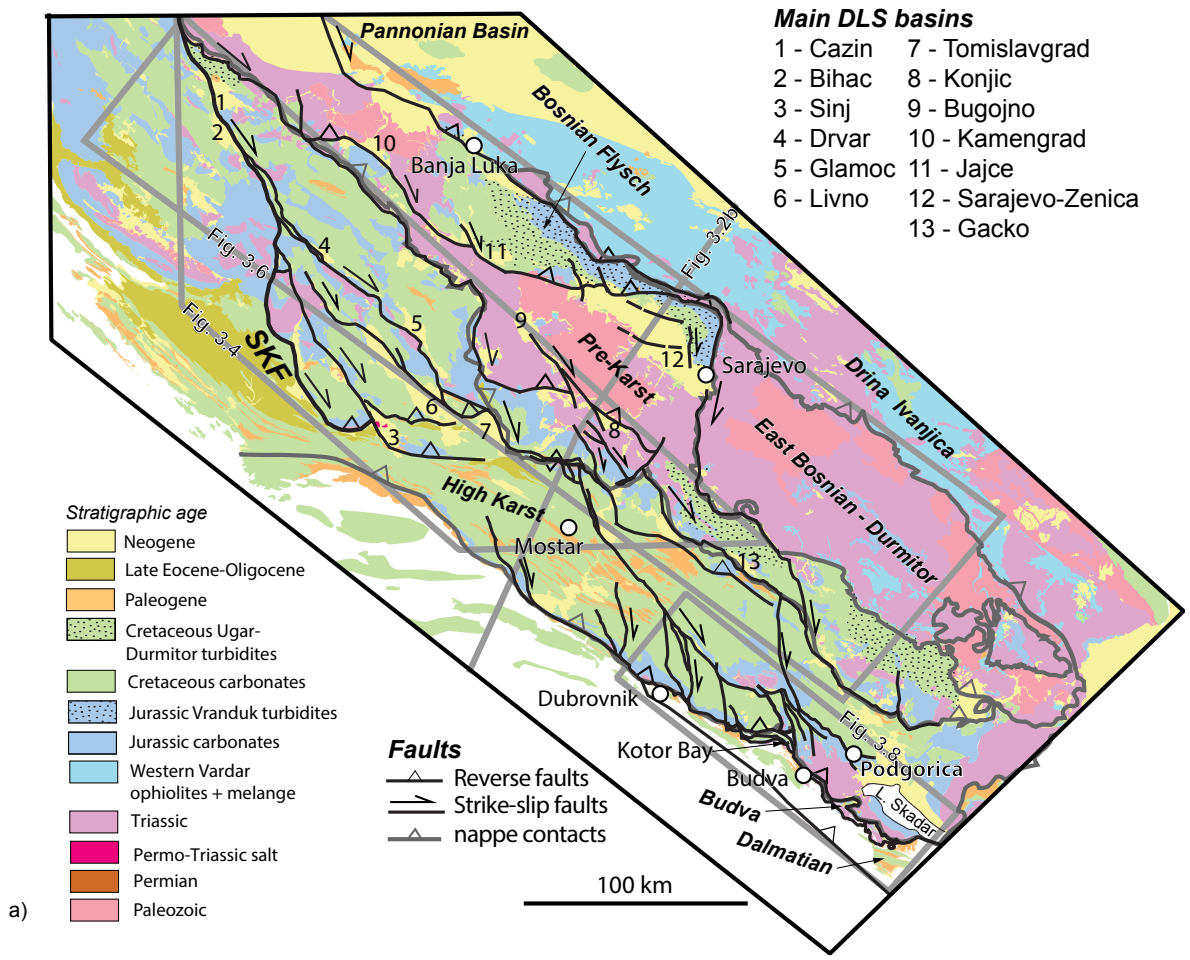


Figure 3.2 a) Geological map of the central and south-eastern part of the Dinarides (simplified from 1:100.000 maps of former Yugoslavia – OGK, Osnova Geoloska Karta) overlaid by the post- 9 Ma fault system mapped in this study and the major nappe contacts depicted in Figure 3.1. Note that other faults, such as late Jurassic - Eocene thrusts or Miocene normal faults, are not displayed in this map for simplicity. This is in contrast with Figure 3.2b, where these faults are displayed. Note also the location of the main Miocene Dinarides Lake System (DLS) basins (Harzhauser & Mandic, 2008; Mandic et al., 2012). Grey polygons are the locations of maps in Figures 3.4, 3.6 and 3.8. The grey line is the location of the cross-section in Figure 3.2b. SKF = Split – Karlovac Fault; *(continued on next page)*

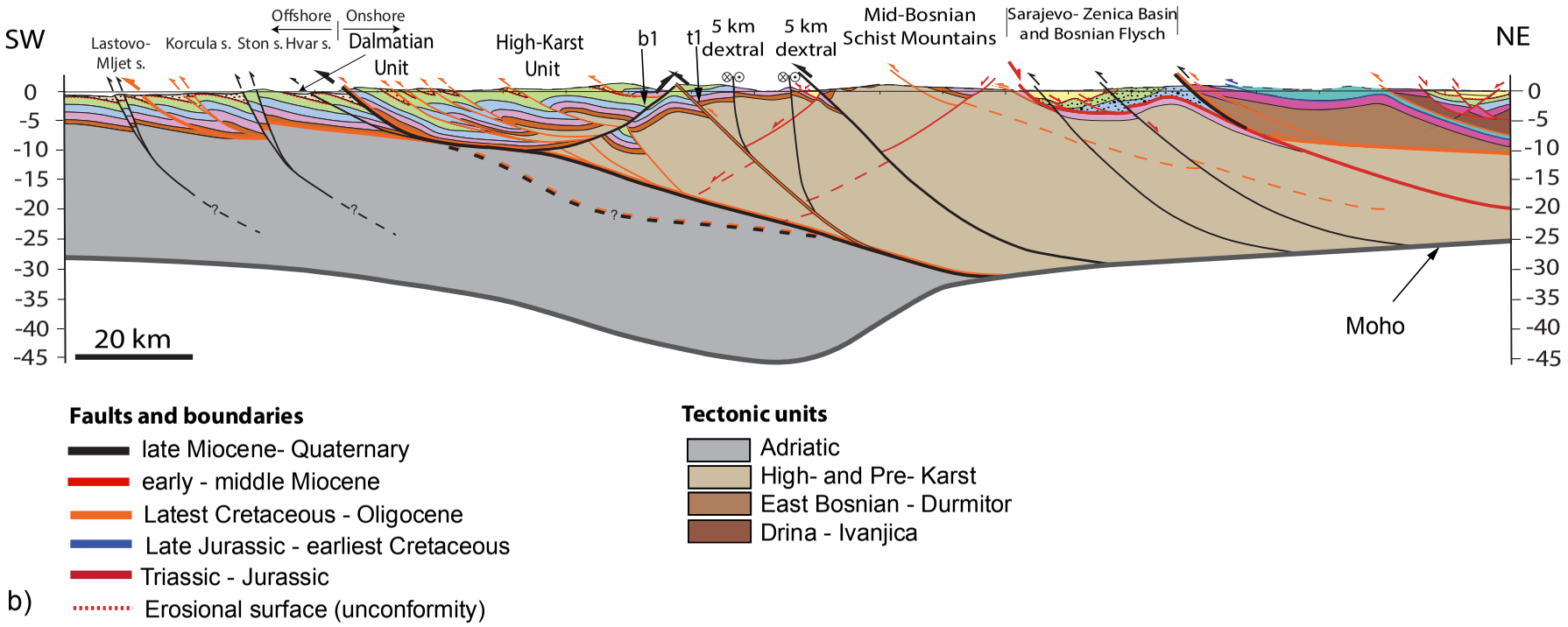


*Figure 3.2 (continued)* b) Cross-section over the central part of the Dinarides (for further details see the description of the same cross-section in Figure 2.11, Chapter 2). Note that colours and symbols of lithostratigraphic units are the same as in Figure 3.2a. Note also the superposition of deformation between older late Jurassic - Eocene thrusts, early-middle Miocene normal faults and younger post- middle Miocene structures. t1 and b1 are the thrust and backthrust discussed in the text and displayed also in Figure 3.6a.

## 3.2 The Dinarides orogenic evolution and the Adriatic indentation

The Dinarides are part of a Mediterranean orogenic system that evolved during Mesozoic–Cenozoic times (Figures 3.1 and 3.2). The opening of a northern branch of the Neotethys Ocean located between Adriatic- and European- derived continental units took place during the Middle Triassic (e.g., Schmid et al., 2008; Stampfli & Borel, 2002). Structures associated with this opening are rather scarce in the presently observed Dinarides nappe stack, but a NE-SW direction of extension has been inferred in the internal Dinarides and the Budva Unit of Montenegro (e.g., Toljić et al., 2013; van Unen et al., 2019). The Neotethys opening in the Dinarides was associated with widespread rifting magmatism and the subsequent formation of a wide passive Adriatic continental margin (e.g., Dimitrijevic, 2001; Pamic, 1984). While the proximal part of this continental margin (SW-wards in Figure 3.2a) recorded almost continuous and thick Triassic–Paleocene shallow-water carbonate sedimentation (in the Dalmatian, High-Karst and Pre-Karst units in Figures 3.1-3.3), its distal parts (NE-wards in Figure 3.2a) recorded gradual subsidence and deepening of a carbonate to marine pelagic facies during Middle Triassic - Lower Jurassic times (Figure 3.3, Korbar, 2009; Schefer, 2010; van Gelder et al., 2015; Vlahovic et al., 2005).

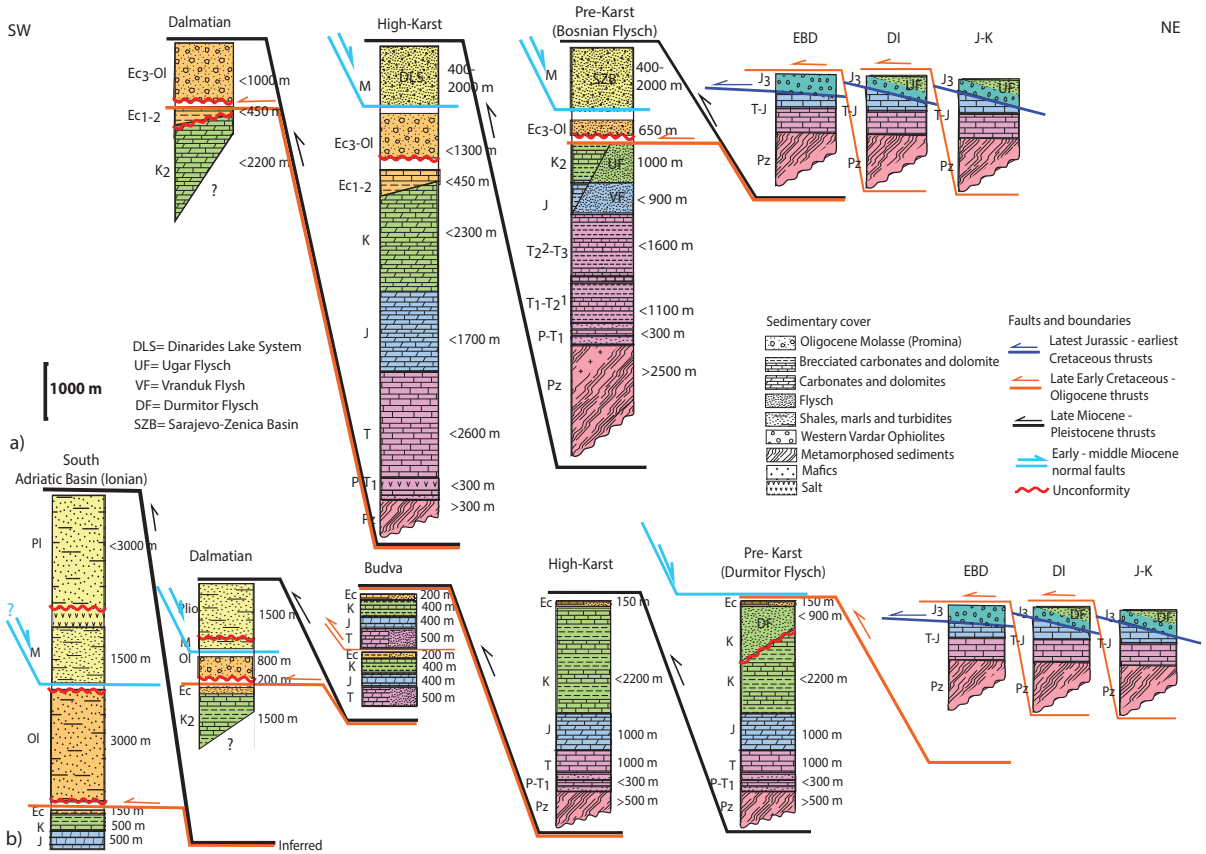


Figure 3.3 Correlation of lithostratigraphic columns across various Dinarides tectonic units. a) the north-western part of the Dinarides; b) the south-eastern part of the Dinarides. All columns are simplified and correlated from surface mapping studies (1:100.000 maps of former Yugoslavia – OGK, Osnova Geoloska Karta), except the South Adriatic column that is derived from offshore wells (see Bega, 2015 for further details). Whenever outcropping, the Variscan

*Figure 3.3 (continued)* basement is overlain by Permian - Lower Triassic continental deposits and/or evaporites. In the external part of Dinarides, upper Lower Triassic - Paleocene carbonates reach 2-3 km in cumulative thickness. Ages: Pl= Pliocene, Pl= Pliocene–Pleistocene, M= Miocene, $Ec_{1-2}$= lower-middle Eocene, $Ec_3$-Ol= upper Eocene - Oligocene, Ec= Eocene, $K_2$= Upper Cretaceous, K= Cretaceous, J= Jurassic, $J_3$= Upper Jurassic, $T_3$= Upper Triassic, $T_2^2$= upper Middle Triassic, $T_2^1$= lower Middle Triassic, $T_1$= Lower Triassic, P-$T_1$= Permo–Triassic, P= Permian and Pz= (locally metamorphosed) Palaeozoic.

The exception is the Middle Triassic formation of the external located Budva graben (Figure 3.3b), which recorded continuous deep-water carbonatic to pelagic sedimentation until Cretaceous times, interrupting the spatial continuity of the Adriatic shallow-water carbonate sedimentation (Cadjenovic et al., 2008; Crne et al., 2011; Gorican, 1994; Vlahovic et al., 2005). Laterally, the Budva unit can be correlated with similar deep-water deposits located in the Krasta-Cukali and Pindos units of Albania and Greece, respectively (Figure 3.1, e.g., Korbar, 2009; Robertson & Shallo, 2000; Schmid et al., 2008).

### 3.2.1 Orogenic deformation in the Dinarides

The onset of the Middle Jurassic Neotethys oceanic subduction continued with a Late Jurassic–earliest Cretaceous obduction of the Western Vardar Ophiolitic unit over the Adriatic margin, which is observed by top- NW to -WNW thrusting of ophiolites and associated ophiolitic melanges overlying in an upper structural position the internal-most units of the Dinarides (Figure 3.1, e.g., Dimitrijević, 1997; Robertson et al., 2009; Schmid et al., 2008). Subduction continued during Cretaceous times and peaked with the latest Cretaceous–earliest Paleogene collision between Adriatic- and European- derived continental units that was associated with the formation of a suture zone at their contact (the Sava Zone, Figure 3.1, Pamić, 2002; Toljić et al., 2018; Ustaszewski et al., 2009). Orogenic movements continued by renewed Eocene – Oligocene shortening, recorded with larger offsets in the external part of the Dinarides and with reduced amplitudes in more internal units (Andrić et al., 2017; Dimitrijević, 1997; Stojadinovic et al., 2017; Ustaszewski et al., 2010). All these Cretaceous – Paleogene orogenic deformations are characterized by NE-SW oriented contraction and have created the presently SW-ward verging Dinarides nappe stack (Figure 3.2b). The peak deformation episodes were associated with the deposition of contractional turbidites ("flysch" deposits) in the footwall of various nappe units. The thickest deposition of such turbidites is observed in the Bosnian Flysch zone (Figure 3.2a), which is located in the footwall of the ophiolite-carrying East Bosnian - Durmitor thrusting and can be possibly correlated laterally with similar turbidites located in the footwall of the adjacent Southern Alps thrusting (the Tolmin Flysch, Dimitrijević, 1997; Goričan et al., 2012; Hrvatović & Pamić, 2005; Tari, 2002). The deposition of the Bosnian Flysch started during Late Jurassic times (the Vranduk Flysch component) and continued with larger amounts during latest Cretaceous (Maastrichtian) times (the Ugar-Durmitor Flysch component, Figures 3.2 and 3.3), while this deposition was locally interrupted by unconformities (Dimitrijević, 1997; Hrvatović, 2006; Hrvatović & Pamić, 2005; Mikes et al., 2008; Schmid et al., 2008). In a more external position, the Eocene thrusting of the High-Karst and Budva units was associated with the coeval sedimentation of turbidites in their footwall and was synchronous and followed elsewhere by the late Eocene – Oligocene deposition of a

shallow-water to alluvial continental regressive sequence (Figure 3.3, e.g., the Promina "molasse", Mrinjek, 1993; Tari and Mrinjek, 1994; Zupanič & Babić, 2011).

These successive orogenic building episodes were followed by a period of early-middle Miocene extension that affected large areas of the Dinarides. This extension was widely observed along the NE contact with the Pannonian Basin, where the Sava Zone was reactivated along its entire strike by the creation of multiple extensional detachments (e.g., Ustaszewski et al., 2010; van Gelder et al., 2015). The extension affected also more external Dinarides areas, where it created many of the basins that are part of the Dinarides Lake System (Figure 3.1, Andrić et al., 2017; Harzhauser et al., 2011; Mandic et al., 2012; van Unen et al., 2019). The 18 Ma onset of extensional deposition observed in these basins post-dates the ~20 Ma onset of back-arc extension observed in the neighbouring southern Pannonian Basin, interpreted to be driven by the roll-back of the Carpathians slab (de Leeuw et al., 2012; Horváth et al., 2015; Mandic et al., 2012; Pavelić & Kovačić, 2018). It also postdates the Oligocene onset of extension observed in the south-eastern part of the Pannonian Basin, near the contact with the Carpathians units (e.g., Erak et al., 2017). In the Dinarides, the amounts of extension observed decreased after 15 Ma (when deposition in smaller basins like Sinj or Gacko terminated) and was still active until 14 Ma in the Sarajevo-Zenica Basin and until 13 Ma in the Livno and Tomislavgrad basins (Figure 3.2, de Leeuw et al., 2011; de Leeuw et al., 2010; Mandic et al., 2011; Sant et al., 2018). Extension peaked at ~15-14 Ma in the neighbouring Pannonian Basin over a 15 Ma transition from alluvial and lacustrine to marine deposition, while gradually expanding southwards until 12.8 Ma (Mandic et al., 2019a; Mandic et al., 2019b; Pavelić & Kovačić, 2018). Interrupted by a short inversion event at the transition between middle and late Miocene, the back-arc extension continued in the southern Pannonian Basin during the late Miocene until ~8 Ma, when the Carpathians subduction zone was locked and the associated thin-skinned shortening ceased (Balázs et al., 2016; Matenco et al., 2016; Matenco & Radivojević, 2012).

### 3.2.2 N- to NE-ward Adriatic indentation in the Dinarides and neighbouring areas

The onset of the N-ward motion and indentation of the Adriatic unit was recorded in the Southern Alps starting with the latest Oligocene – early Miocene, and was associated with a lateral extrusion of the Eastern Alps into the Pannonian Basin starting at ~20 Ma and is still presently observed at a convergence rate of ~2-5 mm/yr (Grenerczy et al., 2005; Handy et al., 2010; Horváth et al., 2015; Ratschbacher et al., 1991). Strike-slip and contractional deformation is observed north and south of the right-lateral Peri-Adriatic Lineament, with larger amounts of upper crustal exhumation northwards (Figure 3.1, Handy et al., 2014; Heberer et al., 2017; Tomljenovic et al., 2008).

In the external Dinarides, the NNW-SSE oriented Split-Karlovac Fault (Figures 3.1 and 3.2) is thought to be one of the major structures formed during the Adriatic indentation (e.g., Ustaszewski et al., 2008), although no kinematic or timing data were so far provided. GPS studies show a 4-5 mm/yr N- to NE- ward present-day movement of the Dinarides with respect to a stable European framework (Grenerczy et al., 2005; Pinter et al., 2005). Furthermore, moderate to strong earthquakes are distributed along many fault systems in the Dinarides (e.g.,

Herak et al., 2009; Ustaszewski et al., 2014), although the kinematics of these faults is largely unknown. The overall Adriatic indentation is thought to have been associated with its counter-clockwise rotation and (continental) subduction, indicated from a high-velocity anomaly observed during geophysical studies beneath the Dinarides (Bennett et al., 2008; Šumanovac & Dudjak, 2016; Šumanovac et al., 2017). Although debated, these studies have inferred that the subducting slab in the SE part of the Dinarides reaches depths of up to 450 km, while remaining at shallower levels NW-wards (Šumanovac et al., 2017).

Although reconstructions generally assume that indentation associated with subduction started in the Dinarides at the same ~20 Ma times as in the Alps (Le Breton et al., 2017), observations indicate different onset ages. Obviously, one cannot define an indentation mechanism in areas of the Dinarides at times where the above described Miocene extension was observed. In more details, the age of the youngest E-W to NE-SW oriented Dinarides thrusts, folds and strike-slip faults located near the contact with or inside the Pannonian Basin is generally thought to post-date either the middle Miocene or the entire Miocene in the centre and north-west (e.g., Fodor et al., 2005; Tomljenović & Csontos, 2001; Tomljenovic et al., 2008; Ustaszewski et al., 2014), or started at around 8.8-8.0 Ma in the south-east (Matenco and Radivojević, 2012; Toljić et al., 2013). Sedimentation continued in some intramontane basins of the Dinarides Lake System during the late Miocene. A 700m thick coarsening upwards succession is observed in limited areas of the Sarajevo-Zenica Basin (the Orlac conglomerates), interpreted to be syn-contractional (Figure 3.2, see discussion in Andrić et al., 2017). Palynological data from the intercalated coal seams provide a good stratigraphic correlation with the 8.8-5.4 Ma age of similar deposits found in the southern part of the Pannonian Basin (Magyar & Geary, 2012; Pantić et al., 1966). The Livno and Tomislavgrad Basin (Figure 3.2) recorded two late Miocene sedimentation cycles divided by an unconformity, which are correlated with the Pannonian Basin stratigraphy at 11.6-8.8 Ma and 8.8-4.5 Ma (Magyar & Geary, 2012; Milojevic & Sunaric, 1962; Milojević & Sunarić, 1964; Pantić & Bešlagić, 1964). The first cycle follows the outline of the two basins, while the second one shows a splitting of depocenters that can be interpreted to be syn-kinematic in respect to contraction and transpression (de Leeuw et al., 2011; van Unen et al., 2019). The cessation of Dinarides lacustrine deposition occurred ~ 5 Ma, which correlates with a regional unconformity observed in the southern Pannonian Basin (Pavelić & Kovačić, 2018; Ustaszewski et al., 2014). All these observations and interpretations suggest that the regional onset of contraction/transpression in the Dinarides and the southern Pannonian Basin inversion started somewhere ~ 8.8-8.0 Ma. We will further refer to this overall deformation event as the post- 9 Ma Adriatic indentation in the Dinarides.

## 3.3 Methodology and approach

We have performed a kinematic study in key areas along the external Dinarides strike that was focused on characterizing the post-Paleogene deformation events. The deformation observed in the lower – middle Miocene sediments of the Dinarides Lake System was used as a key timing indicator to discriminate the latest deformation event from pre-dating tectonic episodes. These sediments were deposited initially during an extensional event that was followed by inversion associated with strike-slip and thrusting, observed locally in the studied

area or elsewhere in the Dinarides (Andrić et al., 2017; van Unen et al., 2019; Žibret & Vrabec, 2016). We started by mapping large-scale structures that inverted the Miocene basins and collecting a new kinematic dataset by studying these structures in higher details. Wherever possible, we followed these structures along their strike outside the basins, where they truncate in map view the inherited pre-Miocene nappe structure. Structures were separated in areas located outside basins per deformation event, which has been done by using superposition criteria derived from cross-cutting or re-activation relationships. Such criteria are in agreement with the kinematics observed in the Miocene basins, which remained the main criteria for discriminating the superposition of deformation and its associated timing.

Since the area is unusually large for one kinematic study (Figure 3.2) we focussed and restricted our analysis only to clear and large offsets faults, identified to have significant stratigraphic offset in map view and observed in the field to be associated with shear zones or faults with large (hundreds of metres to kilometres) displacements. The identification of such large offset shear zones or faults is rather direct in map view, owing the exceptional quality and full coverage of the 1:100.000 scale geological maps available (OGK Former Yugoslavia). We specifically note that most of our measurements are taken in such major shear zones characterized often by the development of wide fault gouge foliations or high density of faults having the same kinematics in a narrow deformation zone. The kinematics of the pre-Miocene deformation is rather known to a large extent from previous regional, structural and kinematic studies (Andrić et al., 2017; Dimitrijević, 1997; Schmid et al., 2008; Ustaszewski et al., 2010), including in the study area (Figure 3.2b, van Unen et al., 2019), as described in the previous chapter. We have used this existing knowledge to further discriminate the kinematics of pre-Miocene events in the field and separate it from the significantly different character of the subsequent deformation, an observation confirmed by superposition criteria.

Field measurements included brittle structures, such as faults with their kinematic sense of shear derived from slickensides, Riedels, or drag-folds, other types of folds, shear foliations and shear-bands. All the kinematic data has been grouped per deformation event and plotted in stereonets (Figures 3.4-3.9). In a first stage, the measured kinematics of large offset faults was grouped by calculating paleostress directions for the same deformation event (Figures 3.4, 3.6, 3.8) by a direct inversion method (Angelier, 1979; Angelier, 1984; Delvaux & Sperner, 2003), accounting for confidence criteria (Sperner & Zweigel, 2010). This means that our study does not utilize the typical paleostress approach where all faults are measured in specific restricted areas where the paleostress field is calculated, but we specifically targeted and measured the kinematics of large offset faults inverting Miocene basins to define more regional paleostress directions. This type of kinematic approach is better suited for the large size of our study area, when compared with the typical local stations paleostress approach measuring all faults that create stress patterns often difficult to connect at regional scale.

Our observations show that the early-middle Miocene normal faults and all predating structures associated with Cretaceous - Paleogene NE-SW oriented shortening, Late Jurassic - earliest Cretaceous ESE-WNW oriented shortening and Middle Triassic NE-SW oriented extension are truncated by a complex interplay between large-offset strike-slip, high-angle reverse faults and thrusts. As expected for such a complex interplay, the analysis has demonstrated that paleostress is not entirely suitable for defining regional tectonic phases because of large amounts of vertical axis rotations and strain partitioning observed near and at

large distance from large-offset structures during the same deformation event. In particular, we observed a drag effect by clockwise rotations of faults and folds situated in the vicinity and truncated by large-offsets dextral shear zones. All this deformation affects the Miocene basins and given the time-span of deformation (post- 9 Ma and presently active), it is likely that these faults and folds formed earlier and were dragged, rotated clockwise and truncated later by the large offset dextral shear zones. For instance, NW-SE to NNW-SSE oriented dextral and NNE-SSW to NE-SW oriented sinistral faults are rotated to NNW-SSE to N-S oriented dextral and NE-SW to ENE-WSW oriented sinistral faults, respectively (Figures 3.4a, 3.6a and 3.8a). At the same time, reactivation of releasing or restraining strike-slip bends or step-overs creates strain partitioning of deformation and calculated paleostress directions due to vertical axis rotations. Such limitations of the paleostress methodology are otherwise well-known, particularly when deformation affects structurally anisotropic rocks (e.g., De Vicente et al., 2009; Jones & Tanner, 1995; Lacombe, 2012), while the exact amounts of vertical axis rotations during dragging or strain-partitioning are generally difficult to restore.

Given these overall limitations, we decided to group faults in a first stage by field observations and during paleostress inversion in two strike-slip and one compressional paleostress fields, no matter that sometimes there is an up to 25° deviation from a theoretical shear planes (Figures 3.4, 3.6 and 3.8b-d). Subsequently we added one other methodology (Andrić et al., 2017; van Gelder et al., 2015), where the observed deformation was described by defining directions of regional tectonic transport in map view and cross-sections. This methodology and the connection between large offset faults observed in the field have demonstrated that these three paleostress fields are in fact the result of the same long-lived deformation event. The differentiation between stress calculations (compression-tension) and strain observations (contraction-extension) is subsequently used in the description of deformation events.

Our field kinematic observations of the early-middle Miocene extensional event and predating deformation are very similar with results of previous studies in the Dinarides outside the studied area. Therefore, although used in the documentation of field structures below, we have decided to focus our structural analysis only to structures associated with the inversion of Miocene basins. This has led to the definition of a post- middle Miocene fault system that spans across the entire studied area of the central and south-eastern Dinarides (Figure 3.2a). Since a large part of this fault system is still presently active, we have furthermore correlated our kinematic data with previous studies on GPS motions, crustal stress patterns, seismicity, crustal geophysics and other geodynamic quantifications. This correlation has been performed in the Dinarides and at the larger-scale of the Adriatic continental micro-plate, in order to connect regionally observed deformation patterns and derive a genetic mechanism.

## 3.4 Kinematic data along the Dinarides strike

The observed post-Paleogene structures are either normal faults that formed during the onset of early-middle Miocene basin sedimentation or a combination between strike-slip connected with high angle reverse faults or thrusts that post-date (i.e. truncate) the entire Miocene sedimentation. These strike-slip and contractional structures are connected by forming an anastomosing system of faults that truncate most of the studied Dinarides area from the NW to

the SE (Figure 3.2a). These structures may be geometrically grouped in three main areas based on the amplitude and character of deformation, i.e. the Split-Karlovac faults system, the Bosnian Flysch and connecting faults system, and the Budva unit and connecting faults system (Figures 3.4, 3.6 and 3.8, respectively).

### 3.4.1 The Split-Karlovac faults system

In the NW part of our studied area, the Split-Karlovac faults system was mapped in the field to be composed of one main fault zone in the NW that gradually branches off SE-wards to four main dextral strike-slip faults (Figure 3.4a).

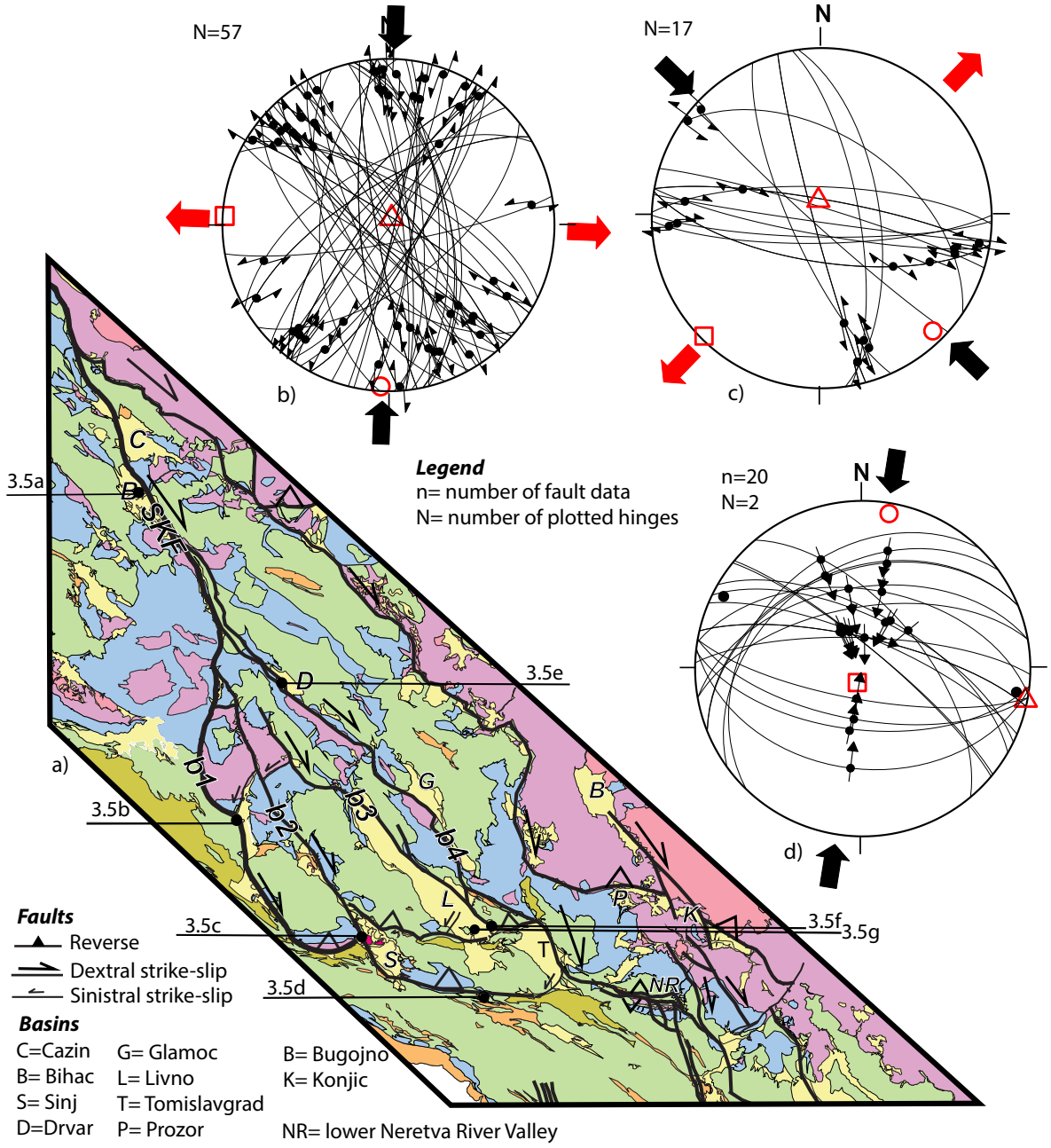


Figure 3.4 Structural map and kinematic data for the Split-Karlovac and connecting fault system. Note that only structures active in the post- 9 Ma phase of deformation are displayed in the map and plotted on stereonets (Schmidt projection, lower hemisphere). In stereonets,

*Figure 3.4 (continued)* lines with arrow symbols are projections of fault planes with kinematic sense of shear, while thick black dots are projections of fold hinges. a) Geological map with structures active during the post- 9 Ma phase of deformation. b1-4 are individual branches of the fault system. SKF = Split-Karlovac Fault (branch b1 of the fault system). Same conventions and legend as in Figure 3.2a. Location of the map is displayed in Figure 3.2a; b) Stereoplot showing NW-SE to NNW-SSE oriented dextral and their conjugate NNE-SSW to ENE-WSW oriented sinistral strike-slip faults. The calculated paleostress field shows N-S oriented compression and E-W oriented tension; c) Stereoplot showing WNW-ESE oriented dextral and NNW-SSE oriented sinistral strike-slip faults. The calculated paleostress field shows NW-SE oriented compression and NE-SW oriented tension; d) Stereoplot showing reverse faults and two sub-horizontal fold hinges, the calculated paleostress field shows N-S to NNE-SSW oriented compression.

In outcrops, often larger offset WNW-ESE to N-S oriented dextral strike-slip faults are associated with smaller offset NNW-SSE to NE-SW oriented conjugate sinistral faults. These faults define two strike-slip paleostress fields, one with a N-S oriented compression direction and one with a NW-SE oriented compression direction (Figure 3.4b,c). In map scale, the large-offset dextral faults change their strike and connect to thrusts or high-angle reverse faults (Figure 3.4a). This is observed in outcrops by numerous WNW-ESE to WSW-ENE oriented large offset thrusts and high-angle reverse faults associated with few similarly oriented (drag-) folds, which define a N-S to NNE-SSW oriented compressional stress field (Figure 3.4d). All these structures truncate, reactivate or fold the lower-middle Miocene sediments of the basins and the pre-Miocene nappe structure (Figure 3.4a). The large-offsets strike-slip faults can be often observed at the present-day basin margins (Figure 3.4a), which suggests transpressive movements associated with uplift and exhumation.

In the NW part of the studied area, near the Cazin and Bihac basins, the Split-Karlovac deformation is focused on one main NNW-SSE oriented fault that is located at the western margin of the former and the eastern margin of the latter (Figure 3.4a). In outcrops, NNW-SSE oriented dextral shear zones cross-cut inherited and similarly oriented normal faults that are observed, for instance in the Upper Jurassic limestones at the eastern margin of the Bihac Basin (Figure 3.5a). The lower-middle Miocene sediments are truncated by similarly oriented normal faults that are tilted together with the bedding near the margins affected by faulting. However, the Split-Karlovac Fault itself (fault b1 in Figure 3.4a) and its vicinity is affected by significant diapirism of the Permo-Triassic salt and other evaporites (Šušnjara et al., 1992; Tišljar, 1992), which makes a clear discrimination of tectonic deformation rather difficult. This is rather obvious by the uplift of diapirs along the fault in its central part and in the Sinj Basin, east of the junction between two major branches of the system (Figure 3.4a, see also de Leeuw et al., 2010).

From the north-west to the south and south-east, the strike-slip deformation is gradually being distributed along a wide area where the previously mapped Split-Karlovac Fault is the westward branch of our post- middle Miocene fault system (fault b1 in Figure 3.4a). Along this fault trace, often dextral transpressive truncations and drag-folding of the steeply dipping (50-60°) Upper Eocene – Oligocene Promina beds is observed (Figure 3.5b). In the same area, deformation is also associated with smaller-offset NE-SW oriented sinistral strike-slip faults and shear zones with fault gouge foliations that reach kilometres offsets (NE of point 5b in

Figure 3.4a). More to the SE, the Split-Karlovac Fault changes strike and become a high-angle reverse fault, where the Triassic clastics and limestones in the hanging-wall are thrusted over gradually tilted Promina and lower Miocene sediments of the Sinj Basin (SE termination of fault b1 in Figure 3.4a).

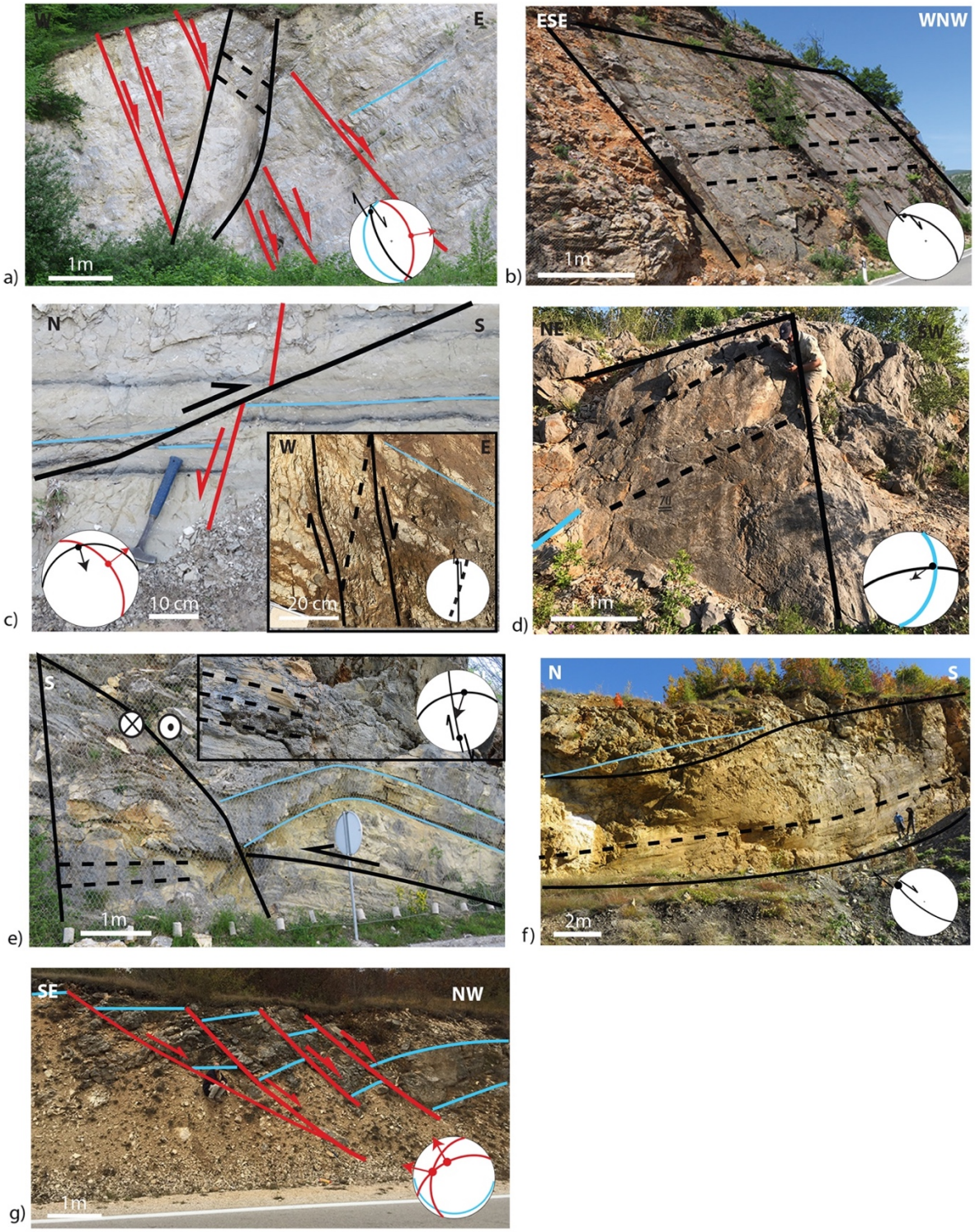


Figure 3.5 Interpreted field photos illustrating structures and their kinematics in the area of the Split-Karlovac and connecting fault system (locations in Figure 3.4a). Red lines: early–middle Miocene faults, black lines: post- 9 Ma faults, blue lines: bedding. a) One NW-SE oriented dextral strike-slip shear zone cross-cutting (E)NE-dipping normal faults in Jurassic limestones

*Figure 3.5 (continued)* along the NE flank of the Bihac Basin; b) One large offset NW-SE oriented dextral strike-slip fault truncating Cretaceous limestone deposits along the Split-Karlovac Fault; c) One small-offset S-vergent reverse fault cross-cuts a NE-dipping normal fault, adjacent to a N-S oriented dextral strike-slip fault gauge zone with Riedel shears in lower Miocene lacustrine sediments of the Sinj Basin; d) One high-angle SW-vergent reverse-sinistral fault in Cretaceous limestones located in the footwall of a large-offset high-angle reverse fault; e) One NNW-SSE oriented dextral strike-slip fault cross-cuts a low-angle SSW-vergent reverse fault and drag folding in Jurassic limestones situated along the SW flank of the Drvar Basin. The upper right inset shows slickensides along the strike-slip fault plane; f) Large-offset NW–SE oriented dextral strike-slip shear zone truncating Miocene sediments and Cretaceous limestones in the SE part of the Livno Basin; g) One system of NW-dipping normal faults located in the Livno Basin.

To the NE, the second branch of the Split-Karlovac faults system (fault b2 in Figure 3.4a) offsets the Promina beds and the Miocene sediments of the Sinj Basin near its SE-ward termination. This deformation is visible in the basin, for instance by centimetres to metres scale ENE-WSW oriented thrusts and N-S oriented strike-slip faults and shear zones that truncate centimetres- to metres-scale offsets normal faults (Figure 3.5c). Truncation of stratigraphic markers shows that the offset of this second dextral strike-slip branch is in the order of a few kilometres in the north and increases to 10-15 km in the Sinj Basin (Figure 3.4a). At its SE termination, the dextral strike-slip branch changes its strike and connects with a reverse fault. The offset of this reverse fault gradually decreases eastwards as observed by the stratigraphic duplication of Jurassic – Cretaceous limestones in its hanging-wall emplaced over Cretaceous – Oligocene limestones and clastics (including Promina beds) of the footwall (Figure 3.4a). In outcrops, reverse faults often show a strike-slip component that changes from dextral in the west to sinistral in the east (Figure 3.5d).

One other branch of the Split-Karlovac faults system (fault b4 in Figure 3.4a) crosses the SW margin of the Drvar and Glamoc basins. In more details, NNW-SSE oriented dextral strike-slip faults changes their strike to or truncate ~S-vergent fault-bend folds affecting the Lower Cretaceous sediments and offsets Cretaceous limestones that border the western margin of the Drvar Basin (Figure 3.5e). This dextral deformation also cross-cuts normal faults observed at the SW margin of the Glamoc Basin. To the SE, the third and fourth branches of the Split-Karlovac system (faults b3 and b4, Figure 3.4a) truncate the SE part of the Livno Basin, where they form a large transpressive structure that splays and transfer offsets between dextral strike-slip to high angle reverse faults and transpressive structures. In this area, a 7-10 m thick shear zone made up by a foliated fault gouge can be observed, which has a clear NW-SE oriented dextral strike-slip character (Figure 3.5f). The foliation is made up of fault gouge material that contains remnants of sheared Cretaceous limestones and Miocene lacustrine marls. This shearing also truncates the system of domino-tilted normal faults observed in the Miocene sediments (Figure 3.5g), while forming large drag-folds by tilting these strata to sub-vertical positions. The deformation associated with the overall transpressive structure at the SE margin of the Livno Basin is transferred to the eastern margin of the Tomislavgrad basin by swinging its strike to E-W and backwards along a system of reverse faults associated with large drag-folding of the Cretaceous – Oligocene carbonates and clastic sediments in its footwall (Figure 3.4a). In fact, it is rather clear that Livno and Tomislavgrad formed as one basin during the

Miocene extension and were separated by a subsequent uplift associated with the transpressive system located at the present SE margin of the Livno Basin (see also de Leeuw et al., 2011). Further to the SE (Figure 3.4a), the dextral fault at the eastern margin of the Tomislavgrad Basin changes again its strike and is connected to a system of N- and S- vergent high angle reverse faults that make the connection with the dextral fault observed along the Neretva River Valley.

### 3.4.2 The Bosnian Flysch and connecting faults system

The second group of structures made up by strike-slip combined with reverse faults cross-cutting or reactivating the Miocene basins and pre-Miocene orogenic structure are observed along a wide zone combining the southern margin of the East Bosnian – Durmitor unit, the Bosnian Flysch and the southern margin of the Mid-Bosnian Schist Mountains (Figure 3.6a). In outcrops, often large-offset WNW-ESE to N-S oriented dextral strike-slip faults are associated with smaller offset NNW-SSE to ENE-WSW oriented conjugate sinistral strike-slip faults. These faults define two strike-slip paleostress fields, one with a NNE-SSW oriented compression direction and one with a NW-SE oriented compression direction (Figure 3.6b,c). Large-offset dextral faults change their strike and connect to thrusts or high-angle reverse faults (Figure 3.6a). These WNW-ESE to WSW-ENE oriented large offset thrusts and high-angle reverse faults define a NNE-SSW oriented compressional stress field (Figure 3.6d). The reverse faults can often be associated with drag and upright folds with ~E-W to WNW-ESE oriented hinges. All these structures deform or truncate the lower-middle Miocene sediments and the genetically associated normal faults in the Kamengrad, Jajce, Mrkonjic Grad, Sarajevo-Zenica and Konjic basins and the pre-Miocene nappe structure located along their flanks (Figure 3.6a). Large offset faults are generally dextral transpressive or high-angle reverse verging southwards, which suggests significant exhumation of the basins and their flanks.

In the NW, normal faults are often cross-cut or observed in the vicinity of strike-slip faults (Figure 3.7a). Normal faults with similar orientations are furthermore observed in the lower part of the lower-middle Miocene sediments of the Kamengrad basin (Figure 3.7b), which are covered or absent in the upper stratigraphy of this basin. A large NNW-SSE oriented dextral strike-slip fault with an offset in the order of 7 km offsets the Miocene fill of the Kamengrad basin (Figure 3.6a).

A NNW-SSE oriented dextral strike-slip shear zone with a displacement in the order of 10 km offsets also the Miocene basin fills of the Mrkonjic Grad and Jajce basins (Figure 3.6a). This shear zone is visible in both the Miocene sediments and the Lower Cretaceous limestones situated along their flank, where it forms large fault planes with clear slickensides (Figure 3.7c) or shear zones with fault gouge foliations. To the SE, this fault zone changes gradually its strike to NW-SE and WNW-ESE, and is connected with an E-W oriented shear zone with reverse, sometimes oblique offset and S-ward vergence. In outcrops, this shear zone is observed as an up to 4m thick foliated fault gouge that contains numerous brittle S-C and C-C' shear-bands or Riedel structures (Figure 3.7d). This shear zone drag-folds the strata or other foliated fault-gouge material in its footwall.

The Bosnian Flysch zone flanking the Sarajevo-Zenica Basin (Figure 3.6a) retains a large amount of deformation that recorded both the pre-Miocene orogenic evolution, the Miocene extension and the subsequent inversion affecting the basin and its flanks (see also van Unen et

al., 2019). The latter structures are made up by large offset dextral strike-slip shear zones, high-angle reverse faults and thrusts with top-S sense of shear, layer parallel shearing and E-W oriented folds. For instance, often layer-parallel top-S shearing affects the finer members of the turbidite beds, observed by brittle shear bands and asymmetric folds (Figure 3.7e). The contact zone between the East – Bosnian Durmitor and Bosnian Flysch units is often re-activated with a top-S sense of shear along high-angle reverse faults associated with metres scale drag-folds (Figure 3.7f).

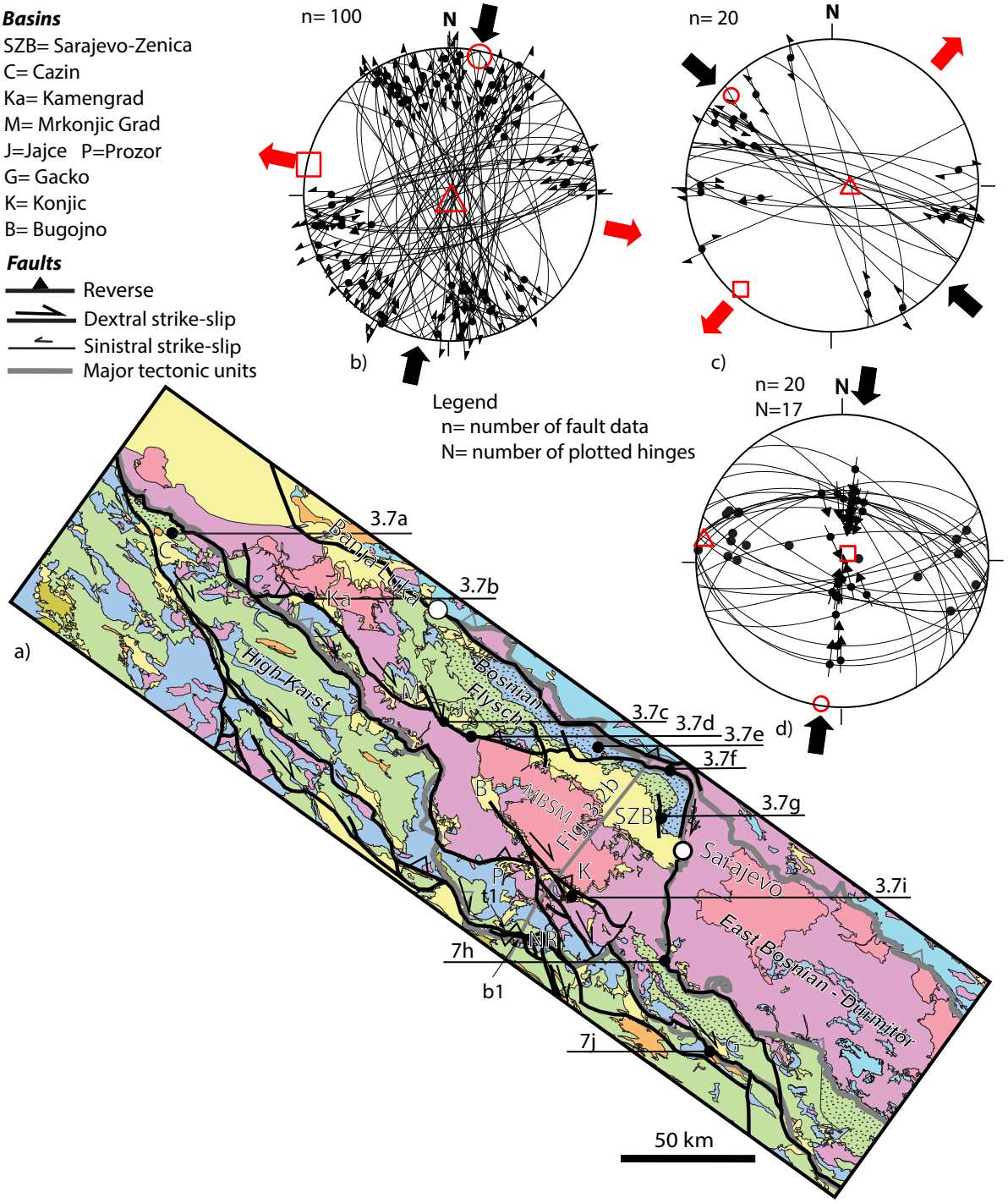


Figure 3.6 Structural map and kinematic data for the Bosnian Flysch and connecting fault system. Note that only structures active in the post- 9 Ma phase of deformation are displayed

*Figure 3.6 (continued)* in the map and plotted on stereonets (Schmidt projection, lower hemisphere). In stereonets, lines with arrow symbols are projections of fault planes with kinematic sense of shear, while thick black dots are projections of fold hinges. MBSM=Mid-Bosnian Schist Mountains. a) Geological map with structures active during the post- 9 Ma phase of deformation. Same conventions and legend as in Figure 3.2a. Location of the map is displayed in Figure 3.2a. t1 and b1 are the thrust and backthrust discussed in the text and displayed also in Figure 3.2b; b) Stereoplot showing NW-SE to N-S oriented dextral and their conjugate NNE-SSW to ENE-WSW oriented sinistral strike-slip faults. The calculated paleostress field shows NNE-SSW oriented compression and ESE-WNW oriented tension; c) Stereoplot showing WNW-ESE oriented dextral and NNW-SSE oriented sinistral strike-slip faults. The calculated paleostress field shows NW-SE oriented compression and NE-SW oriented tension; d) Stereoplot showing reverse faults with S- and N- sense of shear, and ~E-W oriented fold hinges. The calculated paleostress field shows NNE-SSW oriented compression.

At the eastern margin of the Sarajevo-Zenica Basin, a major NNW-SSE to N-S oriented dextral strike-slip shear zone, made up by several fault branches, cross-cuts both the Miocene basin sediments and the adjacent uppermost Cretaceous turbidites (Figure 3.7g). These branches are often observed by metres-thick foliated fault gouges with clear slickensides or corrugations, associated with brittle shear bands and Riedel shears. South of the Sarajevo-Zenica Basin, the eastern termination of the East Bosnian - Durmitor unit is most likely a large offset dextral fault that gradually changes strike and connects to an E-W oriented high-angle reverse fault (Figure 3.6a). The gradual change is characterized by the formation of NW-SE to WNW-ESE oriented dextral transpressive and positive flower structures, observed in the uppermost Cretaceous calci-turbidites of the Bosnian Flysch (Figure 3.7h). The total offset recorded by the dextral strike-slip system located at the eastern termination of the Sarajevo-Zenica Basin is rather difficult to calculate, but by accounting for the change in strike of the Bosnian Flysch and overlying East Bosnian – Durmitor unit (Figures 3.1 and 3.6a, the Sarajevo "sigmoid" of Dimitrijević, 1997) this offset can be estimated at 15-20 km.

South of the Mid-Bosnian Schists Mountains, one other transpressional strike-slip system can be observed in the southern part of the Bugojno Basin, that more to the south cross-cuts and offsets dextrally the Konjic Basin to the ESE from the Prozor Basin to the WNW (Figure 3.6a). The Miocene sediments of the Konjic Basin are affected by numerous up to 30m offset syn-depositional normal faults and by 3-4 subsequent major dextral shear zones associated with transpressional or high-angle reverse faults. For instance, a NW-SE oriented reverse shear zone crosscuts the centre of the basin and is associated with drag folding and tens of metres spaced fault branches (Figure 3.7i). The total cumulated offsets of this dextral system is in the order of 10-15 km (Figure 3.6a).

Further to the SE, the continuation of this fault system is less clear in map view (Figure 3.6a), but outcrops show numerous strike-slip faults, either WNW-ESE to NNW-SSE dextral or NNW-SSE to NNE-SSW sinistral that truncate often pre-existing normal faults. For instance, the Jurassic limestones and clastic sediments located on the SW flank of Gatsko Basin (Figure 3.6a) show ENE-WSW oriented normal faults that are truncated by WNW-ESE oriented dextral strike-slip faults (Figure 3.7j).

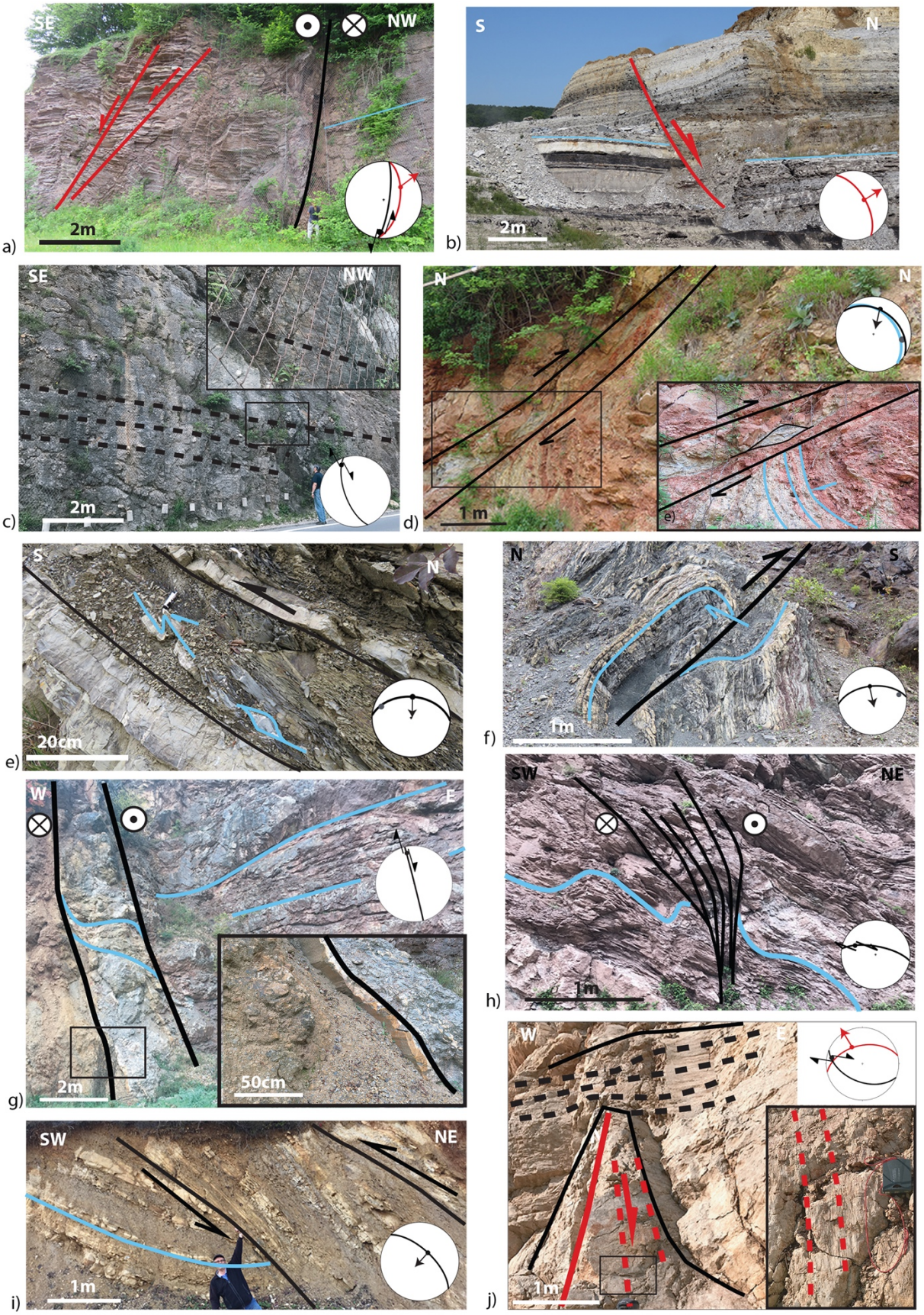


Figure 3.7 Interpreted field photos illustrating structures and their kinematics in the area of the Bosnian Flysch and connecting fault system (locations in Figure 3.6a). Red lines: early–middle Miocene faults, black lines: post- 9 Ma faults, blue lines: bedding. a) One NNE-SSW oriented

*Figure 3.7 (continued)* sinistral strike-slip shear zone adjacent to NE-dipping normal faults truncating uppermost Cretaceous turbidites of the Ugar Flysch along the NE flank of the Cazin Basin; b) One large-offset (~15 m) NE-dipping normal fault truncating the Miocene sediments of the Kamengrad Basin; c) One NW-SE oriented dextral strike-slip fault truncating Cretaceous limestones, part of a larger system of similarly oriented dextral strike-slip faults that offsets with ~10 km the Jajce from Mrkonjic Grad basins; d) One S-vergent reverse shear-zone truncating Cretaceous limestones located south of the Jajce Basin. The bottom right inset shows brittle shear-bands and Riedel shears formed in the fault gouge foliation and drag-folding in the footwall; e) One S-vergent reverse shear-zone associated with brittle shear-bands and asymmetric folds with a WNW oriented hinge located in the Upper Jurassic turbidites of the Vranduk Flysch; f) One S-vergent reverse fault associated with drag folds with an E-W oriented hinge, located in the Upper Jurassic – lowermost Cretaceous ophiolitic mélange; g) One NNW–SSE oriented dextral strike-slip shear zone with kilometres-size offset truncating the uppermost Cretaceous turbidites of the Ugar Flysch. The bottom right inset shows corrugations inside the ~2 m thick fault gouge foliation; h) Transpressional flower structure made up of WNW-ESE oriented dextral strike-slip faults truncating the uppermost Cretaceous turbidites of the Ugar Flysch; i) High-angle SW-vergent reverse fault associated with drag folding truncating the lower – middle Miocene sediments of the Konjic Basin; j) WNW-ESE oriented dextral strike-slip fault cross-cutting a NW-dipping normal fault truncating Jurassic limestones at the contact with the Miocene sediments of the Gatsko Basin. The bottom right inset shows the dip slip slickensides of the normal fault.

### 3.4.3 The Budva unit and connecting faults system

Similar to the Bosnian Flysch zone, the Budva unit of Montenegro was intensively deformed during both the pre-Miocene orogenic evolution and the Neogene extension followed by inversion (van Unen et al., 2019). The most recent episodes of deformation include numerous normal faults observed in the Budva and neighbouring units that truncate sediments as young as the Eocene and, therefore, are considered to be Miocene in age by correlation with the syn-depositional normal faults found in the Dinarides Lake System basins. These normal faults are inverted or subsequently truncated by a complex system of strike-slip, transpressional, high-angle reverse and thrust faults. In outcrops, large-offset WNW-ESE to N-S dextral strike-slip faults are associated with smaller offset NNW-SSE to ENE-WSW oriented conjugate sinistral strike-slip faults (Figure 3.8b,c). These faults define two strike-slip paleostress fields, one with a NNE-SSW oriented compression direction and one with a NW-SE oriented compression direction. However, differently from previous areas, a significantly higher number of E-W to NW-SE oriented thrusts and high-angle reverse faults have been measured in the Budva unit (Figure 3.8d), which in map-scale are connected with (sub-)units or nappe contacts and are connected with or truncated by NNW-SSE oriented dextral strike-slip faults (Figure 3.8a). The reverse faults are often associated with drag and upright folds with ~E-W to WNW-ESE oriented hinges, observed mainly at (sub-)units contacts in the Kotor Bay and across the Budva unit (Figure 3.8a). Large offset faults are generally S-vergent thrusts or NNW-SSE oriented dextral faults that gradually increase their offset from a few kilometres in the NW to more than 10 km in the SE.

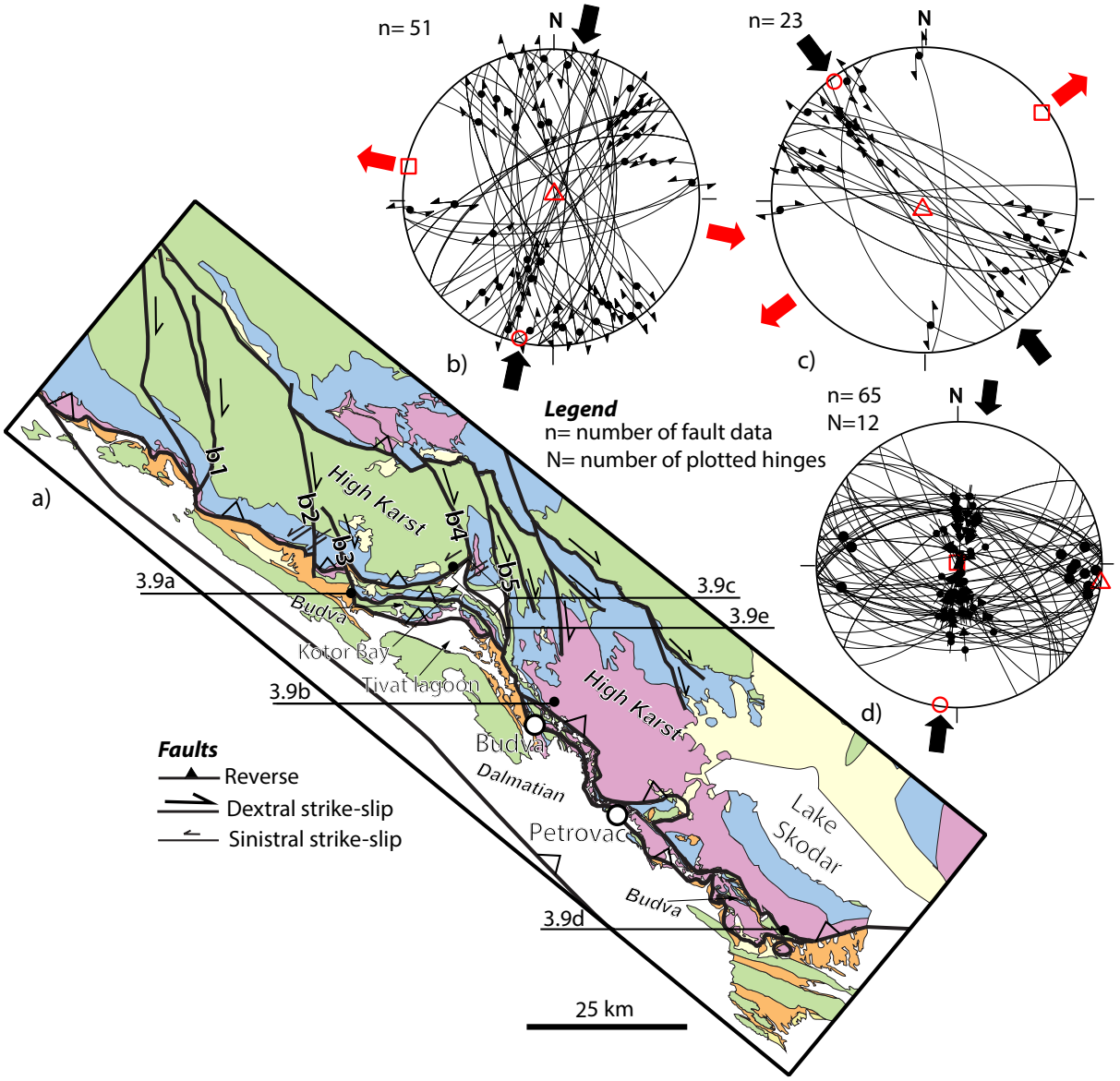


Figure 3.8 Structural map and kinematic data for the Budva zone and connecting fault system. Note that only structures active in the post- 9 Ma phase of deformation are displayed in the map and plotted on stereonets (Schmidt projection, lower hemisphere). In stereonets, lines with arrow symbols are projections of fault planes with kinematic sense of shear, while thick black dots are projections of fold hinges. a) Geological map with structures active during the post- 9 Ma phase of deformation. Same conventions and legend as in Figure 3.2a. Location of the map is displayed in Figure 3.2a; b) Stereoplot showing NW-SE to N-S oriented dextral and their conjugate NNE-SSW to ENE-WSW oriented sinistral strike-slip faults. The calculated paleostress field shows NNE-SSW oriented compression and ESE-WNW oriented tension; c) Stereoplot showing WSW-ENE to WNW-ESE oriented dextral and NNW-SSE to N-S oriented sinistral strike-slip faults. The calculated paleostress field shows NW-SE oriented compression and NE-SW oriented tension; d) Stereoplot showing reverse faults with N and S sense of shear and ~E-W oriented fold hinges. The calculated paleostress field shows NNE-SSW oriented compression.

NW of the Kotor Bay area, three large scale dextral strike-slip faults have map offsets in the order of 3, 5 and 7 km (b1, b2 and b3, respectively, in Figure 3.8a). In all situation, these faults displace the thrusting contact of the High Karst unit, while the latter fault (b3) makes the NW-

ward termination of the Budva unit in Montenegro. Numerous strike-slip faults have been observed in outcrops, typically by large fault planes with thick slickensides affecting the Mesozoic limestones, locally associated with top-S high-angle reverse faults (Figure 3.9a). More to the SE, a NNW-SSE oriented dextral shear zones displaces with 18 km both the High-Karst over Budva and the Budva over Dalmatian units contacts along the eastern margins of the Kotor Bay and Tivat lagoon (branch b5 in Figure 3.8a). This shear zone is visible by dextral zones of fault gauge foliations or dextral faults truncating earlier normal faults (Figure 3.9b) associated locally with lower offset NNE-SSW oriented sinistral strike-slip faults (Figure 3.9c). Other smaller offset dextral strike slip faults are observed in the Budva unit more to the SE (Figure 3.8a).

Three types of high-angle reverse and thrust faults can be observed in outcrops in the external High Karst – Budva – Dalmatian areas (Figure 3.8a). The NW-SE oriented High Karst over Budva and Budva over Dalmatian units contacts formed initially during the top-SW Eocene Dinarides nappe stacking. These contacts as well as smaller-offsets thrusts composing the Budva sub-units geometry have been partial reactivated by a later deformation episode that created reverse faults with top-S sense of shear, asymmetric- and drag folding with E-W oriented hinges (Figure 3.8d). In the field, the latter set is observed truncating the post-Eocene normal faults. Typical deformation in outcrops are observed for instance by high-angle reverse faults truncating Middle Triassic deep-water limestones or by reactivating the low-angle High Karst – Budva contact observed by the oblique thrusting of Triassic limestones over Eocene clastic turbidites (Figure 3.9d). At major thrust contacts, cataclastic shear zones are associated with a large number of isoclinal-, upright-, drag- and asymmetric- folds with E-W to WNW-ESE oriented hinges.

The two types of major structures, NW-SE to N-S oriented dextral faults and top-S ESE-WNW to NW-SE oriented high-angle reverse faults or thrusts gradually change their strike and connect with each other in the footwall of the High-Karst thrusting (Figure 3.8a). The connection is done in such a way that the map-scale dextral strike-slip faults displace the High-Karst unit, the Budva unit and the Eocene turbidites of the Dalmatian located at the contact with the Budva unit. However, these map-scale dextral strike-slip faults do not displace the Cretaceous limestones of the Dalmatian unit. The connection between dextral strike-slip and different thrusts can be observed, for instance, in the Kotor Bay, where a NNW-SSE oriented dextral strike-slip fault (b4 in Figure 3.8a) must connect with the High-Karst thrust (Figure 3.9e), while the similarly oriented, larger offset dextral strike-slip branch located a few kilometres more to the east connects with the Budva thrust (b5 in Figure 3.8a). At regional scale, the deformation transfer from dextral strike-slip gradually increases the amount of southward thrusting and associated exhumation of the High Karst unit from a few kilometres in the NW to more than 30 km in the SE. The increase in exhumation associated with the increase in thrusting leads to the gradual exposure of older (Triassic) rocks observed SE-wards in the High Karst unit (Figure 3.8a). When accounting for the internal deformation observed inside the onshore exposed Budva and Dalmatian units, the total amount of post- Middle Miocene S- to SSW- ward thrusting is likely in the order of 40-50 km only in the offshore exposed segment of the external High-Karst to Dalmatian units.

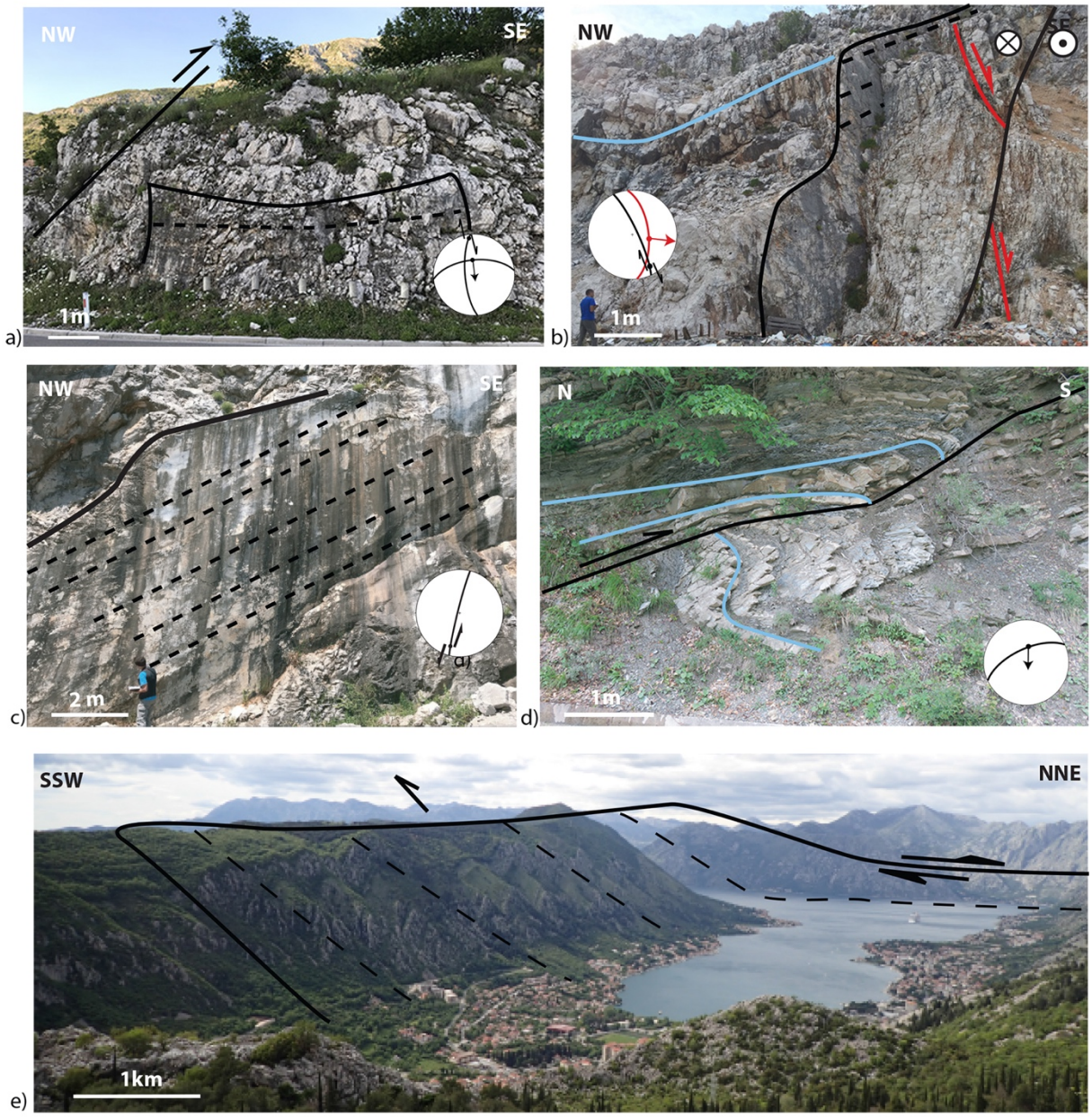


Figure 3.9 Interpreted field photos illustrating structures and their kinematics in the area of the Budva unit and connecting fault system (locations in Figure 3.8a). Red lines: early–middle Miocene faults, black lines: post- 9 Ma faults, blue lines: bedding. a) One NNW-SSE oriented dextral strike-slip fault and one high-angle S-vergent reverse fault truncating Cretaceous limestones, part of a larger shear zone made up by NNW-SSE oriented dextral strike-slip faults separating the Budva from Dalmatian units; b) One NW–SE oriented dextral strike-slip faults cross-cutting an ESE-dipping normal fault in Triassic carbonates of the High Karst unit; c) One large offset NNE-SSW oriented sinistral strike-slip fault truncating Cretaceous limestones of the High-Karst unit; d) One S-vergent reverse fault associated with drag folding deforming Eocene turbidites of the Budva unit; e) Large-scale overview of the Kotor Bay illustrating the transfer from dextral strike-slip faulting in the NNW to S-ward thrusting to the SSE.

## 3.5 Interpreting the kinematic data at regional scale

When connecting kinematic observations across all studied areas, it is rather clear that the pre-Miocene nappe system together with the Miocene basins of the Dinarides Lake System are affected by two deformation events along the strike of the entire Dinarides, which postdate the main period of orogenic structuration that ended during the Paleogene.

The first deformation event is characterized by syn-depositional normal faults that are genetically associated with the onset of early-middle Miocene sedimentation. Such normal faults were observed in all studied basins (Kamengrad, Drvar, Glamoc, Sinj, Livno, Tomislavgrad, Mrkonjic Grad, Jajce, Sarajevo-Zenica, Konjic, Gatsko, e.g., Figures 3.4-3.9) and provide critical timing constraints for the superposition of deformation. Although not targeted specifically by our kinematic analysis (i.e. not displayed in Figures 3.4, 3.6, 3.8), we have observed that large offset normal faults indicate roughly NE-SW extension, while smaller offsets normal faults show NW-SE oriented extension. The NE-SW direction of extension has been previously observed to have larger effects also in other Dinarides basins of Bosnia and Herzegovina, Croatia, and Slovenia (e.g., Andrić et al., 2017; van Unen et al., 2019; Žibret & Vrabec, 2016). Therefore, we are in agreement with these previous studies that a period of early-middle Miocene extension has affected all external areas of the Dinarides.

More importantly, our study has defined for the first time the kinematics, geometry and regional effects of a second major deformation event that post-dated the sedimentation in the Miocene basins by inverting, truncating or otherwise deforming their entire infill. As described above, this deformation must have started after ~9 Ma. In all areas, outcrop kinematics indicate that deformation may be characterized by three paleostress groups, two strike-slip (NW-SE and N-S to NNE-SSW compression, with NE-SW and E-W to WNW-ESE tension, respectively) and one compressional (N-S to NNE-SSW oriented compression, Figures 3.4, 3.6 and 3.8). The strike-slip faults observed in outcrops have large WNW-ESE to N-S oriented dextral offsets, while the conjugate NNW-SSE to ENE-WSW oriented sinistral strike-slip faults have generally low offset. In outcrops, reverse faults often have an oblique transpressional component and large-offset faults have a southward vergence, while the ones verging northwards have low offsets.

In map view, the post- 9 Ma faults form a large anastomosing system that spans from the Cazin Basin in the NW to the connection with the Albanides in the SE (Figures 3.1 and 3.2a). In outcrops and in map scale, the WNW-ESE to N-S oriented large offset dextral faults gradually change their strike and connect to large offset E-W to WNW-ESE oriented high-angle reverse faults or thrusts. In almost all situations, these fault segments were already observed previously and drawn on geological maps (Basic Geological Maps of former Yugoslavia, scale 1:100.000). However, only the Split-Karlovac Fault has been previously interpreted as a dextral strike-slip structure (branch b1 in our Split-Karlovac system, Figures 3.1 and 3.4a, e.g., Chorowicz, 2016; Ustaszewski et al., 2008).

The timing of the Split-Karlovac Fault is the least controlled in our study, owing to the association of deformation with diapirs made up of salt and other evaporites and poor Miocene outcrops along this fault (Figure 3.4a). Along this fault segment, the mapped deformation affected both the upper Eocene – Oligocene Promina beds and the locally overlying lower-middle Miocene sediments. However, the degree of deformation is significantly different: while

the Promina beds are clearly truncated by this fault and often tilted to sub-vertical positions by drag-folds, Miocene sediments appear to be less deformed, while their degree of tilting is significantly lower, generally 20-40°. While it is possible that this difference in the degree of deformation observed is an effect of differential movements against the fault plane during the post- 9 Ma deformation event, it is also possible that the Split-Karlovac Fault has been initiated earlier, during the late Eocene – Oligocene deposition of the Promina beds, and deformation continued later, after 9 Ma. This earlier initiation is justified by the observation of thick Promina molasse deposition limited to the west and south of the Split-Karlovac Fault, while to the east and north such deposition is fairly limited (Figure 3.2a). However, erosional removal during subsequent transpressional (re-)activation along the Split-Karlovac Fault could have played a significant role in this present-day thickness variability.

In contrast, all other branches of the strike-slip and reverse faults system are much less or not affected by diapirism. These branches truncate both the Promina beds and Miocene sediments, whenever present, and must have been (re-)activated with a large offset after 9 Ma. There is just one kinematic study published so far documenting a late Eocene-Oligocene deformation in the Sarajevo-Zenica Basin, which is characterized by shortening with a NE-SW oriented compression direction (Andrić et al., 2017). Such a compression direction is partly incompatible with the activation of the NW-SE to NNW-SSE dextral strike-slip along the Split-Karlovac Fault and, therefore, the first hypothesis of significant (re-)activation after 9 Ma seems more likely. Therefore, we conclude that most strike-slip connected with reverse faults along the entire Split-Karlovac system must post-date 9 Ma and has likely reactivated an inherited Paleogene thrust.

The cumulative dextral strike-slip and reverse faulting appears to be similar in the order of 60-70 km in various across-strike orogenic segments. However, this amount is distributed differently along the Dinarides orogenic strike (Figure 3.2). In the NW, the largest amount of deformation (~50 km) is retained by the branches of the Split- Karlovac system, while more internal areas (e.g., Kamengrad Basin) have lower amounts of deformation (~10-15 km). In the centre, the largest amount of deformation is taken up by the Sarajevo – Zenica Basin together with its eastern Bosnian Flysch and East Bosnian – Durmitor units' change in strike along the Sarajevo "sigmoid" (~50 km), while deformation southwards in the Konjic Basin and Neretva valley has lower values (~20 km). In the SE, the largest amount of deformation is taken up by the external High-Karst and Budva units and its NNW-SSE connected dextral strike-slip faults (~50 km), while more internal units recorded lower amounts of deformation (5-10 km). Please note that these calculations do not account for the offshore internal deformation and the thrusting of the Dalmatian unit over the Adriatic foreland, which is likely significant in the Montenegro sector (e.g., Bega et al., 2015). The overall deformation shows a gradual transfer of dextral strike-slip, transpression and shortening from the internal Dinarides in the NW to the external Dinarides in the SE. The total amount of cumulative displacements across the entire system is difficult to estimate due to the unclear amount of offset transfer between individual structures, but must be somewhere in the order of 150-200 km.

One special note is required for what has been previously described as the Pre-Karst thrusted unit of the Dinarides (Figures 3.1 and 3.2a). This unit has been introduced originally as a transitional paleogeographic realm between the Middle Triassic – Paleocene shallow-water carbonates of the external Dinarides and a more internal tectonostratigraphic unit characterized

by deep water Upper Jurassic – Cretaceous turbidites (i.e. "flysch", see also Aubouin et al., 1970). In subsequent studies, the Paleozoic basement and the overlying continental to shallow-water Triassic to Cretaceous cover together with the overlying deformed Bosnian Flysch has been often grouped in an individual thrusted unit in the pre-Miocene Dinarides nappe stack (e.g., Schmid et al., 2008 and references therein). Our field observations show that in most Bosnia north-west of the Neretva River (NW of NR in Figure 3.6) the contact between the Pre-Karst and High-Karst units never retains the typical SW-ward thrusting kinematics of the pre-Miocene deformation (the Dinaric vergence of Schmid et al., 2008; Tari, 2002). We observed that this fault is either a NW-SE to WNW-ESE oriented dextral strike-slip fault or an E-W oriented thrust with top- S to SSW-wards kinematics, or even a normal fault (Figure 3.2a). In other situations, the fault simply does not exist, the interpreted unit contact being a map interpretation connecting two faults with different kinematics (such as two post- 9 Ma strike-slip faults or a Dinaric thrust with a post- 9 Ma strike-slip fault, Figure 3.2). It is rather clear that the segments of this contact with large offset are part of the post- 9 Ma dextral strike-slip and reverse faults system. Therefore, we suggest abandoning the term "Pre-Karst" as a pre-Miocene thrusted unit of the Dinarides.

## 3.6 Mechanics of deformation

The post- 9 Ma deformation observed in outcrops and map scale demonstrate in all areas that large offset WNW-ESE to N-S oriented dextral strike-slip faults transfer gradually their displacements to E-W to NNW-SSE oriented dextral transpressive faults and ultimately to E-W to WNW-ESE oriented thrusts and high-angle reverse faults. Such structures are observed throughout the entire studied area (Figure 3.2). Whenever the deformation is taken up by one large offset dextral strike-slip fault, the offsets remains roughly constant along its dextral strike outside transfer zones (outside grey areas in Figure 3.10). In the transfer zone, the offset of reverse faults is maximum near the dextral fault, while decreasing gradually at farther distance, often until complete disappearance. The gradual decrease in offset along these reverse faults is actually an effect of transferring the deformation to the next structure composed of another dextral fault that transfers again gradually its offset to one other thrust (Figure 3.10). The transfer of deformation from one structure to the next one can be done in two ways: either the gradual decrease in thrusting offset is taken up by a gradual increase of dextral offset along the adjacent strike-slip fault (situation 1, Figure 3.10a), or the gradual decrease in reverse offset is taken up by a gradual increase in offset along an opposite vergent reverse fault connected with one other dextral strike-slip fault (situation 2, Figure 3.10a). Situation 1 is the most common one observed, such as along the Split-Karlovac system (Figure 3.4). Situation 2 is observed for instance on the structures connecting the Livno and Tomislavgrad basin (Figure 3.4), or more obvious along the Neretva River Valley (NR in Figure 3.6). Interesting is the situation of this later area where dextral strike-slip faults connect to both a thick-skinned thrust and a thin-skinned backthrust (t1 and b1 in Figure 3.2b, NR in Figure 3.6a). These structures transfer rapidly their offsets in such a way that the thrust offset increases and is larger W-wards, while the backthrust offset increases and is larger E-wards (which is the situation of the cross -section in Figure 3.2b). This also raises the possibility of transferring deformation between a thin-skinned and a thick-skinned strike-slip system along lateral or oblique ramps.

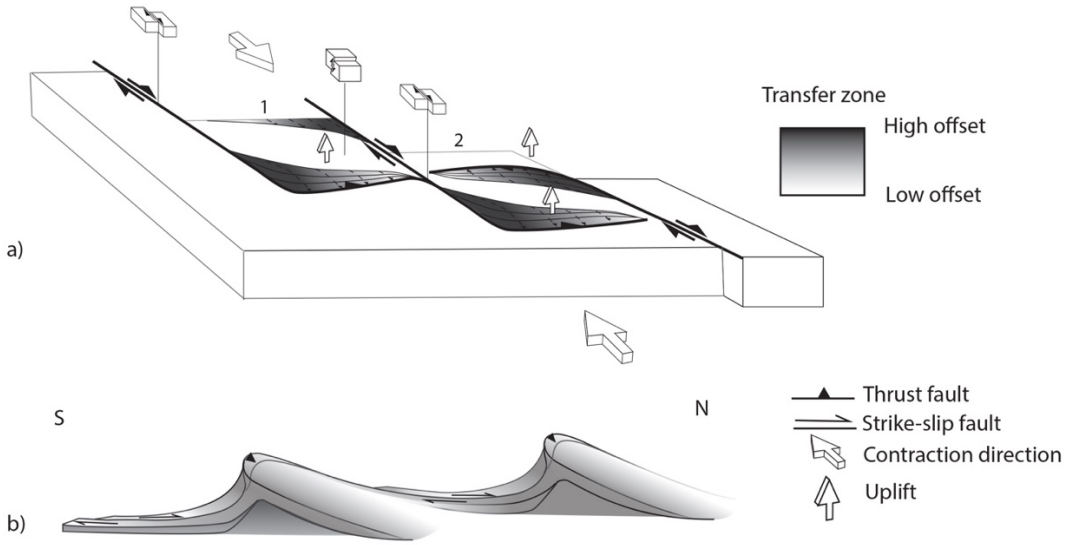


Figure 3.10 Cartoons illustrating structural mechanisms of strain partitioning and transfer depicted by our study for the post- 9 Ma deformation event. a) 3D view of strain transfer between dextral strike-slip faults via restraining step-overs and/or restraining bends. The transfer of deformation between strike-slip faults is achieved in two ways: 1) a gradual decrease in thrusting offset is taken up by a gradual increase of dextral offset along the adjacent strike-slip fault; 2) a gradual decrease in reverse offset is taken up by a gradual increase in offset along an opposite vergent reverse fault connected with one other dextral strike-slip fault; b) 3D view of offset transfer between two reverse faults via a dextral strike-slip fault.

Given the connection between the large-offset dextral strike-slip and high-angle reverse faults or thrusts observed in outcrops and at map scale, it is rather clear that the two types of paleostress fields (strike-slip and compression) defined by the post- 9 Ma structures do not reflect two distinct deformation events but are rather an effect of partitioning deformation along highly curved faults. The same strain partitioning creates also two different strike-slip paleostress fields defined by our outcrop-scale post- 9 Ma structures, which show N-S to NNE-SSW and NW-SE oriented compression combined with E-W to ESE-WNW and NE-SW oriented tension, respectively, in the entire studied area. Such strain partitioning is obviously an effect of clockwise rotations and drag-folding in the vicinity of major strike-slip faults.

In fact, such curved structures formed during a deformation event that was characterized regionally by N-S to NNE-SSW oriented compression, which is mostly oblique to the inherited NW-SE oriented Cretaceous – Paleogene nappe stack. The WNW-ESE to N-S oriented large offsets dextral strike-slip faults may be interpreted as lateral or oblique ramps accommodating the transfer of shortening across an inherited NW-SE oriented nappe stack. High amounts of cumulative offset recorded by the system of curved dextral to reverse faults are observed in the Bosnian Flysch and the Budva unit of Montenegro. These areas contain deep-water to pelagic sediments, which are rheologically weaker when compared with the Paleozoic basement and Mesozoic shallow-water carbonatic cover deposited in the neighbouring units. As these areas have always recorded much larger amounts of deformation when compared with elsewhere in the external part of the Dinarides, this strain localisation is likely the result of focussing deformation in rheologically weak zones (see also van Unen et al., 2019).

The overall transfer mechanisms from strike-slip to high-angle reverse faulting can be described as a special class of continental restraining bends or stepovers (e.g., Biddle &

Christie-Blick, 1985; Cunningham & Mann, 2007 and references therein). As long as the rheology of rocks affected by deformation is homogenous, such as the typical High-Karst shallow water carbonate platform overlying the Variscan basement and Permian – lowermost Triassic clastics, the strike-slip deformation is dominant and transfers its offset between various fault branches across shorter segments of high-angle reverse faults. Whenever inherited weakness zones with a favourable orientation are present, such as the Bosnian Flysch or the Budva unit, deformation localizes in thrusts or oblique reverse faults that are dominant over shorter segments of strike-slip faulting.

## 3.7 Towards understanding the post- 9 Ma Dinarides deformation in a larger geodynamic context

The patterns of post- 9 Ma deformation mapped across the central and south-eastern Dinarides partly fit the overall framework of Adriatic indentation, as defined by many previous studies (Figure 3.11a,b, e.g., Handy et al., 2010; Pinter et al., 2005). The overall N-S to NNE-SSW directions of compression derived from our observed structures inferring N- to NNE-ward indentation of Adria is in general agreement with N- to NE- ward direction of movement derived by GPS studies in the Dinarides by taking as a reference a stable European framework (Figure 3.11b, e.g., D'Agostino et al., 2008; Grenerczy et al., 2005; Métois et al., 2015). While GPS movement vectors are oriented more N-wards in the NW Dinarides and the neighbouring Southern Alps, this movement gradually changes to NNE and NE towards the Pannonian Basin and the central and south-eastern part of the Dinarides (Figure 3.11b). Across the Adriatic Sea, GPS studies indicate a N- to NE-ward movement of the Apennines along trajectories that can be generally connected with the ones observed in the Dinarides, Pannonian Basin, and Southern and Eastern Alps (Figure 3.11b). The situation changes in the SE located Ionian domain, starting with the Albanides that record a ~1-5 mm/yr motion towards the NW in their external and towards the SE in their internal parts, while the Hellenides record much larger motions of ~10-36 mm/year, gradually rotating from S- to SW-ward following the structural vergence of the orogen in the overall direction of the Aegean slab-roll back (Jouanne et al., 2012; Kahle et al., 2000; Métois et al., 2015; Nocquet, 2012).

The N-S to NNE-SSW direction of compression derived by our paleostress analysis is also in general agreement with modelled averages of the present-day maximum horizontal stress ($S_H$) field in the Dinarides (Figure 3.11b). This modelled stress component indicates a gradual change from N-S orientations in the NW to NE-SW orientations in the SE Dinarides, which is compatible with the overall Adria indentation (Bada et al., 2007; Heidbach et al., 2007; Heidbach et al., 2010). Towards the Hellenides, this stress field changes to more E-W directions, which is a combined effect of a similarly oriented compression in external areas and perpendicular N-S to NNE-SSW oriented extensional deformation elsewhere, inferred to be the result of the S- to SSW-wards slab roll-back combined with gravitational spreading of the Aegean lithosphere (Heidbach et al., 2007; Konstantinou et al., 2017). A similar situation is observed in the Apennines (Figure 3.11b), where the NW-SE $S_H$ orientations are the result of a NE-SW oriented extension.

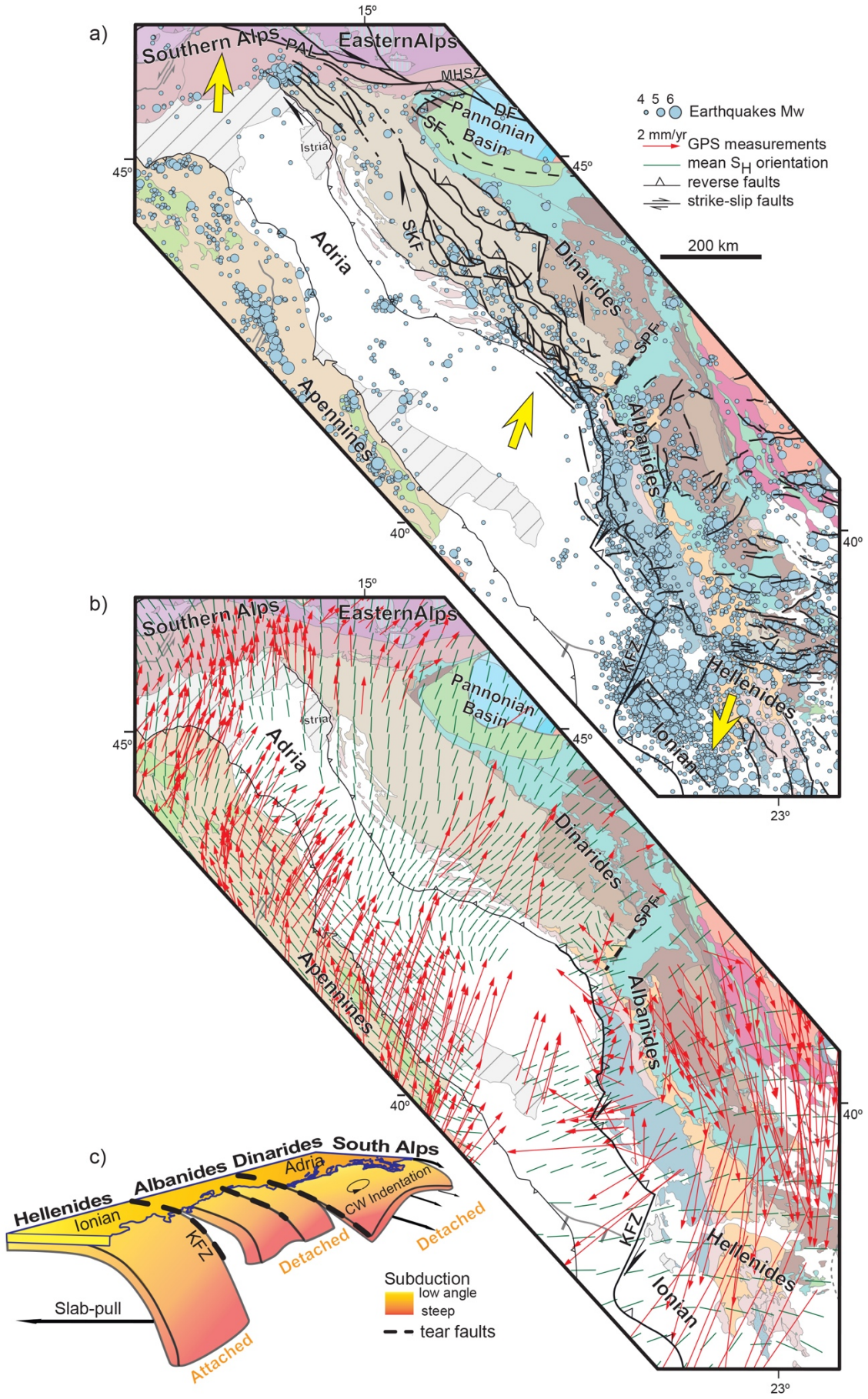


Figure 3.11 The post- 9 Ma deformation mapped in the studied Dinarides area correlated in

*Figure 3.11 (continued)* the larger Alps-Dinarides-Albanides-Hellenides-Apennines context. a) Tectonic map of the Dinarides and neighbouring orogens (adapted from Schmid et al., 2008; Schmid et al., 2011, legend and conventions presented in Figure 3.1) overlaid by the post- 9 Ma deformation, and seismicity. The post- 9 Ma fault pattern in the Dinarides, Pannonian Basin, Southern and Eastern Alps is taken from our results and previous studies (Heberer et al., 2017; Moulin et al., 2016; Tomljenović and Csontos, 2001; Tomljenovic et al., 2008; Ustaszewski et al., 2014; van Gelder et al., 2015; Vrabec and Fodor, 2006; Vrabec et al., 2006). Only presently active seismogenic faults are displayed in the Albanides and Hellenides (Caputo et al., 2012; Pavlides et al., 2010; Pérouse et al., 2017). Only the orogenic front is displayed in the Apennines. Only earthquakes with magnitude greater than 4 are displayed, their location is taken from the USGS earthquakes catalogue (https://earthquake.usgs.gov/earthquakes/), corrected by local studies whenever available (e.g., Herak et al., 2009; Pérouse et al., 2017). SKF = Split - Karlovac Fault; KFZ = Kefalonia Fault Zone; SPF = Skutari – Pec Fault; PAL = Peri-Adriatic Lineament; SF = Sava Fault; DF = Drava Fault; MHSZ = Mid-Hungarian Shear Zone; b) The same tectonic map as in Figure 3.11a (same conventions) overlaid by the present-day stress distribution and GPS horizontal motions. The GPS horizontal motions are displayed in an Eurasian fixed reference framework (D'Agostino et al., 2008; Grenerczy et al., 2005; Jouanne et al., 2012; Métois et al., 2015; Nocquet, 2012). The mean present-day maximum horizontal stress orientation ($S_H$) is compiled from previous studies (Bada et al., 2007; Heidbach et al., 2007; Heidbach et al., 2010; Pierdominici & Heidbach, 2012); c) Conceptual cartoon illustrating the lateral transition in the subduction and collision system between the Dinarides, Albanides and Hellenides. The cartoon infers subduction of continental mantle lithosphere disconnected from an oceanic slab by the Oligocene slab detachment beneath the Dinarides (Andrić et al., 2018), subduction of thinned continental lithosphere disconnected from an oceanic slab by previous slab detachment beneath the Albanides and subduction of oceanic and continental mantle lithosphere in a continuous Aegean slab beneath the Hellenides. The three areas are separated by slab tears. The cartoon also infers that the post- 9 Ma deformation accommodates the differential movement between the N- to NE-ward Adriatic indentation and continental subduction and the SW-ward movement driven by the Aegean slab pull.

To the NW of the Apennines, the $S_H$ orientation gradually changes to NE-SW in the Adriatic Sea, interpreted to be a combination between horizontal gradients of the gravitational potential energy, the long-wavelength of the Africa-Europe convergence zone and the Adriatic indentation (Métois et al., 2015; Pierdominici & Heidbach, 2012).

Larger clusters of earthquakes are observed in the central Dinarides and the SE Budva zone in areas that are spatially juxtaposed over the mapped post- 9 Ma fault system (Figure 3.11a). Therefore, it is very likely that our post- 9 Ma fault system is seismically active, although more precise localisation of this seismicity in local studies and details on focal mechanisms are generally scarce (Figure 3.11a, see also Bada et al., 2007; Herak et al., 2009; Šumanovac et al., 2017; Ustaszewski et al., 2014).

In this overall context, it is rather clear that the post- 9 Ma fault system mapped in the central and SE part of the Dinarides accommodates the differential motion between the N- to NE-ward indentation of Adria and the S- to SW-ward movement of the Hellenides and SE Albanides, driven by the roll-back of the Aegean slab. How exactly the deformation connects between the Alps and the Albanides-Hellenides? This is a difficult question given the local nature and problematic age of faults in many kinematic studies across the entire system. To the NW (Figure 3.11a), a significant number of NW-SE to WNW-ESE oriented larger offsets dextral strike-slip faults, associated with E-W to ENE-WSW oriented reverse faults and smaller offset NE-SW to

NNE-SSW oriented sinistral strike-slip faults has been mapped to be either latest Miocene – Quaternary, Pliocene - Quaternary or as a result of active and neotectonic deformation along the Peri-Adriatic Lineament or southwards in the NW-most part of the Dinarides (e.g., Heberer et al., 2017; Moulin et al., 2016; Tomljenović & Csontos, 2001; Tomljenovic et al., 2008; Ustaszewski et al., 2014; van Gelder et al., 2015; Vrabec & Fodor, 2006; Vrabec et al., 2006). The northern part of this fault system connects with the latest Miocene – Quaternary deformation of the Mid-Hungarian Shear Zone, Sava and Drava faults (e.g., Fodor et al., 2005; Fodor et al., 1998), which are located N to NE of the faults mapped in our study (Figure 3.11a). The southern part of the fault system (immediately north of the Istria peninsula, Figure 3.11a) likely connects with or transfer deformation to our observed Split-Karlovac and Bosnian Flysch faults systems. The larger offset strike-slip and thrusting focussed in the external part of the High-Karst, Budva and Dalmatian units of the SE Dinarides connect with the late Miocene – Quaternary faults in the external parts of the onshore and offshore Albania (Ionian and pre-Apulian zones, possibly also Krasta-Cukali unit in Figure 3.1, Bega, 2015; Roure et al., 2004; Vilasi et al., 2009). More to the SE towards the Hellenides (Figure 3.11a), the active thrusting is focussed in the external-most part of the orogenic wedge, close to the main deformation front (Caputo et al., 2012; Pavlides et al., 2010; Pérouse et al., 2017). This thrusting is displaced by NNE-SSW oriented dextral faults, among which the largest is the seismically active Kefalonia Fault Zone, a fault that started its activity at ~5 Ma (Louvari et al., 1999; Menant et al., 2016; Pérouse et al., 2017).

The zones where the overall structural kinematics, GPS motions, present-day horizontal stress and seismicity distributions change across the entire Dinarides - Albanides - Hellenides orogens are the Kefalonia Fault zone and the Skutari - Pec (or Shkoder - Peja) Fault zone (Figure 3.11a). The first fault zone is thought to be the surface expression of a young tear fault in the Aegean subduction system separating subduction of continental crust to the NW from subduction of oceanic crust to the SE (Figure 3.11b, Evangelidis, 2017; Pearce et al., 2012). The second fault zone is interpreted to be the expression of an older transformant fault that separated the Mesozoic carbonate facies evolution (e.g., Aubouin & Dercourt, 1975; Robertson & Shallo, 2000; Velaj et al., 1999) and shows significant Miocene normal faulting offset accommodating an increase in roll-back subduction to the SE (Le Breton et al., 2017; Schmitz et al., 2017) of a transitional Adriatic-Ionian continental lithosphere affected by significant normal faulting (Bega, 2015). Therefore, the interpretation of a gradual transition from an Adriatic indentation inducing continental subduction and N- to NE-ward movements in the Dinarides, to an Albanides – Hellenides area located NW of the Kefalonia Fault and characterized by subduction of thinned continental lithosphere, and, ultimately, to subduction of oceanic lithosphere and slab roll-back SE of the Kefalonia Fault (Figure 3.11c) seems justified.

## 3.8 Conclusions

Among the many examples available worldwide, the Neogene evolution of the Adriatic microplate in the Mediterranean domain provides one of the best places to understand indentation effects in terms of the relationship between deep lithosphere and mantle processes and the structural evolution of neighbouring orogens. Understanding the interplay between

various mechanisms invoked for the Adriatic indentation was hampered by the lack of structural and kinematic data in the Dinarides, an orogen situated at the critical transition between the Alps, Albanides and Hellenides, and across the Adriatic margin of the Apennines. Starting from the scarcely available information for the post-Paleogene evolution, we have re-visited the less known area of the central and south-eastern Dinarides by focussing on collecting a new kinematic dataset for structures formed during the Adriatic indentation that postdate the main orogenic evolution.

In agreement with previous studies, our data shows that the lower-middle Miocene sediments of the Dinarides Lake System have been deposited during a period of extension that affected the entire orogen across its strike. Furthermore, we demonstrate for the first time that extension was followed by a period where strike-slip deformation was intimately associated with reverse faulting and thrusting. Starting from the early-middle Miocene basins, we have mapped how WNW-ESE to N-S oriented dextral strike-slip faults transfer gradually their offsets to E-W to NNW-SSE oriented dextral transpressive faults and ultimately to E-W to WNW-ESE oriented thrusts and high-angle reverse faults. This entire deformation was driven by a stress field that changes its compressional orientation along the orogenic strike from N-S in the NW to NNE-SSW in the SE.

The overall transfer mechanism from strike-slip to high-angle reverse faulting can be described as a special class of continental restraining bends or stepovers. As long as the rheology of rocks affected by deformation is homogenous, the strike-slip deformation is dominant and transfers its offset between various fault branches across shorter segments of high-angle reverse faults. Whenever large-scale inherited weakness zones with a favourable orientation are present, such as units containing deep-water sediments that recorded significant deformation during the previous orogenic evolution, deformation localizes in thrusts or oblique reverse faults that are dominant over shorter segments of strike-slip faults. Strike-slip faults transfer their offset to thrusts in such a way that the offset changes along their strikes.

The observation of the regional early-middle extension in the Dinarides infers that there were no indentation effects prior to 9 Ma in this orogen. The geodynamic mechanism driving this period of extension that gradually reduces its effects towards the external parts of the orogen and has maximum amplitudes during the ~17-15 Ma Miocene Climatic Optimum (Mandic et al., 2012; Sant et al., 2018) are still unclear. One can think of horizontal gradients of the gravitational potential energy, prolongation of the Pannonian back-arc extension far into the Dinarides, roll-back of a Dinarides slab, processes associated with the subduction zone, eduction post-dating the Oligocene slab-break off (e.g., Andrić et al., 2018; Matenco and Radivojević, 2012 and references therein), but all such hypotheses remain speculative.

The onset of indentation that started in the Dinarides at ~9 Ma was likely associated with a differential motion of Adria in respect to the S- to SW- ward movement of a Hellenides area situated SE of the Kefalonia Fault, driven by the Aegean slab-roll back, facilitated by the thinned continental to oceanic nature of the Ionian lithosphere involved in the subduction system. The system of strike-slip, reverse and thrust faults mapped in the Dinarides that likely continues or transfers its offset to the NW until the Southern Alps and to the SE in the external part of the Albanides is nothing else but a large-scale crustal horizontal drag zone accommodating ~150-200 km of differential motion between the Adriatic indentation and Aegean slab roll-back in post- 9 Ma times. Partitioning the deformation related to the Adriatic

indentation in the Apennines and Hellenides may be certainly influenced by asthenospheric flow around subducted slabs and moments of slab tearing or detachment, as previously inferred (e.g., Faccenna et al., 2014; Király et al., 2018; Le Breton et al., 2017). But such studies are qualitative because they ignore a correct quantification of the timing and geometry of deformation in the Dinarides and need to be re-visited.

## Chapter 4.

# Coupled kinematic and thermal modelling across the Dinarides orogen: implications on the maturity of potential source rocks and paleo fluid-flow

*This chapter is based on:*
*van Unen, M., Nader, F. H., Darnault, R., Rudkiewicz, J.-L., & Matenco, L. (2019). Coupled kinematic and thermal modelling across the Dinarides orogen: implications on the maturity of potential source rocks and paleo fluid-flow. In preparation*

## 4.1 Introduction

Collisional orogens commonly involve crustal accretion mechanisms during the migration of subduction zones and contractional deformation towards the orogenic foreland (Beaumont et al., 1999; Doglioni et al., 2007; Lallemand et al., 1994). The foreland-ward migration of contractional deformation and accretion can be associated with syn- and post-tectonic exhumation, erosion and/or extension (Ellis et al., 1999). The sedimentation and erosion rates, shear heating and Moho heat flow supply, significantly affects the temperature distribution, fluid flow, and petroleum system potential throughout the formation of these collisional orogens (Faccenda et al., 2008; Huerta,1998; Roure et al., 1993; Swennen et al., 2000). The use of restorations, such as balanced cross-sections, has provided the critical quantification required to derive the structural geometries and kinematic relationships in such collisional orogens (Davis et al., 1983; Mitra, 1994; Roure & Sassi, 1995; Vergés et al., 1995). Such restorations are generally conducted across regional cross-sections and led to better estimating the amounts of shortening, subsidence and exhumation, as well as erosion and sedimentation through time (e.g. Callot et al., 2010; Zoetemeijer et al., 1993). Thermal (basin) modelling has been used to simulate porous medium deformation, heat transfer, and hydrocarbon generation and migration, taking into account the realistic mechanisms of deformation through time (Schneider, 2003). Since paleo-fluid flow must have affected the host-rock through a chain-series of chemical and mineralogical reactions, leading to phases such as observed in fracture filling cements, coupling basin modelling with diagenetic studies is a valuable tool to derive quantitative predictions of reservoir properties, constraining the paleo-temperatures, fluid flow evolutions, and timing of hydrocarbon generation and trapping (e.g. Roure et al., 2005; Schneider et al., 2000; Vilasi et al., 2006; 2009).

In order to restore balanced cross-sections, the tectonic evolution across the area must be well constrained. The Dinarides is a collisional orogen where the mechanics of deformation through space and time have been recently studied in detail (Figure 4.1, see also Chapters 2 and 3). The main tectonic units of the Dinarides orogen formed during the Late Cretaceous – Oligocene period of continental collision (Schmid et al., 2008). A period of extension spanning the late Oligocene- Middle Miocene times followed, which resulted in the formation of the Dinarides Lake system (Erak et al., 2017; Harzhauser et al., 2008; 2011; Mandic et al., 2012; Stojadinović et al., 2017). From latest Miocene times renewed shortening affected the Dinarides, and remains active at present-day (van Unen et al., 2019). Although the present-day surface geometry and the regional kinematic history are well documented, estimates of shortening and exhumation rates during the tectonic evolution across the Dinarides remain speculative to a large extent. In order to derive quantitative predictions of reservoir properties, constraining paleo-temperatures, fluid flow evolution and timing of hydrocarbon generation and trapping, we have analyzed an orogenic transect in the SE external Dinarides (Figure 4.2).

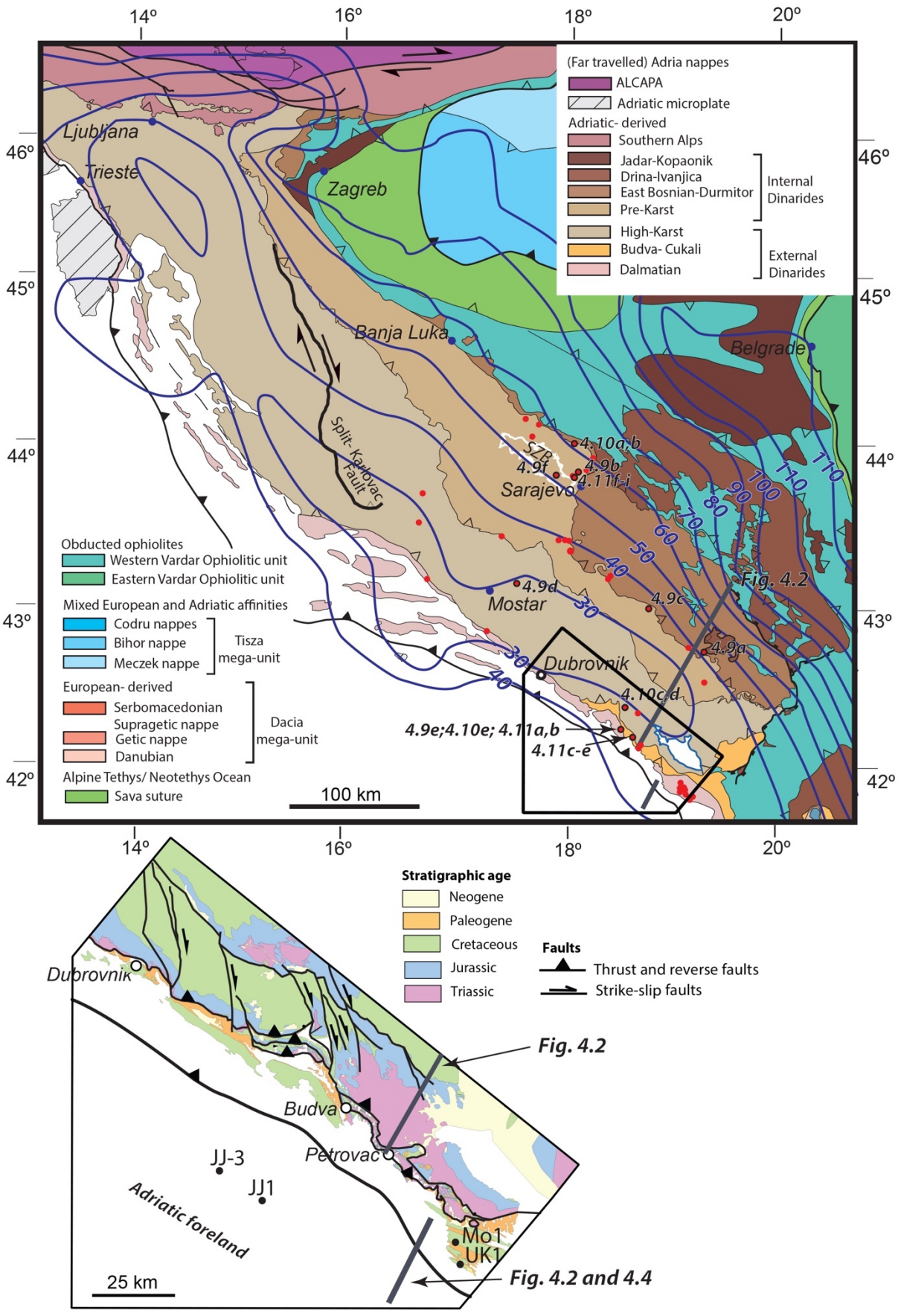


Figure 4.1 Tectonic map of the Dinarides and their junction with the Alps in the NW and the Albanides in the SE (location in the upper right inset, modified from Schmid et al. 2008). Blue

*Figure 4.1 (continued)* dots= cities, red dots= location of samples used for the petrographic and geochemistry study, red dots with thick black outline= location of the samples analyzed during the petrography study described in Figures 4.9-4.11. Blue lines represent the surface heat flow values in mW/m2 (after Milivojević, 1993 and Milivojević & Martinović, 2005). Gray lines are the locations of the crustal-scale cross-section (Figure 4.2) and the seismic line (Figure 4.4). SZB= Sarajevo-Zenica Basin. The lower left inset is an enlargement of the SE part of the external Dinarides, which is indicated by the black box in the main tectonic map. The lower left inset can be described as a more detailed tectonic map indicating the main faults. Within this inset the traces of the cross-section and the seismic line, and the location of wells are shown.

The construction of this section was aided by the interpretation of seismic lines in the offshore Montenegro, where larger amounts of shortening by thrusting are observed. The combination between offshore quantification and previous onshore interpretations (see Chapter 2) has allowed the construction of a cross-section in the southern Serbia - Montenegro sector of the Dinarides (Figures 4.1 and 4.2). Shortening, exhumation and erosion through time, were investigated by kinematically restoring this section into its pre-orogenic configuration. Based on the thermal model, the maturity of source rocks and reservoir properties (i.e., porosity, permeability) have subsequently been modelled along the restored cross-section through geological time. The tectonic-related paleo-fluid flow history has also been deduced from preliminary petrography and geochemistry investigations on representative fracture-cemented rocks in terms of diagenesis. This combined analysis has allowed us to quantify the differences in shortening and slip-rates, exhumation and subsidence rates, fluid-flow, maturity of source rocks, as well as erosion and sedimentation rates, and their impact on the hydrocarbon potential.

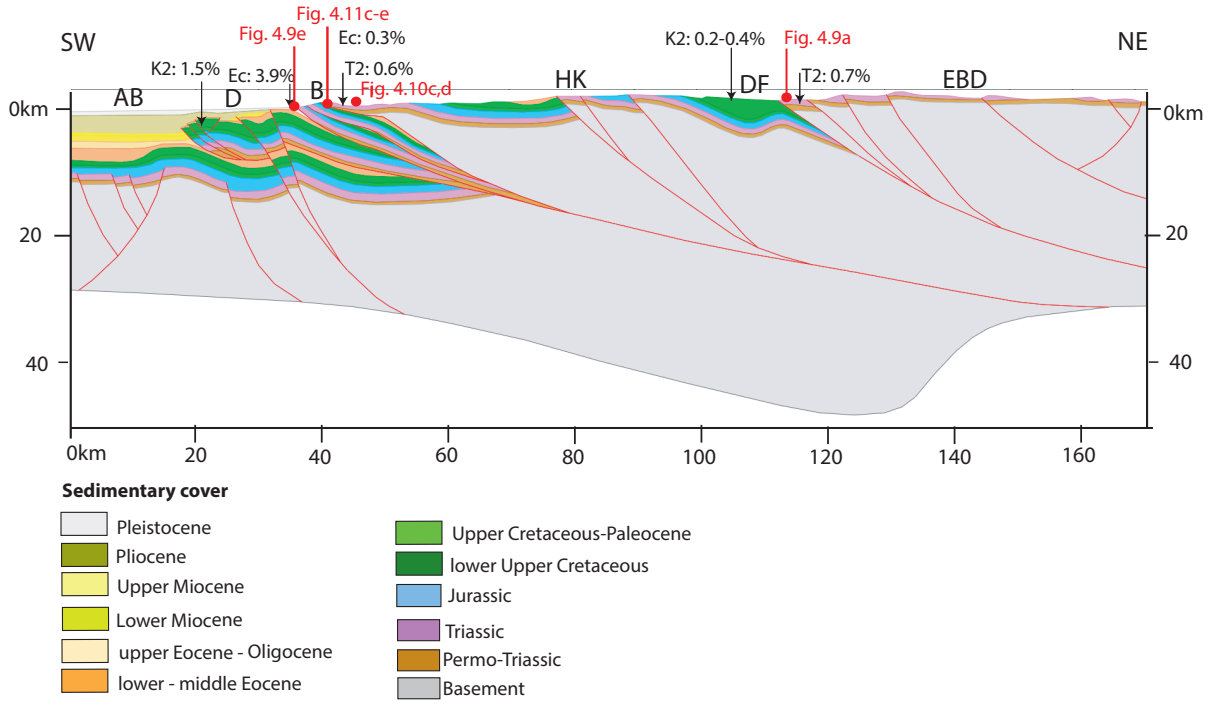


Figure 4.2 Regional orogenic cross-section that extends from the East Bosnian-Durmitor unit in southern Serbia toward the South Adriatic Basin in Montenegro. The location of the cross-section is displayed in Figure 4.1. The cross-section was edited in the KronosFlow software. The location of the rock samples from which we determined the TOC values (in %) during our Rock-Eval pyrolysis (Table 4.2) and from previous studies, are demonstrated by black arrows

*Figure 4.2 (continued)* along the surface of the cross-section. The red dots are the locations of the analyzed thin-sections of Figure 4.9-4.11. AB= Adriatic Basin, D= Dalmatian zone, B= Budva zone, HK= High-Karst unit, EBD= East Bosnian-Durmitor unit, DF= Durmitor Flysch. Ec= Eocene, $K_2$= Upper Cretaceous and $T_2$= Middle Triassic.

## 4.2 The evolution of the external Dinarides

### 4.2.1 The tectonic and lithostratigraphic evolution and its relationship with burial and exhumation

The NW-SE trending Dinarides orogen is situated in Central Europe, connecting the Southern Alps in the NW and Albanides/Hellenides in the SE, and has a SW- to S- structural vergence by gradual thrusting over the Adriatic foreland (Figure 4.1). Therefore, the Dinarides are part of the same Mediterranean orogenic system that evolved during Mesozoic–Cenozoic times (Figures 4.1). The opening of a northern branch of the Neotethys Ocean located between Adriatic- and European- derived continental units took place during the Middle Triassic. This was associated in our studied area by the formation of the Budva graben of Montenegro (e.g., Schmid et al., 2008; Stampfli & Borel, 2002; van Unen et al., 2019). To the N and NE of our studied area, the onset of the Middle Jurassic Neotethys oceanic subduction continued with a Late Jurassic–earliest Cretaceous obduction of the Western Vardar Ophiolitic unit over the Adriatic margin and with a latest Cretaceous - Paleogene period of continental collision, where deformation migrated generally to more external areas of the Dinarides (e.g., Andrić et al., 2017; Dimitrijević, 1997; Robertson et al., 2009; Schmid et al., 2008; Ustaszewski et al., 2010). The peak latest Cretaceous and Eocene-Oligocene deformation episodes were associated with the deposition of contractional turbidites ("flysch" deposits) in the footwall of various nappe units episodically during Late Jurassic - Eocene times. These successive orogenic building episodes were followed by a period of early-middle Miocene extension that affected large areas of the external Dinarides (Andric et al., 2017; van Unen et al., 2019) and the onset of the Adriatic indentation in the Dinarides in post- middle Miocene times (post- 9 Ma) that is still presently active (Handy et al., 2010; Herak et al., 2009; Tomljenovic et al., 2008; Ustaszewski et al., 2014). This latter deformation created a large number of connected strike-slip, thrusts and transpressive structures connected with the thrusting over the Adriatic foreland, which closely mirror the present-day seismicity, stress field and horizontal motions in the Dinarides and surrounding areas (see Chapter 3 for further details).

The lithostratigraphy together with burial and exhumation of sediments in the external Dinarides closely mirror the overall orogenic evolution. Post-dating Variscan deformations, Middle Permian deposits, which crop out in the Bosnian Schist Mountains, are made up by shales with coal intercalations, overlain by lagoonal micrites, dolomicrites and shales (Dimitrijević, 1997). The further deposition of the Upper Permian - lowermost Triassic deposits took place in a shallow-marine carbonatic to continental clastic environment, limestones, sandstones and shales being laterally replaced by sabkha-type evaporites (Figure 4.3) that have higher thicknesses in the external areas situated west and southwest of the Split Karlovac Fault (Figure 4.1, Kulušić & Borojević Šoštarić, 2014; Tari, 2002; Tišljar, 1992). These Permo-Triassic evaporites have been gradually buried and exhumed at much later times during the Paleogene - Quaternary deformation event. They have also been reported offshore Croatia and

Montenegro in diapiric structures (Grandić et al., 2010). The continental deposition during lowermost Triassic was replaced throughout the remainder of the Mesozoic-Paleocene by the sedimentation of the Adriatic platform carbonates, where up to 9 km of shallow water limestones were deposited in the external part of the Dinarides (e.g., Vlahović et al., 2005). The exception is the Budva graben (Figure 4.3) that recorded continuous sedimentation of Middle Triassic - Cretaceous deep-water, pelagic carbonates and, interrupting the spatial continuity of the Adriatic shallow-water carbonate sediments. In the Budva graben, the upper Lower Triassic - middle Anisian shallow water dolomites and limestones are intruded or overlain by rifting (sub-) volcanic bodies that are laterally replaced and overlain by deep-water nodular limestones, calcareous turbidites, radiolarites and other pelagic deposition that started in late Anisian times and continued until Eocene times, when sedimentation changed to turbidites (Cadjenovic et al., 2008; Crne et al., 2011; Dimitrijević, 1997; Gorican, 1994; Vlahovic et al., 2005). The total thicknesses of the Triassic – Eocene sediments is more than 3 km in the Budva graben (Zappaterra, 1990).

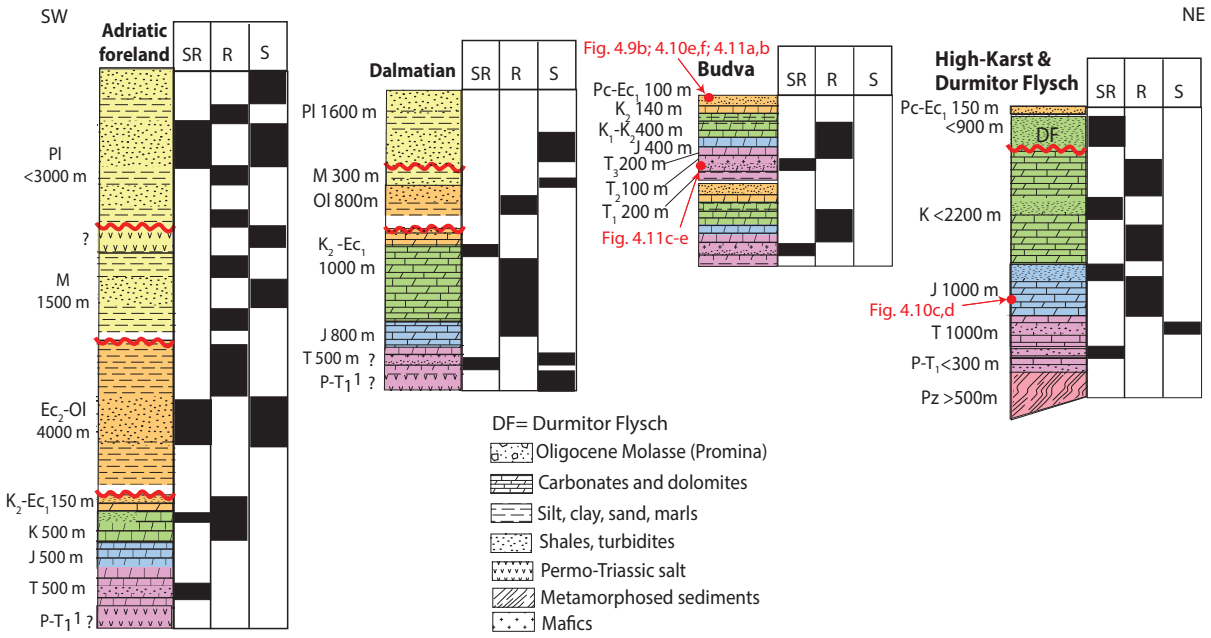


Figure 4.3 Generalized lithostratigraphic columns, indicating the source rock, reservoir rock, and seal rock intervals. The red numbers refer to Figures 4.9-4.11, which demonstrate the location of the analyzed samples.

The overall shallow-water sedimentation was also interrupted during another extensional episode that resulted in the Early Jurassic formation of the horst and graben geometry of the (South) Adriatic Basin that recorded more distal carbonate and clastic sediments. Adriatic Basin horst and graben structures possibly connected the rifted structures of the Alps (i.e. the Belluno Basin) with the ones of the Ionian Basin (Vlahović et al., 2005; Bega, 2015). Outside these deeper areas, the shallow water deposition of the Adriatic platform carbonates (limestones and dolomites) continued in the High Karst and Dalmatian units with short periods of emergence in response to the interplay between eustatic changes and tectonics (Korbar et al., 2001; Tišljar et al., 1998; Velić et al., 2015; Vlahovic, 2005). Significant tectonic events for deposition in the external Dinarides are recorded by the sedimentation of contractional turbidites. The thickest

deposition of such turbidites in our studied area is observed in the Bosnian Flysch zone, where deposition started during Late Jurassic times (the Vranduk Flysch component) and continued with larger amounts during latest Cretaceous (Maastrichtian) times (the Ugar-Durmitor Flysch component, see Chapter 2 and 3), with localized unconformities (Dimitrijević, 1997; Hrvatović, 2006; Hrvatović and Pamić, 2005; Mikes et al., 2008; Schmid et al., 2008). In more external Dinarides positions, the shallow water carbonate sedimentation prevailed until Lutetian times (Cosović et al., 1994). This sedimentation changed during the Eocene thrusting of the High-Karst, Budva and Dalmatian units, which was associated with the coeval sedimentation of up to 500m of turbidites in the footwall of the thrusts, and was partly synchronous or followed elsewhere by the late Eocene – Oligocene deposition of a shallow-water to alluvial continental regressive sequence dominantly made up by carbonate conglomerates, sandstones and breccias (Figure 4.3, e.g., the Promina "molasse", Mrinjek, 1993; Tari & Mrinjek, 1994; Zupanič & Babić, 2011). In the Dalmatian zone, an unconformity is recorded at the transition between Cretaceous and Paleocene carbonates, probably as a flexural response (i.e. forebulge) to thrusting of more internal units, while upper Paleocene to Oligocene clastics are partly eroded by their subsequent thrusting over the Adriatic foreland that was associated with the formation of a Paleogene flexural basin, where 4 km thick clastic sediments were deposited (Velić et al., 2015; Bega, 2015; Figure 4.2 and 4.3).

The external Dinarides were affected by a period of early-middle Miocene extension that created faults with variable offsets, from large-scale detachments and listric normal faulting to small-scale offset normal faults, which also created the Dinarides Lake System, an endemic and endorheic system of lakes that overlaid the previous orogenic structure (Harzhauser & Mandic, 2008; Mandic et al., 2012; Andric et al., 2017, see also Chapters 2 and 3). The largest basin in the Dinarides is the Oligocene–Miocene Sarajevo–Zenica Basin, situated SW of the Bosnian Flysch in Bosnia-and-Herzegovina (Figure 4.1). Inside this basin, a syn-contractional upper Oligocene alluvial and shallow water carbonate sequence intercalated with coals is overlain by an early-middle Miocene mixed clastic and carbonate sediments deposited in an alluvial, deltaic and lacustrine environment, including a 1-2 km thick sequence of conglomerates, deposited in response to large-scale asymmetric extension (Andrić et al., 2017; Hrvatović, 2006). Simultaneously, the deposition of ~1500 m of Miocene clastic sediments took place in the Adriatic foreland overlain locally by the typical sedimentation (including salt) of the Messinian Salinity Crisis (Bega, 2015; Tari, 2002). Up to 3 km of clastic sediments were deposited during the Pliocene - Quaternary times, where the geometry of the sediments shows a flexural foredeep in the Adriatic foreland and thrusting of the Dalmatian nappe, particularly well visible in the offshore Montenegro segment and in neighboring Albania (Figure 4.2; Bertotti et al., 2001; Roure, 2004; Vilasi et al., 2009; Bega, 2015).

### 4.2.2 Petroleum systems

Seismic reflection acquisition was achieved in the South Adriatic Basin within the framework of hydrocarbon exploration. The tectonic structures of the offshore South Adriatic Basin in Montenegro (SE-Dinarides) have been interpreted from such seismic profiles, which often reveal thin-skinned (sub-thrust) structures (Bega, 2015; Bertotti et al., 2001; Dragasević, 1983). The sub-thrust structures have not been indicated from the well logs, and are only interpreted from scarce onshore and offshore seismic lines and gravity data (Glavatovic, 2007).

Well logs provided additional information regarding the characteristics of the sedimentary sequences (Bega, 2015). Within the SE-Dinarides four principal source rock intervals, three reservoir intervals and fours seal intervals have been considered (Bega, 2015; Dubljevic, 2013; Gušić & Jelaska, 1993; Velaj, 2012; Zappaterra, 1994). First, the Anisian turbidite intervals with TOC values of up to 0.7% are considered as primary oil source. Second, the Upper Cretaceous – Middle Eocene shales and marls with up to 1.5% of TOC are thought to be oil- and gas-prone. Third, the Eocene - Oligocene shales with up to 3.9% of TOC are believed to be mainly gas prone (Figures 4.2 and 4.3). Fourth, the Lower Pliocene shales include biogenic gas sources. Potential reservoir intervals are the Cretaceous-Eocene shelf edge and platform carbonates, Oligocene-Lower Pliocene turbidites, and Miocene - Pleistocene siliciclastic intervals. Potential seals above the reservoir units, include overthrusted Permo-Triassic evaporites and Triassic shales, Oligocene and Miocene-Pleistocene intra-formational deep marine shales (Figure 4.3). The Permo - Triassic evaporites have been encountered in some onshore wells (e.g. UK-1 and Mo-1; see Figure 4.1; Bega, 2015).

## 4.3 Methodology

### 4.3.1 Seismic data (South Adriatic Basin, offshore Montenegro)

Five 2D seismic reflection lines were made available to this study by the Montenegro Seismological Observatory (with the agreement of the Montenegro Hydrocarbon Administration). For this study, only one seismic line, that is nearest to the onshore cross-section, and which extends almost in the same direction has been included in this study (Figures 4.1 and 4.2). The length of this seismic line is 36 km and has a maximum depth of 9 seconds TWT (Figure 4.4). The interpretation includes horizon and fault picking. The thicknesses of the different stratigraphic units derived from the JJ-3 well-log of Bega (2015) has been used to obtain the velocities of the different stratigraphic layers by projecting this well (with depth in metres) on the seismic line Y-80-10E (with depth in TWT seconds). These velocities have been used to convert the horizon interpretation of our seismic line from TWT in seconds to depth in metres (Table 4.1).

Table 4.1 Velocity values for the most important sedimentary intervals. Estimated in m/seconds by dividing the sedimentary thicknesses in m from the JJ-3 well with the corresponding sedimentary thickness in seconds (TWT/2) from the seismic line Y-80-10E after Bega, 2015.

| **Age sedimentary interval** | **Type of sediment** | **Velocity (m/s)** |
|---|---|---|
| Pliocene-Pleistocene | Shales and sand | 2062 |
| Miocene | Shales and sand | 2290 |
| Oligocene | Shales and sand | 2920 |
| Paleocene | Carbonates | 4000 |
| Mesozoic | Carbonates | 4374 |

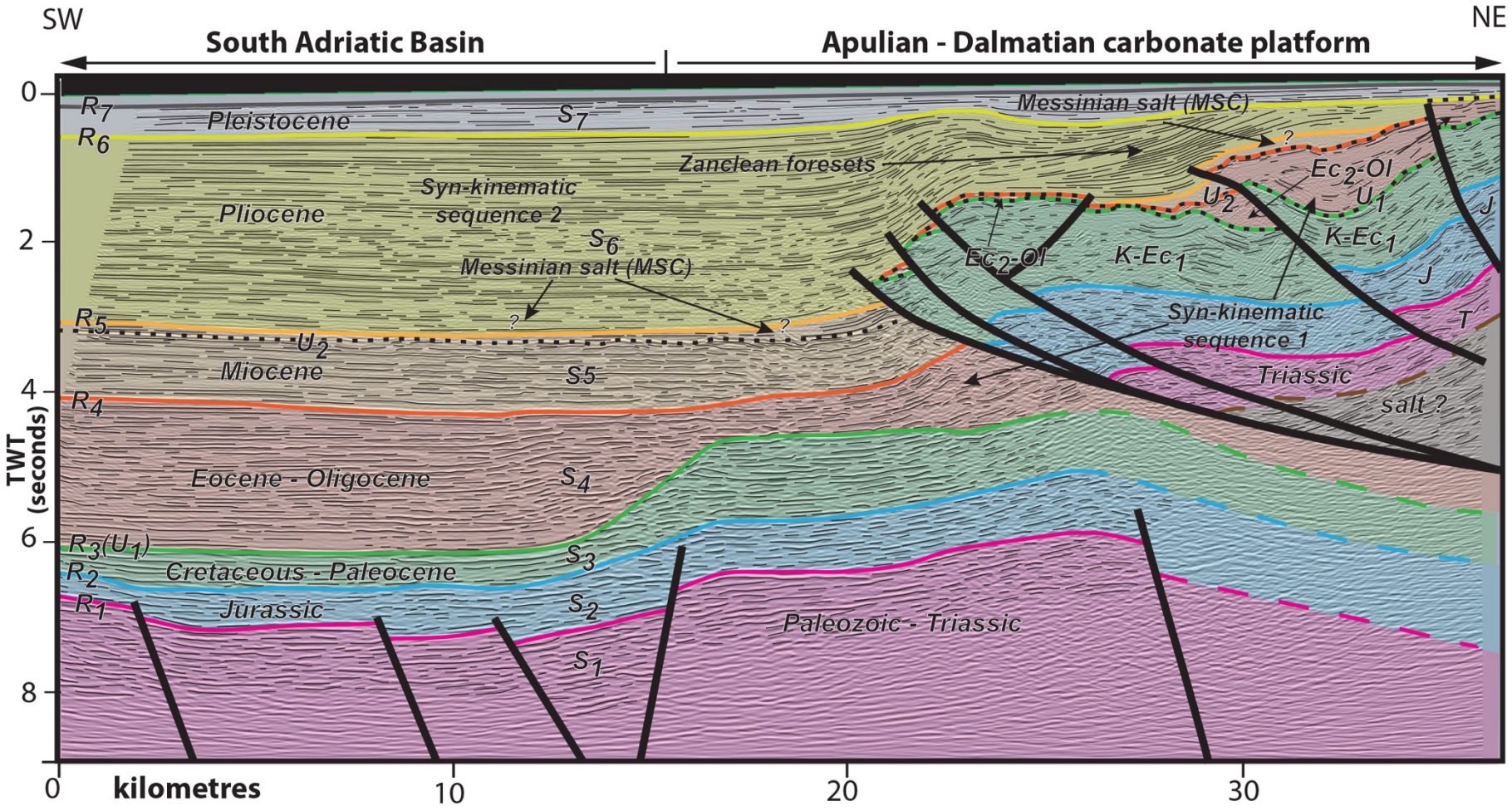


Figure 4.4 Interpreted seismic line (see text for details) situated in offshore Montenegro. The location of the seismic line is displayed in Figure 4.1. U= unconformities, R= horizons and S= stratigraphic packages. $Ec_2$-Ol= middle Eocene-Oligocene, K-$Ec_1$= Cretaceous-lower Eocene. The seismic line was made available by the Montenegro Seismological Observatory and with the agreement of the Montenegro Hydrocarbon Administration.

### 4.3.2 Numerical kinematic restorations and modelling

The present-day configuration of the restored cross-section is 172 km long, and extends through the SE-Dinarides, from the East Bosnian-Durmitor unit in Serbia in the NE towards the offshore Adriatic Basin of Montenegro in the SW (Figure 4.1). The cross-section extends perpendicular to major structures and we have avoided to cross-cut strike-slip faults. Within this study we aimed to identify the minimum amounts of shortening and extension during the main episodes of deformation, which was done by restoring the large-scale structural features that are observed in areas of major deformation. By accounting for the different deformation events and the associated kinematic and geometry changes we have restored the cross-section into its pre-orogenic configuration by the use of the KronosFlow$^{TM}$ software (IFPEN and BeicipFranlab; Figure 4.2). During the loading process of the present-day cross-section, the lithostratigraphic character for each horizon was assigned. The faults are rooted at the Moho (van Unen et al., 2019) and subdivide the cross-sections into different blocks with their own specific grid, each of which with specific grid dimensions. It must be noted that the Moho geometry, in the studied sections, is only validated for the present-day cross-section, which has been constrained from Bouguer gravity data (Šumanovac 2010; Tassis et al., 2013). The past Moho geometry during the evolution remains speculative, but has been constructed by taking into account the deformation events such as moments of rifting (uplift of the Moho) or continental collision (subsidence of the Moho).

The algorithm used for fault related deformation is the moving least square method. This method makes a global approximation of all available (unorganized) data points of the two sliding surfaces (both faults or horizons) and restores towards the region around the point for the best-fit reconstruction (Lancaster & Salkauskas, 1981). The flexural slip geometry driven method was also used to unfold extensional geometries (e.g. Sarajevo-Zenica Basin). This method unfolds objects around a straight line (e.g. fault) and preserves area, volume and line length (Dahlstrom, 1969). The mesh deformation, achieved by KronosFlow$^{TM}$, accounts for proper porous medium deformation, heat transfer, hydrocarbon generation and fluid migration, with no drawbacks on the scale nor the quality of the data obtained through subsequent thermal (basin) modelling. Decompaction between two deformation phases for each step has been calculated, which allows the related geometries to adjust with sediment unloading during backstripping.

### 4.3.3 Numerical basin modelling

TemisFlow$^{TM}$ Basin modelling software (IFPEN and BeicipFranlab) was used to construct a 2D thermal/basin model. Thermal conditions strongly influence the physical and chemical properties of the source rocks (and their associated maturity) as well as the properties of sediments and fluids, and therefore is a critical parameter in the basin model. Using an average geothermal gradient in such a complex collisional orogen is far too simple, as the resulting temperature is mainly depth depended and does not take into account the specific sedimentary intervals. In contrast, solving for conductive heat transfer with adequate boundary conditions and conductivity that depend upon rock composition and porosity (Fourier, 1822; Ungerer et al., 1990) is much more suited for achieving the objectives in this study on the Dinarides orogen. The heat flow across the sediments depend on the tectonic processes, mantle heat flow,

radiogenic heat, heat conductivity and heat capacity of the sediments, and fluid flow processes that transfer heat through the sediments (Lachenbruch, 1970).

We used uniform radiogenic heat for each sedimentary interval where the crust was set at 3.0 $\mu W/m^3$, and for the sedimentary layers varies between 1.25 and 0.01 $\mu W/m^3$ (depending on the sediments) in the presented model (Figure 4.5). This implies that a steady state vertical conduction is assumed per sedimentary interval. In order to optimize the present-day basal heat flow input value we have built multiple models to analyze the effect of the input parameters on the known constrains (such as $T_{max}$ and surface heat flow) across the models. A constant heat flow value at the base of the crust of 40 $mW/m^2$ matched the present-day surface heat flow values estimated in previous studies (Figure 4.1, Jarosinski, 2012; Milivojević, 1993; Milivojević & Martinović, 2005; Miošić et al., 2010; Ravnik et al., 1995; Turrini et al., 2017) and the $T_{max}$ values determined in this study. The thermal regime in crust and sediment is in relation with the deep geodynamic evolution associated with the position of the slab and reflects the modelled Moho geometry. We have kept the basal heat flow of 40$mW/m^2$ constant through time and by doing this we assume that the heat flow contribution from the lithospheric mantle is not varying during the evolution of the orogen. It must be noted that we do not aim to model the whole lithosphere, but rather to detail the sedimentary part of the cross-section. From the thermal models we have deduced the geothermal gradient through space and time. By analyzing the impact of these thermal input parameters on the maturity evolution model, we have focused our results on the moments when the main phases of maturity took place and to connect the maturity patterns with the tectonic evolution.

To determine the hydrocarbon potential the various elements of petroleum systems must be defined (i.e. source rock, seal and reservoir; Figure 4.3). For instance, the source rocks are defined by their type of kerogen (derived from the oxygen index and hydrogen index ratio; van Krevelen, 1950), TOC% and $T_{max}$ values. Potential source rocks have been identified in the field and sampled. In total, 21 samples were analyzed at IFPEN by Rock-Eval pyrolysis. From these samples eight were assigned as potential source rocks, which are of Triassic, Jurassic, Cretaceous, Eocene and Miocene age (Table 4.2). Pyrolysis was done with the Rock-Eval 6 apparatus (at IFPEN), featuring the determination of geochemical changes during maturation (Espitalié et al., 1977). Additional TOC values and petroleum system characteristics have been taken from previous studies (e.g., Bega, 2015; Grandić et al., 2010; Mazzuca et al., 2015; Velić et al., 2015). Vitrinite reflectance (EasyRo%) was simulated in order to estimate maturity levels. The resulting values indicate maturity as follows: immature from 0-0.55%, oil window from about 0.55-1.2%, gas window from 1.2-3.0%, and overmature when values are >3.0% (Teichmüller & Durand, 1983).

Within the basin model transparent faults are assumed, which means that fluid flow along the faults only takes place when there is a juxtaposition between permeable layers. In contrast, when there is a juxtaposition between impermeable layers the fluids will not escape along the faults and are trapped by the impermeable layers. A simplified sedimentary model of the present day section has been used to interpret and discuss the possible fluid-flow through the sedimentary cover by analyzing the relative permeability between the sedimentary intervals. Within this model we distinguished 1) the Permo-Triassic 50/50 shales and sand intervals with the exception of the Dalmatian zone where the Permo-Triassic intervals consist of salt; 2) the Triassic dolostones; 3) the Jurassic and Cretaceous limestones; 4) the Durmitor Flysch with

50/50 shales and sands; and 5) the Eocene to Pleistocene 50/50 shales and sand intervals (Figure 4.5).

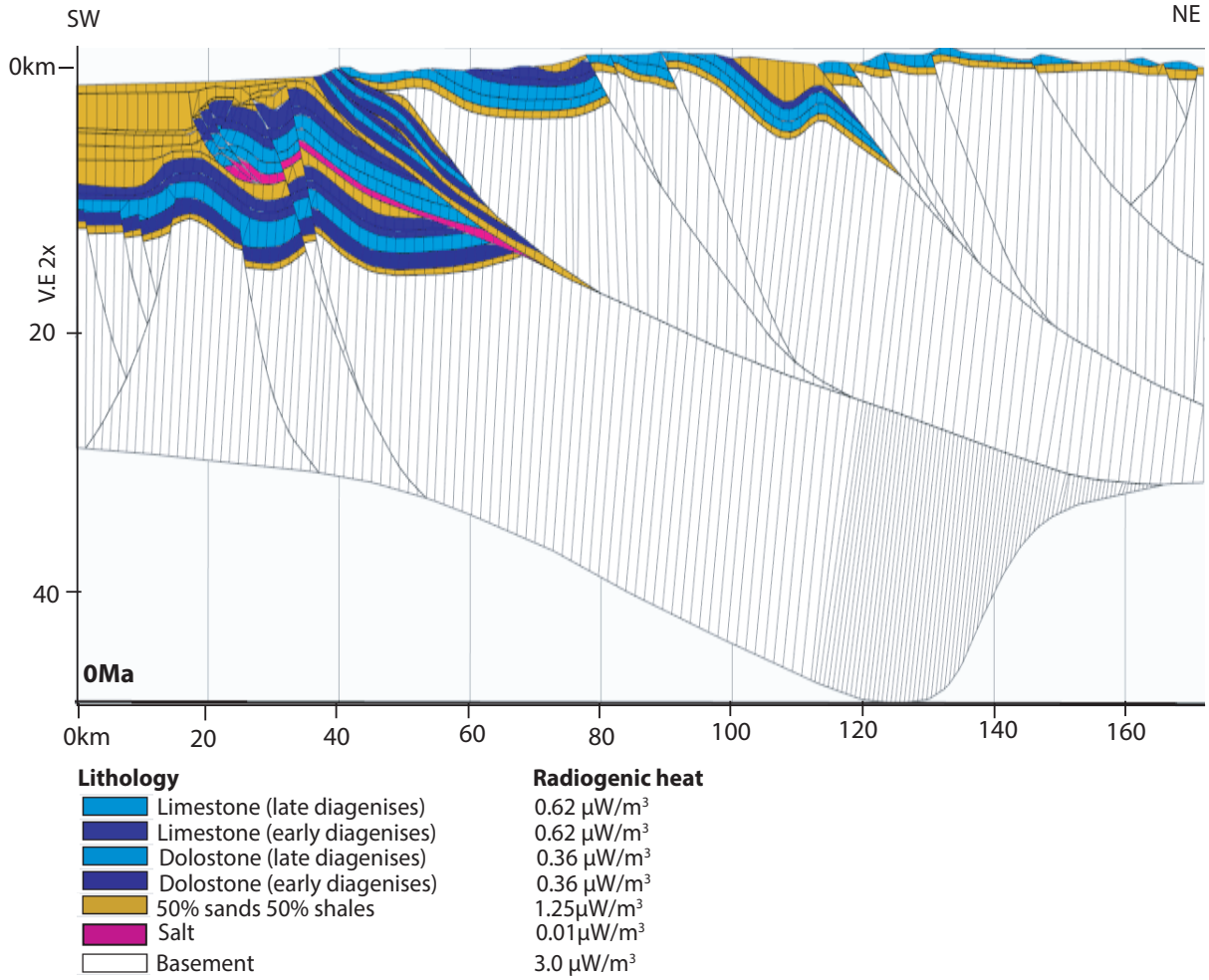


Figure 4.5 Simplified sedimentary model of the restored cross-section, showing the litho-stratigraphic characteristics that have been assigned to the different sedimentary intervals for the 2D numerical models within the KronosFlow software. The vertical and horizontal grey lines inside the cross-sections are the cells generated during the mesh deformation, similar applies for Figures 4.7 and 4.8.

### 4.3.4 Preliminary petrographic and geochemical analyses

Petrographic characterization and stable carbon and oxygen isotope analyses were achieved on representative rock samples from outcrops in the studied area. First, 101 hand-specimens were cut, polished, and stained with Alizarin Red-S and K-Ferricyanide for carbonate minerals characterization. The staining allows the rapid distinction between dolomite and calcite as well as their associated ferroan mineral phases (Dickson, 1966). Out of the studied hand-specimen, 45 thin-sections were prepared, which were stained as well (as mentioned above). Microscopic analyses of the thin-sections were done with a conventional polarized microscope (Nikon Eclipse LV100 POL) under plain polarized light (PPL) and cross-polarized light (XPL), and cathodoluminescence (CL, Nikon eclipse ME600) at IFPEN. The CL method reveals information regarding the chemical composition and exposes textures in minerals that are not

visible under the conventional polarized microscope (Sommer, 1972). Micromill Sampling System (Olympus SZ61) was used at IFPEN to collect about two milligrams of powder samples from each of 46 cement filled veins and 33 different hand-specimen for stable carbon and oxygen isotope analyses. These were done at the Friedrich-Alexander University in Erlangen, Germany. Carbonate powders were reacted with 100% phosphoric acid at 70°C using a Gasbench II connected to a ThermoFisher Delta V Plus mass spectrometer. All values are reported in per mil relative to V-PDB. Reproducibility and accuracy was monitored by replicate analysis of laboratory standards calibrated by assigning δ13C values of +1.95‰ to NBS19 and -46.6‰ to LSVEC and δ18O values of -2.20‰ to NBS19 and -23.2‰ to NBS18. By combining the oxygen isotope composition of the cements (carbonate mineral phase) with the suggested original composition of the parent fluid (from which the mineral precipitated), the mineral-precipitation temperature could be estimated (Talbot & Kelts, 1990).

## 4.4 Results

### 4.4.1 Offshore seismic interpretation

In total seven horizons (R1, oldest, to R7, seabed) and several faults were identified on the interpreted 2D seismic section (Figure 4.4). These horizons and their associated stratigraphic packages (S1 to S7, respectively) were picked mainly based on amplitude reflection characteristics, stratigraphic contacts and terminations.

#### 4.4.1.1 R1 and S1

Description – The deepest horizon R1 can be characterized by high amplitude, sub-parallel, discontinuous reflectors. It is well observed in the Adriatic Basin (SW of the seismic profile), poorly defined in the northeastern part of the Adriatic Basin (Figure 4.4). R1 overlies an overall moderate to high amplitude, sub-parallel to chaotic reflection package (S1), and underlies low to moderate amplitude, sub-parallel, discontinuous reflectors (S2). The R1 horizon is cross-cut and vertically displaced by numerous normal faults (5 faults have been traced in Figure 4.4), which demonstrates horst and graben, and tilted structures. Within the Apulian-Dalmatian domain the R1 horizon is offset and uplifted from the ones in the Adriatic Basin (Figure 4.4).

Interpretation – The R1 reflector has been interpreted to be Late Triassic in age, as it is offset by normal faults forming horst and graben structures, typical features ascribed to the Middle Triassic rifting event that prevailed until the Early Jurassic in the area of the South Adriatic Basin. The sedimentary package below R1 (i.e., S1) has a moderate amplitude, sub-parallel seismic pattern and can be described by the Paleozoic – Triassic sequence. In the duplicated series in the Apulian-Dalmatian the R1 horizon might be underlain by Permo-Triassic salt.

#### 4.4.1.2 R2 and S2

Description – The R2 horizon can be characterized by low to moderate amplitude sub-parallel reflectors, which overlie a seismic interval showing, generally, low amplitude, sub-parallel to chaotic, discontinuous reflectors (S2), and underlie a package with low to moderate amplitude, sub-parallel, more continuous reflectors (S3; Figure 4.4). The clarity of this major reflector across the investigated section is similar to that of R1 (decreasing towards the NE in the Adriatic Basin). Sub-parallel and inclined reflection patterns are observed in the centre and

northeastern part of the profile, specifically on the top of the large horst structure along R1. The R2 horizon, does not seem to be cross-cut by the normal faults that offset the underlying R1 horizon, resulting in the varying overall thickness of S2 package. Similar to the underlying R1 horizon, R2 is offset by a thrust fault representing the transition from the Adriatic Basin to the Apulian-Dalmatian carbonate platform (Figure 4.4).

Interpretation – The age of the R2 horizon can be interpreted to be the top Late Jurassic, since it is not affected by the underlying normal faults ascribed to the Middle Triassic – Early Jurassic rifting event. The S2 package would therefore represent the syn-rift sedimentary sequence, with shallow carbonate facies on the top of horst structures and deeper marine facies in the graben structures. This relates to the generally parallel (though discontinuous) reflectors in the South Adriatic Basin and the inclined higher-amplitude reflectors, that are typical of carbonate ramp build-ups, in the northeastern margin of the Adriatic Basin domain and in the Apulian-Dalmatian domain (i.e., above the large horst structure, Figure 4.4).

#### 4.4.1.3 R3 and S3

Description – The R3 horizon represents high amplitude, relatively parallel and continuous, condensed reflectors (especially in the SW part of the profile). It overlies a seismic interval (S3), which in the South Adriatic Basin, is made up of a relatively thin (<0.5 sec. TWT) package of low to moderate amplitude, parallel reflectors. Whereas, in the centre of the profile towards the NE, the thickness of S3 exceeds 1.5 sec. TWT, featuring, sub-parallel and inclined reflectors with relatively stronger amplitudes. Above R3, the typical configuration of basin-to-margin becomes clear. The overlying reflectors (S4 interval) onlap on the R3 horizon at the NE edge of the Adriatic Basin domain. The NE termination of R3 is unclear, but may be traced similarly to the underlying R2 and R1, dipping below the major thrust faults in the Apulian-Dalmatian domain. Within the Apulian-Dalmatian carbonate platform this R3 horizon could also be traced between 2.5 and 1.0 sec. TWT (Figure 4.4).

Interpretation – The high amplitude reflectors R3 that were picked between 4.2 and 6.0 sec. TWT in the South Adriatic Basin, and between 1.0 and 2.5 sec. TWT in the Dalmatian zone. It represents the top of the Cretaceous-Paleocene platform carbonates and can be associated with an unconformity (U1) based on the observed onlapping reflectors of the S4 package.

#### 4.4.1.4 R4 and S4

Description – The R4 horizon can be characterized by a key high amplitude sub-parallel reflector, which separates an interval of moderate to high amplitude, discontinuous, sub-parallel to inclined reflectors below (S4) from low to moderate amplitude sub-parallel, continuous reflectors above (S5) in the Adriatic Basin. The S4 reflectors onlap and wedge onto the top carbonate platform deposits (R3 unconformity) in the Adriatic Basin domain (Figure 4.4). Towards the NE the S4 package becomes relatively thinner with more chaotic reflectors that are offset by a thrust fault (Figure 4.4). The R4 horizon curves upward just below the thrust fault which offsets its trace about 1.0 sec TWT higher towards the NE.

Interpretation – The R4 horizon can be interpreted to represent the top Oligocene age. By that time, the South Adriatic Basin has been filled by a thick package of sand, silt, clay, marls and turbidites (Figure 4.3) with the seismo-stratigraphic characteristics reported in S4 (e.g. discontinuous, sub-parallel, downlapping reflectors). The thickness variations of S4 indicate

that the sediments are likely derived NE of the South Adriatic Basin and were deposited in the basin structure as prograding deltaic deposits. These sediments can be interpreted to be of Eocene - Oligocene age. Thrusting within the Dalmatian zone was active during the Eocene – Oligocene regional phase of contraction, which dragged the R4 horizon. The prevailing increased thickness of S4 at the contact with the thrust front suggest that this package represents a syn-kinematic sequence corresponding to the Eocene – Oligocene phase of contraction (Figure 4.4). This confirms the dating of the onset of thrusting in the Apulian-Dalmatian domain. Simultaneously, the uplift of the Dalmatian zone resulted in the erosion of the S4 sediments (Figure 4.4). Since, the overlying, younger Miocene sediments are also affected by these thrusts, the latter might have also been re-activated in the later phase of regional contraction.

#### 4.4.1.5 R5 and S5

Description – The R5 horizon is characterized by moderate to high amplitude sub-parallel reflectors in the area of the South Adriatic Basin and moderate to low amplitude reflectors in the Dalmatian zone (Figure 4.4). A seismic reflection-free pattern is observed along this horizon (which could represent the Messinian Salt). This horizon overlies an sedimentary interval (S5) consisting of low to moderate amplitude continuous reflectors in the Adriatic Basin. Furthermore, R5 underlies relatively low amplitude, discontinuous reflectors (S6). Within the South Adriatic Basin S5 is thicker (around 1 sec. TWT) compared to the Dalmatian zone (0 to <0.25 sec. TWT). The S5 reflectors can be associated with channel features in the South Adriatic Basin and within the Dalmatian zone they show a prograding wedge configuration. The R5 reflector is offset by the Apulian-Dalmatian thrust faults.

Interpretation - The age of the R5 reflector can be interpreted to be the top Miocene. The channel geometries reported in S5 package in the South Adriatic Basin can be associated with fluvial type of sediment deposition of Miocene age. R5 is interpreted as well to coincide with a major unconformity especially in the Apulian-Dalmatian domain (U2, Figure 4.4). In the footwall of the fontal thrust fault the strata has a low amplitude prograding wedging configuration. This can be associated with deltaic sedimentation in shallow marine environments during the uplift of the Dalmatian zone, coinciding with the latest Miocene phase of regional contraction and reverse faulting. As such faults offset the Late Miocene (- early Pliocene) sedimentary packages, they must have been active (or reactivated) during the latest Miocene phase of contraction.

#### 4.4.1.6 R6 and S6

Description – The R6 horizon is characterized by moderate to high amplitude, parallel reflectors, which overlies the seismic interval (S6) with varying thicknesses. S6 consists of a variety of seismic reflectors: moderate to high, and blank amplitudes, parallel to subparallel, inclined and discontinuous. The R6 horizon underlies reflectors showing low amplitude (to blank), sub-parallel, continuous characteristics (S7). The S6 reflectors can be associated with channel features in the South Adriatic Basin, and within the Dalmatian zone they show a prograding wedge configuration where the S6 reflectors onlap onto the R5 horizon (Figure 4.4). Besides, the reflectors overlying the frontal thrust faults are curved upwards and show pinch-outs attesting to syn-sedimentary fault activity.

Interpretation – The channel features and wedge shape that are found in the S6 package in the South Adriatic Basin indicate fluvial and deltaic type of sedimentation. S6 shows the typical Zanclean foresets that formed after the Messinian Salinity Crisis as they directly overlie the Messinian unconformity (see also Clauzon, 1990; Gorini et al., 2005). Due to the uplift of the Dalmatian zone during the latest Miocene phase of regional contraction and reverse faulting a major antiform geometry of S6 reflectors above the frontal thrust faults formed. The alternating low to moderate amplitude parallel reflectors of S6 can represent clastic turbidite deposits, which were triggered during the thrust activation associated with slope instability. These faults must have remained active in the Pliocene, suggesting that S6 package represents – at least partially – a syn-kinematic sequence (Figure 4.4).

#### 4.4.1.7 R7 and S7

The R7 horizon represents the seabed, overlying relatively low amplitude, parallel, continuous reflectors – typical of under-compacted deeper marine shale deposits (S7). This S7 package reflectors onlap onto the R6 horizon above the thrust faults in the Apulian-Dalmatian carbonate platform domain (Figure 4.4).

### 4.4.2 Restoration and shortening, subsidence, exhumation, and erosion estimates

The Middle Triassic-Early Jurassic rifting resulted in the formation of the Budva zone and the subsidence of the Adriatic foreland, which can be associated with crustal thinning and the formation of horst and graben structures in the Adriatic foreland (Figure 4.6a).

From Triassic to Late Cretaceous the shallow marine environment resulted in the deposition of the thick carbonate platform in the external Dinarides reaching (overall thicknesses of up to 6 km). Within the Budva zone and the Adriatic Basin, deposition took place in a relatively deeper marine environment, which can be associated with the deposition of thinner sequences of deeper, pelagic carbonates (reaching overall thicknesses of up to 3 km; Figure 4.6b). Most of the shortening in the internal parts of the Dinarides took place during the latest Cretaceous times, which can be characterized by the SW-ward thrusting of the East-Bosnian Durmitor over the Durmitor Flysch zone. This resulted in a minimum of ~20 km of shortening at this thrust contact in addition to ~2 km inside the East Bosnian-Durmitor unit (Figure 4.6b). The footwall descended to depths of about 12 km.

The continued contraction from Eocene - Oligocene times resulted in the SW-vergent low-angle thrusting in the external parts of the Dinarides, with a gradual migration towards the foreland area. The High-Karst over Budva thrust accommodates ~10km of shortening, associated with the exhumation of the High Karst zone of ~ 3km. During this time an additional ~10km of internal shortening took place within the Budva unit. The Budva over Dalmatian thrust accommodates a minimum of ~17km of shortening (Figure 4.6c). The Budva thrusting can be associated with its exhumation of ~ 3km. Most of the shortening, about 48 km, was accommodated by the thrusting of the Dalmatian zone over the Adriatic Basin. This resulted in the subsidence of the Adriatic Basin of about 4 km, which simultaneously experienced the infill of ~ 3000-4000 m of siliciclastic sediments. The Dalmatian thrusting also resulted in the erosion of more than 1 km of Eocene – Oligocene sediments. The total amount of Eocene – Oligocene shortening accommodation is ~85km.

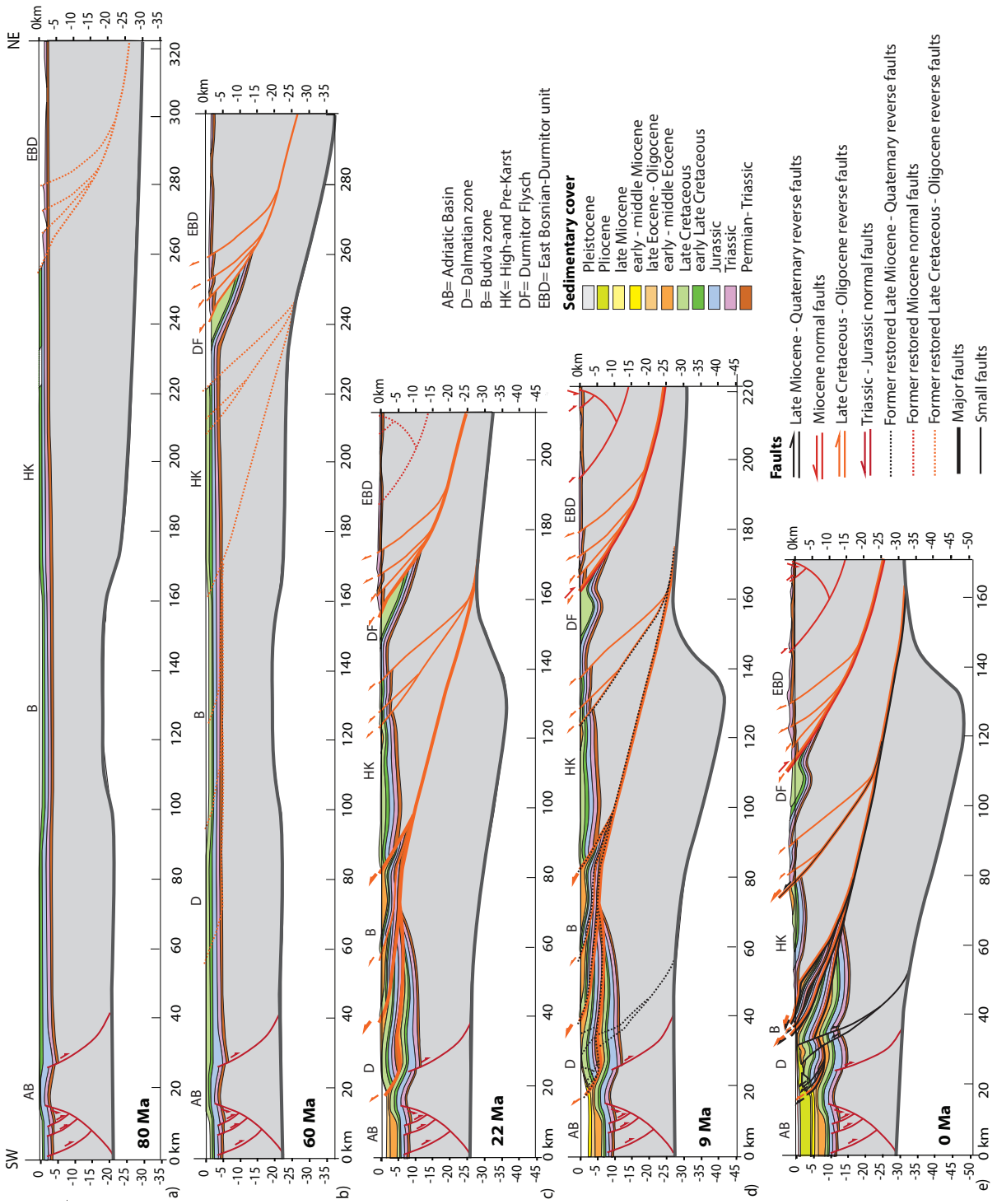


Figure 4.6 Kinematic evolution of the cross-section. AB= South Adriatic Basin, D= Dalmatian zone, B= Budva zone, HK= High-Karst unit, EBD= East Bosnian-Durmitor unit, DF= Durmitor Flysch. a) From Late Triassic – Early Jurassic the Adriatic Basin formed associated with horst-and-graben structures. The carbonate platform build-up took place from Triassic - Cretaceous times; b) The Late Cretaceous period of contraction resulted in the SW-ward thrusting of the East Bosnian-Durmitor unit over the Durmitor Flysch; c) Until Oligocene the gradual migration of contractional deformation toward the orogenic foreland could be associated with southwestward nappe stacking of the High-Karst, Budva and Dalmatian units; d) Miocene extension resulted in the footwall exhumation of the East Bosnian-Durmitor – Durmitor Flysch

*Figure 4.6 (continued)* contact; e) From latest Miocene times contraction induced high-angle reverse faulting and reactivated former structures and nappe contacts in the Dinarides.

During Miocene times about 1500 m of siliciclastic sediments were deposited in the Adriatic Basin, which resulted in basin subsidence. Furthermore, the early – middle Miocene extension reactivated the East-Bosnian Durmitor – Durmitor Flysch thrust contact, associated with the footwall uplift of ~6 km. The minimum amount of horizontal stretch during this phase of extension is >8 km (Figure 4.6d).

The latest Miocene phase of contraction resulted in the formation of high-angle N-and S-vergent reverse faults and the reactivation of former thrust contacts, with most significant reactivation in the foreland area. The High-Karst over Budva thrusting resulted in ~12km of shortening. This can be associated with the erosion of ~3km of Jurassic to Cretaceous sediments in the hangingwall of this thrust contact. During this deformation phase the Budva zone subsided about 10km, its substratum reaching depths of ~17km. About 3 km of additional shortening have been determined in the central part of the High Karst zone (Figure 4.6e). The internal thrusting inside the Budva zone seems to accommodate a minimum of ~15 km of shortening. This can be associated with the erosion of ~ 2 km of Triassic to Eocene sediments. The thrusting of the Budva zone over the Dalmatian zone accommodated about 13km of shortening. This can be associated with the erosion of ~1km of Eocene sediments in the Dalmatian zone. About 5 km of shortening have been accommodated inside the Dalmatian zone, which can be associated with transpressional fold structures that are offset with hundreds of metres by high-angle reverse and/or strike-slip faults that can be traced towards the basement (Figure 4.6e). The Dalmatian over Adriatic foreland thrusting accommodates about 5 km of shortening. Simultaneously, Neogene syn-kinematic sedimentation of more than 4000 m of siliciclastic sediments inside the Adriatic Basin took place (see also Figure 4.4), which can be associated with basin subsidence of ~4km. The overthrusting and uplift (of several km) of the Dalmatian zone can be associated with the erosion of hundreds of metres of Miocene and Pliocene siliciclastic sediments inside the Dalmatian zone. Therefore, the total minimum amount of shortening accommodated from the late Miocene - Quaternary is ~53 km (Figure 4.6e).

### 4.4.3 Thermal model

The heat flow was quantitatively calibrated by means of thermal modelling (TemisFlow™; details in Methodology). From the heat flow model, which reflects the constant heat flow input values at the base of the Moho and the calculated heat flow distribution across the investigated section (up to 80 mW/m$^2$; Figure 4.7a), the evolutions of geothermal gradients in each tectonic unit have been derived (Figure 4.7b). During the Triassic – Early Jurassic rifting the estimated geothermal gradient increases from 17°C/km to about 22°C/km in the Budva zone compared to 19°C/km in the adjacent areas. Until Late Cretaceous times the calculated geothermal gradient had an approximate continuous value of 20°C/km on average across the orogen. After the Cretaceous - Eocene thrusting the deduced geothermal gradient was 14°C/km in the area of the Budva zone, 20°C/km in the South Adriatic Basin and 16°C/km in the High-Karst unit. After the Miocene extension the geothermal gradient was about 25°C/km in the area of the Bosnian-Durmitor Flysch, 18°C/km in the Budva zone, and 26°C/km in the Dalmatian and South

Adriatic Basin. At present-day the geothermal gradient in the Budva zone, Dalmatian zone and South Adriatic Basin is 19°C/km, in the High-Karst zone 18°C/km and in the Bosnian-Durmitor Flysch 20°C/km (Figure 4.7b).

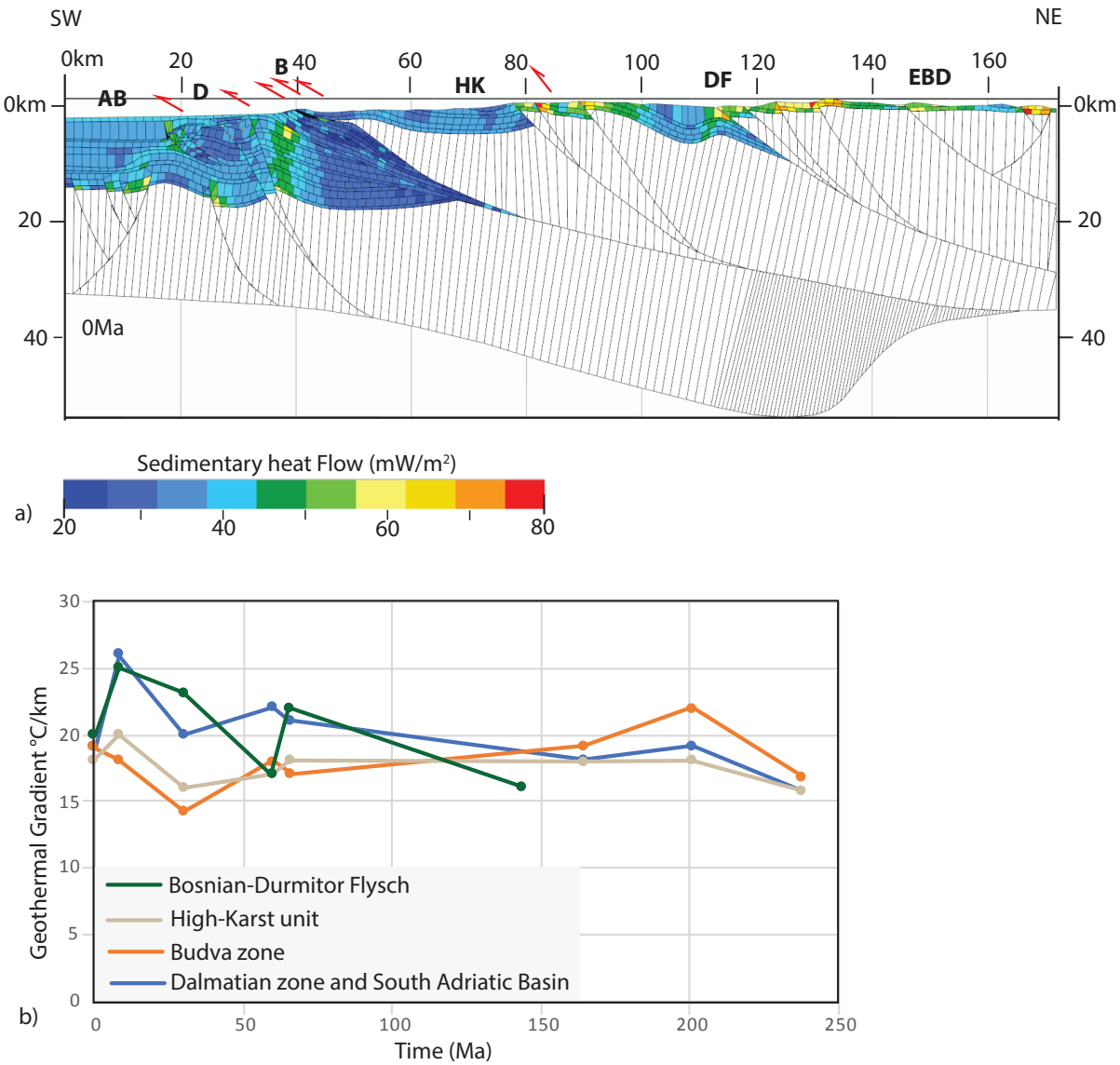


Figure 4.7 a) Heat flow distribution across the sedimentary cover of the present-day cross-section, reflecting the constant basal input heat flow value of 40 mW/m$^2$. This corresponds with the present-day surface heat flow values; b) Diagram demonstrating the variable geothermal gradient across the Dinarides through space and time, which has been extrapolated from the thermal model.

### 4.4.4 Maturity model

The three major source rocks (Triassic, Late Cretaceous - Paleocene, and Eocene - Oligocene; see also Figure 4.3) were investigated in terms of maturation degrees derived from the thermal model. After early Late Cretaceous times Triassic source rocks all across the cross-section reached the oil window, as a result of sufficient burial during sedimentation of the carbonate platform (Figure 4.8a). Within the Dalmatian zone, these Triassic source rocks reached both the oil and gas window (Figure 4.8a).

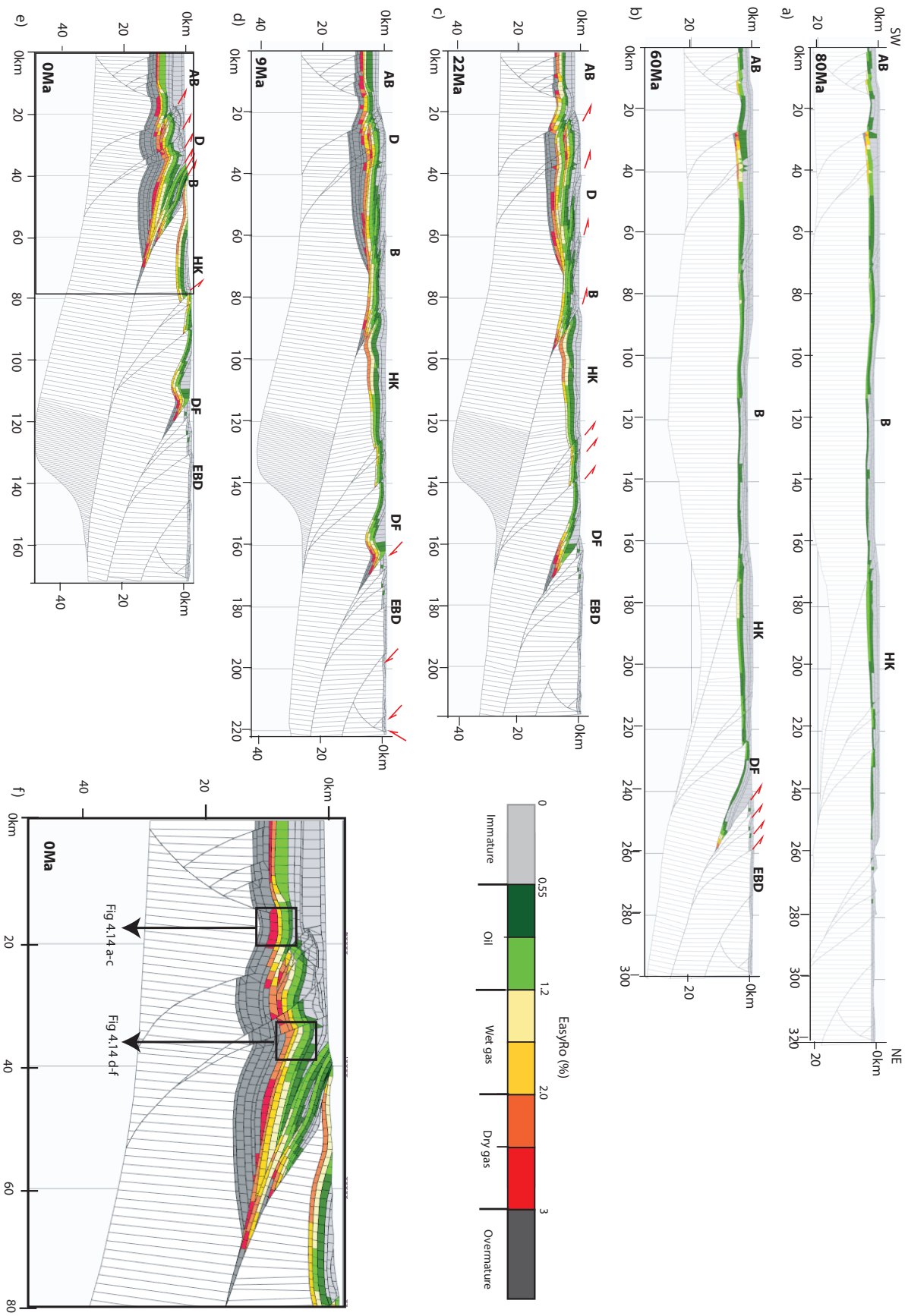


Figure 4.8 Maturity evolution of the restored cross-section. a) Maturation of Middle Triassic source rocks began after sufficient burial was reached during the deposition of the thick

*Figure 4.8 (continued)* carbonate platform across the entire orogen; b) The thrusting of the East Bosnian- Durmitor over the Durmitor Flysch during Late Cretaceous resulted in the burial and the maturation of the Triassic shales and Durmitor Flysch in the footwall of the thrust contact; c) During the Eocene – Oligocene thrusting and sedimentation, Triassic and Cretaceous source rocks became mature all across the area; d) The exhumation of the Durmitor Flysch zone during the early - middle Miocene extension, caused the mature Durmitor Flysch to reach the surface. Simultaneously, the rapid and thick sedimentation in the Adriatic Basin resulted in the maturation of Eocene - Oligocene source rocks; e) Continued thrusting, the reactivation of former thrust and thick sedimentation in the foreland from Late Miocene onwards resulted in increased burial of the footwall areas and an increase in maturation of Middle Triassic, Cretaceous and Eocene - Oligocene source rocks in the Budva zone, Dalmatian zone and South Adriatic Basin; f) Zoom-in of the foreland-area of e), which shows the location of the areas described in Figure 4.14.

These Triassic source rocks, represented by type III kerogens and residual TOC values of 0.7% (Table 4.2), have vitrinite reflectance values between 0.55 and 1.69 Ro%. During the latest Cretaceous – Eocene phase of contraction, deep burial (~12 km) of the footwall of the East Bosnian Durmitor – Bosnian-Durmitor Flysch contact took place. As a result the Triassic source rocks increased in maturity where they reached the oil and gas window (Figure 4.8b). The range in vitrinite reflectance of the Triassic source rocks in the footwall of this thrust contact obtain values between 0.55 and 1.82 Ro%.

The Eocene - Oligocene foreland-ward migration of thrusting can be associated with the burial of the Budva and Dalmatian zones, which resulted in the maturation of source rocks in these zones (Figure 4.8c). Within the Budva zone Triassic source rocks reached the oil and gas window with vitrinite reflectance values between 0.67 and 1.8 Ro%. Within the Dalmatian zone, the Triassic source rocks reached the oil and wet gas window with vitrinite reflectance values between 1.1 and 1.5 Ro%, while Cretaceous source rocks reached the oil window with vitrinite reflectance values between 0.55 and 0.82Ro%. Within the Adriatic foreland the Triassic source rocks became overmature. Cretaceous source rocks reached the oil window in the SW-part and gas window in the NE-part beneath the Dalmatian zone (Figure 4.8c). These Cretaceous source rocks have vitrinite reflectance values between 0.69 and 2.12Ro%. Below the Dalmatian thrust within the Adriatic foreland, Eocene - Oligocene source rocks reached the oil and gas window with vitrinite reflectance values between 0.55 and 1.53Ro%.

As a result of the Oligocene - Miocene sedimentation and the subsiding Adriatic foreland, the Eocene – Oligocene source rocks in the southwestern-most part of the Adriatic foreland reached the oil window. These source rocks have vitrinite reflectance values between 0.6 and 1.1Ro%. Whereas, the NE part of these source rocks beneath the Dalmatian thrust reached the gas window with values of up to 2.4 Ro% (Figure 4.8d).

Continued thrusting and the reactivation of the High-Karst – Budva and Budva – Dalmatian contacts from latest Miocene times onwards can be associated with an increase in burial of the footwall areas (Figure 4.8e,f). During this time, Triassic source rocks reached the oil and gas window in the Budva zone. These source rocks have vitrinite reflectance values between 0.89 and 2.4 Ro%. Cretaceous source rocks in the Budva zone reached the oil window, which have vitrinite reflectance values between 0.55 and 0.94 Ro%. Within the Dalmatian zone Eocene – Oligocene source rocks reached the oil window in the immediate footwall of the Budva contact,

which have vitrinite reflectance values between 0.55 and 0.71 Ro%. The mature Eocene source rocks in the Dalmatian zone can be associated with type III kerogens and TOC values of up to 0.9% (Table 4.2).

Table 4.2 Input data derived from Rock-Eval pyrolysis on samples (N=15) taken from the studied area. Location of the samples is shown by their ID number in Figure 4.2. HK= High-Karst, D= Dalmatian, DF= Durmitor Flysch, UF=Ugar Flysch, VF= Vranduk Flysch, EBD=East Bosnian-Durmitor, M=Montenegro, B= Bosnia-and-Herzegovina, C= Croatia, L. Jurassic= Late Jurassic, $T_{max}$= Maximum temperature (in °C), TOC= Total Organic Carbon content (in %), HI= Hydrogen Index, OI= Oxygen Index (van Krevelen, 1950); I= oil prone (lacustrine), II= oil and gas prone (marine), III= gas prone (terrestrial), IV= none. ln(Estimated Ro)= (0.0078 $T_{max}$) – 1.2 (after Barker & Pawlewicz, 1986).

| # | ID | Age | Unit | $T_{max}$ | TOC | HI | OI | Kerogen | Estimated Ro% |
|---|---|---|---|---|---|---|---|---|---|
| 1 | Ec | Eocene | HK(M) | 441 | 0,3 | 27 | 143 | III | 0.76 (oil-prone) |
| 2 | T2 | Anisian | HK (M) | 415 | 0,62 | 284 | 32 | II | 0.33 (immature) |
| 3 | T2 | Anisian | EBD(M) | - | 0,69 | 3 | 25 | III | - |
| 4 | K2 | Cretaceous | DF(M) | 442 | 0,28 | 25 | 21 | II/III | 0.78 (oil-prone) |
| 5 | K2 | Cretaceous | DF(M) | 433 | 0,38 | 42 | 5 | I/II | 0.63 (oil-prone) |
| 6 | Ec | Eocene | HK(M) | - | 0,3 | 3 | 83 | III | - |
| 7 | Ec | Eocene | D (M) | 442 | 0,9 | 80 | 49 | III | 0.78 (oil-prone) |
| 8 | K2 | Cretaceous | DF(M) | - | 0,2 | 10 | 95 | III | - |
| 9 | K2 | Cretaceous | UF(B) | - | 0,14 | 7 | 114 | III | - |
| 10 | K2 | Cretaceous | UF(B) | 434 | 0,23 | 17 | 143 | III | 0.65 (oil-prone) |
| 11 | J3 | L. Jurassic | VF(B) | - | 0,18 | 0 | 6 | IV | - |
| 12 | T2 | Anisian | EBD(B) | - | 0,15 | 0 | 7 | IV | - |
| 13 | J3 | L. Jurassic | VF(B) | - | 0,12 | 8 | 275 | IV | - |
| 14 | J3 | L. Jurassic | VF(B) | 444 | 0,44 | 50 | 136 | III | 0.81 (oil-prone) |
| 15 | M | Miocene | HK(B) | 435 | 2.87 | 579 | 41 | I | 0.66 (oil-prone) |

### 4.4.5 Coupled diagenetic and tectonic evolution

The preliminary petrographic analyses, which was undertaken in this contribution, is focused on the determination of diagenetic events, based on the characteristics of specific vein-filling calcite and dolomite cements and their mutual cross-cutting relationships (Figures 4.9-4.11). The isotope analyses has contributed to the determination of the fluid-origin of such specific vein-filling phases (Table 4.3 and Figure 4.12). For some veins no isotope analyses have been done, due to the small width of these veins. Based on the different deformation phases derived during the kinematic study, the timing of the fractures/veins has been determined (Figure 4.13). Three major generations of veins have been indicated along the cross-sections, which represent the main episodes of fracturing and cementation.

Table 4.3 Carbon and oxygen isotopic results (N= 46; in permil V-PDB) for different vein-filling (V) and matrix (M) cements.

| Number | Sample Label | Mineralogy | Age host rock | $d^{13}C$ permil V-PDB | $d^{18}O$ permil V-PDB calcite | Cement phase |
|---|---|---|---|---|---|---|
| 1 | V-2 | Calcite | Paleogene | -0,80 | -7,25 | C3 |
| 2 | V-5A | Calcite | Anisian | 2,79 | 0,37 | C3 |
| 3 | V-5B | Calcite | Anisian | 0,87 | 4,69 | C3 |
| 4 | V-13 | Caclite (90%) Dolomite (10%) | Permo-Triassic | 1,10 | -7,04 | C1 |
| 5 | V-18 | Calcite | Late Cretaceous | 1,35 | -4,34 | C1 |
| 6 | V-20 | Calcite | Ugar Flysch | 0,46 | -5,58 | C1 |
| 7 | V-22 | Calcite | Vranduk Flysch | 0,10 | -5,33 | C1 |
| 8 | M-22 | Dolomite | Vranduk Flysch | 0,00 | -5,20 | |
| 9 | V-24 | Calcite | Miocene | -3,01 | -8,15 | C3 |
| 10 | V-31 | Calcite | Miocene | -3,55 | -5,67 | C3 |
| 11 | V-33 | Calcite (95%) Dolomite (5%) | Anisian | 0,37 | -8,87 | C2 |
| 12 | V-40 | Calcite | Anisian | 3,70 | -6,29 | C2 |
| 13 | V-42 | Calcite (95%) Dolomite (5%) | Paleogene | 1,42 | -6,22 | C2 |
| 14 | V-44 | Calcite | Paleogene | -0,75 | -7,59 | C2 |
| 15 | V-46 | Calcite (95%) Dolomite (5%) | Anisian | 1,27 | -6,77 | C2 |
| 16 | V-49 | Calcite | Paleogene | 1,25 | -7,46 | C2 |
| 17 | V-53 | Calcite (90%) Dolomite (10%) | Anisian | -1,05 | -8,85 | C2 |
| 18 | M-53 | Dolomite | Anisian | -0,85 | -6,10 | |
| 19 | V-61 | Dolomite (60%) Calcite (40%) | Anisian | -0,55 | -8,64 | C2 |
| 20 | V-67 | Calcite | Vranduk Flysch | 1,48 | -6,48 | C1 |
| 21 | M-67 | Dolomite | Vranduk Flysch | 1,31 | -5,71 | C1 |
| 22 | V-70 | Calcite (95%) Dolomite (5%) | Ugar Flysch | 2,80 | -4,61 | C1 |
| 23 | V-72 | Calcite | Vranduk Flysch | 0,45 | -4,24 | C1 |
| 24 | V-76A | Dolomite | Vranduk Flysch | -0,76 | -8,56 | C1 |
| 25 | V-76B | Calcite | Vranduk Flysch | -0,94 | -9,77 | C1 |
| 26 | M-76 | Dolomite | Vranduk Flysch | -0,58 | -9,38 | |
| 27 | V-78 | Calcite | Ugar Flysch | 2,10 | -5,81 | C1 |

*Table 4.3 (continued)* Carbon and oxygen isotopic results (N= 46; in permil V-PDB) for different vein-filling (V) and matrix (M) cements.

| Number | Sample Label | Mineralogy | Age host rock | $d^{13}C$ permil V-PDB | $d^{18}O$ permil V-PDB calcite | Cement phase |
|---|---|---|---|---|---|---|
| 28 | V-80 | Calcite (95%) Dolomite (5%) | Vranduk Flysch | 1,75 | -4,24 | C1 |
| 29 | V-82 | Calcite | Vranduk Flysch | 0,91 | -5,44 | C3 |
| 30 | V-84 | Calcite | Vranduk Flysch | 0,35 | -9,50 | C3 |
| 31 | V-92 | Calcite | Triassic | 1,03 | -3,66 | C3 |
| 32 | M-92 | Calcite | Triassic | 1,18 | -3,25 | |
| 33 | V-93 | Calcite | Ugar Flysch | 1,82 | -12,58 | C3 |
| 34 | M-93 | Calcite | Ugar Flysch | 2,07 | -3,10 | |
| 35 | V-94 | Calcite | Cretaceous | 2,33 | -11,54 | C3 |
| 36 | M-94 | Calcite (60%) Dolomite (40 %) | Cretaceous | 2,40 | -2,26 | |
| 37 | V-95A | Calcite | Triassic | 2,46 | -10,33 | C3 |
| 38 | V-95B | Dolomite | Triassic | 2,37 | -5,49 | C1 |
| 39 | M-95 | Calcite | Triassic | 2,31 | -2,93 | |
| 40 | V-97A | Calcite | Cretaceous | -0,61 | -7,76 | C1 |
| 41 | V-97B | Calcite | Cretaceous | -0,73 | -8,11 | C1 |
| 42 | M-97 | Calcite | Cretaceous | 0,91 | -8,02 | C1 |
| 43 | V-99 | Calcite | Jurassic | 3,09 | -1,71 | C2 |
| 44 | M-99 | Calcite (60%) Dolomite (40 %) | Jurassic | 3,28 | -1,88 | |
| 45 | V-101A | Calcite | Cretaceous | 0,91 | -6,84 | C3 |
| 46 | V-101B | Calcite | Cretaceous | 0,77 | -6,99 | C3 |

#### 4.4.5.1 Sedimentary facies (host-rocks) description

The Triassic (cataclastic) sediments in the East Bosnian-Durmitor unit in Montenegro can be characterized by a fine-grained mudstone matrix (Figure 4.9a). The staining of these samples demonstrate a non-ferroan dolomite matrix with ferroan-rich calcite intercalations. The matrix of is non-luminescent to brown dull luminescent under CL and often shows high luminescent intercalations. Samples from the Vranduk Flysch can be characterized as a fine to medium crystalline mud-wackestones (Figure 4.9b). The staining of the matrix indicates a non-ferroan dolomite matrix with ferroan-rich calcite intercalations. The matrix is, generally, non-luminescent under CL with high luminescent intercalations. The Ugar Flysch (Upper Cretaceous) deposits are medium to coarse crystalline wack-packestones with organic matter inclusions (Figure 4.9c). The staining of these samples indicate a non-ferroan dolomite matrix. The matrix is non-luminescent under CL and have high luminescent intercalations. Cretaceous limestones in the High-Karst zone are medium grained wack-packestones (Figure 4.9d). The staining demonstrates a non-ferroan calcite matrix with ferroan calcite intercalations. Under CL

the matrix is orange dull luminescent, and can be associated with some non-luminescent intercalations.

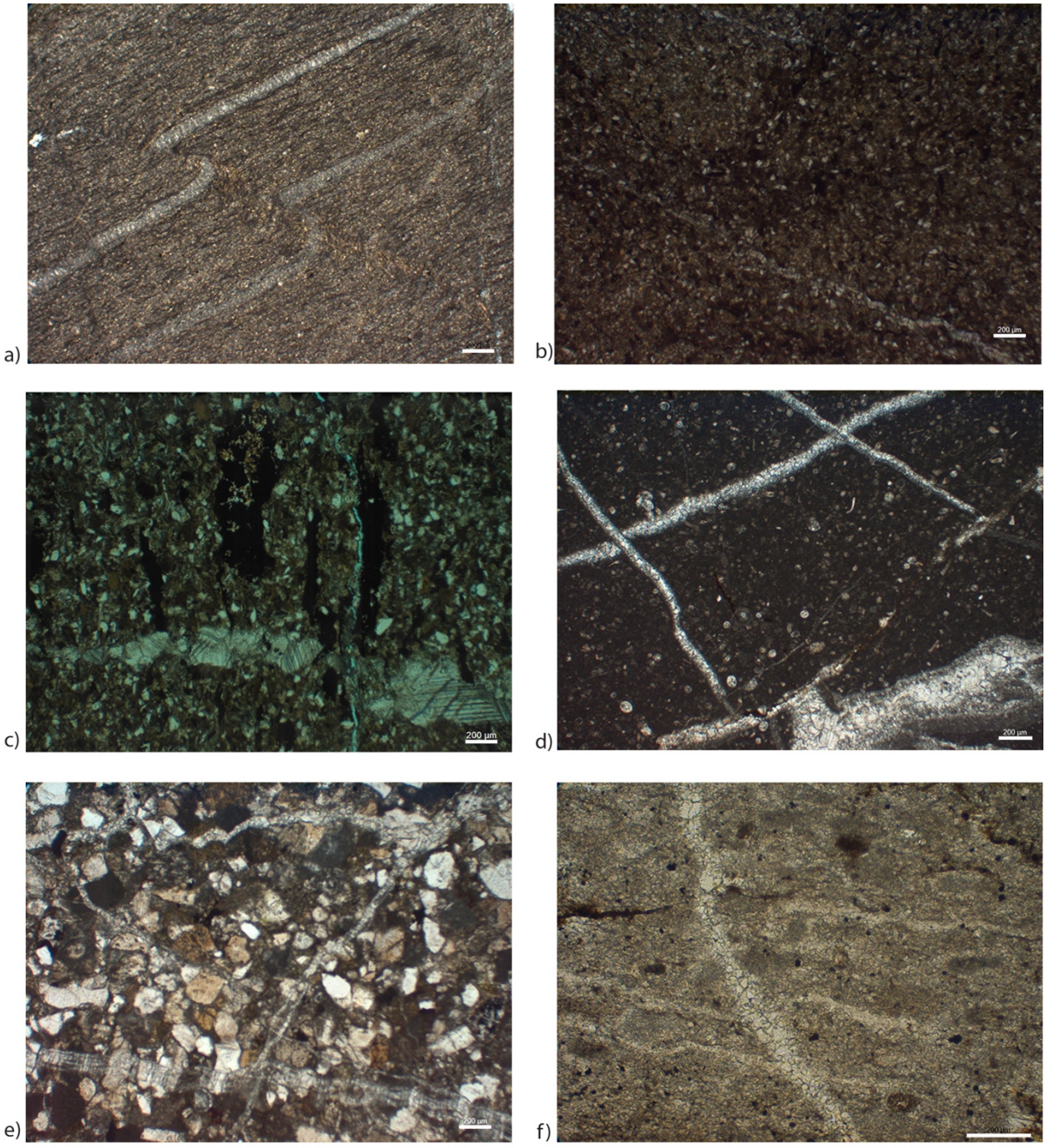


Figure 4.9 Petrographic characteristics of representative rock samples under PPL. Locations of the samples are demonstrated in Figures 4.1 and 4.2. a) Triassic cataclastics in the hangingwall of the East-Bosnian Durmitor – Durmitor Flysch contact; b) Vranduk Flysch sediments in Bosnia-and-Herzegovina; c) Ugar Flysch sediments in Bosnia-and-Herzegovina; d) Cretaceous limestones in the High-Karst zone of central Bosnia-and-Herzegovina; e) Eocene clastic turbidites in the Dalmatian zone of Montenegro; f) Miocene siliciclastics in the Sarajevo-Zenica Basin. Scale bars are 200 μm.

Samples from Eocene clastic turbidites with quartz intercalations in the Dalmatian zone of Montenegro are medium-coarse grained wack-packestones (Figure 4.9e). The staining indicates

a non-ferroan dolomite matrix with ferroan calcite inclusions. Under CL the matrix is dark orange dull luminescent with non-luminescent intercalations.

Samples from the Miocene siliciclastics of the Sarajevo-Zenica Basin are fine to medium grained mud-wackestones (Figure 4.9f). The staining reveals a non-ferroan dolomite matrix. Under CL the matrix is dull orange luminescent with some non-luminescent intercalations.

#### 4.4.5.2 Vein-filling cements

**Late Cretaceous – Eocene contraction**

Within the internal Dinarides, C1 veins have a similar orientation as the NW-SE oriented thrust faults that formed during the Late Cretaceous – Eocene phase of contraction. The C1 veins can be characterized by sparry twinned calcite crystals in the Cretaceous flysch deposits in the footwall of the East Bosnian-Durmitor – Bosnian-Durmitor Flysch contact (Figure 4.9c, 4.10a). Within Triassic carbonates in the hangingwall of this thrust contact the C1 cements have granular textures with less twinning. These vein-filling C1 cements are believed to post-date tectonic stylolites as they extend parallel to stylolites or within them (after opening of stylolites, which became the margins of the veins). The C1 appear purple (ferroan rich calcite) at the margins and pink (non-ferroan calcite) in the center upon staining. Under CL, C1 calcite cements are brown dull luminescent, which is similar to the Triassic host-rocks (Figure 4.10b). The $\delta^{18}O$ values for the C1 calcite are between -9.77 and -2.93‰ V-PDB and the $\delta^{13}C$ values are between -0.94 and 3.09‰ V-PDB (Table 4.3 and Figure 4.12).

**Eocene – Oligocene contraction**

Within the external Dinarides C2 calcite veins have a similar orientation as the NW-SE oriented thrust faults that formed during the Eocene-Oligocene phase of contraction. Within the Jurassic sediments from the hangingwall of the High Karst – Budva thrust contact, sparry calcite veins (C2) cross-cut burial stylolites (Figure 4.10c). Both the matrix of Jurassic and Cretaceous host-rocks and the C2 vein-filling (non-ferroan) cements are dull orange luminescent under CL (Figure 4.10d). Similar types of C2 veins have been observed in the Eocene clastic turbidite deposits in the footwall of the Budva – Dalmatian contact (Figure 4.10e). The matrix of these Eocene turbdities is generally non-luminescent with localized high luminescent intercalations. The C2 veins are slightly darker dull luminescent under CL compared to the Eocene turbidite matrix (Figure 4.10f). The $\delta^{18}O$ values for the C2 veins on average range between -8.87 and -1.71‰ V-PDB and the $\delta^{13}C$ values between -1.05 and +3.70‰ V-PDB (Table 4.3 and Figure 4.12). The C2 veins found in the Jurassic limestones have similar stable isotope values as the Jurassic rock matrix (see Table 4.3, M99).

**Late Miocene – Quaternary contraction**

The C3 calcite veins have similar orientations as the NNW-SSE to WNW-ESE oriented reactivated reverse faults and strike-slip faults, which were formed during the latest Miocene to present-day phase of Adriatic indentation. These C3 veins can be characterized by twinned sparry calcite crystals - radiaxial and bladed crystals are observed as well (Figure 4.11a,c,f,h).

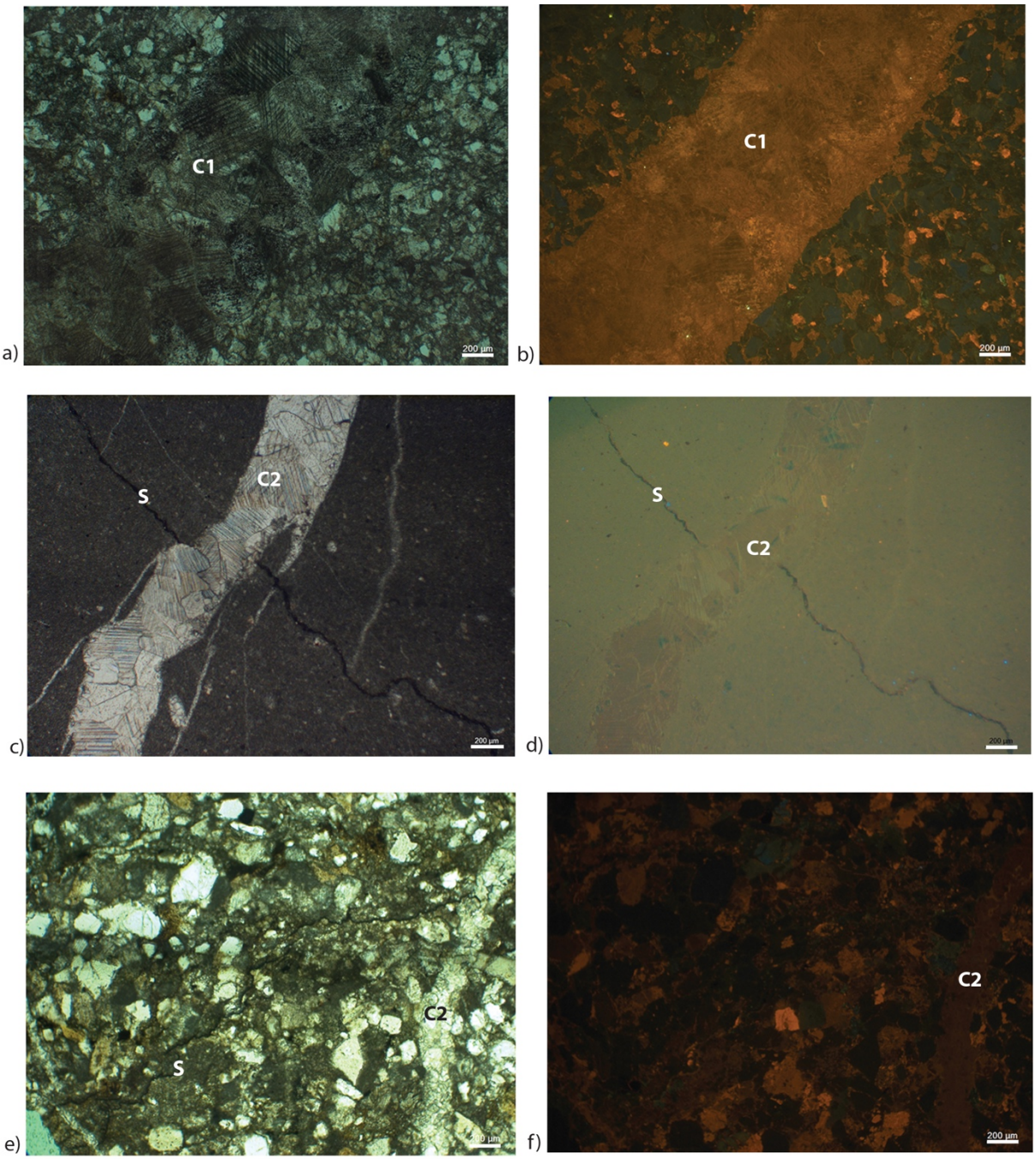


Figure 4.10 Petrographic characteristics of C1 veins associated with the Late Cretaceous – Eocene thrusting and the C2 veins associated with the Eocene - Oligocene thrusting. The location of the analyzed samples are indicated in Figures 4.1 and 4.2. Plain polarized light (PPL) images are on the left and the equivalent cathodoluminescence (CL) images are on the right. a) Vranduk Flysch sample demonstrating a medium-coarse mud- wackestone with a blocky calcite C1 vein with twinned surfaces under PPL; b) under CL this sample has a non-luminescent matrix with bright red luminescent intercalations and the C1 vein has a brown dull luminescence; c) Jurassic limestone sample showing under PPL a fine grained mud-wackstone with blocky C2 veins that cross-cut burial stylolites (S); d) under CL the matrix shows a brown dull pattern, which is similar to that of C2 vein-filling cement; e) Eocene clastic turbidite sample showing a coarse grained pack-grainstone with blocky C2 veins that cross-cut a tectonic stylolite (S) under PPL; f) under CL a non-luminescent matrix with red luminescent intercalations and a dark brown dull luminescent C2 vein is shown. Scale bars are 200 µm.

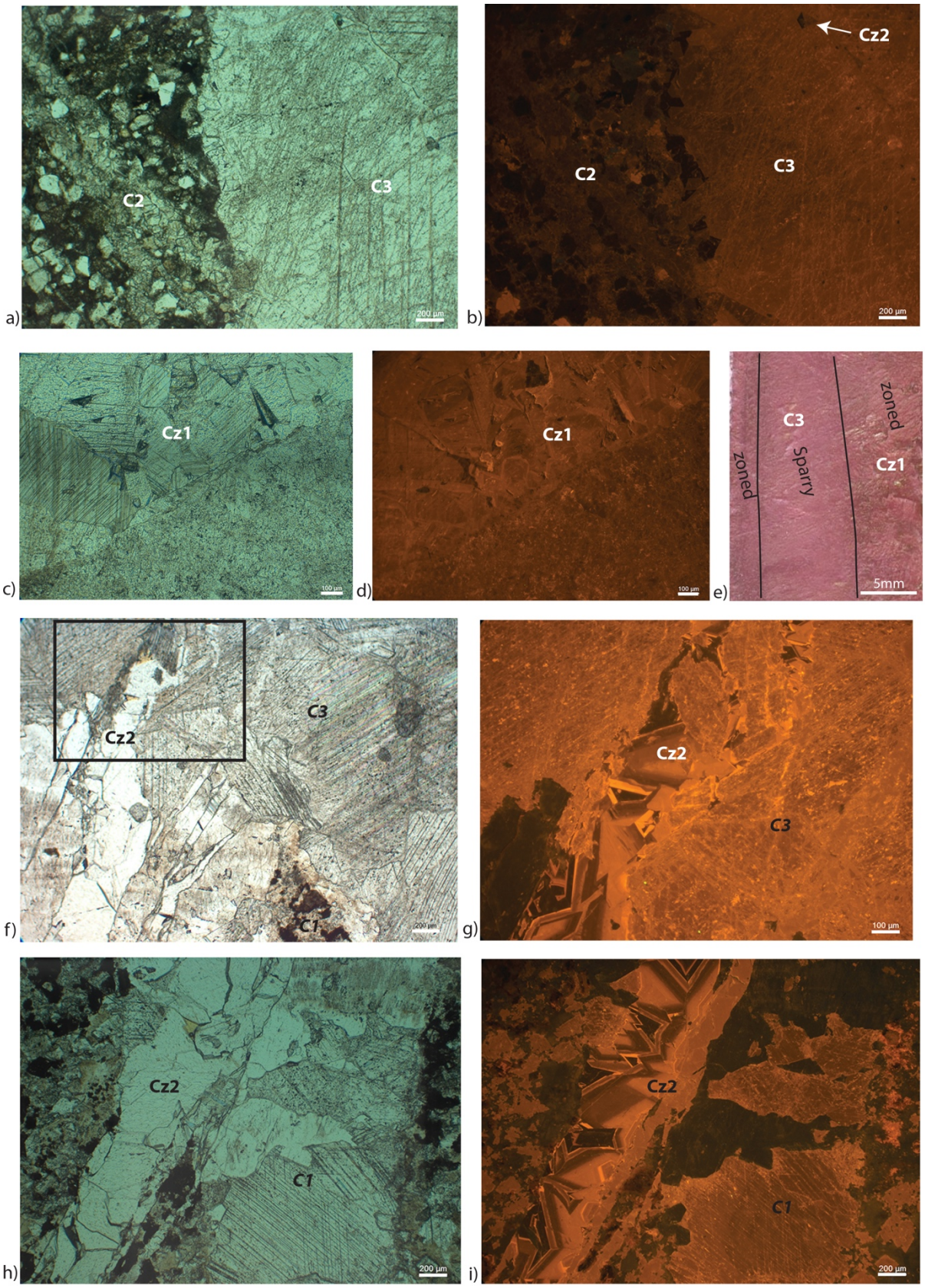


Figure 4.11 Petrographic characteristics of C3 veins, which are often associated with zoned calcite (Cz). The Cz and C3 veins were likely precipitated prior (for the former) and during the Late Miocene – Quaternary thrust reactivation (for the latter), reverse and strike-slip faulting. a) Eocene turbidite sample showing a coarse grained pack-grainstone with blocky C3 veins that cross-cut the former C2 veins and are overgrown by zoned calcite cements (Cz2) under

*Figure 4.11 (continued)* PPL. Scale bar is 200 μm; b) under CL a non-luminescent matrix with red luminescent intercalations and an orange dull with high-luminescent overgrowth textures for the C3 vein is shown. Scale bar is 200 μm; c) Triassic turbidite sample showing a vein filled with zoned calcite crystals (Cz1) associated with twinned surfaces, which was later fractured and filled by C3 cements. Scale bar is 100 μm; d) under CL the Cz1 cement has a dull orange luminescence with bright luminescent zones that are filled with non-luminescent cements. Scale bar is 100 μm; e) Stained hand specimen for the large overview of the superposition relationship between the Cz1 and C3 vein, showing that along the margin of the C3 vein the Cz1 veins extend. Both appear pink during staining, which indicates their non-ferroan calcite content; f) Vranduk Flysch sample showing the blocky twinned texture of the C3 vein under PPL. Scale bar is 200 μm; g) under CL a vein associated with zoned calcite crystals (Cz2) reveals a dull orange luminescence with bright luminescent zones that are filled with non-luminescent cements, which incises the C3 vein. Scale bar is 100 μm; h) under PPL the C1 vein has twinned sparry textures and is being cross-cut by the zoned calcite vein (Cz2). Scale bar is 200 μm; i) the C1 vein appears dull luminescent with non-luminescent overgrowth structures under CL. Scale bar is 200 μm

The staining makes these veins appear pink, indicating their non-ferroan calcite content (e.g., Figure 4.11e). Under CL the C3 vein-filling calcite cements are orange dull luminescent and can often be associated with zoned patterns that have bright red luminescent rims with non-luminescent cements in the center (Figure 4.11b,d,g,i).

Within the Eocene turbidite sediments in the Dalmatian zone of Montenegro, C3 veins cross-cut former C2 veins and are overgrown by CL-zoned Cz2 calcite crystals (Figure 4.11b). These Cz2 crystals thus post-date the C3 vein-filling cements. In the Triassic shales at the footwall of the High Karst – Budva thrust contact, the C3 veins can be characterized by a crack-and-seal type of vein, whereby the C3 vein-filling cements appear to post-date a former vein that had CL-zoned pattern (Cz1; Figure 4.11d). Under CL the central core of C3 veins show cements having orange dull CL-pattern, while the edges of the vein show calcite with faint CL-zoned (bright orange and central non- luminescent patterns; Cz1, Figure 4.11d). The $\delta^{18}O$ values for the C3 veins are between +0.37 and +4.69‰ V-PDB and the $\delta^{13}C$ values are between +0.87 and +2.79‰ V-PDB (Table 4.3 and Figure 4.12).

Within the Vranduk Flysch, along the large ~NNW-SSE oriented dextral strike-slip faults observed at the East-Bosnian Durmitor – Bosnian-Durmitor Flysch contact, the C3 veins can be characterized by twinned sparry calcite crystals (Figure 4.11f). The C3 vein-filling cements pre-date the Cz2 CL-zoned calcites. The C3 vein appears orange dull luminescent and the post-dating Cz2 calcite appears orange luminescent with bright orange zones and non-luminescent centers (Figure 4.11g, i). Note that Cz2, C3 and Cz1 veins post-date the former C1 vein.

Apart from the positive stable isotopes in the Anisian shales of the Budva zone the stable isotope values for the other C3 calcite crystals demonstrate $\delta^{18}O$ values between -2.26 and -12.58‰ V-PDB with $\delta^{13}C$ values between -1.05 and +2.80‰ V-PDB (Table 4.3 and Figure 4.12).

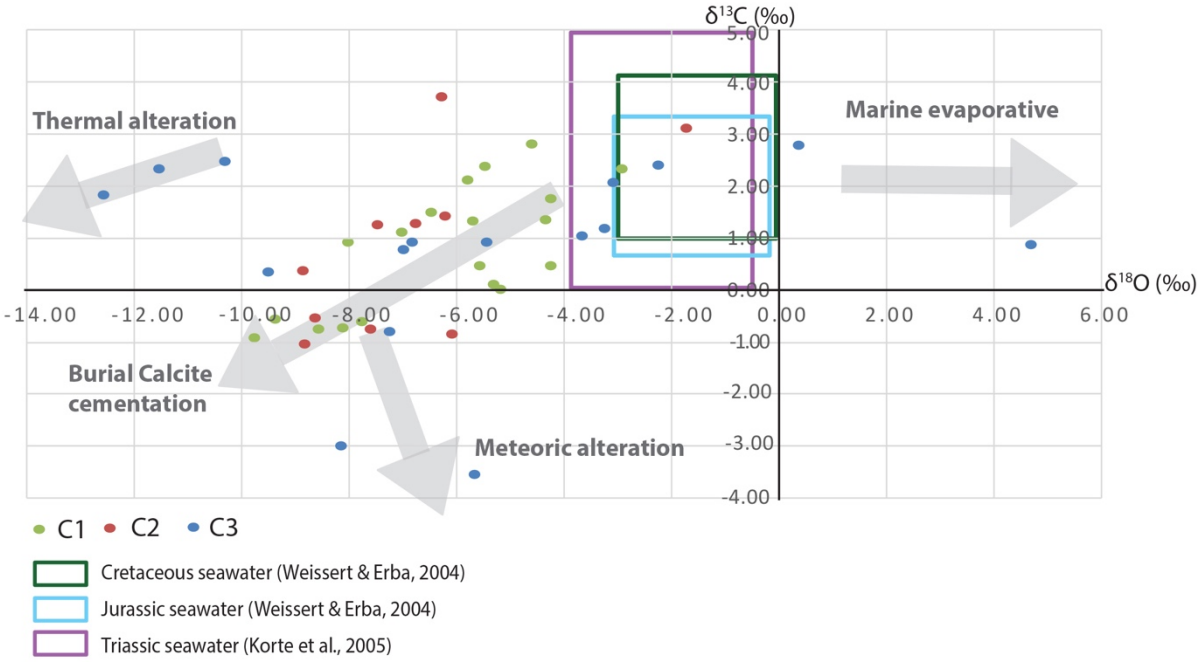


Figure 4.12 Stable carbon and oxygen isotope attributes for calcite cements C1, C2 and C3 and major host-rocks exposed in the study area.

## 4.5 Discussion

### 4.5.1 Tectonic evolution and estimates of shortening, subsidence, sedimentation, exhumation, and erosion rates

The latest Cretaceous thrusting of the East Bosnian-Durmitor over Durmitor Flysch contact in the external Dinarides accommodated ~22 km of shortening over a time span of about 20Ma from 80-60 Ma (Figure 4.6a-b) from which we estimated average slip-rates of ~0.9 mm/yr. This can be associated with sedimentation rates of ~ 0.1 mm/yr of the syn-kinematic turbidites (Durmitor Flysch) in the footwall, which got buried up to 12 km of depth indicating a burial rate of the footwall of ~0.6mm/yr. This syn-tectonic deposition can be associated with the formation of unconformities at the base of the Durmitor Flysch sequence. Due to the absence of deeper structural data in the onshore part (in contrast to the offshore), the amounts of shortening, burial, erosion and sedimentation remain highly speculative. When the deeper structures in the onshore part contains duplication structures, the shortening amounts could increase significantly.

The restoration concept we undertook, suggests that the Eocene – Oligocene phase of contraction retains most of the shortening, which was mostly accumulated in the external-most parts of the Dinarides. This moment dates the transition from thick- to thin-skinned tectonics in the Budva and Dalmatian zones. From this moment onwards there is a contrast between the thin-skinned geometry in the Budva and Dalmatian zones, with a thick-skinned geometry in the High-Karst and more internal parts. The thin-skinned geometry can be characterized by sub-thrust structures, similar to the ones that have been interpreted in Bega (2015) and to the ones observed in the Cukali zone of Albania (see also Velaj, 2015). From the restoration, the total amount of shortening is estimated to be 85 km from 60-22Ma, which can be associated with an overall slip rate of ~2.2 mm/yr (Figure 4.6d). The largest amounts of slip were accommodated

by the thrusting of the Dalmatian zone over the Adriatic foreland with shortening values of about 48 km, indicating slip-rates of ~1.3 mm/yr. The thrusting can be associated with anticlinal fold geometries with large wavelengths during the uplift of the Dalmatian zone (Figure 4.6c), which is typical for the Dinaric phase of contraction. The exhumation of the Dalmatian zone could have resulted in the erosion of the Eocene sedimentary intervals (Figure 4.4). This large-scale thrusting was likely responsible for the ~4 km of basin subsidence, associated with the formation of the foredeep wedge in the Adriatic foreland (see also Bega, 2015). Simultaneously, the first thick sequence of Eocene to Oligocene syn-kinematic siliciclastic deposition of about 4km took place inside this basin (see Figure 4.4 syn-kinematic sequence 1), which is equal to the amount of basin subsidence. From the seismic interpretation these syn-kinematic deposits can be characterized by onlapping sequences onto the carbonate ramp in the NE of the Adriatic foreland (Figure 4.4). However, the 48km of shortening accommodation, estimated from the restoration, of the frontal thrust of the Dalmatian over Adriatic Basin, is probably too high for the relative small size of the foredeep wedge constructed in our profile. This can be solved by assigning part of this shortening to the latest Miocene phase of contraction, which requires for the top Oligocene sedimentary interval to have a deeper position in the present-day profile. The contact between the deeper sedimentary intervals and the sub-thrust structures could not be clearly indicated from the seismic data and well logs, and in previous studies these structures are only interpreted from scarce onshore and offshore seismic lines and gravity data (see also Glavatovic, 2007).

From 22-9Ma, during the phase of extension, stretching rates of > 0.8 mm/yr were reached. The footwall of the East Bosnian-Durmitor – Bosnian-Durmitor Flysch contact got exhumed with about 6 km, which can be associated with exhumation rates of up to ~0.5 mm/yr in the footwall (Figure 4.6d,e). The geometry of the erosional unconformity beneath the Durmitor Flysch indicates the isostatic rebound in the footwall of an extensional detachment, which can be associated with the uplift of the Moho geometry and mantle upwelling.

The restoration of the late Miocene phase of contraction infers a minimum of 53 km of shortening over 9 Ma mostly accommodated in the foreland area (Figure 4.6e). From the total amount of late Miocene shortening an overall slip-rate of about ~5.9 mm/yr can be estimated, which is in close approximation to the velocities of the Adriatic indentation that has been investigated during previous GPS studies (e.g. Bennett et al., 2008; Grenerczy, 2005). The slip rates along the main faults are 1.3 mm/yr at the High-Karst – Budva contact, 1.7 mm/yr at the internal thrusting within the Budva zone, 1.4 mm/yr along the Budva – Dalmatian contact and 0.6 mm/yr at the Dalmatian – South Adriatic Basin contact. Erosion rates of up to 0.3 mm/yr in the hangingwall of the High-Karst – Budva contact, 0.2 mm/yr inside the Budva zone, and more than 0.1mm/yr inside the Dalmatian zone. Within our restored present-day interpretation the thin-skinned structures of the Dalmatian zone are truncated by basement-involved reverse faults, indicating thick-skinned deformation in the Adriatic foreland during the Neogene. These faults have a transpressional structure with a high inclination and have been interpreted to be of late Pliocene – Quaternary age, which is indicated by the wedge structure above the active Dalmatian – Adriatic Basin thrust that is filled with Pliocene sediments (Figure 4.2, 4.4b). The high-angle faults can be associated with the formation of transpressional folds (anticlinal geometries) inside the sediments of the Dalmatian zone, and have a deep-seated basement involved structure. Thus, in our profile the evolved thin-skinned structures during the Eocene

– Oligocene pre-dates a later Neogene phase of contraction that induced the thick-skinned high-angle reverse faults. The Middle Adriatic ridge, situated in the middle of the Adriatic Sea, has an E-W oriented transpressive structure that is distributed along many branches (Scisciani & Calamita, 2009). One of these branches prolongs to and affects the sub-thrust structure in offshore Montenegro (see also Bega, 2015), which is demonstrated in our profiles with the high inclined reverse faults (Figure 4.2 and Figure 2.11). The timing of activity of these high-angle reverse faults is interpreted to be active during Paleogene - Miocene and late Pliocene – Quaternary times, but the higher resolution of this timing remains speculative (Scisciani & Calamita, 2009). Therefore, different scenarios for the superposition relationship between the external sub-thrusts and the high-angle reverse faults could be made (see also Figure 2.11b,c).

Furthermore, the uplift of the Dalmatian zone, likely resulted in the erosion of the Miocene sediments creating unconformities at the top Miocene (U2 in Figure 4.4). During late Miocene – Quaternary times a second period of large syn-kinematic sicliclastic deposition took place (see Figure 4.4 syn-kinematic sequence 2), which can be marked as the main episode responsible for the formation of the foredeep wedge in the Adriatic Basin (see also Picha, 2002). The thick deposition of the syn-kinematic sequence 2 can be associated with the formation of the unconformity at the top Messinian in the Adriatic Basin (Figure 4.4). The basin subsidence of ~4km (with rates of ~0.8 mm/yr) underwent simultaneous infill of 4km of Late Miocene to Pleistocene sediments. The low slip-rates of 0.6 mm/yr of the Dalmatian zone over the Adriatic Basin indicates a low impact of orogenic loading, which unlikely explains the strong basin subsidence. Therefore, the significant basin subsidence is rather related to flexure of the lithosphere associated with subduction relative to this basin, which can be responsible for the accumulation of flexural subsidence (e.g. Wortel & Spakman, 1992; Zoetemeijer et al., 1993). This can be related to the indenting Adriatic plate (see also Chapter 3; Grenerczy et al., 2005; Picha, 2002). Similar flexure of the Adriatic lithosphere has been indicated beneath the Apennine foreland, which is responsible for the formation of the Apennine foredeep basin (see also Bertotti et al., 2002; Royden, 1993).

## 4.5.2 Correlating the diagenetic features with the fluid-flow and thermal evolution

It should be noted that this diagenetic study was only preliminary and further advanced diagenetic analyses need to be considered to better constrain the proposed fluid origins, fluid-flow evolution and fluid-rock interactions.

### 4.5.2.1 Late Cretaceous – Eocene NW-SE oriented fracturing

The Late Cretaceous onset of NE-SW oriented contraction resulted in the formation of NW-SE oriented fractures. Gradual burial during thrusting and deposition resulted in the precipitation of C1 cements inside these fractures (Figure 4.13). These cements show stronger twinning in the footwall areas compared to the hangingwall areas, which is due to more significant shearing burial of the footwall (Figure 4.10a). The C1 veins post-date burial stylolites.

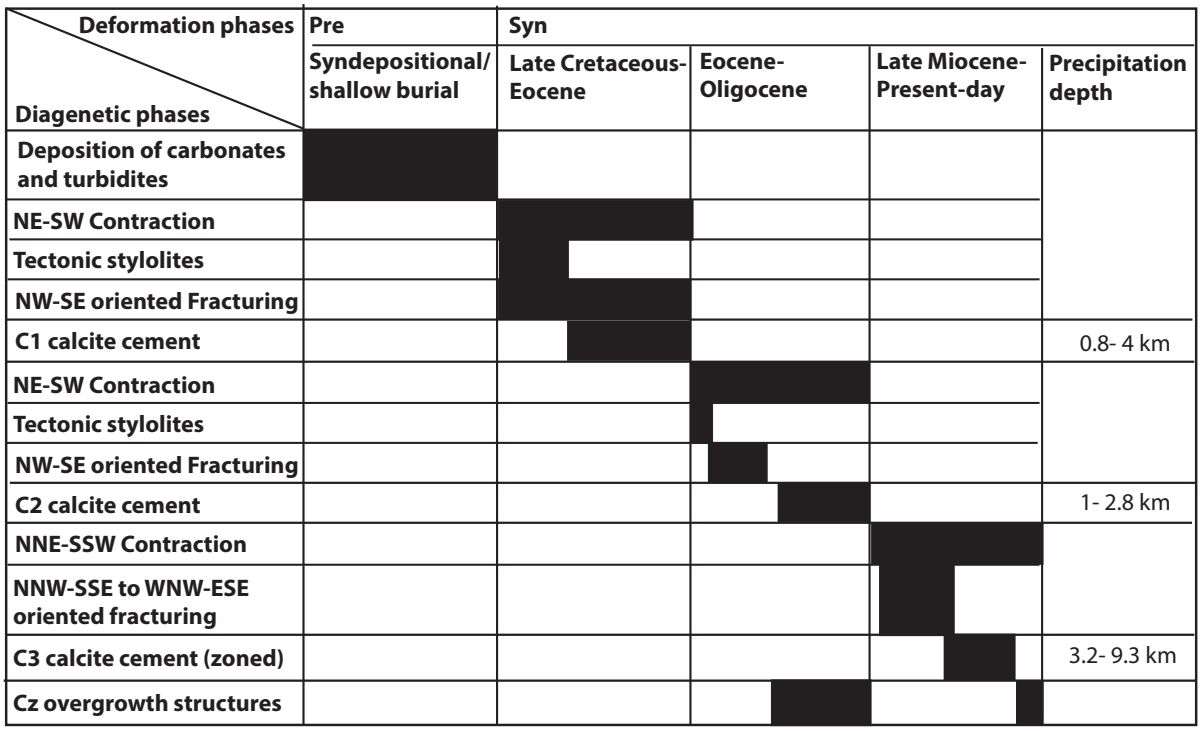


Figure 4.13 Diagenetic evolution (paragenesis) constrained from the preliminary petrography study with the focus on the main phases of deformation and the associated calcite cementation.

The ferroan characteristic of the C1 calcite cements that diminishes towards the center of the veins (disappearing at the center of the veins), suggests two possibilities: first, that the original iron content of the parent fluid was depleted during precipitation; or second, that the precipitation occurred during uplift (or change towards more oxidized realms). The C1 calcite brown dull luminescence and strongly depleted oxygen isotope values (as low as -9.77 ‰ V-PDB; Table 4.3 and Figure 4.12) may also confirm a reduced burial environment prevailing at the time of cementation. As the CL-pattern of the Triassic carbonate matrix is similar to that of the fracture-filling C1 cements, the latter could have been buffered by Triassic formation water during burial (Figure 4.15a). This also suggested by the resulted wide range of oxygen isotope values (-9.77 to -2.93‰ V-PDB) and the $\delta^{18}O$ and $\delta^{13}C$ values decreasing trend (Figure 4.12). Hence, C1 cements that must have precipitated after burial stylolites, appear to have been subsequently affected by burial diagenesis (recrystallization) and crystal deformation, most probably during further thrusting.

Based on the fractionation equation of Friedman & O'Neil (1977), and by assuming that the original parent fluid of C1 cements is Triassic seawater (with $\delta^{18}O$ between -4 and -0.5‰ V-SMOW; Korte et al., 2005), we estimate the precipitation temperatures of these cements to be up to 64°C. With the help of the constructed thermal model, the corresponding burial depth of C1 cements would be between 938m and 4000m (with an average geothermal gradient of 16°C/km in the High-Karst zone). The restoration model, represented in Figure 4.6b, demonstrates that the Durmitor (and equivalent Bosnian) Flysch intervals (Triassic host-rock) were buried to 12 km. The petrographic and geochemical characteristics of the fracture-filling C1 cements in such host-rocks, constrain the precipitation timing an depth, falling with the above mentioned burial depth. In addition, since the isotopic signature of the cement is similar

to the host rock, precipitation from Triassic formation water and/or fluid-rock buffering might have prevailed. Such fluids may also have flown upward through permeable rocks with continuous thrusting.

#### 4.5.2.2 Eocene – Oligocene NW-SE oriented fracturing

The Eocene onset of NE-SW oriented contraction resulted in the formation of NW-SE oriented fractures in the external parts of the Dinarides. The Late Cretaceous – Eocene and Eocene – Oligocene sets of fractures have thus similar orientations. Gradual burial during thrusting and deposition resulted in the precipitation of sparry calcite cements (C2) inside the latter fractures (Figure 4.13). These calcite crystals often have twinned surfaces (e.g. Figure 4.10c), which indicate processes of shearing burial. The C2 calcites have similar dull luminescence as the Jurassic host-rocks (Figure 4.10d). This suggests that during the footwall burial and fracturing, associated with the thrusting, the precipitation of the C2 cements was buffered by the internal fluids from the Jurassic formations. This is in agreement with the similar carbon and oxygen isotope values for the Jurassic matrix with a $\delta^{18}O$ of -1.88‰ V-PDB and a $\delta^{13}C$ of 3.28‰ V-PDB and the C2 vein-filling calcite with a $\delta^{18}O$ of -1.71‰ V-PDB and a $\delta^{13}C$ of 3.09‰ V-PDB (see Table 4.3; e.g., V99 and M99). The precipitation of these cements took place after burial stylolites developed (Figure 4.10c,e). Since staining indicates that these calcites are non-ferroan, the parent fluids prevailing in such burial environment would have a relatively low iron content. Alternatively, calcite cementation occurred in oxidized conditions. From these observations we interpreted the fluid from which the C2 cements were precipitated to be either Jurassic formation seawater or another fluid that has been buffered by Jurassic limestones due long residence time. These fluids have been buried during sedimentation and later released during the Eocene - Oligocene thrusting, resulting in the precipitation of the C2 cements (Figure 4.12; see also Vilasi et al., 2009).

By implementing the obtained $\delta^{18}O$ values for the C2 vein-filling calcites into the fractionation equation of Friedman & O'Neil (1977), assuming that the parent fluid is Jurassic seawater with $\delta^{18}O$ composition between approximately -3.0 and -0.5‰ V-SMOW (Figure 4.12; Weissert & Erba, 2004), the precipitation temperatures could be estimated to be between 29 and 54°C. These temperatures infer a precipitation depth between 1526 and 2842 m (with an average geothermal gradient of 19°C/km in the High-Karst, Budva and Dalmatian zones). This can be correlated to the restoration model of Figure 4.6c, which demonstrates that the Jurassic and Eocene sedimentary intervals (reaching depths of up to 3 km) into which the C2 veins are precipitated, fall within the calculated depth range.

#### 4.5.2.3 Late Miocene – Quaternary NNW-SSE to WNW-ESE oriented fracturing

The late Miocene – Quaternary phase of ~NNE-SSW oriented contraction can be associated with the formation of NNW-SSE to WNW-ESE oriented fractures. The progressive increase in burial of the footwalls of active thrust contacts in the SW-most part of the orogen can be associated with the precipitation C3 sparry calcite cements inside the evolved fractures (Figure 4.13). The observed twinned crystals also indicate processes of shearing burial (Figure 4.11a,f). The wide spread in $\delta^{18}O$ values (between -12.58 and -2.26‰V-PDB) suggests that the precipitation of these cements took place at different elevated temperatures, or from a mixture of fluids having different origins (Figure 4.12). The dull to bright luminescence CL-pattern of

these cements is different than that of the host-rocks. This might indicate that the C3 cements likely have an extrinsic, deep-sourced fluid origin. The position of the detached slab post-Oligocene times is located at the High-Karst – Budva, and Budva – Dalmatian and Dalmatian – Adriatic Basin contacts (Figure 4.15c). This could have resulted in the migration of deep-sourced, probably magmatic-related fluids from the accretionary wedge of the subduction zone towards the surface along active faults and NE of the slab (Figure 4.15d).

Some of these fracture-filling calcites show strong depletion in $\delta^{13}C$ values, typical of values associated with processes of meteoric alteration (Lohmann, 1988). The meteoric alteration could have resulted in the different overgrowth textures and of zoned calcite cements Cz2 (Figure 4.11b,g; e.g., El-Ghali et al., 2013; Permanyer et al., 2015). Correlating the $\delta^{18}O$ values for the C3 calcite veins, the fractionation equation of Friedman & O'Neil (1977), and a magmatic $\delta^{18}O$ composition from Neogene - Quaternary between +6 to +6.9‰ (Seghedi et al., 2004), suggests that the precipitation of such cement might have occurred at temperatures between 62 and 177°C. During this time the geothermal gradient in the Dalmatian zone and Bosnian Flysch are about 19°C/km of the former and 20°C/km of the latter area (Figure 4.7b). This indicates a precipitation depth between about 3263 and 9316 m in the area of the Dalmatian zone and between 3100 and 8850 m in the Durmitor Flysch zone. These depths may be reached in the Eocene turbidites in the Dalmatian zone and in the Durmitor Flysch (Figure 4.6e)

Meteoric alteration processes may have also affected the rocks prior to the deposition of the C3 cements. This has been indicated in the Triassic turbidite sediments in the Budva zone (Figure 4.11c-e) where veins with zoned calcite crystals Cz1 are believed to have precipitated prior to the precipitation of C3 cements, but after the formation of the C1 and C2 veins that formed from Late Cretaceous - Oligocene times. These veins associated with Cz1 cements appear along the margins of the C3 veins (Figure 4.11c,d), which both cross-cut former C2 veins. This can be explained by the process of crack-and-seal, which have a strong relation with zoned calcites cements (e.g., Gaviglio, 1986; Ramsay, 1980). These zoned calcite cements have likely been precipitated from meteoric fluids (El-Ghali et al., 2013), which from our petrography study has been indicated to be dated after Oligocene and before Late Miocene times (Figure 4.15c). The C3 veins, observed in the footwall of the High-Karst – Budva thrust, contact have a dull luminescence, which is different to the non-luminescent Triassic host-rock and therefore could be associated to an external fluid source. The positive oxygen isotopes could indicate a saline fluid source origin (Figure 4.12), possibly related to the original evaporated saline water during Permo-Triassic times (Fiket et al., 2008; Vilasi et al., 2009). These formation waters could have been released during the Late Miocene thrust reactivation associated with the precipitation of the C3 cements inside the evolved fractures. Correlating the assumed positive $\delta^{18}O$ values for the C3 calcite veins, the fractionation equation of Friedman & O'Neil (1977), and a Permo-Triassic seawater $\delta^{18}O$ composition between approximately -4.0 and -0.5‰ V-SMOW (Figure 4.12; Korte et al., 2005), indicates that precipitation occurred at temperatures reaching around 18°C. These temperatures infer a shallow precipitation depth of up to 1000 m (with an average geothermal gradient of 18°C/km in the Budva zone), which are being reached for these Triassic sedimentary intervals in the Budva zone (Figure 4.6e and 4.7b).

#### 4.5.2.4 Possible alternatives to the diagenetic fluid flow model

Other alternatives for the diagenetic fluid flow model could be considered, including extrinsic fluids that are not buffered by or that are not in thermal equilibrium with the host-rock. Such non-thermal equilibria can evolve when the host-rock is being effected by the advection of fluids with different temperatures (see also Roure et al., 2010). For example when the host-rock gets in contact with meteoric water, which can be colder, or hydrothermal fluids, which can be hotter than the host-rock. In order to optimize the knowledge regarding the thermal (dis)equilibrium, micro-thermometry can be applied, which can also help in dating several other diagenetic episodes and in reconstructing the fluid-flow history (see other case studies such as Dewever et al., 2010; Roure et al., 2010; Vilasi et al., 2009). To better constrain and further detail the fluid-rock interactions, other information such as rock temperature, timing and duration of the diagenetic episodes, whether diagenesis takes place in an open- or closed-system, fluid compositions and fluid velocities (i.e. controlling the growth and dissolution of various minerals) need to be acquired (e.g. Ferket et al., 2003; Roure et al., 2010).

This preliminary diagenetic study focused on the main phases of cementation, which are the ones that could clearly be linked to the different deformation events that were well defined at outcrops (van Unen et al., 2019). Although several generations of cements have been sampled, the current petrography and stable isotope study may not be detailed enough to distinguish all possible generations of cements. To distinguish the different generations in more detail, further sampling and stable isotope analysis are necessary. When the isotopic signature of a certain diagenetic phase (e.g. cement) evolves during geological time (burial history, paragenesis), the interpretation of such results regarding the estimated temperatures becomes complicated and has to be taken with care. The presented and interpreted results in this thesis are preliminary and the proposed ranges of deduced temperatures are broad and have to be considered as basic assumptions (that are in line with the scale of the burial/thermal modelling). Reconstruction of the isotope signatures of the key diagenetic phases can be proposed for future research to assess the fluid-flow history in more detail (such as in Dewever et al., 2010; Ferket et al., 2003).

### 4.5.3 Maturity model: petroleum system implications

The maturity model demonstrates that the geodynamic processes have a first order influence on the thermal picture. Together with the organic content of the various formations, this allows to derive an integrated picture of the petroleum systems. Present-day observed seeps at the surface and in well logs confirm presently active petroleum systems in the studied area. As the structures and internal sedimentary intervals of the cross-section have mainly been built from surface kinematic analyses, the deeper sedimentary structures for the onshore part of the cross-section remain speculative. For the offshore part we had better constraints due to available seismic data.

#### 4.5.3.1 Adriatic Basin

From the maturity model three different source rocks intervals have been indicated for the Adriatic foreland. The Triassic shale source rocks reach the oil window from early Late Cretaceous times onwards, which can be associated with burial during sedimentary deposition (Figure 4.14a).

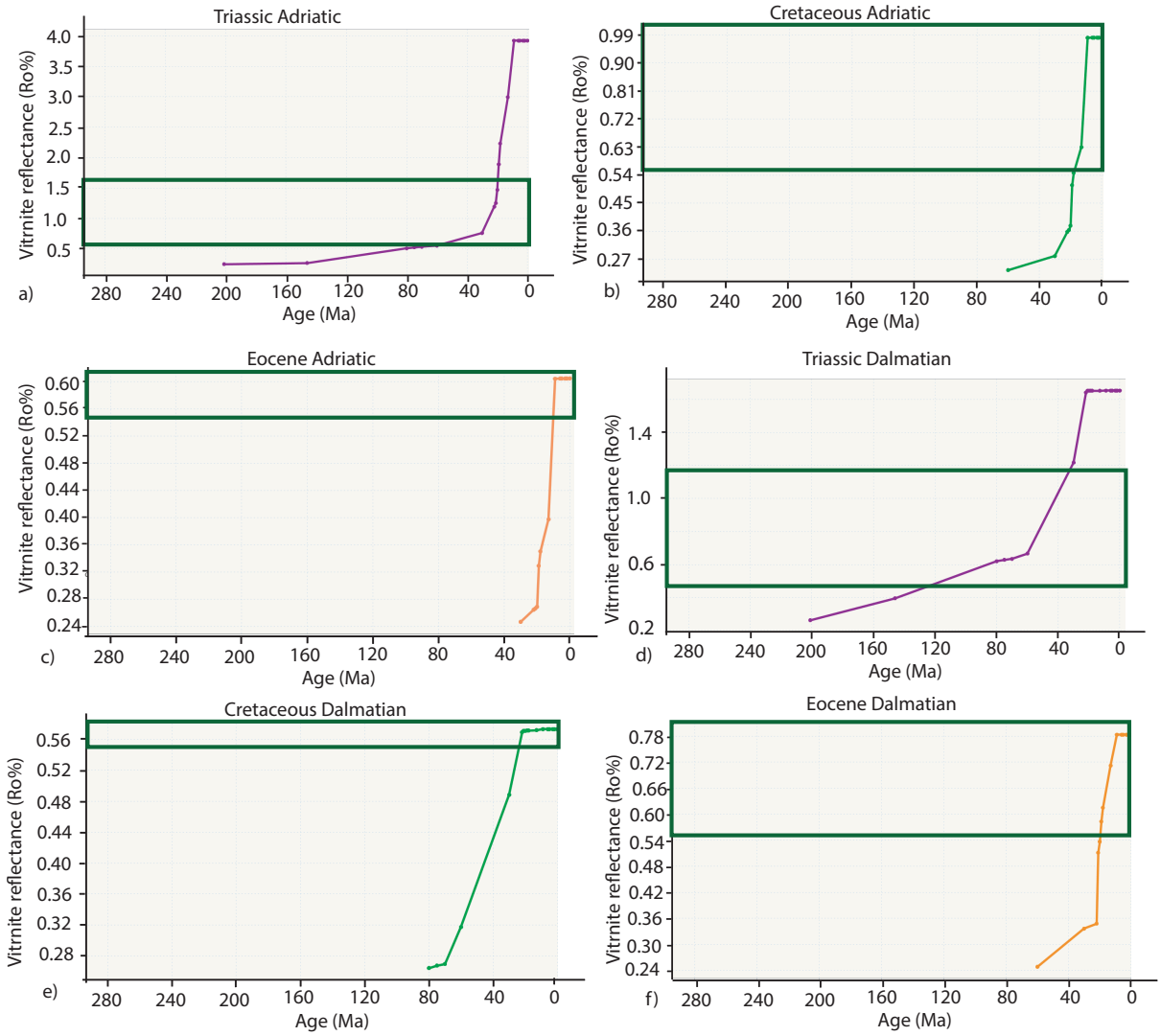


Figure 4.14 Timing of simulated maturation of the different source rocks in the: Adriatic Basin represented by a) Triassic source rocks that reached the oil window and later became overmature, b) Cretaceous source rocks, which reached the oil window, c) Eocene – Oligocene source rocks, which reached the oil window; the Dalmatian zone represented by d) Triassic source rocks that reached the oil and gas window, e) Cretaceous source rocks that reached the oil window, f) Eocene-Oligocene source rocks that reached the oil window. See location of the source rocks in Figure 4.8f.

The Eocene - Oligocene phase of contraction resulted in the first episode of basin subsidence, and subsequently the Triassic source rocks became overmature. This means that the Triassic shale must have yielded their hydrocarbon potential by that time. The Cretaceous limestones and shales reached the oil window after the Eocene – Oligocene phase of thrusting of the Dalmatian zone over the Adriatic foreland (Figure 4.14b). These source rocks started to increase in maturity after the deposition of the thick package of Oligocene – Miocene sediments and remain in the oil window at present-day. The Eocene – Oligocene shales also reached the oil window, later on, as a consequence of basin subsidence and burial associated with the thick package of sedimentary deposition from Oligocene to Pliocene times (Figure 4.14c). These source rocks reached the gas window in the deepest buried parts below the Dalmatian thrust (Figure 4.8e,f).

The main reservoirs in the Adriatic foreland can be assigned to the Cretaceous - Eocene platform carbonates and the Oligocene and Miocene - Pleistocene turbidite intervals (Figure 4.3). From the petrography study (in the Budva zone), we determined that the precipitation of the Cz1 calcite cements can be related to meteoric fluid flow processes that occurred after the Eocene - Oligocene phase of contraction, but prior to the latest phase of Miocene contraction and fracturing (Figure 4.11c,d). If similar meteoric alteration processes occurred in the Adriatic foreland (and/or margin), the porosity and permeability of the carbonate intervals and their reservoir potential could be enhanced. As these meteoric alteration processes took place before the Late Miocene oil charge, the potential for the amount of oil to be trapped in the reservoirs increases. The presence of hydrocarbons can be validated by oil shows that have been found within the JJ-3 well in the Cretaceous-Eocene carbonate sequences at a depth of 4134 m (Bega, 2015; Velaj, 2012) and within the JJ-1 well gas shows have been determined in the Oligocene flysch sequence (Velaj, 2012).

Potential seals can be assigned to Neogene shale intervals and low permeable salt sheets. The fluids from the Triassic source rock intervals could be trapped along the Dalmatian – South Adriatic Basin thrust contact by the juxtaposing impermeable salt layers. When the overlying Neogene sediments would have a high sealing capacity the hydrocarbon migration from the Cretaceous and Eocene – Oligocene source rocks could also be prevented.

The fluids from the Triassic and Cretaceous source rocks in the Adriatic foreland could migrate through the permeable dolostone and limestone intervals towards the Dalmatian – South Adriatic Basin thrust fault (Figure 4.5). These fluids can be blocked by the low permeable layers (e.g. salt) in the hangingwall of this thrust contact. Additionally, the migration of fluids from these source rocks can be trapped by overlying low permeability Cenozoic seal rocks.

#### 4.5.3.2 Dalmatian zone

The Middle Triassic shales entered the oil window in the Dalmatian zone upon Early Cretaceous times, which can be related to the deposition of the carbonate platform build-up (Figure 4.14d). Soon after the Eocene phase of thrusting of the Budva zone over the Dalmatian zone and the footwall burial, the Triassic source rocks reached the gas window. As a result of this phase of Eocene thrusting and burial of the Dalmatian zone the Cretaceous limestones and Eocene turbidites entered the oil window, which currently remain in the oil window (Figures 4.8e and 4.14e).

Overlying Cretaceous - Eocene carbonate and Eocene – Oligocene turbidite intervals could serve as potential reservoir rocks for the Triassic and Cretaceous source rocks (Figures 4.3 and 4.5). From the petrography study and the identification of the zoned calcite cements, meteoric alteration might have taken place after the Eocene – Oligocene (Cz1 precipitation) and Late Miocene (Cz2 precipitation) thrusting. This could have enhanced the reservoir potential of the carbonate and clastic turbidite intervals. This implies that the highest potential for oil entrapment in the enhanced reservoirs could have taken place after the latest Miocene thrusting, when Triassic and Cretaceous source rocks increased their maturity distribution in the oil window (Figure 4.8e). This implies, that from the Late Miocene onwards these reservoirs could be charged with oil by the Triassic and Cretaceous source rocks. Numerous oil seeps have been encountered in Cretaceous carbonates along the Dalmatian coast of Montenegro (Velaj, 2012), indicating a presently active petroleum system.

Potential seal rocks in the Dalmatian zone are found in the overlying Neogene (shale) sediments (Figure 4.3). Furthermore, the hydrocarbons could migrate from their lower structural position towards the higher anticline geometries inside the Dalmatian zone (Figure 2). This anticline structure could represent a structural trap (Spahić et al., 2014). When the Neogene (shale) sediments are expected to have low permeabilities, the hydrocarbons from below could be prevented from escaping to the surface. Compared to the South Adriatic Basin, the petroleum system potential of the Dalmatian zone is lower. This is due to the thinner overlying Neogene seal rocks as a result of erosion during uplift of the Dalmatian zone (during late Miocene – Quaternary times), and the absence of overlying impermeable salt layers.

#### 4.5.3.3 Onshore Dinarides

The interpretation of the restored cross-section is based on surface kinematics with low constraints on the deeper structures for the onshore parts, as mentioned above. Within the Budva zone, Triassic and Cretaceous source rocks were simulated to be mature and in the oil window from early Late Cretaceous onwards. The deepest parts of the Triassic source rocks also reached the gas window from Late Miocene (Figure 4.8e,f). In the area of the High-Karst, Budva and Dalmatian zones, the carbonate rocks have likely enhanced in porosity and permeability due to meteoric dissolution and karstification, when these zones uplifted after the Eocene – Oligocene (Figure 4.8c) and Late Miocene (Figure 4.8e) periods of thrusting. This has been indicated from the zoned calcite cements inside the Budva and Dalmatian zones, which suggest to be formed due to meteoric alteration processes pre (Cz1)- and post (Cz2)-dating Late Miocene times (Figure 4.11b,d). This could have enhanced the reservoir potential of the carbonate intervals and their potential to be charged by the underlying source rocks after late Miocene times (when most of the hydrocarbon generation took place). However, as these permeable carbonate rocks crop-out at the surface in the Budva and High-Karst zones, the sealing capacity within this area is low and the hydrocarbons would have escaped towards the surface (Figure 4.5 and 4.8e).

The mature source rocks in the hinterland in the internal parts of the orogen already took place during the build-up of the Triassic – Late Cretaceous carbonate platform, but these were eroded and exhumed during the Miocene phase of extension. At present-day the Triassic and Cretaceous source rocks are in the oil and gas windows, and the outcropping (Bosnian-) Durmitor flysch sediments are in the oil window (Figure 4.8e). The petrography study indicates that meteoric alteration associated with the precipitation of zoned calcite cements (Cz2) took place after the Late Miocene phase of contraction within fractures developed in the Vranduk Flysch (Figure 4.11f). This could suggest that meteoric alteration increased the reservoir potential of the turbidites and possibly also that of the carbonate sediments, but only after the late Miocene. Modelling demonstrates that hydrocarbon generations most probably ended by the Late Cretaceous - Eocene thrusting. As no significant permeability increase have been indicated from the petrography study prior to this phase of thrusting, the reservoir potential at that time could have been low. This together with the Miocene uplift could have resulted in the escape of the generated hydrocarbons, which happened prior to the increase in reservoir potential after Late Miocene times (as indicated from the Cz2 veins from the petrography study). This can be validated by the present-day absence of hydrocarbon seeps at the surface within the Bosnian Flysch zone. Also, the present-day seal capacity in this area could be low as the carbonate and turbidite sediments, which enhanced in permeability after the suggested Late

Miocene meteoric alteration (e.g. Figure 4.10f-i), are presently surface-exposed. This implies that even if hydrocarbons were trapped in potential reservoirs, such hydrocarbons most likely escaped through the permeable layers towards the surface at the present-day (Figure 4.5).

### 4.5.4 Integrated conceptual rock fluid deformation model

Three types of fluid flow have been considered throughout the formation of the Dinarides orogen, which are internal formation fluids, meteoric fluids and deep-sourced mantle fluids. They are believed to induce significant impact on potential reservoir rocks. Hence, together with the modelling of the maturation of source rocks (inferring generated hydrocarbons), constraining the diagenetic fluid flow evolution helps in better defining the potential petroleum systems. By analyzing the sedimentary model and the permeability characteristics of the different sedimentary intervals, possible fluid pathways can be described – although 3D modelling remains necessary to investigate the related fluid flow pertinently (this was not in the scope of the present study).

During the Late Cretaceous – Oligocene thrusting, burial of the footwall areas and uplift of the hangingwall areas took place. In general, this can be associated with the upward migration of formation fluids towards the surface (Figure 4.15a,b). Additionally, meteoric fluids would migrate from high elevated areas towards lower elevated areas associated with erosional surfaces (Figure 4.15b). During the foreland-ward migration of thrusting and slab retreat in the same direction deep-sourced mantle fluids are expected to migrate along the active thrusts towards the surface (Figure 4.15c). Once these fluids reach the sedimentary cover they will migrate through permeable layers towards less compacted areas.

Upon the exhumation of the Bosnian and Durmitor Flysch zone during the early - middle Miocene extension, no significant changes in permeability are believed to take place as indicated from the petrography study. During the slab-retreat, the deep-sourced fluids will likely continue to migrate through the permeable layers towards the surface and the SW (Figure 4.15c).

During the latest phase of Miocene contraction the reactivation of the East Bosnian-Durmitor – Bosnian Flysch (in Bosnia-and-Herzegovina) contact can be associated with the precipitation of calcite cements (C3) with a deep-sourced fluid origin. Prior and after the deposition of these C3 cements, meteoric alteration of the fractures took place (as indicated from the zoned calcite cements Cz). This can be associated with the meteoric fluid flow from local highs to lower areas (Figure 4.15d). In the foreland area of Montenegro the renewed thrust (reactivation) from late Miocene – Quaternary can be associated with the migration of deep sourced fluids from the accretionary wedge (of the presently observed slab) towards the surface along active thrusts, which resulted in the precipitation of the C3 cements (as observed in the Budva and Dalmatian zones, Figures 4.11a-e). Due to the strong compaction of the sediments in the deep buried Budva zone during the overthrusting of the High Karst zone, the permeability decreases and therefore fluids will be squeezed out towards the surface (Figure 4.5 and 4.15d). The fluids inside the Dalmatian zone will migrate towards the local antiform structures through high permeable layers where they can be trapped beneath low permeable shales (Figures 4.5 and 4.15d). Within the offshore South Adriatic Basin fluids can migrate through deep permeable layers (dolostones and limestones) towards the local highs in the NE where they will be trapped at the Dalmatian – South Adriatic Basin thrust contact. This is, because the hangingwall of this

thrust contact is covered by impermeable sediments such as Permo-Triassic salt sheets or Triassic shales, which block the fluids from the deeper sediments of the South Adriatic Basin to migrate upwards along the fault (Figures 4.5 and 4.15d).

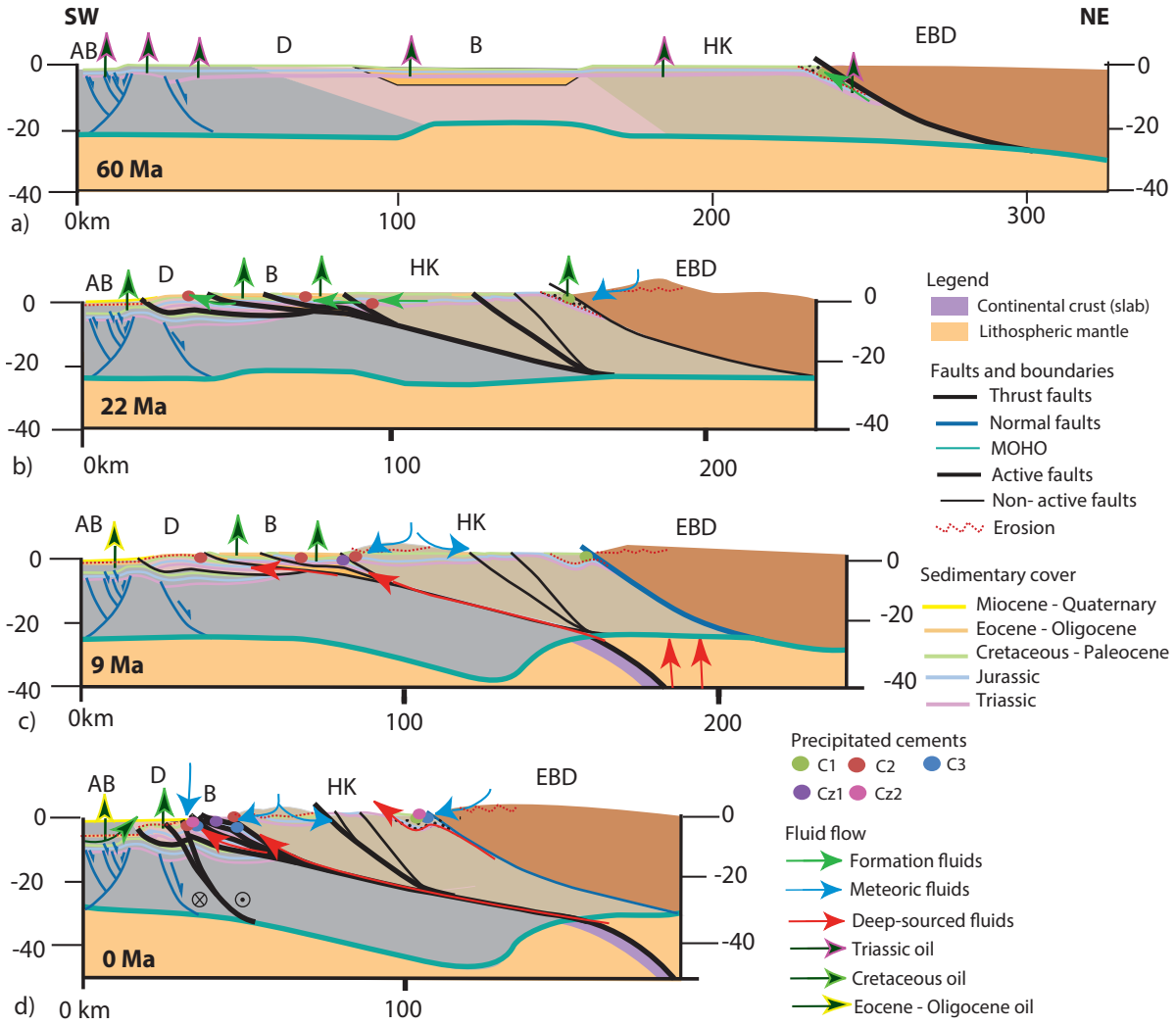


Figure 4.15 Conceptual fluid-flow model showing also potential hydrocarbon migrations. Above the vertical zero line the topography is sometimes exaggerated in order to better show the processes. a) The latest Cretaceous moment of continental collision and associated SW-ward thrusting in the internal part of the Dinarides can be associated with the precipitation of C1 calcite cements from Triassic formation waters. Simultaneously, Triassic source rocks generated oil all across the area; b) The SW-ward thrusting in the external Dinarides can be associated with the reactivation and migration of Jurassic formation waters, which resulted in the precipitation of C2 cements in fractures. Simultaneously, Cretaceous source rocks generated oil in the Durmitor Flysch, Budva zone and Adriatic Basin; c) Until Late Miocene, the foreland migrated slab can be associated with enhanced deep-sourced fluid flow towards the surface NE of the slab. Meteoric fluids could have resulted in the precipitation of Cz1 zoned calcite cements observed in the foreland area of Montenegro. Sedimentation in the Adriatic basin resulted in the generation of oil from Eocene – Oligocene source rocks; d) The Late Miocene reactivation of former thrust contacts in the foreland of the SE-Dinarides can be associated with the migration of deep-sourced fluids from the detached slab along the active thrusts towards the surface, which resulted in the precipitation of C3 cements inside fractures. Meteoric fluid flow

*Figure 4.15 (continued)* contributed to the precipitation of post-dating Cz2 zoned calcite cements, which overgrow and cross-cut the C3 veins.

## 4.6 Conclusions

Kinematic restoration and basin modelling along one major regional cross section across the Dinarides orogen, together with preliminary petrographic and geochemical studies on representative rock samples resulted in the following conclusions:

The kinematic restoration of the large-scale structural features resulted in constraining the minimum amounts of shortening, subsidence, sedimentation rates, exhumation and erosion, which helped, subsequently, in analyzing the maturity evolution, paleo fluid-flow and petroleum potential.

The integrated approach of kinematic restoration, thermal modelling (and associated maturation of source rocks and petroleum system modelling), and diagenesis study resulted in investigating viable petroleum system(s) and possible hydrocarbon generation and trapping episodes, as well as proposing a conceptual model for fluid-flow rock deformation. Consequently, the timing of hydrocarbon charging as well as possible reservoir properties evolution through fluid-rock interactions have been constrained.

Erosional unconformities have been linked to syn-kinematic deposition of sediments during episodes of fault activity (assigned to specific deformation events), among which the major ones have been observed in the Durmitor Flysch, and inside the Dalmatian zone and Adriatic Basin. During the Late Cretaceous ~22km of shortening was accommodated by the East-Bosnian Durmitor – Durmitor Flysch contact, associated with the syn-kinematic deposition of the Durmitor Flysch. During the Eocene – Oligocene phase of contraction, thrusting migrated towards the foreland, which accommodated a total amount of ~85km of shortening. Most of this shortening was accommodated by the Dalmatian over Adriatic foreland thrusting, which resulted in significant basin subsidence (due to tectonic loading) and the initiation of the flexural basin. This can be associated with syn-kinematic siliciclastic sedimentation and the formation of erosional unconformities. This phase of thrusting marks the onset of the transition of the thick- to thin-skinned geometry of the Budva and Dalmatian zones, whereas in the High-Karst and the more internal parts a thick-skinned geometry prevails in our concept. The Late Miocene – Quaternary phase of contraction accommodated a total amount of ~53km of shortening, which resulted in another major episode of flexural basin subsidence associated with syn-kinematic deposition and the formation of unconformities. This episode of basin subsidence is likely linked to the migrating subduction zone. In contrast to the onshore parts, the offshore part of Montenegro, has been described in detail due to the available seismic lines, which aided in dating the thrust activity by the interpretation of unconformities and stratigraphic characteristics.

Within our cross-section, high-angle basement involved reverse faults cross-cut the structures in the Adriatic foreland and Dalmatian zone (Figure 4.2). This suggests that a thick-skinned tectonic regime post-dates the thin-skinned emplacement of the Dalmatian zone over the Adriatic foreland (i.e. the external sub-thrust structures). The high-angle basement involved transpressional reverse faults can be interpreted to be a prolongation of the E-W oriented

transpressive structure of the Middle Adriatic Ridge, which is situated in the middle of the Adriatic sea.

The Late Cretaceous – Eocene thrusting in the internal Dinarides resulted in the precipitation of C1 sparry calcite cements, which have been buffered by Triassic formation waters and seem to have deposited at depths between 813 and 4000 m. The Eocene – Oligocene thrusting in the external Dinarides can be associated with the precipitation of C2 twinned sparry calcite cements, that were precipitated at depths between 1000 and 2800 m. These cements have likely been precipitated from Jurassic formation waters as indicated from their CL-patterns and the stable carbon and oxygen isotope data. Both C1 and C2 represent fluids that were trapped in the host-rocks and or buffered by the latter due to long residence time. Such fluids might have flown due to thrusting deformation towards the external part of the Dinarides and upwards. They were followed by a first phase of calcite cement precipitation (Cz1) in developed fractures in the Budva zone, probably associated with meteoric fluid processes related to exhumation. After the Late Miocene, deep-sourced fluids from the accretionary wedge are expected to flow along the active thrust contacts and towards the area NE of the slab, which resulted in the precipitation of C3 twinned sparry calcite cements. Meteoric alteration of these cements resulted in the precipitation of zoned calcite crystals (Cz2), which have been encountered in the Eocene turbidites in the Dalmatian zone of Montenegro and in the Vranduk Flysch in Bosnia-and-Herzegovina.

The Eocene – Oligocene and late Miocene – Quaternary phases of thrusting resulted in the main periods of maturation of Triassic, Cretaceous and Eocene – Oligocene source rocks. Meteoric fluid alterations could have enhanced the fracture and dissolution porosity of the Cretaceous - Eocene platform carbonates and Eocene - Oligocene turbidites, increasing their reservoir potential prior to hydrocarbon charging. Generally speaking, the highest petroleum system potential has been suggested to be in the South Adriatic Basin and Dalmatian zone. The large impermeable salt sheets in the Dalmatian zone could serve as a high capacity seal rock. These layers prevent the hydrocarbons from the source rocks of the South Adriatic Basin to escape along the sealed Dalmatian – South Adriatic Basin thrust contact.

Since we estimated the minimum amounts of shortening, more optimistic hypotheses regarding the petroleum potential are possible and should be investigated (e.g., by means of seismic, gravity and well data) to better estimate the oil and gas potential of the Dinarides. Also, in order to get a better integrated reconstruction of the fluid flow additional basin modelling – particularly 3D simulations – has to be done, which will allow to simulate the overpressure evolution across the cross-sections. In order to improve the thermal calibration of the basin models, the paleo-geothermal gradient or heat flow must be better quantified in the external parts of the Dinarides orogen. Besides, the diagenesis study was only preliminary within the scope of this study. Further, advanced diagenetic analyses will certainly better constrain the proposed fluid origins, fluid-flow evolution and fluid-rock interactions.

## Chapter 5.

# Concluding remarks: integrated geological observations and numerical modelling results

The principal aim of the research presented in this thesis was to link the effects of the kinematic tectonic evolution (at crustal- and lithospheric- scale) with the thermal, paleo fluid-flow and organic matter maturity evolutions during the formation of the Dinarides collisional orogen by means of a new numerical basin model (Figure 5.1). The extensive field kinematic studies across the orogen performed in this study, made it possible to construct two large-scale profiles and subsequently reconstruct one of these cross-sections into its pre-orogenic configuration, on which basin modelling was applied.

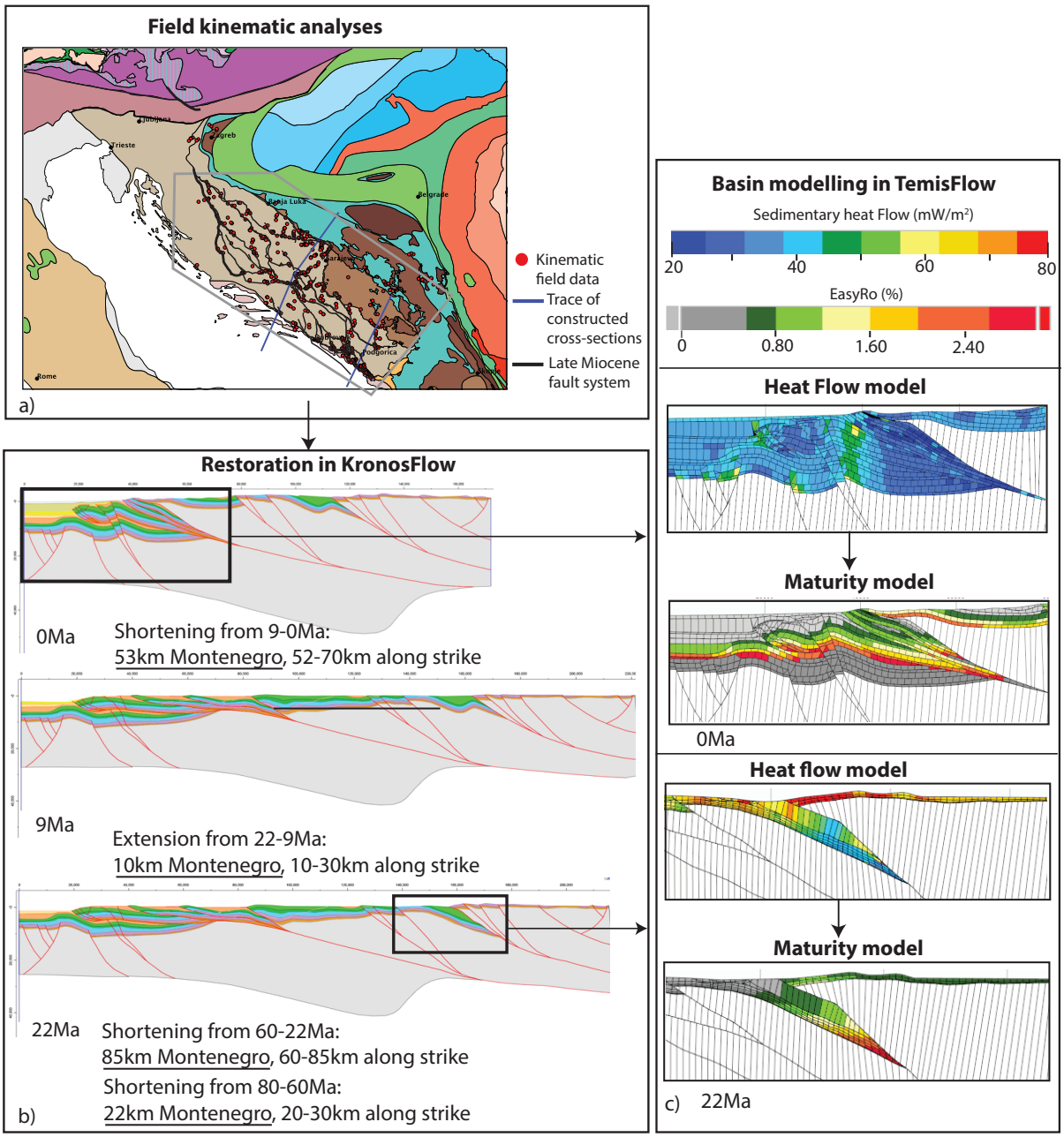


Figure 5.1 Summary of the performed workflow during this thesis. a) First, a detailed kinematic study across the Dinarides, which aided in the construction of two regional cross-sections; b) One of these regional cross-sections was restored into its per-orogenic configuration, which demonstrates the various amounts of shortening; c) Numerical basin modelling allowed to simulate the heat flow and maturity evolution of the restored cross-section.

## 5.1 Regional and large-scale tectonic evolution and sedimentation

The large-scale field study in the Dinarides orogen led to new insights in understanding the relation between subduction and collisional processes. The Late Cretaceous – Eocene phase of contraction resulted in the accommodation of shortening by the SW-ward thick-skinned thrusting of the East-Bosnian Durmitor over the Bosnian-Durmitor Flysch. During this time the crustal root gradually migrates with time from the NW of the Sava zone to the NW of the High-Karst contact (see Figure 2.13). This is facilitated by the gradual migration of the slab towards the orogenic front and by the large amounts of crustal-scale thick-skinned thrusting, which duplicate a significant part of the Adriatic basement. Flexural subsidence and deepening of the footwall can be associated with the syn-kinematic deposition of the Ugar-Durmitor Flysch sequences and the Eocene flysch sequences more to the foreland, associated with the formation of unconformities over the hanging-walls and over the flexural forebulges.

The Eocene – Oligocene thrusting has been recorded in the foreland area of the external parts of the Dinarides. This thrusting has a foreland-ward migration, which can be related the migration of a subduction zone in the same direction. For the SE-profile a total shortening of 85km was estimated during this period of contraction. Within the central profile similar amounts of shortening are expected, which have been estimated to be in the order of ~60 km (see also Balling et al., 2016). The Eocene – Oligocene thrusting phase marks the onset of the transition from a thick-skinned geometry to a thin-skinned geometry of the Budva and Dalmatian zones, whereas the geometry of the High-Karst and more internal units remains thick-skinned based on our interpretation. This is different to the profile in the central Dinarides, where a thin-skinned geometry has been interpreted for the SW-part of the High-Karst zone (Figure 2.11a). In both profiles, the crustal root is expected to have been formed in response to basement thrusting at the transition between the thick- and thin-skinned geometries (Figure 2.13b,c). During this time flexural subsidence took place in the South Adriatic Basin of the Montenegro profile, which can be related to the tectonic loading of the Dalmatian zone during thrusting (accommodating a shortening amount of ~48km for this thrust alone). Simultaneous with the 4 km of basin subsidence the first sequence of syn-kinematic deposition inside the Adriatic Basin took place. The total amount of Eocene – Oligocene shortening was estimated to be ~85km.

From early – middle Miocene a phase of extension resulted in the formation of the Miocene basin system and the uplift and reactivation of the East-Bosnian Durmitor – Bosnian-Durmitor Flysch contact. A later phase of contraction could be dated by the superposition relationship with the Miocene extensional features and sediments, to be activated during post-9 Ma times. The post-9Ma phase of contraction has been linked to the indentation of the Adriatic microplate, which induced a large-scale system of strike-slip faults that gradually transfer their offsets to thrusts and high-angle reverse faults. Most of the accumulated shortening induced during this latest phase of contraction, has been localized in rheological weak zones in the foreland area of Montenegro with a total amount of ~53km of shortening. During this phase a second period of rapid flexural subsidence of ~4km took place in the Adriatic Basin of the Montenegro profile, which can be associated with the syn-kinematic deposition of Neogene – Quaternary sediments. This episode of basin subsidence likely developed due to the presence of the subduction zone,

rather than to be a consequence of orogenic loading by the few amounts of thrusting (>5km) that have been simulated from the restoration. For the amount of at least 53 km of shortening to be accumulated in the SE-Dinarides from Late Miocene onwards, an additional slab-retreat of more than 53km compared to the position of the slab during Oligocene times is expected (see also Chapter 2 Figure 2.13b,c). Within the central Dinarides profile no such large-scale basin subsidence has been observed in the offshore trace of the cross-section constructed in this thesis (see Chapter 2 Figure 2.11a).

The Middle Adriatic Ridge, situated in the middle of the Adriatic Sea, has an E-W oriented transpressive structure, and is distributed along many branches (e.g., Scisciani & Calamita, 2009 and references therein). One of these branches was interpreted to extend to and affect the structures in offshore Montenegro (see also Bega, 2015). The transpressional structure of the Middle Adriatic Ridge is demonstrated in our profiles by the high inclined reverse faulting (Figure 2.11). In our interpretations (Figure 2.11b,c), we have followed the typical age of these transpressional structures, which is demonstrated as a two stage deformation (Paleogene-Miocene and late Pliocene - Quaternary), while the higher resolution of this timing remains speculative (Scisciani & Calamita, 2009). This is the reason for the two interpretations for the Montenegro section (Figure 2.11b,c), where either the thin-skinned sub-thrusting pre-dates a later phase of high-angle basement involved reverse faulting (Figure 2.11b), or where the thin-skinned sub-thrusting post-dates the high-angle reverse faulting (Figure 2.11c).

## 5.2 Numerical basin modelling in collisional systems

The 2D basin models have been used to integrate the burial and thermal history during the tectonic evolution of the Dinarides orogen, which simulates the timing of hydrocarbon generation as a reflection of the thermal model (Figure 5.1c). The present-day variable surface heat flow distribution across the Dinarides can be linked to the crustal-scale deformation processes, the radiogenic heat of the sediments, compaction of the sedimentary intervals and the active subduction dynamics (associated with variations in the Moho geometry). As the subducting slab is currently located in a far external position of the Dinarides orogen, the heat flow increases towards the hinterland NE of the slab where the surface heat flow is higher compared to the lower surface heat flow values in the proximity of the slab. In general, fast slip-rates (compared to relative slow erosion rates) results in the deep burial of the footwall areas of active thrust contacts. The deep burial results in a transient heat field, which decreases the conductivity, permeability and heat flow of the deepest buried sediments in the footwall areas, where potential source rocks are often overmature (e.g. Figure 5.1c).

The numerical modelling applied on the cross-section shows the importance of the amounts of erosion and sedimentation during the main phases of deformation on the maturity pattern. The main viable petroleum system potential has been indicated in the offshore Adriatic Basin and Dalmatian zone of Montenegro. Within the Adriatic Basin, Cretaceous and Eocene – Oligocene source rocks started to generate hydrocarbons after the Eocene – Oligocene thrusting and basin subsidence associated with syn-kinematic deposition of potential seal rocks. After this phase of thrusting these source rocks continued to generate hydrocarbons. The presence of impermeable layers of Permo-Triassic salt in the Dalmatian zone and the overlying Neogene – Quaternary seal rocks make it likely that the hydrocarbons could be trapped there.

## 5.3 Integrated fluid flow model

Within this study the fluid flow is being analyzed in terms of the sedimentary model and the associated permeabilities of the different sedimentary intervals, which has been coupled with the diagenetic study. The relative timing of the different diagenetic events allowed to date the fluid (as well as hydrocarbon) flow with the main episodes of fracture formation. The inferred fluid-rock interactions allowed basic suggestions regarding reservoir properties enhancement or destruction. This together with the restoration and maturity basin model can indicate whether the moment of hydrocarbon generation took place at a suitable time for the fluids to migrate and to be trapped in potential reservoir units or structural traps. This is important for the definition of the petroleum potential of an orogen.

Fluids are expected to flow through permeable layers, which are being pushed towards the orogenic foreland during the main phases of foreland-ward thrusting. The stable isotope data indicated rock-buffered fluids (producing C1 and C2 cements, and probably further destroying reservoir properties) during the first two main episodes of Late Cretaceous and Eocene contraction. Subsequently, meteoric fluid alterations resulted in an increase in permeability and reservoir potential, which is a consequence of uplift, erosion and folding after the Eocene – Oligocene phase and the post-9Ma phase of contraction (as indicated by the dated Cz1 and Cz2 veins). The increase in permeability allows the fluids and hydrocarbons to migrate towards these potential reservoirs. Additionally, the migration of the subduction zone towards the orogenic foreland together with the active thrust fronts, could have resulted in deep-sourced fluid flow along the active thrusts towards the surface and the hinterland (associated with the precipitation of C3 cements). Further advanced diagenesis study on such cements and associated fluids might bring additional information and constraints with respect to the reservoir properties evolution in the external Dinarides.

# References


Andersen, T. B., Jamtveit, B., Dewey, J. F., & Swensson, E. (1991). Subduction and eduction of continental crust: major mechanisms during continent-continent collision and orogenic extensional collaps, a model based on the south Norwegian Caledonides, Terra Nova, 3, 303-310. doi: 10.1111/j.1365-3121.1991.tb00148.x

Andrić, N., Sant, K., Matenco, L., Mandic, O., Tomljenović, B., Pavelić, D., Hrvatović, H., Demir, V., & Ooms, J. (2017). The link between tectonics and sedimentation in asymmetric extensional basins: Inferences from the study of the Sarajevo–Zenica Basin. Marine and Petroleum Geology, 83, 305-332. doi: 10.1016/j.marpetgeo.2017.02.024

Andrić, N., Vogt, K., Matenco, L., Cvetković, V., Cloetingh, S., & Gerya, T. (2018). Variability of orogenic magmatism during continental collision: A numerical modelling approach, Gondwana research, 56, 119-134. doi: 10.1016/j.gr.2017.12.007

Angelier, J. (1979). Determination of the mean principal directions of stresses for a given fault population. Tectonophysics, 116, 17-26.

Angelier, J. (1984). Tectonic analysis of fault slip data sets, Journal of Geophysical Research: Solid Earth, 89(B7). doi: 10.1029/JB089iB07p05835

Artemieva, I. M., Thybo, H. & Kaban, M. K. (2006). Deep Europe today: geophysical synthesis of the upper mantle structure and lithospheric processes over 3.5 Ga. Geological Society of London, Memoirs, 32(1), 11-44. doi: 10.1144/GSL.MEM.2006.032.01.02

Aubouin, J., Blanchet, R., Cadet, J.-P., Celet, P., Charvet, J., Chorowicz, J., Cousin, M., & Rampnoux, J.-P. (1970). Essai sur la géologie des Dinarides. Bulletin de la Société Géologique de France, 12(6), 1060-1095. doi: 10.2113/gssgfbull.S7-XII.6.1060

Aubouin, J. & Dercourt, J. (1975). Les transversales dinariques dérivent-elles de paléofailles transformantes? Compte Rendu Academie des Sciences, 281, 347-350.

Bada, G., Horváth, F., Dövényi, P., Szafián, P., Windhoffer, G. & Cloetingh, S. (2007). Present-day stress field and tectonic inversion in the Pannonian basin. Global and Planetary Change, 58, 165-180.

Balázs, A., Matenco, L., Magyar, I., Horváth, F. & Cloetingh, S. (2016). The link between tectonics and sedimentation in back-arc basins: New genetic constraints from the analysis of the Pannonian Basin. Tectonics, 35, 1526–1559.

Balazs, A., Evgueni, B., Matenco, L., Vogt, K., Francois, T., & Cloetingh, S. (2017). Symmetry during the syn- and post-rift evolution of extensional back-arc basins: The role of inherited orogenic structures. Earth and Planetary Science Letters, 462, 86-98. doi: 10.1016/j.epsl.2017.01.015

Balling, P., Tomljenović, B., & Ustaszewski, U. (2016). Along-strike shortening variations across the external Dinarides quantified by means of balanced cross-sections. Abstract Bonn, 16th Symposium on Tectonics, Structural Geology and Crystalline Geology.

Barker, Ch,E., & Pawlewicz, M.J. (1986). The correlation of vitrinite reflectance with maximum temperature in humic organic matter. Paleogeothermics. Edited by G. Buntebarth and L. Stegena, Springer-Verlag Berlin Heidelberg: Lecture Notes in Earth Sciences, 5

Beaumont, C., Munoz, J. A., Hamilton, J., & Fullsack, P. (2000). Factors controlling the Alpine evolution of the central Pyrenees inferred from a comparison of observations and

geodynamical models. Journal of Geophysical Research, 105(B4), 8121-8145. doi: 10.1029/1999JB900390

Bega, Z. (2015). Hydrocarbon Exploration Potential of Montenegro - a Brief Review, Journal of Petroleum Geology, 38(3), doi: 10.1111/jpg.12613

Bennett, R. A., Hreinsdóttir, S., Buble, G., Bašić, T., Bačić, Ž., Marjanović, M., Casale, G., Gendaszek, A., & Cowan, D. (2008). Eocene to present subduction of Southern Adria mantle lithosphere beneath the Dinarides, Geology, 36(1), 3-6. doi: 10.1130/G24136A.1

Berner, R. (1981). A new geochemical classification of sedimentary environments. Journal of Sedimentary Petrology, 51, 359-365.

Bertotti, G., Picotti, V., Chilovi, C., Fantoni, R., Merlini, S., & Mosconi, A. (2001). Neogene to Quaternary sedimentary basins in the south Adriatic (Central Mediterranean): Foredeeps and lithospheric buckling. Tectonics, 20 (5), 771-787.

Bertotti, G., Casolari, E., & Picotti, V. (2002). The Gargano Promontory: a Neogene contractional belt within the Adriatic plate. *Terra Nova, 11 (4),* 168-173. doi: 10.1046/j.1365-3121.1999.00243.x

Bertotti, G., Mosca, P., Juez, J., Polino, R. & Dunai, T., 2006. Oligocene to present kilometres scale subsidence and exhumation of the Ligurian Alps and the Tertiary Piedmont Basin (NW Italy) revealed by apatite (U-Th)/He thermochronology: correlation with regional tectonics. Terra Nova, 18, 18-25.

Biddle, K.T. & Christie-Blick, N. (1985). Strike-Slip Deformation, Basin Formation, and Sedimentation. SEPM Soc. Sedim. Geol., 37, 1-34.

Bortolotti, V., Chiari, M., Marroni, M., Pandolfi, L., Principi, G., & Saccani, E. (2012). Geodynamic evolution of ophiolites from Albania and Greece (Dinaric-Hellenic belt): one, two, or more oceanic basins?. International Journal of Earth Sciences, 102(3), 783-811. doi: 10.1007/s00531-012-0835-7

Brun, J.-P., & Faccenna, C. (2008). Exhumation of high-pressure rocks driven by slab rollback. Earth and Planetary Science Letters, 272(1-2), 1-7. doi: 10.1016/j.epsl.2008.02.038

Burov, E., & Yamato, P. (2008). Continental plate collision, P-T-t-z conditions and unstable vs. stable plate dynamics: Insights from thermo-mechanical modelling. Lithos, 103(1-2), 178-204. doi: 10.1016/j.lithos.2007.09.014

Burov, E., Francois, T., Agard, P., Le Pourhiet, L., Meyer, B., Tirel, C., Lebedev, S., Yamato, P., & Brun, J.-P. (2014). Rheological and geodynamic controls on the mechanisms of subduction and HP/UHP exhumation of crustal rocks during continental collision: Insights from numerical models. Tectonophysics, 631, 212-250.

Cadjenović, D., Kilibarda, Z., & Radulović, N. (2008). Late Triassic to Late Jurassic evolution of the Adriatic Carbonate Platform and Budva Basin, Southern Montenegro. Sedimentary Geology, 204(1-2), 1-17. doi: 10.1016/j.sedgeo.2007.12.005

Callot, J.-P., Breesch, L., Guilhaumou, N., Roure, F., Swennen, R., & Vilasi, N. (2010). Paleo-fluids characterisation and fluid flow modelling along a regional transect in Northern United Arab Emirates (UAE). Arabian Journal of Geosciences, 3 (4), 413-437. doi: 10.1007/s12517-010-0233-z

Chaftez, H.S. (1972). Surface Diagenisis of Limestone. Journal of Sedimentary Research, 42, 325-329. doi: 10.1306/74D7253B-2B21-11D7-8648000102C1865D

Caporali, A., Aichhorn, C., Barlik, M., Becker, M., Fejes, I., Gerhatova, L., Ghitau, D., Grenerczy, G., Hefty, J., Krauss, S., Medak, D., Milev, G., Mojzes, M., Mulic, M., Nardo, A., Pesec, P., Rus, T., Simek, J., Sledzinski, J., Solaric, M., Stangl, G., Stopar, B., Vespe, F. & Virag, G. (2009). Surface kinematics in the Alpine-Carpathian-Dinaric and Balkan region inferred from a new multi-network GPS combination solution. Tectonophysics, 474, 295-321.

Caputo, R., Chatzipetros, A., Pavlides, S. & Sboras, S. (2012). The greek database of seismogenic sources (GreDaSS): State-of-the-art for northern greece. Ann. Geophys., 55, 859-894.

Chorowicz, J., 2016. Genesis of the Pieniny Klippen Belt in the Carpathians: Possible effects of a major paleotransform fault in the Neo-Tethyan domain. Comptes Rendus Geosci., 348, 15-22.

Chiari, M., Djerić, N., Garfagnoli, F., Hrvatović, H., Krstić, M., Levi, N., Malasoma, A., Marroni, M., Menna, F., Nirta, G., Pandolfi, L., Principi, G., Saccani, E., Stojadinović, U., & Trivić, B. (2011). The geology of the Zlatibor-Maljen area (western Serbia): A geotraverse across the ophiolites of the Dinaric-Hellenic collisional belt. Ofioliti. 36(2), 139-166. Retrieved from https://www.researchgate.net/publication/257330703

Clauzon, G. (1990). Restitution de l'évolution géodynamique néogène du bassin du Roussillon et de l'unité adjacente des Corbières d'après les données écostratigraphiques et paléogéographiques. Paléobiologie continentale, 17, 125-155

Cortecci, G & Reyes, E., Berti, G., & Casati, P. (1981). Sulfur and oxygen isotopes in Italian marine sulfates of Permian and Triassic ages. Chemical Geology, 34, 65-79. doi: 10.1016/0009-2541(81)90072-3.

Cosović, V., Baloncić, D., Koić, M., Marjanac, T., Moro, A., Gušić, I., & Jelaska, V. (1994). Paleontological evidence of Paleogene transgression on Adriatic carbonate platform. Geologie Mediterraneenne, 21, 49-53.

Črne, A. E., Weissert, H., Goričan, Š., & Bernasconi, S. M. (2011). A biocalcification crisis at the Triassic-Jurassic boundary recorded in the Budva Basin (Dinarides, Montenegro). Geological Society of America Bulletin, 123(1-2), 40-50. doi: 10.1130/B30157.1

Cunningham, W.D. & Mann, P. (2007). Tectonics of strike-slip restraining and releasing bends. Geol. Soc. London, Spec. Publ., 290, 1.

Cvetković, V., Pécskay, Z., & Šarić, K. (2013). Cenozoic igneous tectonomagmatic events in the Serbian part of the Balkan Peninsula: inferences from K/Ar geochronology. Acta Volcanologica 10, 111–120.

Davis, D., Supper, J., & Dahlen, F.A. (1983). Mechanics of fold-and-thrust belts and accretionary wedges. JGR Solid Earth, 88 (B2), 1153-1172. doi: 10.1029/JB088iB02p01153

D'Agostino, N., Avallone, A., Cheloni, D., D'Anastasio, E., Mantenuto, S., & Selvaggi, G. (2008). Active tectonics of the Adriatic region from GPS and earthquake slip vectors. Journal of Geophysical Research, 113, B12413. doi: 10.1029/2008JB005860

Dahlstrom, C.D.A. (1969). Balanced cross-sections. Canadian Journal of Earth Sciences, 6 (4), 743-757. doi: 10.1139/e69-069

Davy, P. & Cobbold, P.R. (1988). Indentation tectonics in nature and experiment. 1. Experiments scaled from gravity. Bull. Geol. Inst. Uppsala, 14, 129-141.

De Leeuw, A., Mandic, O., Krijgsman, W., Kuiper, K., & Hrvatović, H. (2011). A chronostratigraphy for the Dinaride Lake System deposits of the Livno-Tomislavgrad Basin: the rise and fall of a long-lived lacustrine environment in an intra-montane setting. Stratigraphy, 8/1, 29-43. doi: 10.1016/j.tecto.2012.01.004

De Leeuw, A., Mandic, O., Krijgsman, W., Kuiper, K., & Hrvatović, H. (2012): Paleomagnetic and geochronologic constraints on the geodynamic evolution of the central Dinarides. Tectonophysics, 530-531, 286 - 298. doi: 10.1016/j.tecto.2012.01.004

De Leeuw, A., Mandic, O., Vranjković, A., Pavelić, D., Harzhauser, M., Krijgsman, W., & Kuiper, K.F. (2010). Chronology and integrated stratigraphy of the Miocene Sinj Basin (Dinaride Lake System, Croatia). Palaeogeography, Palaeoclimatology, Palaeoecology, 292, 155-167. doi: 10.1016/j.palaeo.2010.03.040

De Vicente, G., Vegas, R., Muñoz-Martín, A., Van Wees, J.D., Casas-Sáinz, A., Sopeña, A., Sánchez-Moya, Y., Arche, A., López-Gómez, J., Olaiz, A. & Fernández-Lozano, J. (2009). Oblique strain partitioning and transpression on an inverted rift: The Castilian Branch of the Iberian Chain. Tectonophysics, 470, 224-242.

Delvaux, D. & Sperner, B. (2003). Stress tensor inversion from fault kinematic indicators and focal mechanism data: the TENSOR program. In: New Insights into Structural Interpretation and Modelling (D. Nieuwland Ed.). Geological Society, London, Special Publications, 212, 75-100.

Dewever, B., Berwouts, I., Swennen, R., Breesch, L., & Ellam, R.M. (2010). Fluid flow reconstruction in karstified Panormide platform limestones (north-central Sicily): Implications for hydrocarbon prospectivity in the Sicilian fold and thrust belt. Marine and Petroleum Geology, 27(4), 939-958. doi: 10.1016/j.marpetgeo.2009.10.018

Dickson, J.A.D. (1966). Carbonate identification and genesis as revealed by staining. Journal of sedimentary petrology, 36 (2), 491-505. doi: 10.1306/74D714F6-2B21-11D7-8648000102C1865D

Dimitrijević, M. D. (2001). Dinarides and the Vardar Zone: a short review of the geology. Acta Vulcanologica, 13(1-2), 1-8. doi: 10.1400/19061

Dimitrijević, M. D. (1997). Geology of Yugoslavia. 2nd edition, Geoinstitute, Belgrade, Serbia.

Dimitrijević, M. N., & Dimitrijević, M. D. (1987). The turbiditic basins of Serbia. Serbian Academy of Sciences and Arts Department of Natural & Mathematical Sciences, Monograph, 61, 304.

Djerić, N., & Gerzina, N. (2008). Late Triassic radiolarians from the Ovcar-Kablar Gorge (SW Serbia). Annales Geologiques de la Peninsule Balkanique, 69(39-47). doi: 10.2298/GABP0869039D

Djerić, N., Gerzina, N., & Schmid, S. M. (2007). Age of the Jurassic Radiolarian Chert Formation from the Zlatar Mountain (SW Serbia). Ofioliti, 32(2), 101-108. Retrieved from https://earth.unibas.ch/tecto/Members/Schmid/Publications/105_Djericetal_2007.pdf

Doglioni, C., Carminati, E., Cuffaro, M., & Scrocca, D. (2007). Subduction kinematics and dynamic constraints. Earth-Science Reviews, 83(3-4), 125-175. doi: 10.1016/j.earscirev.2007.04.001

Dohmen, P. (2012). The balance between orogenic shortening and back arc extension in the internal nappes of the Dinaric, (Bachelor Thesis). Library of Utrecht University, Utrecht, The Netherlands: University of Utrecht

Downes, H. (2005). Origin and significance of spinel and garnet pyroxenites in the shallow lithospheric mantle in Western Europe and NW Africa. Ofioliti, 30(2).

Dragasević, T. (1983). Oil geological exploration in the Montenegro Offshore in Yugoslavia. Nafta 34 (7-8) 397-404.

Dubljević, V. (2013). Oil and gas in Montenegro. Ministry for Economic Development, Government of Montenegro, Geological Survey of Montenegro.

Duretz, T. & Gerya, T.V. (2013). Slab detachment during continental collision: Influence of crustal rheology and interaction with lithospheric delamination. Tectonophysics, 602, 124-140.

El-Ghali, M.A.K., El Khoriby, E.H., Mansuberg, H., Morad, S., & Ogle, N. (2013). Distribution of carbonate cements within depositional facies and sequence stratigraphic framework of shoreface and deltaic arenites, Lower Miocene, the Gulf of Suez rift, Egypt. Marine and Petroleum Geology, 45, 267-280.

Ellis, S., Beaumont, C., & Pfiffner, A. (1999). Geodynamic models of crustal-scale episodic tectonic accretion and underplating in subduction zones. Journal of Geophysical Research, 1041(B7), 15169-15190

Erak, D., Matenco, L., Toljić, M., Stojadinović, U., Andriessen, P. A. M., Willingshofer, E., & Ducea, M. N. (2017). From nappe stacking to extensional detachments at the contact between the Carpathians and Dinarides – The Jastrebac Mountains of central Serbia. Tectonophysics, 710–711, 162-183. doi: 10.1016/j.tecto.2016.12.022

Erdös, Z., Huismans, R. S., & van der Beek, P. (2015). First-order control of syntectonic sedimentation on crustal-scale strucure of mountain belts, Journal of Geophysical Research:Solid Earth, 120(7), 5362-5377. doi: 10.1002/2014JB011785

Espitalié, J., Laporte, J.L., Madec, M., Marquis, F., Leplat, P., Paulet, J. & Boutefeu, A. (1977). Méthode rapide de caractérisation des roches mères, de leur potentiel pétrolier et de leur degré d'évolution. Revenu Institut Français du Pétrole, 32, 23-42.

Evangelidis, C.P. (2017). Seismic anisotropy in the Hellenic subduction zone: Effects of slab segmentation and subslab mantle flow. Earth Planet. Sci. Lett., 480, 97-106.

Faccenda, M., Gerya, W.V., & Chakraborty, S. (2008). Styles of post-subduction collisional orogeny: Influence of convergence velocity, crustal rheology and radiogenic heat production. Lithos, 103, 257-287. doi: 10.1016/j.lithos.2007.09.009

Faccenna, C. & Becker, T.W. (2010). Shaping mobile belts by small-scale convection. Nature, 465, 602-605.

Faccenna, C., Becker, T. W., Conrad, C. P., & Husson, L. (2013). Mountain building and mantle dynamics. Tectonics, 32, 1-15. doi: 10.1029/2012TC003176

Faccenna, C., Piromallo, C., Crespo-Blanc, A., Jolivet, L. & Rosetti, F. (2004). Lateral slab deformation and the origin of the western Mediterranean arcs. Tectonics, 23, TC1012, doi:10.1029/2002TC001488.

Faccenna, C., Becker, T. W., Auer, L., Billi, A., Boschi, L., Brun, J.-P., Capitanio, F. A., Funiciello, F., Horvàth, F., Jolivet, L., Piromallo, C., Royden, L., Rossetti, F., & Serpelloni, E. (2014). Mantle dynamics in the Mediterranean. Reviews of Geophysics, 52(3), 283-332. doi: 10.1002/2013RG000444

Ferket, H., Swennen, R., Ortuno, S., & Roure, F. (2003). Reconstruction of the fluid flow history during Laramide foreland fold and thrust belt development in eastern Mexico:

cathodoluminescence and $\delta^{18}O - \delta^{13}C$ isotope trends of calcite-cemented fractures. Journal of Geochemical Exploration, 78-79, 163-167. doi:10.1016/S0375-6742(03)00119-5

Fiket, A., Alajbeg, A., Strmic Palinkas, S., Tari-Kovacic, V., Palinkas, L., & Spanenberg, J. (2008). Organic geochemistry of Jurassic-Cretaceous source rocks and oil seeps from the profile across the Adriatic-Dinaric carbonate platform. Geologica Carpathica, 59, 3, 225-236.

Fischer, M. P., Woodward, N. B., & Mitchell, M. M. (1992). The kinematics of break-thrust folds. Journal of Structural Geology, 14(4), 451-460. doi: 10.1016/0191-8141(92)90105-6

Fodor, L., Bada, G., Csillag, G., Horvath, E., Ruszkiczay-Rudiger, Z., Palotas, K., Sikhegyi, F., Timar, G. & Cloetingh, S. (2005). An outline of neotectonic structures and morphotectonics of the western and central Pannonian Basin. Tectonophysics, 410, 15-41.

Fodor, L., Jelen, B., Marton, E., Skaberne, D., Car, J. & Vrabec, M. (1998). Miocene-Pliocene evolution of the Slovenian Periadriatic fault: Implications for the Carpathians extrusion models. Tectonics, 17, 690-709.

Fourier, J. (1822). Théorie Analytique de la Chaleur. Chez Firmin Didot, Père et fils, Libraires pour les mathématiques, l'architecture hydraulique et la marine, Rue Jacob, 24, 1-638

Forte, A. M., Cowgill, E., & Whipple, K. X. (2014). Transition from a singly vergent to doubly vergent wedge in a young orogen: The Greater Caucasus. Tectonics, 33(11), 2077-2101. doi: 10.1002/2014TC003651

Friedman, I., & O'Neil, J.R. (1977). Composition of stable isotopic fractionation factors of geochemical interest. M. Fleisher (Editor), Data of Geochemistry, 6th U.S. Geological Survey, Professional paper, 440, 1-12

Frisch, W., Dunkl, I. & Kuhlemann, J. (2000). Post-collisional orogen-parallel large-scale extension in the Eastern Alps. Tectonophysics, 327, 239-265.

Gallhofer, D., von Quadt, A., Peytcheva, I., Schmid, S. M., & Heinrich, C. A. (2015). Tectonic, magmatic, and metallogenic evolution of the Late Cretaceous arc in the Carpathian-Balkan orogen. Tectonics, 34, 1813–1836. doi: 10.1002/ 2015TC003834

Gaviglio, P. (1986). Crack-seal mechanism in a limestone: a factor of deformation in strike-slip faulting. Tectonophysics 131, 247-255

Gerya, T. V., & Yuen, D. A. (2003). Rayleigh-Taylor instabilities from hydration and melting propel `cold plumes' at subduction zones. Earth and Planetary Science Letters, 212(1-2), 47-62. doi: 10.1016/S0012-821X(03)00265-6

Glavatovic, B. (2007). Seismogenic model for Montenegro: Overview of relevant data. First Workshop for the Nato Science for Peace Project, No. 983054, 7-9 November 2007, Slovenia.

Goričan, Š. (1994). Jurassic and Cretaceous radiolarian biostratigraphy and sedimentary evolution of the Budva Zone (Dinarides, Montenegro). Memoires de Geologie, 18, 177, Lausanne, Swiss

Goričan, Š., Karamata, S., & Batočanin-Srećković, D., (1999). Upper Triassic (Carnian-Norian) Radiolarians in Cherts of Sjenica (SW Serbia) and the Time Span of the Oceanic Realm Ancestor of the Dinaridic Ophiolite Belt. Bulletin T. CXIX de l'Academie serbe des sciences et des arts, 39, 141-149.

Goričan, Š., Košir, A., Rožič, B., Šmuc, A., Gale, L., Kukoč, D., Celarc, B., Črne, A. E., Kolar-Jurkovšek, T., & Placer, L. (2012). Mesozoic deep water basins of the eastern Southern Alps

(NW Slovenia). Paper presented at 29th IAS Meeting of Sedimentology, Journal of Alpine Geology, 55, 1-44, Schladming, Austria

Gorini, C., Lofi, J., Duvail, C., dos Reis, A.T., Guennoc, P., Le Strat, P., & Mauffret, A. (2005). The Late Messinian salinity crisis and Late Miocene tectonism: interaction and consequences on the physiography and post-rift evolution of the Gulf of Lions margin. Marine and Petroleum Geology. 22 (6-7). doi:10.1016/j.marpetgeo.2005.03.012.

Grandić, S., Kratković, I., & Rusan, I. (2010). Hydrocarbon potential assesment of the slope deposits along the SW Dinarides carbonate platform edge. NAFTA, 61 (7-8), 325-338

Grenerczy, G., Sella, G., Stein, S., & Kenyeres, A. (2005). Tectonic implications of the GPS velocity field in the Northern Adriatic region, Geophysical Research Letters, 32(L16311), 1-4. doi: 10.1029/2005GL022947.

Gušić, I., & Jelaska, V. (1993). Upper Cenomanian – Lower Turonian sea-level rise and its consequences on the Adriatic-Dinaric carbonate platform. Geologische Rundschau, 82, 676-686.

Handy, M. R., Schmid, S. M., Bousquet, R., Kissling, E., & Bernoulli, D. (2010). Reconciling plate-tectonic reconstructions of Alpine Tethys with the geological-geophysical record of spreading and subduction in the Alps. Earth-Science Reviews, 102(3-4), 121-158. doi: 10.1016/j.earscirev.2010.06.002

Handy, M.R., Ustaszewski, K. & Kissling, E. (2014). Reconstructing the Alps–Carpathians–Dinarides as a key to understanding switches in subduction polarity, slab gaps and surface motion. Int. J. Earth Sci., 104, 1-26.

Harzhauser, M., & Mandic, O. (2008). Neogene lake systems of central and South-Eastern Europe: Faunal diversity, gradients and interrelations. Paleogeography, Paleoclimatology, Paleoecology, 260(3-4), 417-434.
doi: 10.1016/j.palaeo.2007.12.013

Harzhauser, M., Mandic, O., Latal, C. & Kern, A. (2011). Stable isotope composition of the Miocene Dinaride Lake System deduced from its endemic mollusc fauna. Hydrobiologia, 682, 27-46.

Heberer, B., Reverman, R.L., Fellin, M.G., Neubauer, F., Dunkl, I., Zattin, M., Seward, D., Genser, J. & Brack, P. (2017). Postcollisional cooling history of the Eastern and Southern Alps and its linkage to Adria indentation. Int. J. Earth Sci., 106, 1557-1580.

Heidbach, O., Rajabi, M., Cui, X., Fuchs, K., Müller, B., Reinecker, J., Reiter, K., Tingay, M., Wenzel, F., Xie, F., Ziegler, M.O., Zoback, M.-L. & Zoback, M. (2018). The World Stress Map database release 2016: Crustal stress pattern across scales. Tectonophysics, 744, 484-498.

Heidbach, O., Reinecker, J., Tingay, M., Müller, B., Sperner, B., Fuchs, K. & Wenzel, F. (2007). Plate boundary forces are not enough: Second- and third-order stress patterns highlighted in the World Stress Map database. Tectonics, 26.

Heidbach, O., Tingay, M., Barth, A., Reinecker, J., Kurfess, D. & Muller, B. (2010). Global crustal stress pattern based on the World Stress Map database release 2008. Tectonophysics, 482, 3-15.

Heidbach, O., Custodio, S., Kingdon, A., Mariucci, M.T., Montone, P., Müller, B., Pierdominici, S., Rajabi, M., Reinecker, J., Reiter, K., Tingay, M., Williams, J., & Ziegler,

M. (2016). Stress Map of the Mediterranean and Central Europe 2016, GFZ Data Service. doi: 10.5880/WSM.Europe2016.

Herak, D., Herak, M. & Tomljenovic, B. (2009). Seismicity and earthquake focal mechanisms in North-Western Croatia. Tectonophysics, 465, 212-220.

Heuret, A., & Lallemand, S. (2005). Plate motions, slab dynamics and back-arc deformation. Physics of The Earth and Planetary Interiors, 149(1-2), 31-51. doi: 10.1016/j.pepi.2004.08.022

Horváth, F., Musitz, B., Balázs, A., Végh, A., Uhrin, A., Nádor, A., Koroknai, B., Pap, N., Tóth, T., & Wórum, G. (2015). Evolution of the Pannonian basin and its geothermal resources. Geothermics, 53, 328-352. doi: 10.1016/j.geothermics.2014.07.009

Houseman, G. & England, P. (1993). Crustal thickening versus lateral expulsion in the Indian-Asian continental collision. J. Geophys. Res.: Solid Earth, 98, 12233-12249.

Hrvatović, H. (2006). Geological Guidebook through Bosnia and Herzegovina (ISBN: 9958-9351-3). Sarajevo, Bosnia and Herzegovina: Geological Survey of Federation Bosnia and Herzegovina.

Hrvatović, H., & Pamić, J. (2005). Principal thrust-nappe structures of the Dinarides. Acta Geologica Hungarica, 48/2, 133-151. doi: 10.1556/AGeol.48.2005.2.4

Huerta, A. D., Royden, L. H., & Hodges, K. V. (1998). The thermal structure of collisional orogens as a response to accretion, erosion, and radiogenic heating. Journal of geophysical research, 103 (B7), 15287-15302.

Iancu, V., Berza, T., Seghedi, A., Gheuca, I., & Hann, H.-P. (2005). Alpine polyphase tectono-metamorphic evolution of the South Carpathians: A new overview. Tectonophysics, 410(1-4), 337-365. doi: 10.1016/j.tecto.2004.12.038

Ilić, A., & Neubauer, F., (2005). Tertiary to recent oblique convergence and wrenching of the Central Dinarides: Constraints from a palaeostress study. Tectonophysics, 410(1-4), 465-484. doi: 10.1016/j.tecto.2005.02.019

Ilić, A., Neubauer, F., & Handler, R. (2005). Late Paleozoic–Mesozoic tectonics of the Dinarides revisited: Implications from 40Ar/39Ar dating of detrital white micas. Geology, 33(3), 233-236. doi: 10.1130/G20979.1

Jammes, S., & Huismans, R. S. (2012). Structural styles of mountain building: Controls of lithospheric rheologic stratificatio and extensional inheritance, Journal of Geophysical Research: Solid Earth, 117. doi: 10.1029/2012JB009376

Jolivet, L., & Faccenna, C. (2000). Mediterranean extension and the Africa-Eurasia collision. Tectonics, 19(6), 1095-1106. doi: 10.1029/2000TC900018

Jolivet, L., & Brun, J.-P. (2010). Cenozoic geodynamic evolution of the Aegean. International Journal of Earth Sciences, 99(1), 109-138. doi: 10.1007/s00531-008-0366-4

Jolivet, L., Faccenna, C., Heut, B., Labrousse, L., Le Pourhiet, L., Lacombe, O., Lecomte, E., Burov, E., Denèle, Y., Brun, J.-P., Philippon, M., Paul, A., Salaün, G., Karabulut, H., Piromallo, C., Monié, P., Gueydan, F., Okay, A.I., Oberhänsli, R., Pourteau, A., Augier, R., Gadenna, L. & Driussi, O. (2013). Aegean tectonics: Strain localisation, slab tearing and trench retreat. Tectonophysics, 597–598(0), 1-33. doi: 10.1016/j.tecto.2012.06.011

Jolivet, L., Faccenna, C., Becker, T., Tesauro, M., Sternai, P. & Bouilhol, P. (2018). Mantle Flow and Deforming Continents: From India-Asia Convergence to Pacific Subduction. Tectonics, 37, 2887-2914.

Jolivet, L., Menant, A., Sternai, P., Rabillard, A., Arbaret, L., Augier, R., Laurent, V., Beaudoin, A., Grasemann, B., Huet, B., Labrousse, L. and Le Pourhiet, L., 2015. The geological signature of a slab tear below the Aegean. Tectonophysics, 659, 166-182.

Jones, R.R. & Tanner, G.P.W. (1995). Strain partitioning in transpression zones. Journal of Structural Geology, 17, 793-802.

Jouanne, F., Mugnier, J.L., Koci, R., Bushati, S., Matev, K., Kuka, N., Shinko, I., Kociu, S. & Duni, L. (2012). GPS constraints on current tectonics of Albania. Tectonophysics, 554-557, 50-62.

Kahle, H.G., Cocard, M., Peter, Y., Geiger, A., Reilinger, R., Barka, A. & Veis, G. (2000). GPS-derived strain rate field within the boundary zones of the Eurasian, African, and Arabian Plates. J. Geophys. Res. - Solid Earth, 105, 23353-23370.

Kastelić, V., & Carafa, M. (2012). Fault slip rates for the active External Dinarides thrust-and-fold belt. Tectonics. doi: 10.1029/2011TC003022

Király, Á., Faccenna, C. & Funiciello, F. (2018). Subduction Zones Interaction Around the Adria Microplate and the Origin of the Apenninic Arc. Tectonics, 37, 3941-3953.

Kissling, E., Schmid, S. M., Lippitsch, R., Ansorge, J., & Fügenschuh, B. (2006). Lithosphere structure and tectonic evolution of the Alpine arc: new evidence from high-resolution teleseismic tomography. Geological Society of London, Memoirs, 32, 129-145. doi: 10.1144/GSL.MEM.2006.032.01.08

Konstantinou, K.I., Mouslopoulou, V., Liang, W.T., Heidbach, O., Oncken, O. & Suppe, J. (2017). Present-day crustal stress field in Greece inferred from regional-scale damped inversion of earthquake focal mechanisms. J. Geophys. Res.: Solid Earth, 122, 506-523.

Korbar, T. (2009). Orogenic evolution of the External Dinarides in the NE Adriatic region: a model constrained by tectonostratigraphy of Upper Cretaceous to Paleogene carbonates. Earth-Science Reviews, 96(4), 296-312. doi: 10.1016/j.earscirev.2009.07.004

Korte, C., Kozur, H.W., & Veizer, J. (2005). δ13C and δ18O values of Triassic brachiopods and carbonate rocks as proxies for coeval seawater and palaeotemperature. Paleogeography, Paleoclimatology, Paleoecology, 226(3-4), 287-306. doi: 10.1016/j.palaeo.2005.05.018

Kreemer, C., Holt, W. E., & Haines, A. J. (2003). An integrated global model of present-day plate motions and plate boundary deformation. Geophysical Journal International, 154(1), 8-34. doi: 10.1046/j.1365-246X.2003.01917.x

Kulušić, A., & Borojević Šoštarić, S. (2014). Dinaride evaporite mélange: Diagenisis of the Kosovo Polje evaporites. Geologia Croatica, 67/1, 59–74. doi: 10.4154/gc.2014.05

Lachenbrach, A. (1970). Crustal temperature and heat productivity implications on the linear heat flow relation. Journal of Geophysisical Research, 75, 3291-3300.

Lacombe, O. (2012). Do fault slip data inversions actually yield ‘‘paleostresses’’ that can be compared with contemporary stresses? A critical discussion. Comptes Rendus Geoscience, 344, 159-173. doi: 10.1016/j.crte.2012.01.006

Lacombe, O., & Bellahsen, N. (2016). Thick-skinned tectonics and basement-involved fold–thrust belts: insights from selected Cenozoic orogens. Geological Magazine, 1-48. doi: 10.1017/S0016756816000078

Lallemand, S.E., Schurle, P., & Malavieille, J. (1994). Coulomb theory applied to accretionary and nonaccretionary wedges : Possible causes for tectonic erosion and/or frontal accretion. Journal of Geophysical Research, 99, 12033-12055

Lancaster, P., & Salkauskas, K. (1981). Surfaces generated by moving least-squares methods. Mathematics and Computation, 37, 141–158

Le Breton, E., Handy, M.R., Molli, G. & Ustaszewski, K. (2017). Post-20 Ma Motion of the Adriatic Plate: New Constraints From Surrounding Orogens and Implications for Crust-Mantle Decoupling. Tectonics, 36, 3135-3154.

Lippitsch, R., Kissling, E., & Ansorge, J. (2003). Upper mantle structure beneath the Alpine orogen from high-resolution teleseismic tomography. Journal of Geophysical Research, 108(B8). doi: 10.1029/2002JB002016

Lohmann, K.C. (1988). Geochemical patterns of meteoric diagenetic systems and their application to studies of paleokarst. In: James, N.P., Choquette, P.W. (Eds.), Paleokarst. Springer-Verlag, 58–80.

Louvari, E., Kiratzi, A.A. & Papazachos, B.C. (1999). The Cephalonia Transform Fault and its extension to western Lefkada Island (Greece). Tectonophysics, 308, 223-236.

Magyar, I. & Geary, D.H. (2012). Biostratigraphy in a Late Neogene Caspian-Type Lacustrine Basin: Lake Pannon, Hungary. In: O.W. Baganz, Y. Bartov, K. Bohacs and D. Nummedal (Eds.), Lacustrine sandstone reservoirs and hydrocarbon systems. AAPG Memoir 95, pp. 255-264.

Mandic, O., de Leeuw, A., Bulić, J., Kuiper, K. F., Krijgsman, W., & Jurišić-Polšak, Z. (2012). Paleogeographic evolution of the Southern Pannonian Basin: 40Ar/39Ar age constraints on the Miocene continental series of Northern Croatia. International Journal of Earth Sciences, 101(4), 1033-1046. doi: 10.1007/s00531-011-0695-6

Mandic, O., de Leeuw, A., Vukovic, B., Krijgsman, W., Harzhauser, M., & Kuiper, K.F. (2011). Palaeoenvironmental evolution of Lake Gacko (NE Bosnia and Herzegovina): impact of the Middlle Miocene Climatic Optimum on the Dinaride Lake System. Palaeogeography, Palaeoclimatology, Palaeoecology, 299/3-4: 475-492. doi: 10.1007/s00531-011-0695-6

Mandic, O., Hajek-Tadesse, V., Bakrač, K., Reichenbacher, B., Grizelj, A. & Miknić, M. (2019a). Multiproxy reconstruction of the middle Miocene Požega palaeolake in the Southern Pannonian Basin (NE Croatia) prior to the Badenian transgression of the Central Paratethys Sea. Paleogeogr., Paleoclimatol., Paleoecol., 516, 203-219.

Mandic, O., Sant, K., Kallanxhi, M.-E., Ćorić, S., Theobalt, D., Grunert, P., de Leeuw, A. & Krijgsman, W. (2019b). Integrated bio-magnetostratigraphy of the Badenian reference section Ugljevik in southern Pannonian Basin - implications for the Paratethys history (middle Miocene, Central Europe). Global Planet. Change, 172, 374-395.

Marović, M., Djoković, I., Pešić, L., Radovanović, S., Toljić, M., & Gerzina, N. (2002). Neotectonics and seismicity of the Southern margin of the Pannonian basin in Serbia. In S. Cloetingh, F. Horvath, G. Bada, A. Lankreijer (Eds.), Neotectonics and surface processes: the Pannonian Basin and Alpine/Carpathian System (Vol. 3, pp. 277-295). Katlenburg-Lindau, Germany: European Geosciences Union

Márton, E., Drobne, K., Cosović, V., & Moro, A. (2003). Palaeomagnetic evidence for Tertiary counterclockwise rotation of Adria. Tectonophysics, 377, 143–156. doi: 10.1016/j.tecto.2003.08.022

Matenco, L., & Radivojević, D. (2012). On the formation and evolution of the Pannonian Basin: Constraints derived from the structure of the junction area between the Carpathians and Dinarides. Tectonics, 31(6), TC6007. doi: 10.1029/2012TC003206

Matenco, L., Krézsek, C., Merten, S., Schmid, S., Cloetingh, S., & Andriessen, P. (2010). Characteristics of collisional orogens with low topographic build-up: an example from the Carpathians. Terra Nova, 22(3), 155-165. doi: 10.1111/j.1365-3121.2010.00931.x

Matenco, L., Munteanu, I., ter Borgh, M., Stanica, A., Tilita, M., Lericolais, G., Dinu, C., & Oaie, G. (2016), The interplay between tectonics, sediment dynamics and gateways evolution in the Danube system from the Pannonian Basin to the western Black Sea. Science of The Total Environment, 543, 807–827. doi: 10.1016/j.scitotenv.2015.10.081.

Mazzuca, N., Bruni, A., & Joppen, T. (2015). Exploring the potential of deep targets in the South Adriatic Sea: insight from 2D basin modelling of the Croatian offshore. Geologia Croatica, 68(3). 237-246. doi: 104154/gc.2015.18

Meissner, R. & Mooney, W. (1998). Weakness of the lower continental crust: a condition for delamination, uplift, and escape. Tectonophysics, 296, 47-60.

Menant, A., Jolivet, L., & Vrielynck, B. (2016). Kinematic reconstructions and magmatic evolution illuminating crustal and mantle dynamics of the eastern Mediterranean region since the late Cretaceous, Tectonophysics, 675, 103-140. doi: 10.1016/j.tecto.2016.03.007

Métois, M., D'Agostino, N., Avallone, A., Chamot-Rooke, N., Rabaute, A., Duni, L., Kuka, N., Koci, R. & Georgiev, I. (2015). Insights on continental collisional processes from GPS data: Dynamics of the peri-Adriatic belts. J. Geophys. Res.: Solid Earth, 120, 8701-8719.

Mikes, T., Christ, D., Petri, R., Dunkl, I., Frei, D., Báldi-Beke, M., Reitner, J., Wemmer, K., Hrvatović, H., & von Eynatten, H. (2008). Provenance of the Bosnian Flysch, Swiss Journal of Geosciences, 101(0), 31-54. doi: 10.1007/s00015-008-1291-z

Milivojević, M., & Martinović, M. (2005). Geothermal Energy Possibilities, Exploration and Future Prospects in Serbia. Proceedings World Geothermal Congress, Antalya, Turkey, 24-29 April 2005

Milivojević, M.G. (1993). Geothermal model of the earths crust and lithosphere for the territory of Yugoslavia: some tectonic implications. Studia Geophysica et Geodaetica, 37, 265-278.

Milojević, R. & Sunarić, O. (1962). Geoloski prikaz lezista lignita Prolog u Livanjskom ugljenonosnom basenu (Geological investigation of lignite Prolog in the Livno coal basin). Geoloski glasnik, 6, 85-101.

Milojević, R. & Sunarić, O. (1964). Pokušaj stratigrafskog raščlanjavanja slatkovodnih sedimenata Duvanjskog basena i neki ekonomsko geološki momenti u razvoju ugljenih facija (An attempt to stratigraphically separate the freshwater sediments of the Duvanj basin and some economic and geological moments in the development of coal basin). Geološki glasnik, 9, 59-75.

Miošić, N., Samardžić, N., & Hrvatović, H. (2010). The Current Status of Geothermal Energy Use and Development in Bosnia and Herzegovina. Proceedings World Geothermal Congress 2010 Bali, Indonesia, 25-29 April 2010.

Mladenović, A., Trivić, B., & Cvetković, V. (2015). How tectonics controlled post-collisional magmatism within the Dinarides: Inferences based on study of tectono-magmatic events in the Kopaonik Mts. (Southern Serbia). Tectonophysics, 646(0), 36-49. doi: 10.1016/j.tecto.2015.02.001

Molnar, P., England, P., & Martinod, J. (1993). Mantle dynamics, uplift of the Tibetan Plateau, and the Indian monsoon. Reviews of Geophysics, 31(4), 357-396. doi: 10.1029/93RG02030

Moulin, A., Benedetti, L., Rizza, M., Jamšek Rupnik, P., Gosar, A., Bourlès, D., Keddadouche, K., Aumaître, G., Arnold, M., Guillou, V. & Ritz, J.-F. (2016). The Dinaric fault system: Large-scale structure, rates of slip, and Plio-Pleistocene evolution of the transpressive northeastern boundary of the Adria microplate. Tectonics, 35, 2258-2292.

Mrinjek, E. (1993). Sedimentology and depositional setting of alluvial Promina Beds in Northern Dalmatia. Geologia Croatica, 46(2), 243-261. Retrieved from https://hrcak.srce.hr/19915

Munteanu, I., Willingshofer, E., Matenco, L., Sokoutis, D. & Cloetingh, S. (2014). Far-field contractional polarity changes in models and nature. Earth Planet. Sci. Lett., 395, 101-115.

Nocquet, J.-M. (2012). Present-day kinematics of the Mediterranean: A comprehensive overview of GPS results. Tectonophysics, 579, 220-242.

O'Brien, J. J., & Lerche, I. (1988). Impact of heat flux anomalies around salt diapirs and salt sheets in the gulf coast on hydrocarbon maturity: models and observations. Golf coast association of geological societies, XXXVIII, 231-243.

Pamić, J. (2002). The Sava-vardar Zone of the Dinarides and Hellenides versus the Vardar Ocean. Eclogae Geologicae Helvetiae, 95(1), 99-113.

Pamić, J., Balogh, K., Hrvatović, H., Balen, D., Jurković, I., & Palinkaš, L. (2004). K–Ar and Ar–Ar dating of the Palaeozoic metamorphic complex from the Mid-Bosnian Schist Mts., Central Dinarides, Bosnia and Hercegovina. Mineralogy and Petrology, 82, 65–79. doi: 10.1007/s00710-004-0041-9

Pamić, J., Gušić, I., & Jeleska, V. (1998). Geodynamic evolution of the Central Dinarides. Tectonophysics, 297, 251-268.

Pamić, J., Tomljenović, B., & Balen, D. (2002). Geodynamic and petrogenetic evolution of Alpine ophiolites from the central and NW Dinarides: an overview. Lithos, 65(1-2), 113-142. doi: 10.1016/S0024-4937(02)00162-7

Pamić, J. J. (1984). Triassic Magmatism of the Dinarides in Yugoslavia. Tectonophysics, 109(3-4), 273-307. doi: 10.1016/0040-1951(84)90145-8

Pantić, N., Ercegovac, M. & Pantić, V. (1966). Palinološka ispitivanja i stratigrafija terestrično-limničkih tercijarnih naslaga u Zeničko-Sarajevskom basenu (Palinological investigations and stratigraphy of terrestrial and limestone tertiary deposits in the Zenica-Sarajevo basin). Geološki anali Balkanskog poluostrva 32, 183-210.

Pantić, N.K. & Bešlagić, A. (1964). Palinološke analize mrkog uglja i lignita iz Livanjskog tercijarnog bazena (Palinological analyzes of brown coal and lignite from the Livno Tertiary basin). Geološki anali Balkanskog poluostrva, 31, 127-133.

Pavelić, D. & Kovačić, M. (2018). Sedimentology and stratigraphy of the Neogene rift-type North Croatian Basin (Pannonian Basin System, Croatia): A review. Mar. Petrol. Geol., 91, 455-469.

Pavlides, S., Caputo, R., Sboras, S., Chatzipetros, A., Papathanasiou, G. & Valkaniotis, S. (2010). The Greek catalogue of active faults and seismogenic sources. Bull. Geol. Soc. Greece, 43, 486-494.

Pearce, F.D., Rondenay, S., Sachpazi, M., Charalampakis, M. & Royden, L.H. (2012). Seismic investigation of the transition from continental to oceanic subduction along the western Hellenic Subduction Zone. J. Geophys. Res.: Solid Earth, 117.

Peral, M., Király, Á., Zlotnik, S., Funiciello, F., Fernàndez, M., Faccenna, C. & Vergés, J. (2018). Opposite Subduction Polarity in Adjacent Plate Segments. Tectonics, 37, 3285-3302.

Pérouse, E., Sébrier, M., Braucher, R., Chamot-Rooke, N., Bourlès, D., Briole, P., Sorel, D., Dimitrov, D. & Arsenikos, S. (2017). Transition from collision to subduction in Western Greece: the Katouna–Stamna active fault system and regional kinematics. Int. J. Earth Sci., 106, 967-989.

Picha, F. (2002). Late orogenic strike-slip faulting and escape tectonics in frontal Dinarides-Hellenides, Croatia, Yugoslavia, Albania, and Greece. AAPG Bulletin, 86, 1659–1671.

Picotti, V., & Pazzaglia, F. J. (2008). A new active tectonic model for the construction of the Northern Apennines mountain front near Bologna (Italy). Journal of Geophysical Research, 113(B08412), 1-24. doi: 10.1029/2007JB005307

Pierdominici, S. & Heidbach, O. (2012). Stress field of Italy — Mean stress orientation at different depths and wave-length of the stress pattern. Tectonophysics, 532-535, 301-311.

Pinter, N., Grenerczy, G., Weber, J., Stein, S., & Medak, D. (2005). The Adria Microplate: GPS Geodesy, Tectonics and Hazards. Nato Science Series: IV: Earth and Environmental Sciences. (Vol. 61). Dordrecht, The Netherlands: Springer

Piromallo, C., & Morelli, A. (2003). P wave tomography of the mantle under the Alpine-Mediterranean area, Journal of Geophysical Research, 108(B2), 2065. doi: 10.1029/2002JB001757

Platt, J. P., Behr, W. M., Johanesen, K., & Williams, J. R. (2013). The Betic-Rif Arc and Its Orogenic Hinterland: A Review. Annual Review of Earth and Planetary Sciences, 41(1), 313-357. doi: 10.1146/annurev-earth-050212-123951

Pubellier, M., & Morley, C. K. (2014). The basins of Sundaland (SE Asia): Evolution and boundary conditions. Marine and Petroleum Geology, 58, Part B, 555-578. doi: 10.1016/j.marpetgeo.2013.11.019

Rampnoux, J.-P. (1970). Regards sur les Dinarides internes yougoslaves (Serbie-Monténégro oriental): Stratigraphie, evolution paléogéographique, magmatisme. Bulletin de la Société géologique de France, 12, 948–966.

Ramsay, J.G. (1980). The crack-seal mechanism of rock deformation. Nature 284, 135-139

Ratschbacher, L., Frisch, W., Linzer, H.G. & Merle, O. (1991). Lateral extrusion in the Eastern Alps; Part 2, Structural analysis. Tectonics, 10, 257-271.

Ravnik, D., Rajver, D., Poljak, M., & Živčić, M. (1995). Overview of the geothermal field of Slovenia in the area between the Alps, the Dinarides and the Pannonian basin. Tectonophysics, 250 (1–3), 135-149. doi: 10.1016/0040-1951(95)00031-X

Regard, V., Faccenna, C., Martinod, J. & Bellier, O. (2005). Slab pull and indentation tectonics: insights from 3D laboratory experiments. Phys. Earth Planet Int., 149, 99-113.

Robertson, A., & Shallo, M. (2000). Mesozoic-Tertiary tectonic evolution of Albania in its regional Eastern Mediterranean context. Tectonophysics, 316, 197-254.

Robertson, A., Karamata, S., & Sarić, K. (2009). Overview of ophiolites and related units in the Late Palaeozoic-Early Cenozoic magmatic and tectonic development of Tethys in the northern part of the Balkan region. Lithos, 108(1-4), 1-36. doi: 10.1016/j.lithos.2008.09.007

Rosenberg, C.L., Brun, J.P., Cagnard, F., & Gapais, D. (2007). Oblique indentation in the Eastern Alps: Insights from laboratory experiments. Tectonics, 26.

Roure, F., & Sassi, W. (1995). Kinematics of deformation and petroleum system appraisal in Neogene foreland fold-and-thrust belts. Petroleum Geoscience, 1, 253-269. doi: 10.1144/petgeo.1.3.253

Roure F., Roca E., & Sassi W. (1993). The Neogene evolution of the Outer Carpathian flysch units (Poland, Ukraine and Romania): kinematics of a foreland fold and thrust belt system. Sedimentary Geology, 86, 177-201.

Roure, F., Andriessen, P, Callot, J. P., Faure, J. L., Ferket, H., Gonzales, E., Guilhaumou, N., Lacombe, O., Malandain, J., Sassi, W., Schneider, F., Swennen, R., and Vilasi, N. (2010). The use of palaeo-thermo-barometers and coupled thermal, fluid-flow, pore-fluid pressure modelling for hydrocarbon and reservoir prediction in fold and thrust belts. Geological Society London, 348, 87-114. doi: 10.1144/SP348.6

Roure, F., Swennen, R., Schneider, F., Faure, J.I., Ferket, H., Guilhaumou, N., Osadetz, K., Robion, P., & Vandeginste, V. (2005). Incedence and importance of tectonics and natural fluid migration on reservoir evolution in foreland fold-and-thrust belts. Oil & Gas science and Technology - Revenue IFP, 60, 67-106.

Roure, F., Fili, I., Najaz, S., Cadet, J.P., Mushka, K., & Bonneau, M. (2004). Kinematic Evolution and Petroleum Systems—An Appraisal of the Outer Albanides. In: K.R. McClay (Ed.), Thrust tectonics and hydrocarbon systems. AAPG Memoir 82, pp. 474-493.

Royden, L. H. (1993). The tectonic expression of slab pull at continental convergent boundaries. Tectnonics, 12, 303-325

Sant, K., Andrić, N., Mandic, O., Demir, V., Pavelić, D., Rundić, L., Hrvatović, H., Matenco, L., & Krijgsman, W. (2018). Magneto-biostratigraphy and paleoenvironments of the Miocene freshwater sediments of the Sarajevo-Zenica Basin. Paleogeogr., Paleoclimatol., Paleoecol., 506, 48-69.

Schefer, S. (2010). Tectono-metamorphic and magmatic evolution of the Internal Dinarides (Kopaonik area, Southern Serbia) and its significance for the geodynamic evolution of the Balkan Peninsula, (Doctoral Dissertation). Basel, Switzerland: University of Basel

Schefer, S., Cvetković, V., Fügenschuh, B., Kounov, A., Ovtcharova, M., Schaltegger, U., & Schmid S. (2011). Cenozoic granitoids in the Dinarides of Southern Serbia: age of intrusion, isotope geochemistry, exhumation history and significance for the geodynamic evolution of the Balkan Peninsula. International Journal of Earth Sciences, 100(5), 1181-1206. doi: 10.1007/s00531-010-0599-x

Schefer, S., Egli, D., Missoni, S., Bernoulli, D., Gawlick, H.-J., Jovanović, D., Krystyn, L., Lein, R., Schmid, S. M., & Sudar, M. (2010). Triassic sediments in the Internal Dinarides (Kopaonik area, Southern Serbia): stratigraphy, paleogeographic and tectonic significance. Geologica Carpathica, 61(2), 89-109. doi: 10.2478/v10096-010-0003-6

Schmid, S., Bernoulli, D., Fügenschuh, B., Matenco, L., Schefer, S., Schuster, R., Tischler, M., & Ustaszewski, K. (2008). The Alpine-Carpathian-Dinaridic orogenic system: correlation

and evolution of tectonic units. Swiss Journal of Geosciences, 101(1), 139-183. doi: 10.1007/s00015-008-1247-3

Schmid, S.M., Bernoulli, D., Fügenschuh, B., Matenco, L., Schefer, S., Oberhänsli, R., & Ustaszewski, K. (2011). Tracing the closure of Neotethys from the Alps to Western Turkey II: Similarities and differences between Dinarides, Hellenides and Anatolides-Taurides. Geophysical Research Abstracts, 13, EGU2011- 4000.

Schmid, S.M., Kissling, E., Diehl, T., van Hinsbergen, D.J.J. & Molli, G. (2017). Ivrea mantle wedge, arc of the Western Alps, and kinematic evolution of the Alps-Apennines orogenic system. Swiss J. Geosci., 110, 581-612.

Schmitz, B., Ustaszewski, K., Wemmer, K., Onuzi, K., & Muceku, B. (2017). Kinematics and age of the orogen-perpenticular Shkodër-Peja-Normal-Fault, northern Albania, 13th Workshop on Alpine Geological Studies, Zlatibor, Serbia.

Schneider, F. (2003). Basin modelling in complex area: examples from eastern Venezuelan and Canadian foothills. Oil and Gas Science and Technology, Revue de l'IFP, 58, 313–324.

Schneider, F., Wolf, S., Faille, I., & Pot, D. (2000). A 3D Basin Model for Hydrocarbon Potential Evaluation: Application to Congo Offshore. Oil & Gas Science and Technology, Revenue de l'IFP, 55 (1), 3-13

Scisciani, V. & Calamita, F. (2009). Active Intraplate Deformation within Adria: Examples from the Adriatic Region. Tectonophysics, 476, 57-72. doi: 10.1016/j.tecto.2008.10.030

Seghedi, I., Downes, H., Szakács, A., Mason, P.R.D., Thirlwall, M.F., Roşu, E., & Pécskay, Z. (2004). Neogene – Quaternary magmatism and geodynamics in the Carpathian – Pannonian region: a synthesis. Lithos, 72, 117-146. doi: 10.1016/j.lithos.2003.08.006

Sengör, A. M. C., Özeren, M. S., Keskin, M. SakInç, M., ÖzbakIr, A. D., & Kayan, I. (2008). Eastern Turkish high plateau as a small Turkic-type orogen: Implications for post-collisional crust-forming processes in Turkic-type orogens. Earth-Science Reviews, 90(1-2), 1-48. doi: 10.1016/j.earscirev.2008.05.002

Smit, J.H.W., Cloetingh, S.A.P.L., Burov, E., Tesauro, M., Sokoutis, D. & Kaban, M. (2013). Interference of lithospheric folding in western Central Asia by simultaneous Indian and Arabian plate indentation. Tectonophysics, 602, 176-193.

Sommer, S. E. (1972). Cathodoluminescence of carbonates, 2. Geological applications. Chemical Geology, 9, 275-284. doi: 10.1016/0009-2541(72)90065-4.

Spahić, D., Wygrala, B., & Rundić, Lj. (2014). A Few Remarks on Hydrocarbon Resource Assessment Within the Dinaric Thrust and Fold Belt. NAFTA, (3), 244-249.

Sperner, B., & Zweigel, P. (2010). A plea for more caution in fault-slip analysis, Tectonophysics, 482(1-4), 29-41. doi: 10.1016/j.tecto.2009.07.019

Stampfli, G. M., & Borel, G. D. (2002). A plate tectonic model for the Paleozoic and Mesozoic constrained by dynamic plate boundaries and restored synthetic oceanic isochrones. Earth and Planetary Science Letters, 196(1–2), 17-33. doi: 10.1016/S0012-821X(01)00588-X

Stojadinović, U., Matenco, L., Andriessen, P. A. M., Toljić, M., & Foeken, J. P. T. (2013). The balance between orogenic building and subsequent extension during the Tertiary evolution of the NE Dinarides: Constraints from low-temperature thermochronology. Global Planet. Change, 103(0), 19-38. doi: 10.1016/j.gloplacha.2012.08.004

Stojadinović, U., Matenco, L., Andriessen, P., Toljić, M., Rundić, L., & Ducea, M. N. (2017). Structure and provenance of Late Cretaceous–Miocene sediments located near the NE

Dinarides margin: Inferences from kinematics of orogenic building and subsequent extensional collapse. Tectonophysics, 710–711, 184-204. doi: 10.1016/j.tecto.2016.12.021

Šumanovac, F. (2010). Lithosphere structure at the contact of the Adriatic microplate and the Pannonian segment based on the gravity modelling. Tectonophysics, 485(1-4), 94-106. doi: 10.1016/j.tecto.2009.12.005

Šumanovac, F., & Dudjak, D. (2016). Descending lithosphere slab beneath the Northwest Dinarides from teleseismic tomography. Journal of Geodynamics, 102, 171-184. doi: 10.1016/j.jog.2016.09.007

Šumanovac, F., Markušić, S., Engelsfeld, T., Jurković, K., & Orešković, J. (2017). Shallow and deep lithosphere slabs beneath the Dinarides from teleseismic tomography as the result of the Adriatic lithosphere downwelling. Tectonophysics, 712, 523-541. doi: 10.1016/j.tecto.2017.06.018

Šušnjara, A., Sakač, K., Jelen, B. & Gabrić, A. (1992). Upper Permian Evaporites and Associated Rocks of Dalmatia and Borderline Area of Lika and Bosnia. Geol. Croatica, 45, 95-114.

Swennen, R., Muska, K., & Roure, F. (2000). Fluid circulation in the Ionian fold and thrust belt (Albania): implications for hydrocarbon prospectivity. Journal of Geochemical Exploration 69, 629–634.

Talbot, M.R., & Kelts, K. (1990). Paleolimnological Signatures from Carbon and Oxygen Isotopic Ratios in Carbonates, from Organic Carbon-Rich Lacustrine Sediments: Chapter 6. M 50: Lacustrine Basin Exploration: Case Studies and Modern Analogs, 99-112

Tari, V. (2002). Evolution of the northern and western Dinarides: a tectonostratigraphic approach. In G. Bertotti, K. Schumann, S. Cloetingh (Eds.), Neotectonics and surface processes: the Pannonian Basin and Alpine/Carpathian System, Stephan Mueller Special Publication Series (pp. 105-120). Katlenburg-Lindau, Germany: Copernicus.

Tari, V., & Mrinjek, E. (1994). The Role of Palaeogene Clastics in the Tectonic Interpretation of Northern Dalmatia (Southern Croatia). Geol. Croatica, 1, 127-138.

Teichmüller, M., & Durand, B. (1983). Fluorescence miscroscopical rank studies on liptinites and vitrinites in peat and coals and comparison with results of the Rock-Eval pyrolysis. International Journal of Coal Geology, 2, 197-230.

Tišljar, J. (1992). Origin and Depositional Environments of the Evaporite and Carbonate Complex (Upper Permian) from the Central Part of the Dinarides (Southern Croatia and Western Bosnia). Geol. Croatica, 45, 115-126.

Toljić, M., Matenco, L., Ducea, M. N., Stojadinović, U., Milivojević, J., & Đerić, N. (2013). The evolution of a key segment in the Europe–Adria collision: The Fruška Gora of northern Serbia. Global and Planetary Change, 103(0), 39-62. doi: 10.1016/j.gloplacha.2012.10.009

Toljić, M., Matenco, L., Stojadinović, U., Willingshofer, E., & Ljubović-Obradović, D. (2018). Understanding fossil fore-arc basins: Inferences from the Cretaceous Adria-Europe convergence in the NE Dinarides. Global and Planetary Change, 171, 167-184. doi: 10.1016/j.gloplacha.2018.01.018

Tomljenović, B. & Csontos, L. (2001). Neogene-Quaternary structures in the border zone between Alps, Dinarides and Pannonian Basin (Hrvatsko zagorje and Karlovac Basins, Croatia). Int. J. Earth Sci., 90, 560-578.

Tomljenovic, B., Csontos, L.S, Marton, E.E. & Marton, P.T., 2008. Tectonic evolution of the northwestern Internal Dinarides as constrained by structures and rotation of Medvednica Mountains, North Croatia. Geol. Soc. London, Spec. Publ., 298, 145-167.

Turner, F.J. (1953). Nature and dynamic interpretation of deformation lamellae in calcite of three marbles. American Journal of Sciences, 251 (4), 276–298. doi: 10.2475/ajs.251.4.276

Turrini, C., Bosica, B., Ryan, P., Shiner, P., Lacombe, O., & Roure, F. (2017). 3D structural and thermal modelling of Mesozoic petroleum systems in the Po Valley Basin, northern Italy. Petroleum Geoscience, 24, 172-196. doi: 10.1144/petgeo2017-031

Ustaszewski, K., Herak, M., Tomljenović, B., Herak, D., & Matej, S. (2014). Neotectonics of the Dinarides–Pannonian Basin transition and possible earthquake sources in the Banja Luka epicentral area. Journal of Geodynamics, 82, 52-68. doi: 10.1016/j.jog.2014.04.006

Ustaszewski, K., Kounov, A., Schmid, S. M., Schaltegger, U., Krenn, E., Frank, W., & Fügenschuh, B. (2010). Evolution of the Adria-Europe plate boundary in the northern Dinarides: From continent-continent collision to back-arc extension. Tectonics, 29(6), TC6017. doi: 10.1029/2010TC002668

Ustaszewski, K., Schmid, S., Fügenschuh, B., Tischler, M., Kissling, E., & Spakman, W. (2008). A map-view restoration of the Alpine-Carpathian-Dinaridic system for the Early Miocene, Swiss Journal of Geosciences, 101(0), 273-294. doi: 10.1007/s00015-008-1288-7

Ustaszewski, K., Schmid, S. M., Lugović, B., Schuster, R., Schaltegger, U., Bernoulli, D., Hottinger, L., Kounov, A., Fügenschuh, B., & Schefer, S. (2009). Late Cretaceous intra-oceanic magmatism in the internal Dinarides (northern Bosnia and Herzegovina): Implications for the collision of the Adriatic and European plates. Lithos, 108(1-4), 106-125. doi: 10.1016/j.lithos.2008.09.010

van Gelder, I. E., Matenco, L., Willingshofer, E., Tomljenović, B., Andriessen, P. A. M., Ducea, M. N., Beniest, A., & Gruić, A. (2015). The tectonic evolution of a critical segment of the Dinarides-Alps connection: Kinematic and geochronological inferences from the Medvednica Mountains, NE Croatia. Tectonics, 34, 1952–1978. doi: 10.1002/2015TC003937

van Gelder, I.E., Willingshofer, E., Sokoutis, D., & Cloetingh, S.A.P.L. (2017). The interplay between subduction and lateral extrusion: A case study for the European Eastern Alps based on analogue models. Earth Planet. Sci. Lett., 472, 82-94.

van Unen, M., Matenco, L., Nader, F.H., Darnault, R., Mandic, O., & Demir, V. (2019). Kinematics of foreland-vergent crustal accretion: inferences from the Dinarides evolution. Tectonics, 38, doi: 10.1029/2018TC005066.

van Krevelen, D.W. (1950). Graphical-statistical method for the study of structure and reaction processes of coal. Fuel, 29, 269-84

Velaj, T., Davison, I., Serjani, A., & Alsop, I. (1999). Thrust Tectonics and the Role of Evaporites in the Ionian Zone of the Albanides. AAPG Bulletin, 83, 1408-1425.

Velaj, T. (2012). Tectonic style and hydrocarbon evaluation of duplex Kruja zone in Albania. NAFTA, 63 (7-8), 236-242.

Velaj, T. (2015). New ideas on the tectonic of the Kurveleshi Anticlinal Belt in Albania, and the perspective for exploration in its subthrust. Petroleum, 1(4). doi: 10.1016/j.petlm.2015.10.013

Velić, J., Malvić, T., Cvetković, M., & Velić, I. (2015). Stratigraphy and petroleum geology of the Croatian part of the Adriatic Basin. Journal of Petroleum Geology, 38(3), 281-300. doi: 10.1111/jpg.12611

Vergés, J., Millan, H., Roca, E., Mufioz, J. A. & Marzo, M. (1995). Eastern Pyrenees and related foreland basins: pre-, syn- and post-collisional crustal-scale cross-sections. Marine and Petroleum Geology, 12, 8, 893-915

Vergés, J., & Fernàndez, M. (2012). Tethys–Atlantic interaction along the Iberia–Africa plate boundary: The Betic–Rif orogenic system. Tectonophysics, 579(0), 144-172. doi: 10.1016/j.tecto.2012.08.032

Vilasi, N., Swennen, R., & Roure, F. (2006). Diagenesis and fracturing of Paleocene–Eocene carbonate turbidite systems in the Ionian Basin: The example of the Kelçyra area (Albania). Journal of Geochemical Exploration, 89, 409–413.

Vilasi, N., Malandain, J., Barrier, L., Callot, J.-P., Amrouch, K., Guilhaumou, N., Lacombe, O., Muska, K., Roure, F. & Swennen, R. (2009). From outcrop and petrographic studies to basin-scale fluid flow modelling: The use of the Albanian natural laboratory for carbonate reservoir characterisation. Tectonophysics, 474, 367-392.

Vlahović, I., Tišljar, J., Velić, I., & Matičec, D. (2005), Evolution of the Adriatic Carbonate Platform: Palaeogeography, main events and depositional dynamics, Paleogeography, Paleoclimatology, Paleoecology, 220(3-4), 333-360. doi: 10.1016/j.palaeo.2005.01.011

Vogt, K., Matenco, L., & Cloetingh, S. (2017a). Crustal mechanics control the geometry of mountain belts. Insights from numerical modelling. Earth Planetary Science Letters, 460, 12-21. doi: 10.1016/j.epsl.2016.11.016

Vogt, K., Willingshofer, E., Matenco, L., Sokoutis, D., Gerya, T., & Cloetingh, S. (2017b). The role of lateral strength contrasts in orogenesis: A 2D numerical study. Tectonophysics, In press, corrected proof. doi: 10.1016/j.tecto.2017.08.010

Vrabec, M., & Fodor, L. (2006). Late Cenozoic tectonics of Slovenia: structural styles at the northeastern corner of the Adriatic microplate]. In: N. Pinter, G. Gyula, J. Weber, S. Stein and D. Medak (Eds.), The Adria Microplate: GPS Geodesy, Tectonics and Hazards. Springer Netherlands, Dordrecht, 151-168.

Vrabec, M., Pavlovčič-Prešeren, P., & Stopar, B. (2006). GPS study (1996-2002) of active deformation along the Periadriatic fault system in northeastern Slovenia: tectonic model. Geologica Carpathica, 57(1), 57-65.

Weber, J., Vrabec, M., Pavlovčič-Prešeren, P., Dixon, T., Jiang, Y., & Stopar, B. (2010). GPS-derived motion of the Adriatic microplate from Istria Peninsula and Po Plain sites, and geodynamic implications. Tectonophysics, 483(3-4), 214-222. doi: 10.1016/j.tecto.2009.09.001

Willett, S., Beaumont, C., & Fullsack, P. (1993). Mechanical model for the tectonics of doubly vergent compressional orogens. Geology, 21(4), 371-374. doi: 10.1130/0091-7613(1993)021<0371:MMFTTO>2.3.CO;2

Willingshofer, E., Sokoutis, D., Luth, S. W., Beekman, F., & Cloetingh, S. (2013). Subduction and deformation of the continental lithosphere in response to plate and crust-mantle coupling. Geology, 41(12), 1239-1242. doi: 10.1130/G34815.1

Wölfler, A., Kurz, W., Fritz, H., & Stüwe, K. (2011). Lateral extrusion in the Eastern Alps revisited: Refining the model by thermochronological, sedimentary, and seismic data. Tectonics, 30, TC4006, doi: 10.1029/2010tc002782.

Wortel, M.J.R., & Spakman, W. (1992). Structure and dynamics of subducted lithosphere in the Mediterranean region. Proceedings of the Koninklijke Nederlandse Akademie van Wetenschappen, 95, 325-347.

Wortel, M.J.R., & Spakman, W. (2000). Subduction and Slab Detachment in the Mediteranean-Carpathian Region. Science, 290, 1910-1917.

Zappaterra, E. (1990). Carbonate Paleogeographic Sequences of the Periadriatic Region. Bolletino Societa Geologico Italiana, 109, 5-20

Zappaterra, E. (1994): Source-Rock Distribution of the Periadriatic Region. AAPG Bulletin, 78/3, 333-354.

Žibret, L., & Vrabec, M. (2016). Paleostress and kinematic evolution of the orogen-parallel NW-SE striking faults in the NW External Dinarides of Slovenia unraveled by mesoscale fault-slip data analysis, Geologia Croatica, 69, 295-305. doi: 10.4154/gc.2016.30

Ziegler, P. A., Cloetingh, S., & van Wees, J.-D. (1995). Dynamics of intra-plate compressional deformation: the Alpine foreland and other examples, Tectonophysics, 252(1-4), 7-22. doi: 10.1016/0040-1951(95)00102-6

Zoetemeijer, R., Cloetingh, S., Sassi, W., & Roure, F. (1993). Modelling of piggyback Modelling of piggyback-basin stratigraphy: record of tectonic evolution. Tectonophysics, 226, 253-269.

Zupanič, J., & Babić, L. (2011). Sedimentary evolution of an inner foreland basin margin: Paleogene Promina Beds of the type area, Mt. Promina (Dinarides, Croatia). Geologia Croatica, 64(2), 101-120. Retrieved from https://hrcak.srce.hr/71039

# About the Author

The author of this thesis was born on July 20, 1992 in The Hague, The Netherlands. In 2014 she earned her Bachelor's degree in Geology, and in 2016 her Master's degree (cum laude) in Earth Structure & Dynamics, from the Faculty of Earth Sciences, University of Utrecht, The Netherlands. In April 2016 she started her PhD project at the Geoscience Department at IFP Energies Nouvelles, France and in the Tectonics Research Group of the Earth Sciences Department of Utrecht University, The Netherlands.